Moore, G.F., Taira, A., and Klaus, A., et al., 2001
Proceedings of the Ocean Drilling Program, Initial Reports Volume 190

5. Site 1174[1]

Shipboard Scientific Party[2]

SITE SUMMARY

Site 1174 (ENT-03A) is located in the protothrust zone of the Nankai accretionary prism and was designed to sample a zone of incipient prism deformation. When combined with our reference Site 1173 (~11 km seaward) and Site 808 (~2 km landward at the frontal thrust), Site 1174 provides a transect of stratigraphy, structural data, physical properties, and geochemical gradients across the deformation front of the accretionary prism.

We recognized five lithostratigraphic units and three subunits at Site 1174. Unit I (slope-apron facies) is Quaternary in age and extends from the seafloor to a sub-bottom depth of 4.00 meters below seafloor (mbsf). This facies is composed mostly of mud that was deposited on the lowermost trench slope by hemipelagic settling. Unit II (trench-wedge facies) is Quaternary in age and includes three subunits. Subunit IIA (axial trench–wedge facies) extends from 4.00 to 314.55 mbsf and is characterized by thick sand turbidites, silt turbidites, and hemipelagic mud. The lithologies of Subunit IIB (314.55–431.55 mbsf) are limited to silt turbidites and hemipelagic mud, whereas Subunit IIC (431.55–483.23 mbsf) is composed of hemipelagic mud, volcanic ash, and silt turbidites. The gradual transformation in facies character downsection is consistent with a change in depositional environment from the outer trench wedge to abyssal floor. Unit III (upper Shikoku Basin facies) is Quaternary to Pliocene in age and extends from 483.23 to 660.99 mbsf. Lithologies within this unit include hemipelagic mudstone and volcanic ash; the lower unit boundary coincides with the deepest identifiable bed of vitric tuff. In contrast, Unit IV (lower Shikoku Basin facies) contains mostly bioturbated mudstone with sporadic interbeds and nodules of carbonate-cemented claystone and siliceous claystone. Replacement of glass shards by smectite and zeolites (clinoptilolite or heulandite) increases gradually with depth and is more extreme in

[1]Examples of how to reference the whole or part of this volume.
[2]Shipboard Scientific Party addresses.

Ms 190IR-105

finer-grained deposits. As a consequence, both ash to bentonite diagenesis and temporal changes in pyroclastic influx govern the lithologic distinction between the upper and lower Shikoku Basin facies. The unit boundary shifts upsection as Shikoku Basin deposits migrate toward the Nankai deformation front and become increasingly affected by rapid burial and heating beneath the trench wedge. The lowermost stratigraphic unit at Site 1174, Unit V, begins at a depth of 1102.45 mbsf. We drilled only 8.86 m of variegated claystone in this middle Miocene volcaniclastic facies.

Deformation bands are well developed between 218 and 306 mbsf and are concentrated in two oppositely inclined sets striking at 033° with the acute bisectrix inclined 10°NW from vertical. They occur immediately above a narrow but abruptly sheared interval, which with indications of reverse movement and a paleomagnetically restored southeast dip, may be a backthrust. Between 470 and 506 mbsf, fractured and markedly steepened bedding may represent a thrust; no significant deformation was seen in the cores equivalent to the thrust apparent on the seismic profile at 550 mbsf. Narrow, widely spaced zones of fractures and brecciation characterize the interval between 688 and 807 mbsf. Between 807.6 and 840.20 mbsf an irregular downward increase in intensity of inclined fractures and fineness of brecciation defines the décollement, which is thicker and more heterogeneous than at Site 808 and more thoroughly comminuted in its lower part. The underthrust sediments show little tectonic deformation; however, zones of significant bed steepening were noted between 950 and 1000 mbsf and around 1020 mbsf, the latter accompanied by evidence for shear deformation.

Nannofossil assemblages are indicative of Pleistocene (Subzone NN21b) to middle Miocene (Zone NN6) ages. Twenty-three biostratigraphic events are recognized. Nannofossils are common and generally moderately preserved in the Pleistocene, whereas Pliocene and Miocene nannofossils are rare and mostly poorly preserved. Sedimentation rates based on biostratigraphy are 630–770 m/m.y. for the late Quaternary and are significantly lower (11–125 m/m.y.) for deposits older than 0.8 Ma.

Paleomagnetic results indicate that the Brunhes Chron (0–0.78 Ma) ranges from 0 to 544.70 mbsf and extends through the trench-wedge turbidites. The Matuyama Chron occurs from 544.70 to 685.95 mbsf, the Gauss Chron, from 685.95 to 727.85 mbsf, and the Gilbert Chron, from 727.85 to 802.07 mbsf. High magnetic intensities occur from 0 to ~550 mbsf, below which they drop to low values to the bottom of the hole.

The main characteristics of the interstitial water concentration-depth profiles at Site 1174 are similar to those at Site 808. There is an intense, very shallow, sulfate reduction zone, alkalinity and ammonium concentrations peak in the uppermost 200 m of the section, and the solutes that are controlled by fluid-rock reactions, such as Cl, Na, and Si, have sharp changes in their gradients at a depth that corresponds to the boundary between the trench wedge and Shikoku Basin facies (lithostratigraphic Unit II/III boundary). At the depth that corresponds to the thrust intersection (~470 ± 5 mbsf), there are also significant excursions, most distinctly exhibited in the Cl and Si concentrations, that may indicate hydrologic activity. The chemical changes across the major tectonic feature, the décollement, are subtler, but a high-resolution record of pore fluid chemistry was recovered across and within the Nankai Trough décollement for the first time. A local Cl maximum of 496 mM within the décollement decreases smoothly to ~485 mM ~50 m above the décollement zone, whereas there is a very sharp decrease (~10 mM) in the 10 m below the structure. The cause of the Cl maximum in the décollement is as yet unclear. A low-Cl zone in the 200-m interval below the décollement, with minimum concentrations that are ~17% diluted relative to seawater, occurs at an almost identical distance below the décollement at Site 808. The dilution, however, is ~21% at Site 808, ~17% at Site 1174, and considerably less (~9%) at reference Site 1173. In the lowermost ~100 m of the underthrust section, Cl concentrations increase, approaching seawater concentration at 1110 mbsf. Hydration reactions in the lower volcaniclastic or an underlying upper basement fluid flow system may be responsible for the increase in the Cl concentrations.

Dissolved silica concentrations appear to be controlled by biogenic silica dissolution in the trench-wedge sediments, by volcanic ash diagenesis in the upper Shikoku Basin facies, and by the low-Cl source plus in situ silicate reactions at >70° to ~130°C in the lower Shikoku Basin facies. Dissolved sulfate increases below the sulfate reduction zone, 1–2 mM below the upper and lower Shikoku Basin facies boundary sediments, at ~660 mbsf, reaching 8–10 mM below the depth interval of the Cl minimum and remaining constant to the bottom of the section. At Site 1173 the first sulfate increase below the sulfate reduction zone is observed at a much shallower burial depth, ~400 m shallower than at Site 1174. The sulfate distributions at these sites may reflect a dynamic relationship among sedimentation rates, temperature, and microbial sulfate reduction rates.

Organic matter decreases with depth and total organic carbon (TOC) values are low (0.90 to 0.11 wt%; average = ~0.38 wt%) in the core. The C/N ratios indicate the presence of marine organic matter with only a slight increase in the upper trench–wedge facies (~200 mbsf) and in the lower Shikoku Basin facies below the décollement (~1000 mbsf). Discrete intervals of elevated methane concentrations are present between 225 and 700 mbsf. Minor amounts of ethane (200–800 mbsf) and propane (400–650 and 950–1110 mbsf) are probably attributable to some in situ thermal maturation of organic matter.

Microorganisms were enumerated in 40 samples collected from the surface to 1100 mbsf at Site 1174. With the exception of two samples with low abundances (~1.8×10^6 cells/cm^3) in the sandy layers at 26 and 66 mbsf, abundances from the surface to 400 mbsf were close to values predicted based on data from previous Ocean Drilling Program (ODP) sites. Abundances were lower than predicted below 400 mbsf. The decrease may relate to the relatively high temperature gradient at Site 1174. Cell counts dropped below the detection limit at 528 mbsf and remained so until just above the décollement. Abundances at 778 and 789 mbsf were 4.8 and 4.2×10^6 cells/cm^3, respectively; no cells were detected below these depths. Nineteen whole-round samples were used to inoculate anaerobic growth media and were maintained at the estimated in situ temperature. Samples were chosen from the surface through the known hypothermophilic region (113°C) (Blöchl et al., 1997), and subsamples at five depths were targeted for incubation at in situ pressure and temperature.

Porosities within the axial and outer trench–wedge facies (Subunits IIA and IIB) are characterized by high variability and generally decrease with depth. Porosity decreases across the boundary between the outer trench–wedge and trench to basin transition facies (Subunit IIB/IIC boundary). Within the transitional facies, porosities are less scattered and decrease slightly with depth. The upper Shikoku Basin facies (Unit III) is characterized by nearly constant porosities, which is a deviation from normal compaction trends. Surprisingly, a high velocity interval between 510 and 520 mbsf is associated with an interval of elevated porosity. At the top of the lower Shikoku Basin facies (Unit IV; ~660 mbsf) another high-velocity interval is present. Porosities within the lower Shikoku Basin facies resume a compaction trend of decreasing porosity with depth. Porosities increase sharply by 2%–4% at the top of the underthrust sequence. This porosity increase is accompanied by a decrease in velocity and increase of electrical conductivity. However, the anisotropy of electrical conductivity is higher in the underthrust sediments than above the décollement zone. Porosities and velocities increase with depth within the underthrust sediments, whereas electrical conductivities decrease. In contrast to Site 808, porosities within the décollement are not significantly lower than above and below it, although values are somewhat scattered.

Uncalibrated gas-permeameter measurements were made throughout the section. Shallower than 600 mbsf, silt-rich and ash horizons showed higher values than the silty clays. The axial trench–wedge sands gave the highest values and the lowermost silty clays recovered gave the lowest.

In situ temperature measurements to a depth of 65.5 mbsf and laboratory thermal conductivity measurements indicate a near-surface heat flow of 180 mW/m^2. If heat flow is purely conductive and steady state, a temperature of ~140°C is projected for the bottom of the hole.

OPERATIONS

Transit from Site 1173 to Proposed Site ENT-03A (Site 1174)

The bit was pulled from Hole 1173A, clearing the seafloor at 1930 hr on 6 June. After the positioning beacon was released and recovered at 2100 hr, the vessel started moving to proposed Site ENT-03A (Site 1174) in dynamic positioning (DP) mode. The drill string was recovered during the transit and the bit cleared the rotary table at 0445 hr on 7 June, officially ending Hole 1173A. A positioning beacon was dropped at 0700 hr on 7 June, establishing Site 1174.

Site 1174

The precision depth recorder indicated a water depth of 4754.4 meters below rig floor (mbrf). An eight-drill collar advanced hydraulic piston corer/extended core barrel (APC/XCB) bottom-hole assembly (BHA) was made up with an 11.4375-in roller cone bit, a lockable float valve, a seal bore drill collar, landing saver sub, top sub, head sub, nonmagnetic drill collar, five 8.25-in drill collars, one tapered drill collar, six joints of 5.5-in drill pipe, and a crossover sub to 5-in drill pipe. The drill string was tripped to the seafloor, the bit was positioned at 4741.1 meters below sea level (mbsl) (4752.4 mbrf), and core was taken but did not recover any sediment. The bit was repositioned at 4746.1 mbsl (4757.4 mbrf) and Hole 1174A was successfully spudded at 1735 hr on 7 June. Core 1H recovered 4.4 m of sediment, establishing the drilling depth as 4751.2 mbsl (4762.5 mbrf).

Hole 1174A

Cores 1H to 8H were cored from 0 to 64.4 mbsf and recovered 47.04 m (73%) (Tables T1, T2). Fine-grained sand and silts likely caused the somewhat low core recovery. The force required to pull the APC barrel out of the formation increased until it reached 70,000 lb on Core 7H. Core 8H resulted in a partial stroke with only 3 m of penetration, so the coring system was changed over to the XCB.

T1. Coring summary, p. 87.

T2. Coring summary by section, p. 89.

Core 9X was cut from 64.4 to 74.1 mbsf. When we tried to retrieve the core barrel, it could not be pulled free from the BHA. A 50-bbl sepiolite pill was pumped past the core barrel in an effort to clean out any sands/silts that might be causing it to jam, but this did not help, and the entire drill string had to be recovered. The bit cleared the rotary table at 0130 hr on 9 June, officially ending Hole 1174A.

When the BHA reached the rig floor, it was discovered that the core barrel was stuck inside the nonmagnetic outer drill collar. After the core barrel was finally dislodged, one of the XCB latching mechanisms (dogs) was found to have failed. A 1.5-in-long piece was missing from the middle of the latch dog. One of the remaining ends of the latch was still locked inside the XCB body and had rotated outward, pinning the core barrel in place. This is the first known occurrence of this type of failure, and the cause is as yet unknown.

Hole 1174B

The decision was made to set a drill-in-casing (DIC) system in Hole 1174B to case off the loose sands near the seafloor in preparation for an 1150-m-deep penetration through the protothrust and décollement zones. Eleven joints of 11.75-in casing (142.2 m) were made up with a new 14.75-in sawtooth casing bit welded on the end and hung off on the moonpool doors. A 9.875-in tri-cone bit was made up to the drilling assembly and was spaced out ~1 m ahead of the casing bit. Once the drilling assembly was attached to the casing assembly, a DIC reentry funnel was attached to the DIC drive bushing. The completed DIC assembly was then lowered to the seafloor.

While we assembled the DIC system, it was necessary to allow the ship to drift with the current. After the DIC assembly had reached the seafloor, another hour of maneuvering in DP mode was required to move the vessel back on location. Hole 1174B was spudded at 0943 hr on 10 June.

The DIC was first jetted into ~50 mbsf with maximum jetting parameters of 45 strokes per minute (spm), 400 psi, and 5000–10,000 lbs weight on bit (WOB). Then the DIC was drilled into 143.67 mbsf (4906.17 mbrf) with maximum drilling parameters of 80 spm, 1050 psi, 8000–10,000 lbs WOB, 10 rpm, and 6000–9000 ft-lb of torque. Total time for emplacement was ~7.25 hr, and no problems were encountered.

The rotary shifting tool (RST) was then deployed on the wireline to unlatch the DIC. The weight of the DIC casing, ~22,000 lb, was slacked off in preparation for unlatching. The RST had to be worked through the DIC three times before a definite indication of the release sleeve shifting was observed. The drill string was then picked up, and the weight of the DIC system was lost, indicating that it had released properly.

We intended to have Hole 1174B penetrate a relatively thick section that might be unstable; therefore, the decision was made to round trip the drill string to remove the DIC drive sub and then reenter with a standard rotary core barrel (RCB) BHA. Thus, the drill string was recovered.

The DIC BHA was broken out, and an RCB BHA was made up. The RCB was tripped to the seafloor and the vibration-isolated television (VIT) camera frame was lowered to the seafloor in preparation for reentry. The search for the DIC reentry funnel began at 1830 hr on 11 June, and the funnel was first sighted visually at ~2315 hr. At 2347 hr on 11 June, Hole 1174B was reentered and the VIT was recovered. The bit was lowered into the hole with moderate drag until the bit had reached 52.5 mbsf, where some resistance was encountered. The top drive was picked up, and the bit had to be worked down all the way through the cased section.

Hole 1174B was then cored from 143.7 to 265.8 mbsf (4906.2 to 5028.3 mbrf) with high erratic torque. At this depth the bit became stuck. The drill string was worked for 1 hr, and 120,000 lb of overpull was required to free the bit. The bit was raised up inside the casing with drag and high erratic torque all the way. The bit was eventually raised to 50 mbsf (4852 mbrf), where the high erratic torque finally disappeared.

The bit was lowered once again, encountering an obstruction at 52.5 mbsf (4854.5 mbrf). The bit was worked through this problem area inside the casing several times until it was thought that the obstruction was no longer a threat to the coring operations. The bit was then lowered back down into the open hole, encountering fill at 172.5 mbsf (4935 mbrf). After the hole was washed and reamed to bottom, coring resumed.

Some further insight into the mysterious high erratic torque previously observed while coring in Hole 1174B appeared in the top of Core 20R. A piece of chewed-up metal ~3 in long, 1.5 in wide, and 0.25 in thick was recovered. Additional pieces of metal were found in other succeeding cores. Unfortunately, the origin of the metal is still not clear.

While retrieving Core 40R from 524.3 mbsf (5286.8 mbrf), the forward core winch wireline parted at the crown with the core barrel at 3664 mbrf. The frayed end of the wireline caught in the oil saver on top of the swivel and T-bar clamps were used to pull the parted wireline up through the top drive. Preparations were then made to string the parted wireline back over the crown sheave and reattach it to the coring winch. However, when the derrick man reached the crown, he discovered that the outboard wireline crown sheave had failed.

Approximately one-third of the sheave rim on the outboard side had separated from the sheave body. A used sheave was located on board and was installed to replace the failed sheave.

The parted wireline was strung over the replacement sheave and reattached to the core winch with cable clamps. The parted wireline was recovered along with the core barrel, which contained 9.21 m of core. The forward core winch was secured, and the aft core winch, which had 9600 m of new wireline on it, was placed into service. A total of 8.25 hr of down time was incurred as a result of the parted wireline and failed sheave.

Although rotation and circulation were maintained while we recovered the parted wireline and replaced the failed sheave, a wiper trip was carried out before we resumed coring operations. The bit was pulled to 128.43 mbsf (4890.93 mbrf) inside the DIC casing shoe. Once the bit was back inside the casing, an overdue maintenance of the drill line (slip and cut) was carried out. The bit was then lowered to 459.86 mbsf

(5222.36 mbrf), where slight drag was encountered. The top drive was picked up and the hole was washed and reamed to 524.3 mbsf. Approximately 7 m of soft fill was encountered in the bottom of the hole. RCB coring then resumed, and Cores 41R to 102R were recovered from 533.9 to 1119.8 mbsf (5882.3 mbrf). After the DIC was drilled in to 143.7 mbsf, Hole 1174B was continuously cored through 976.1 m of section. Recovery was 577.57 m (60%).

Because some gas was detected in the formation, the hole was displaced with 280 bbl of heavy mud. After the hole was displaced, the pipe was pulled out of the hole with no rotation or circulation. When the bit reached 398.2 mbsf (5160.3 mbrf), a tight spot was encountered and the pipe was worked without picking up the top drive. A 60,000-lb overpull was being applied to the drill string when the pipe came free. However, the drill string weight was ~70,000 lb lighter, indicating that the drill string had parted, and the pipe trip continued. The drill string had parted 467 m above the seafloor.

Once the drill pipe was clear of the seafloor, the two seafloor positioning beacons were given release commands. The primary beacon released and was recovered. However, the backup beacon failed to release and was not recovered. Once the beacon was on board and the end of the pipe was near the rig floor, the thrusters and hydrophones were raised and the vessel began the 2-hr transit to proposed Site ENT-05A (Site 1175).

The end of the drill pipe cleared the rig floor at 2230 hr on 22 June. The pin connection on the bottom of drill pipe stand number 26 had failed. Lost in the hole were a 9.875-in RCB bit, a mechanical bit release, an outer core barrel, a top sub, a head sub, seven 8.25-in drill collars, a transition drill collar, six joints of 5.5-in drill pipe, a crossover sub, and 75 joints of 5-in drill pipe.

LITHOSTRATIGRAPHY

We recognized five lithostratigraphic units at Site 1174 (Fig. F1) and were able to correlate these with units previously described at Sites 808 and 1173 (Table T3). Unit boundaries are diachronous between the sites.

F1. Stratigraphic column, p. 38.

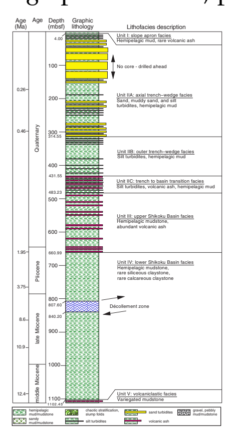

T3. Stratigraphic relations, p. 101.

Unit I (Slope-Apron Facies)

Unit I is Quaternary in age and extends from the seafloor to a subbottom depth of 4.00 mbsf (Fig. F1; Table T3). The dominant lithology is brown to gray mud (silty clay to clayey silt). A pale brown glass-rich ash layer at 3.38 mbsf is normally graded and 22 cm in thickness. The mud is generally structureless and contains clay minerals with less abundant glass, lithic fragments, quartz, feldspar, siliceous microfossils (mostly diatoms), and calcareous nannofossils (mostly coccoliths) (see "Site 1174 Smear Slides," p. 110). Deposition occurred ~50 m above the trench floor by way of hemipelagic settling and, perhaps, muddy turbidity currents.

Unit II (Trench-Wedge Facies)

Unit II is Quaternary in age and 479.23 m in thickness (Fig. F1; Table T3). Subunit IIA (axial trench–wedge facies) consists of 310.55 m of sand, silty to muddy sand, silt to sandy silt, silty clay to clayey silt; one very thin bed of pale gray volcanic ash is at 257 mbsf. We drilled through an inferred sand-rich interval without coring from 67.43 to 143.70 mbsf. Recovered beds of black, dark gray, and greenish gray sand and silty sand range from thick (30–100 cm) to very thick (>100 cm), typically with normal grading (Fig. F2), sharp bases, and gradational tops. Grain size varies from silt to granule (Fig. F3) but is predominantly medium to coarse sand. Thicker intervals of sand are typically soupy. Layers of sandy silt and silt range from medium bedded (10–30 cm) to very thin bedded (1–3 cm) or laminated (<1 cm). Lower contacts are sharp, scoured, or loaded, whereas tops are gradational. Grain size typically fines upward, and plane-parallel laminae are common in the upper parts of beds. The sand and silt deposits contain subrounded to subangular grains of quartz, feldspar, and lithic fragments together with lesser amounts of ferromagnesium minerals, volcanic glass, microfossils, and mica (see **"Site 1174 Smear Slides,"** p. 110). Fine-grained sulfide and framboidal pyrite are present throughout Subunit IIA as a black mottling.

Hemipelagic settling and fine-grained turbidity currents probably caused sedimentation of muddy interbeds in Subunit IIA. The sandy beds are turbidites. Their overall seismic-stratigraphic position and textures and bed thicknesses are all consistent with deposition in the axial portion of the trench wedge. The upper 18 m of the trench wedge is lithologically similar to Unit I at Site 808 (Shipboard Scientific Party, 1991) but does not contain contorted or overturned beds indicative of slump folding. Incipient deformation in the protothrust zone has lifted strata ~50 m above the trench floor. Thus, we cannot rule out the possibility that some of the silty sand beds assigned to Subunit IIA were deposited from axial flows that lapped onto the lowermost slope, and the change to Unit I may be transitional.

The top of Subunit IIB is at the base of a thick silty sand bed at 314.55 mbsf (Section 190-1174B-19R-1, 55 cm). This subunit consists predominantly of silty clay to clayey silt (Fig. F4) with laminae to medium beds of silt and sandy silt. Laminae of volcanic ash are also present. Subunit IIB is very similar to Subunit IA at Site 1173; both probably were deposited in the outer trench–wedge environment.

The top of Subunit IIC (trench to basin transition) is located at the top of a prominent ash bed at 431.55 mbsf (Section 190-1174B-31R-2, 105 cm). This subunit consists of silty claystone to clayey siltstone, volcanic ash, and thin beds of laminated silt to sandy silt. This subunit is equivalent to Subunit IB at Site 1173 and Unit III at Site 808. The base of Subunit IIC is defined by the deepest occurrence of a discrete silt bed (>1 cm) at 483.23 mbsf (Section 190-1174B-36R-5, 73 cm). Thinner silt laminae are sporadically present deeper in the hole.

Unit III (Upper Shikoku Basin Facies)

Unit III is Pliocene to Quaternary in age and 177.76 m in thickness (Fig. F1; Table T3). This unit consists predominantly of silty claystone to clayey siltstone with interbeds of volcanic ash (Fig. F5) and is equivalent to Unit II at Site 1173 and Subunit IVA at Site 808. The deepest unequivocal ash bed at 660.99 mbsf (Section 190-1174B-55R-2, 49 cm) defines the base of Unit III. This particular ash bed is somewhat unusual in that calcareous nannofossils are mixed with unaltered and partially altered volcanic glass. One other deposit of mixed nannofossil-rich mud and volcanic glass is present in Unit III. Many of the ash beds in Unit III contain partially altered volcanic glass, and the finer-grained

F2. Medium- to fine-grained graded sand and mud chips in Subnit IIA, p. 39.

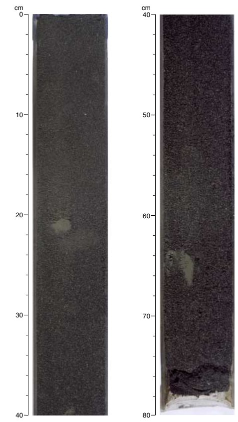

F3. Granule fragments in sand from Subunit IIA, p. 40.

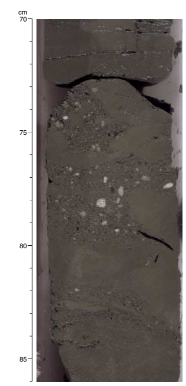

F4. Silty claystone from Subunit IIB containing the trace fossil *Chondrites*, p. 41.

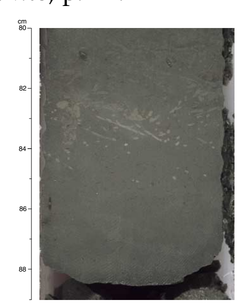

examples display more alteration than coarser-grained beds. This alteration pattern differs from that at Site 1173, where only the lower portion of the upper Shikoku Basin facies showed signs of ash alteration.

Unit IV (Lower Shikoku Basin Facies)

Unit IV is Miocene to Pliocene in age and consists of 441.46 m of mostly bioturbated silty claystone to clayey siltstone (Figs. F6, F7), with minor calcareous and siliceous claystone (Fig. F1; Table T3). Most of the siliceous claystones are probably altered ash beds because they contain particles of cryptocrystalline silica, smectite, zeolite, and opaque minerals (Table T4). The boundary between Unit III and Unit IV, therefore, is controlled partially by diagenetic alteration, as also documented at Sites 1173 and 808. Attempts to correlate ash stratigraphy at Sites 1173 and 1174 met with limited success (Fig. F8). The total thickness of ash-rich Subunit IB and Unit II at Site 1173 (261 m) is greater than the equivalent thickness of Subunit IIC and Unit III at Site 1174 (229.44 m). This discrepancy, together with the smaller number of identifiable ashes at Site 1174, indicates that the diagenetic front of ash alteration migrates upsection as the Shikoku Basin strata are buried progressively beneath the axial trench wedge. Thickness variations also may have been affected by variable sedimentation rates within Shikoku Basin.

Unit V

Unit V begins at a depth of 1102.45 mbsf (Section 190-1174B-102R-CC, 26 cm) and consists of 8.86 m of variegated silty claystone (Fig. F1; Table T3). The probable age is middle Miocene, but recovery from this interval was very poor. The claystone ranges in color from greenish gray to mottled green and red. Even though silicic tuff beds were not recovered, we believe this variegated hemipelagic claystone represents the top of the same volcaniclastic facies as encountered at Site 808 (Shipboard Scientific Party, 1991).

X-Ray Diffraction Mineralogy

The results of X-ray diffraction (XRD) analyses of randomly oriented bulk-sediment powders are shown in Figure F9, and all data are listed in Tables T5 and T6. The average values of normalized relative mineral abundance in Subunit IIA are quartz = 35%, plagioclase = 19%, calcite = 1%, and total clay minerals = 45%. These values are typical of the entire trench-wedge facies. Quartz content decreases slightly within Unit III (mean = 37%), whereas calcite content increases (mean = 4%). A subtle increase in quartz content occurs below the Unit III/IV boundary; this compositional gradient is followed by a reduction in quartz below ~700 mbsf. Total clay mineral content, conversely, increases gradually below the trench-wedge deposits. Average contents of total clay minerals are 46% in Unit III and 49% in Unit IV. This modest increase in clay mineral abundance is probably a consequence of both diagenetic alteration of disseminated volcanic glass and a decrease in particle size within the hemipelagic mudstones of the Shikoku Basin. Plagioclase content decreases steadily beneath the base of Unit II, probably in response to an overall decrease in grain size. Calcite content is erratic in Unit IV as a result of scattered nannofossil-rich beds and nodules of carbonate.

The peak-area ratio of (101) cristobalite to (100) quartz also changes with stratigraphic position (Fig. F9). The pattern of silica alteration is

F5. Two volcanic ash layers from the upper Shikoku Basin, p. 42.

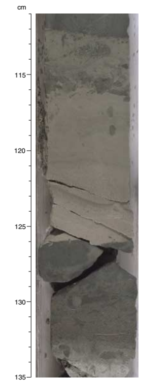

F6. Silty claystone with foraminifers from the lower Shikoku Basin, p. 43.

F7. Silty claystone with the trace fossil *Zoophycos,* p. 44.

T4. XRD analysis of bulk-powder volcanic ash samples, p. 102.

F8. Distribution and thickness of volcanic ash layers, Sites 1173 and 1174, p. 45.

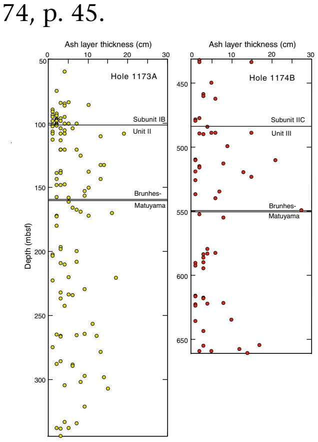

more complicated at Site 1174 than at Site 1173 because the effects of burial beneath the Nankai trench wedge are superimposed on trends inherited from burial and heating in the Shikoku Basin. Smear-slide observations show that diatoms become increasingly scarce in Cores 190-1174B-18R and 19R (305–315 mbsf) and disappear in Core 20R (~325 mbsf) and below. The inferred temperature range for that depth interval is 50°–60°C. The cristobalite to quartz ratio decreases toward and beneath the base of Unit II then increases at ~605 mbsf. The peak-area ratio decreases again at ~660 mbsf just below the boundary between Units III and IV.

XRD analysis of representative volcanic ash beds shows a clear transformation downsection from glass-rich deposits with crystals of plagioclase and quartz to smectite-rich claystone or bentonite (Table T4). Some of the samples analyzed are nearly pure smectite (Fig. F10). A second common alteration product within the lower portion of the upper Shikoku Basin facies is undifferentiated clinoptilolite-heulandite. Similar alteration products were documented at Site 808 (Shipboard Scientific Party, 1991). It is interesting to note, however, that zeolites are not present in the altered ash layers from Hole 1173A (see **"Site 1173 Smear Slides,"** p. 78). This difference may be a function of either reaction temperature or reaction time.

STRUCTURAL GEOLOGY

A variety of deformation structures is present at Site 1174, summarized in relation to lithostratigraphy in Figure F11. All the numerical data are given in Table T7. The chief features at the site are (1) deformation bands developed in the upper part of the hole, (2) zones of fractured and, in places, distinctly steepened bedding within a zone of protothrusting, (3) the basal décollement, and (4) the relatively little-deformed underthrust section. The distribution with depth of the main core-scale structures is portrayed in Figure F12.

Hole 1174A

All the cores retrieved from Hole 1174A, which reached 67.61 mbsf, show approximately horizontal bedding with a distinct fissility in places and a complete absence of deformation.

Hole 1174B

Horizontal bedding with fissile intervals also typifies Hole 1174B down to 464 mbsf, although there is evidence of some slump folding with associated steepened bedding. However, within this largely horizontally bedded interval, we define a structural domain in which deformation bands are concentrated.

Deformation Bands

The shallowest example of a deformation band that we recognized, albeit weakly developed, is at 199 mbsf, indicating that tectonic deformation is acting on sediments that have undergone surprisingly little burial and lithification. The main development of deformation bands arises between 218 and 306 mbsf. The structures appear to be best developed in silty claystones that lack bioturbation. They are manifest in

F9. Abundances of clay minerals, quartz, plagioclase, and calcite, p. 46.

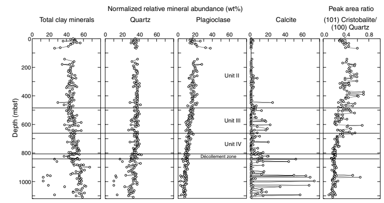

T5. Peak intensities and peak areas from XRD analysis, p. 103.

T6. Normalized relative mineral abundances based on XRD analysis, p. 108.

F10. X-ray diffractograms of unaltered and altered volcanic ash, p. 47.

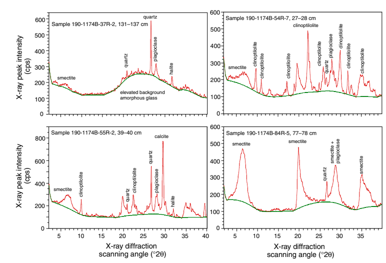

F11. Overall distribution of deformation structures, p. 48.

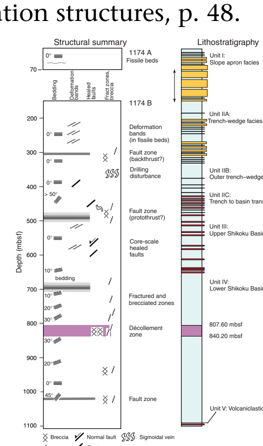

T7. Structural data, p. 112.

the core face as roughly planar dark zones between ~1 and 8 mm across and are commonly in paired, oppositely inclined arrays. Bands can abruptly decrease in width (Fig. **F13A**) and bifurcate into twin strands that coalesce a few millimeters along the band (Fig. **F13B**). Such observations are in line with earlier descriptions of deformation bands in the Nankai prism (e.g., Maltman et al., 1993), where at the microscopic scale, the bands have various kinklike and shear-zonelike aspects. On occasion, it was possible with the Site 1174 cores to detect a sense of displacement along the bands; in all the observed cases, this was a reverse sense.

Figure **F14** shows the orientations of all the deformation bands we observed. Despite the diversity of orientations of the structures in the cores, paleomagnetic correction (see **"Paleomagnetism,"** p. 10, in the "Explanatory Notes," chapter) revealed a concentration into two distinct sets, both with a strike of 033°—roughly that expected if the bands are due to prism contraction. The lesser dihedral angle between the two sets is 67°, the bisector of which is inclined 10° from vertical toward the northwest. The few cases where sense of movement was discernible from the bands are consistent with the principal shortening being shallowly inclined and bisecting the obtuse angle between the sets, which is congruent with typical kink-band geometry. A few millimeter-wide planar zones, which we classified as deformation bands, were observed at much deeper levels: 510 and 590 mbsf. Both cases, unusually, are developed in and confined to thin bands of volcanic ash.

The concentration of the majority of the deformation bands between ~200 mbsf and a sheared interval at 306 mbsf is striking. This latter horizon is a fault zone a mere 35 cm thick consisting of foliated breccia with fragments as small as a few millimeters in length and a distinctly inclined fabric (Fig. **F15**). It therefore contrasts markedly with the little disturbed sediments above and particularly with the virtually undeformed material below. Indications of reverse movement such as small parasiticlike folds imply that the structure may be a thrust. Paleomagnetic reorientation of the fold axial planes (Fig. **F16A;** great circle labeled 1) and the inclined fractures (Fig. **F16** great circle labeled 2.) suggest that the fault is a southeast-dipping feature, possibly a backthrust within the prism. The deformation bands may therefore record pervasive strain in the hanging wall of this fault. An alternative explanation for the localization of deformation bands involves some lithologic influence on their development. At the present site their lower limit approximately coincides with the transition from the trench-wedge to outer trench–wedge facies; at Site 808 of Leg 131, where deformation bands were observed at deeper levels, their lower boundary corresponds to the top of the Shikoku Basin sediments.

Protothrust Domain

The shear zone mentioned above is the shallowest of a number that appear irregularly throughout the section above the basal décollement. Their distribution with depth is depicted in Figure **F12.** For 157 m below the one already described, there is very little deformation and bedding dips rarely depart from horizontal, although core recovery was relatively poor. Abrupt, therefore, is the 1.5-m-thick zone of fine rubble at 463.0 mbsf, which may or may not be of natural origin. The underlying 2.6-m-interval was unrecovered. Between 467.10 and 469.95 mbsf is an interval of fractured and steepened bedding (Fig. **F17**), in places vertical, followed by a 6.55-m unrecovered interval and then virtually unde-

F12. Distribution of bedding dips and deformation structures with depth, Hole 1174B, p. 49.

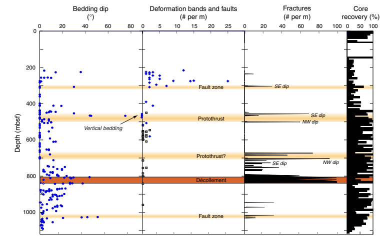

F13. Deformation bands displaying varying width and the tendency to bifurcate, p. 50.

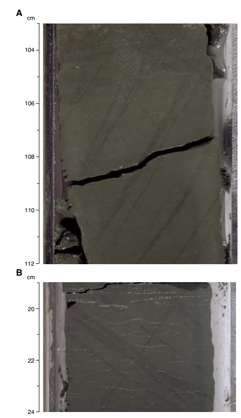

F14. Stereographic projections of deformation bands illustrating the effectiveness of paleomagnetic reorientation, p. 51.

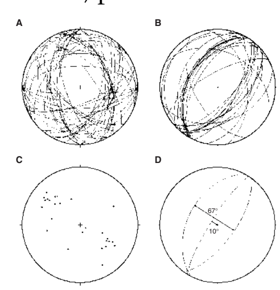

formed subhorizontal beds. A 30-cm-thick zone of shearing at 504 mbsf (Fig. **F16C**) ends this zone of deformation as the underlying cores, to depths well over 600 mbsf, show approximately horizontal beds with little deformation.

Seismically Imaged Protothrust

The significance of the above observations, and indeed one underlying reason for drilling Site 1174, is that seismic interpretations show a prism protothrust at this location. In the preliminary seismic depth section, this protothrust is at a depth of ~550 mbsf, yet we saw no deformation in the cores from around that depth. Good core recovery constrains any thrust located at such depths in unrecovered material to have a thickness <5 m. On the basis of the core data, therefore, a protothrust of significant thickness at this site must be represented by the structures between ~463 and 500 mbsf mentioned above. The beds could be steepened by fault-related folding similar to that inferred for the frontal thrust at Sites 573 (Shipboard Scientific Party, 1986) and 808 (Taira, Hill, Firth, et al., 1991), but details at this site remain unclear. The vertical thickness of the fault zone is a maximum of 41 m if all rubble and unrecovered intervals are included, in comparison to the 30 m reported from Site 808.

Deeper Fractured and Brecciated Zones

Further intervals of fractures and brecciation are present between 688 and 807 mbsf, the latter being the top of the décollement (Fig. **F12**). The appearance of these intervals of broken core is highly variable, and it is possible that those lacking fabric have been artificially induced or that naturally fractured intervals have been enhanced by the coring process. Those zones with a clear alignment of clasts or some regularity of fractures are thought to be natural, but even here their appearance varies. Nowhere are they thick, ranging between 10 and 90 cm. Some cores contain more than one of these zones, separated by intact material, but they are typically many meters apart. Preliminary analysis suggests that some of the fracture fabrics dip toward the southeast; the significance of this remains unclear. The intensified fracturing between 699 and 720 mbsf, sharply bounded at its base and including a northwest-dipping fracture fabric, is shown on Figure **F12** as a fault zone. It may correspond to a protothrust apparent at these depths on the seismic section.

Core-Scale Healed Faults

Small faults are present throughout Site 1174, but they become noticeably more common between ~495 and 611 mbsf. The faults appear as dark seams no more than a millimeter or two across, commonly braided and distinctly curviplanar to irregular (Fig. **F18**). Offset markers are infrequent but, where observed, in almost all cases show a normal sense of displacement, typically between a millimeter and a centimeter. The faults are vertical to steeply inclined; any breakage along them reveals slickensides and, commonly, down-dip slickenlines. These structures are more commonly developed than at Site 1173 and less widespread than similar structures at Site 808 and so could be recording either increasing tectonic strain or greater burial. Their apparently random strike after paleomagnetic reorientation (Fig. **F19**) indicates a lack of tectonic influence. In line with previous interpretations, the faults probably reflect the effects of burial compactional strains on these clayey silt lithologies at this degree of lithification.

F15. Inclined fractures, part of a deformed horizon that may represent a prism backthrust, p. 52.

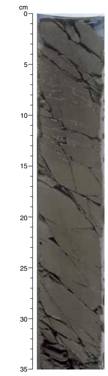

F16. Stereographic projections of fractures related to prism faults, p. 53.

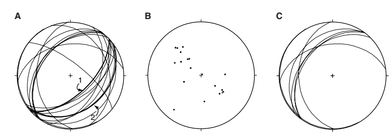

F17. Steepened bedding and inclined fractures, p. 54.

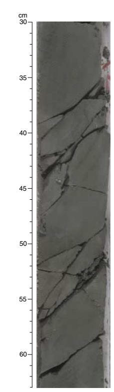

F18. Bifurcating, healed normal fault, p. 55.

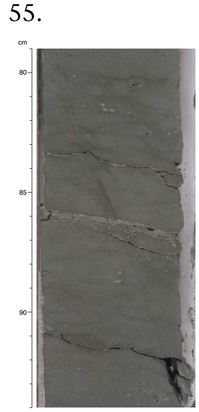

Décollement

The deepest of the brecciated intervals reported above is found at 784 mbsf and is underlain by generally intact sediment with moderate dips as deep as 807 mbsf. Here a distinctive set of planar, inclined fractures divides the cores into trapezoidal blocks (Fig. F20A) that decrease downward in size eventually to be replaced by brecciated material (Fig. F20B). The overall orientation of the fractures is shown in Figures F21A and F21B.

We take the onset of these distinctive, inclined fractures to mark the top of the basal décollement at 807.6 mbsf. The striking feature of the décollement zone is the heterogeneity of the deformation, which in a general way increases downward in intensity. Bedding is irregularly steepened in the zone (Fig. F21C). The topmost 3 m (disregarding unrecovered core) consists largely of the trapezoidal blocks mentioned above, mostly 5 cm and more in length, but the size of the blocks tends to diminish in the underlying 7 m of core until intervals with fragments on the scale of millimeters are common. Six meters or more of unrecovered core separates these foliated breccias from 7 m of much more uniformly comminuted material, with only rare clasts exceeding 1 cm in length and a foliated aspect being variably developed (Fig. F22). The base of this zone contains a few larger blocks but also a 20-cm interval of very finely pulverized material. Just 60 cm below this, a further interval of finely broken sediment is underlain by intact sediment; this contact, at 840.20 mbsf, clearly marks the décollement base. The décollement zone therefore has a vertical thickness at this site of 32.6 m. Because the core containing the base of the structure (Core 190-1174B-73R) was almost completely recovered, any allowance for unseen material would increase this figure by <1 m.

The brecciated aspect of the décollement zone is similar to that reported from Site 808 and contrasts with, for example, that of the northern Barbados prism with its scaly clay and S-C fabrics (Maltman et al., 1997). Nevertheless, there are some differences between the décollement cores from Sites 1174 and 808, such as a 13-m greater thickness at Site 1174. Also, the greater proportion of relatively intact intervals suggests a somewhat more heterogeneous deformation. The meters-long sections of comminuted material reported here were not seen at Site 808, although with the less successful recovery there it is possible such material exists but was simply not retrieved.

Underthrust Domain

The underthrust sediments show little deformation overall, as at Site 808. Between 950 and 1000 mbsf, bedding dips >20° were recorded, and at ~1020 mbsf, a 40-cm-thick zone of shallowly inclined slickensided fractures and nearby bedding dips up to 54° testify to some localized tectonic deformation in these downgoing sediments (Fig. F12). The rest of the section, however, is characterized by subhorizontal bedding. Rare, weakly developed healed normal faults and dewatering features (e.g., Fig. F23) probably record early compaction processes.

Uncalibrated Gas-Permeability Measurements

Measurements from Site 1174 are presented in Figure F24. Figure F25 provides a further illustration of the fine resolution that is made available by the instrument. It is important to reemphasize, however, that

F19. Stereographic projections of core-scale healed faults, p. 56.

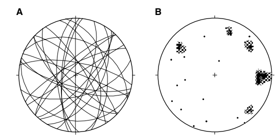

F20. Details of the décollement zone showing breakage into angular blocks and comminution of sediments, p. 57.

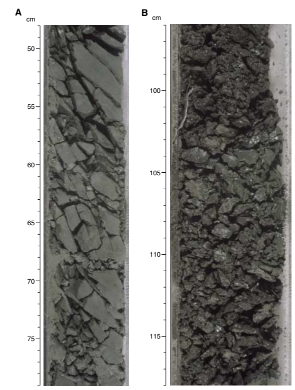

F21. Stereographic projections of structures related to the décollement, p. 58.

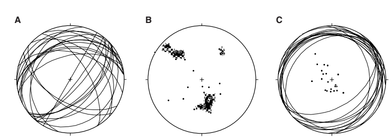

F22. Details of fracturing across the décollement zone, p. 59.

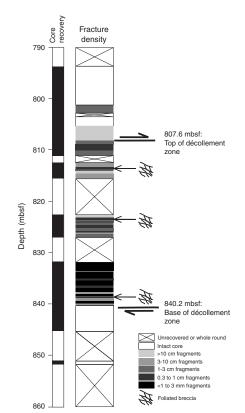

the shipboard results summarized here are semiquantitative measurements based on nitrogen flow in water-saturated sediments.

The sediments in Hole 1174A, reaching only 68 mbsf, were soft and delicate, but the determinations were sufficient to document the contrast in values between the interturbidite silty clays, which measured $<10^{-16}$ m^2, the sandy intervals, which exceeded 10^{-13} m^2, and the thick layers of black sand, which approached 10^{-11} m^2. In Hole 1174B, the sands of the axial-trench turbidites were generally too soft to allow reliable measurement, but two attempts gave measurements $>10^{-13}$ m^2, whereas the silty clays yielded values within an order of magnitude above and below 10^{-16} m^2.

The lower part of the trench sediments, lacking the thick sand intervals, generally showed values $\sim10^{-16}$ m^2 or slightly greater, but measurements well over 10^{-15} m^2 were given by siltier horizons and some ash bands. Thicker ash bands show some variation in detail, illustrated in Figure F25. Also yielding values an order of magnitude greater than the normal silty clays were the bioturbated intervals that involve ash fragments.

Below 480 mbsf, in the Shikoku Basin facies, the cores consistently gave measurements that deviate little from 10^{-16} m^2 (apart from a few aberrant values near 600 mbsf that are not understood). This consistency includes the horizons of ash at these depths, which presumably give values less than shallower equivalents because of their greater degree of alteration. It also includes the décollement zone, that is, it applies to those fragments >~3 cm across that were large enough to allow measurement. Such clasts may not, of course, represent the permeability of the intervening, more highly sheared material. The underthrust sediments show some variation in appearance, such as degree of bioturbation and diagenetic alteration to carbonate, but all these materials gave measurements that deviated little from 10^{-16} m^2. In the lowest recovered sediments, values of 10^{-17} m^2 and less were obtained.

F23. Example of a dewatering structure in the underthrust sediments, p. 60.

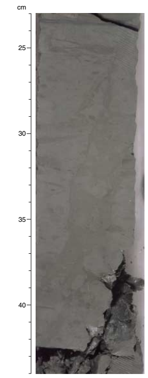

F24. Variation of uncalibrated gas-permeameter measurements with depth, p. 61.

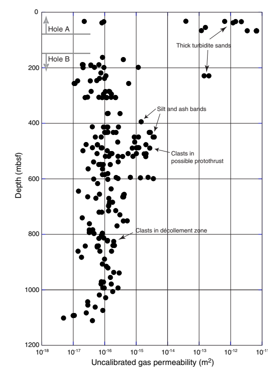

F25. Fine-scale variations in volcanic ash, p. 62.

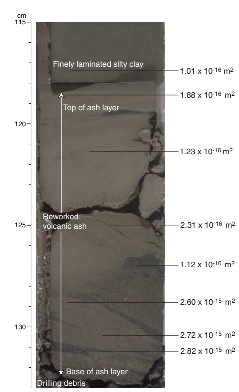

BIOSTRATIGRAPHY

Introduction

Sediments recovered from Site 1174 provide a continuous sedimentary record from the Quaternary through the middle Miocene. The biostratigraphic outline was provided by calcareous nannofossils using the zonation schemes of Gartner (1977) and Martini (1971) with zonal modifications proposed by Young (1998) (Table T8). The interval (core and section) and depth (mbsf) constraints of calcareouse nannofossil events recognized in Site 1174 are reported in Table T9. The epoch boundaries have been placed as in Table T10. For ranges of calcareous nannofossils at Site 1174 see Tables T11 and T12.

Calcareous Nannofossils

Hole 1174A

Hole 1174A was cored to 67.61 mbsf and contained upper Quaternary nannofossil assemblages assigned to Subzones NN21b and NN21a. Calcareous nannofossils are common to frequent throughout the sequence and mostly well to moderately preserved. The main assemblage is composed of placoliths (*Emiliania huxleyi* and *Gephyrocapsa* spp.) with

T8. Recognized nannofossil events, p. 121.

T9. Interval and depth constraints of calcareous nannofossil events, p. 122.

a highly diverse subordinate assemblage. Reworked specimens, mainly discoasterids, sphenoliths, and reticulofenestrids of Pliocene to Miocene age, were encountered sporadically. The only event found in Hole 1174A was the onset of the *E. huxleyi* acme defining the base of Subzone NN21b (0.085 Ma), observed between Samples 190-1174B-7H-CC and 8H-2, 74–75 cm.

T10. Epoch boundaries, p. 123.

T11. Calcareous nannofossil range chart (Zones NN21–NN19), p. 124.

T12. Calcareous nannofossil range chart (Zones NN18–NN6), p. 128.

Hole 1174B

Hole 1174B was washed to 143.7 mbsf. The sediments recovered were assigned to Zone NN21 of the Pleistocene through Zone NN6 of the middle Miocene. Cores 190-1174B-1R to 39R (143.7 to 513.21 mbsf) yield mostly moderately to well-preserved nannofossil assemblages. Nannofossils are common throughout the Pleistocene sequence. Beginning in Sample 190-1174B-40R-CC (523.81 mbsf) nannofossils decrease drastically in abundance alongside a decline to poorer preservation. Nannofossil assemblages are strongly affected by mechanical breakage and dissolution, with several intervals barren of nannofossils (Samples 190-1174B-41R-CC to 42R-CC, 49R-CC, 64R-CC to 65R-3, 103–104 cm, 66R-CC, 68R-CC, 74R-CC, 77R-CC to 78R-CC, 80R-CC, 83R-CC, 87R-CC to 88R-CC, 97R-CC). A few samples exhibit strong overgrowth, which mainly affected discoasterids and reticulofenestrids in Samples 190-1174B-55R-CC to 56R-CC (668.08 to 671.61 mbsf), 59R-CC (706.45 mbsf), 71R-CC (815.49 mbsf), 82R-CC (922.46 mbsf), 84R-CC (946.55 mbsf) and 93R-CC (1031.08 mbsf). Therefore, the proper position of the biostratigraphic events defining zonal boundaries may actually be in the barren intervals. This could explain discrepancies observed between ages retrieved from paleomagnetic data and biostratigraphic ages. The biostratigraphic analysis of further samples may resolve these problems.

Pleistocene

The Pleistocene includes the interval from 150.99 to 639.41 mbsf. Moderately to poorly preserved Pleistocene nannofossils were recovered from Sample 190-1174B-1R-CC to 52R-CC. The Pleistocene assemblages older than 0.26 Ma are characterized by the dominance of gephyrocapsids. Reworked Neogene taxa such as discoasterids, *Reticulofenestra pseudoumbilicus,* and *Sphenolithus* spp. were found in low numbers throughout the Pleistocene samples.

The base of Subzone NN21a, marked by the first occurrence of *E. huxleyi* (0.26 Ma), was placed between Samples 190-1174B-3R-CC and 4R-CC. The last occurrence of *Pseudoemiliania lacunosa* (0.46 Ma) was observed between Samples 190-1174B-16R-CC and 17R-CC bounding the negatively defined Zone NN20 to the bottom. The last occurrence of *Reticulofenestra asanoi* (0.8 Ma; between Samples 190-1174B-43R-CC and 44RH-3, 75–76 cm) and its first occurrence (1.06 Ma, between Samples 190-1174B-47-CC and 48H-CC) provide further datums to subdivide Zone NN19. The Pleistocene/Pliocene boundary was placed between Samples 190-1174B-52R-CC and 53R-3, 79–80 cm, according to the first appearance of *Gephyrocapsa oceanica* (1.77 Ma), which approximates the epoch boundary. Further analysis of relative abundances of the different *Gephyrocapsa* morphotypes may provide a higher biostratigraphic resolution for Zone NN19.

Pliocene

Cores recovered from 645.7 to 778.19 mbsf were assigned to the Pliocene. The Pliocene sediments contain mostly poorly preserved nannofossils in Samples 190-1174B-53R-CC and 67R-4, 75–76 cm. The abundance of nannofossils is generally lower than in the Pleistocene sediments. The Pliocene nannofossil assemblages are dominated by different morphotypes of reticulofenestrids and discoasterids; associated are mainly *Coccolithus* spp., *Calcidiscus* spp., and sphenoliths. Reworked specimens were encountered sporadically.

The last occurrence of *Discoaster brouweri* (1.95 Ma) was used to determine the top of Zone NN18 between Samples 190-1174B-53R-CC and 54R-CC. After an interval in which nannofossils were rare and poorly preserved (Samples 190-1174B-55R-CC and 56R-CC), the last occurrence of *Discoaster pentaradiatus* (2.52 Ma) was recorded between Samples 190-1174B-56R-2, 75–76 cm, and 56R-CC, assigning the level to Zone NN17. The top of Zone NN16 is marked by the last occurrence of *Discoaster surculus* (2.55 Ma) in Samples 190-1174B-56R-CC and 57R-2, 75–76 cm. The last occurrence of *R. pseudoumbilicus* (>7 µm) was used to define the boundary between Zones NN16 and NN15 (3.75 Ma) between Samples 190-1174B-62R-CC and 63R-CC. The last occurrence of *Amaurolithus* spp. (4.0 Ma, top of Zone NN14) in Sample 190-1174B-65R-5, 74–75 cm, was observed at the base of a barren sequence (Samples 190-1174B-64R-CC and 65R-3, 103–104 cm). The top of Zone NN14 (4.13 Ma) was indicated by the first appearance of *Discoaster asymmetricus* between Samples 190-1174B-66R-3, 75–76 cm, and 66R-4, 71–72 cm. The event that identifies zonal boundaries between Zones NN13 and NN12 was not recognized, that is, the first occurrence of *Ceratolithus cristatus* at the top of Zone NN12 (5.05 Ma). The first occurrence of this rarely observed species was recorded in Sample 190-1174B-63R-CC, which is above the last occurrence of *Amaurolithus* spp. (Zone NN14). The last occurrence of *Discoaster quinqueramus* (5.54 Ma) at the top of Subzone NN11b, which approximates the Pliocene/Miocene boundary (5.32 Ma), was observed between Samples 190-1174B-67R-4, 75–76 cm, and 67R-6, 75–76 cm.

Miocene

Sediments recovered from Sample 190-1174B-67R-6, 75–76 cm (784.19 mbsf), to the bottom of Hole 1174B (1111.3 mbsf) contain Miocene nannofossils. The generally poorly preserved Miocene nannofossil assemblage mainly consists of placoliths, diverse discoasterids, and sphenoliths.

The top of Subzone NN11a, marked by the first occurrence of *Amaurolithus spp.* (7.2 Ma), was assessed between Samples 190-1174B-73R-CC and 74R-3, 41–42 cm. The first occurrence of *D. quinqueramus* was used to define the boundary between Zones NN10 and NN11 (8.6 Ma) between Samples 190-1174B-75R-CC and 79R-CC. The last occurrence of *R. pseudoumbilicus* (>7 µm) marking the top of Subzone NN10a (9.0 Ma) was observed between Samples 190-1174B-76R-CC and 79R-CC. The range of *Discoaster hamatus* defines the boundaries of Zone NN9 (9.63–10.7 Ma). Its top occurrence was observed in Sample 190-1174B-80R-4, 75–76 cm, and the first occurrence between Samples 190-1174B-81R-CC and 82R-2, 74–75 cm. The basis of Zone NN8 is marked by the first occurrence of *Catinaster coalitus* (10.83 Ma) between Samples 190-1174B-85R-4, 75–76 cm, and 85R-CC. This event approximates the late/middle Miocene boundary (11.2 Ma). The first occurrence of *Discoaster kugleri* marking the boundary between Zones NN7 and NN6 (11.8 Ma) was recorded between Samples 190-1174B-96R-CC and 98R-CC. The first occurrence of *D. kugleri* is problematic because intergrades with *Discoaster deflandrei* are commonly found below the first occurrence datum (Young, 1998). In the same interval, the last occurrence of *Orthorhabdus serratus* (12.3 Ma) was recorded. The last common occurrence of *Cyclicargolithus floridanus* (13.2 Ma) between Samples 190-1174B-99R-CC and 100R-CC provides a further datum to subdivide Zone NN6. The absence of *Sphenolithus heteromorphus,* the last occurrence of which defines the top of NN5 (13.6 Ma), and the first occurrence of large (>7 µm) *R. pseudoumbilicus* (13.4 Ma) between Samples 190-1174B-101R-CC and 102R-CC suggests the assignment to Zone NN6. Sample 190-1174B-102R-CC from the bottom of the hole does not yield any age diagnostic nannofossils.

PALEOMAGNETISM

Introduction

After measuring the natural remanent magnetization (NRM), all sections of the archive half of the core were partially demagnetized using alternating-field (AF) magnetization up to 30 mT in increments of 5 mT at 5-cm intervals to remove magnetic overprints. Two oriented discrete samples were routinely collected from each section of the working half of the core primarily for shore-based analysis of the anisotropy of magnetic susceptibility. Additional measurements of polarity and basic magnetic character of selected discrete samples were used to aid in the interpretation of the archive long-core magnetization record. Most of the discrete samples were demagnetized up to 60 mT in 5-mT increments to permit principal component analysis. Rock magnetic experiments were conducted to identify the magnetic minerals at Site 1174.

Paleomagnetic Results

The majority of NRM inclinations for all sections are strongly biased toward steep inclinations of ~60°–80°. The steep inclinations observed are interpreted as magnetic overprints acquired during drilling; a problem identified on many previous Deep Sea Drilling Project (DSDP) and ODP legs. These overprints were successfully removed by AF demagnetization at 30 mT (see **"Paleomagnetism,"** p. 14, in the "Site 1173" chapter). Stable magnetic remanent inclinations were measured after AF demagnetization. These inclinations provide information about middle Miocene to Holocene magnetic polarity changes and were used in conjunction with the standard geomagnetic polarity time scale (GPTS) of Cande and Kent (1995) to date the sediments.

Declinations obtained from rotated archive-half core pieces after AF demagnetization aided in core orientation corrections and structural analysis such as fracture fabric analysis (see **"Structural Geology,"** p. 10).

Hole 1174A

The sediments of Units I and II in Hole 1174A, consisting of sandy and silty turbidites, show stable paleomagnetic remanence after AF demagnetization. All recovered sediment from Hole 1174A is included in the Brunhes Chron (0–0.78 Ma) based on the predominantly normal polarity inclinations. In contrast to these stable normal polarity inclinations, three reversed polarity inclinations were observed at 29.5 mbsf (Section 4H-5, 10 cm), 51.95 mbsf (Section 7H-1, 5 cm), and 61.58 mbsf

(Section 8H-4, 5 cm) (Fig. F26). Intensity values are high in both the reversed and normal polarity inclinations. Zijderveld analysis (Fig. F27) suggests that these short reversal events show the possibility of geomagnetic polarity changes during short geomagnetic excursions.

Hole 1174B

Inclination changes in Hole 1174B were compared with the GPTS of Cande and Kent (1995). However, noisy inclination changes from 544.7 (Section 43R-1, 110 cm) to 685.95 mbsf (Section 57R-6, 15 cm) complicate the identification of reversed polarity events. Magnetic intensity of this zone shows a distinct low value. Further rock magnetic analysis will also be needed in order to identify reasons for the scattered inclinations.

The paleomagnetic remanence shows characteristic magnetic intensity zones similar to those of Hole 1173A (Fig. F28). Multisensor track (MST) susceptibility values also follow a similar pattern (see "Physical Properties," p. 29). Based on these characteristic intensity and susceptibility changes, the sediments can be divided into four distinct zones (Fig. F28). High magnetic intensities (intensity Zone [IZ] 1) range from 0 to 553.25 mbsf (Section 44R-1, 35 cm). The termination of this zone does not correspond with a lithostratigraphic boundary (Fig. F28). There is a sudden decrease of magnetic intensity that extends to 763.1 mbsf (Section 65R-6, 60 cm). This low-intensity zone (IZ 2) with a slightly high intensity subzone (IZ 2′) was also observed at Hole 1173A. From 763.1 to 941.7 mbsf (Section 85R-6, 60 cm), intensities increase slightly (IZ 3). Below this, intensities return to very low values for the remainder of the hole (IZ 4).

Rock Magnetism

Rock-magnetic experiments were conducted to identify the magnetic minerals of the four major intensity zones (Fig. F29). Thermal demagnetization of multicomponent isothermal remanent magnetization (Lowrie, 1990) was used as the primary means of identifying magnetic minerals. For these experiments, orthogonally applied fields of 1.0, 0.3, and 0.1 T were used to generate the isothermal remanent magnetization (IRM) components. The samples were then demagnetized using 15 thermal steps from 50° to 650°C (Fig. F29). Greigite was determined to be the main magnetic carrier in IZ 1, identified by a saturation isothermal remanent magnetization (sIRM) of 300 mT and an unblocking temperature (T_{ub}) of ~400°C. IZ 2 is believed to contain both greigite and magnetite, as indicated by a smooth IRM acquisition curve that reaches an sIRM value of ~200 and 800 mT, and the identification of two T_{ub} values of ~600°C. Low-intensity values in this zone indicate that greigite is probably the dominant carrier of magnetism. IZs 3 and 4 are determined to contain magnetite as indicated by the T_{ub} values of 500°–600°C and a narrow sIRM curve point of 300 mT. Similar IRM curves that slightly increase up to ~800 mT were observed for both IZs 3 and 4, indicating that a small amount of greigite is also present, although the high intensities of IZs 3 and 4 suggest that magnetite is probably the dominant magnetic carrier.

F26. Paleomagnetic inclination, declination, and intensity, Hole 1174A, p. 63.

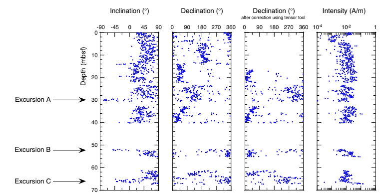

F27. Zijderveld diagrams of excursions, Hole 1174A, p. 64.

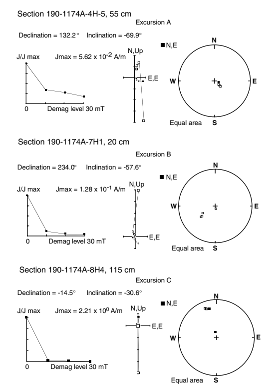

F28. Magnetic intensity zones, Sites 1174 and 1173, p. 65.

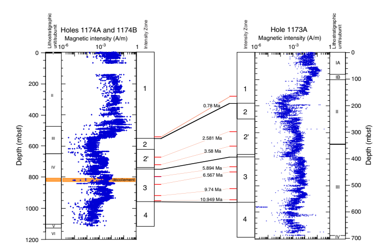

F29. Rock-magnetic experiments, Hole 1174B, p. 66.

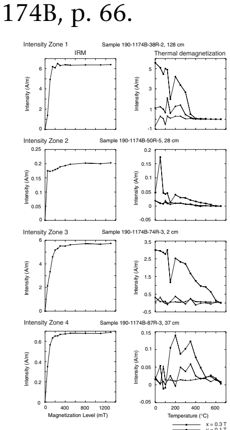

Magnetostratigraphy

Site 1174 magnetostratigraphy is based on polarity changes determined by measuring the inclination of the archive half of the core after AF demagnetization at 30 mT. Many middle Miocene to Pleistocene magnetic polarity records were identified using biostratigraphic datums (calcareous nannofossils; see **"Biostratigraphy,"** p. 14) and correlated to the GPTS of Cande and Kent (1995) (Fig. **F30**). The identified chrons and subchrons are given in Table **T13.**

F30. Magnetostratigraphy, p. 67.

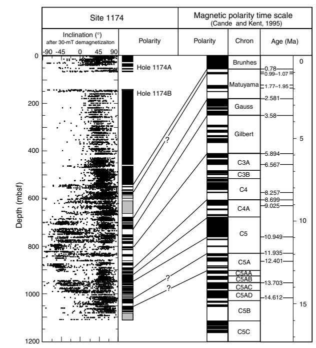

A magnetic polarity change from normal to reversed at 544.7 mbsf (Section 190-1174B-42R-7, 25 cm) is interpreted as the Brunhes/Matuyama Chron boundary dated at 0.78 Ma (Cande and Kent, 1995). The Matuyama Chron (0.780–2.581 Ma) is interpreted to occur at 543.15–685.95 mbsf (Section 190-1174B-57R-6, 15 cm). Although this section of the hole is characterized by a predominantly reversed polarity, only a few normal events are identifiable during the Matuyama Chron (see **"Hole 1174B,"** p. 18).

T13. Depths and ages of magnetic chrons and subchrons, p. 132.

The Gauss Chron (2.581–3.58 Ma), interpreted to occur at 685.95–727.85 mbsf (Section 190-1174B-62R-1, 135 cm), is characterized by a change to a predominantly normal polarity. The magnetic polarity change at 727.85–802.12 mbsf (Section 190-1174B-69R-7, 75 cm) is interpreted as the Gilbert Chron. The termination of the Gilbert Chron and the beginning of Chron C3 is identified at 802.12 mbsf (Section 190-1174B-69R-7, 75 cm). The polarity boundary at 890.15 mbsf (Section 190-1174B-79R-1, 85 cm) is interpreted as the beginning of Chron C4A. A normal polarity inclination interval observed from 901.40 (Section 190-1174B-80R-2, 90 cm) to 947.15 mbsf (Section 85R-1, 5 cm) is identified as Chron C5n.

Sedimentation Rates

Comparison of the magnetostratigraphy and biostratigraphy is shown in Figure **F31.** A marked change of sedimentation rate from 69.83 to 4.07 cm/k.y. occurs at 544.7 mbsf (~1 Ma) within the upper Shikoku Basin facies. A second change from 4.07 to 3.53 cm/k.y. occurs at 793.92 mbsf within the lower Shikoku Basin facies (Fig. **F31**).

F31. Age-depth plot, p. 68.

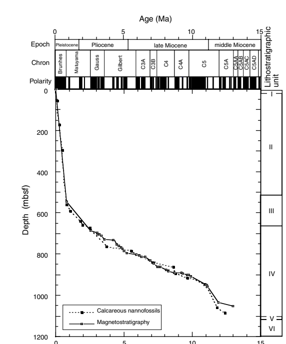

Comparison of Site 1174 to Site 1173

Clear geomagnetic records were identified at both Sites 1173 and 1174. Clearly definable chron boundaries include the Brunhes/Matuyama (0.78 Ma) and Matuyama/Gauss (2.581 Ma). The Gauss/Gilbert (3.58 Ma) and Chron C4/C5 (9.74 Ma) boundaries were also identified but were not as clearly defined.

Correlation between Sites 1173 and 1174 was also performed using zones and peaks of high and low intensity. The first distinct low-intensity peak at 578.49 mbsf in Hole 1174B is correlated to a low-intensity peak at 179.29 mbsf in Hole 1173A (Section 190-1173A-20H-1, 115 cm) in the upper part of lithostratigraphic Unit II (Fig. **F32**). The top of another low-intensity peak at 763.19 mbsf can be correlated to 391.99 mbsf in Hole 1173A (Section 190-1173A-42X-3, 15 cm). Therefore, sediments in the upper part of Site 1174 (lithostratigraphic Unit I to the top of Unit III) correspond to the upper part of lithostratigraphic Unit II in Hole 1173A.

F32. Magnetic polarity reversals at Sites 1173, 1174, and 808, p. 69.

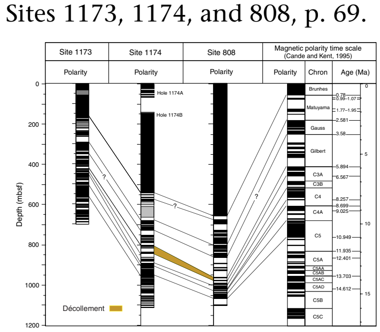

This comparison of magnetic intensity peaks, zones, and magnetostratigraphic results suggests that the upper part of Hole 1174A, consisting mainly of trench turbidites of the Nankai Trough, is about three times thicker than the equivalent sediments in Hole 1173A. In contrast, the thickness of the upper and lower Shikoku Basin facies is similar to that of Hole 1173A.

Comparison of Site 1174 to Site 808

The relationship between Site 1174 and Site 808 previously drilled during Leg 131 (Taira, Hill, Firth, et al., 1991) can be clarified by magnetostratigraphy (Fig. **F32**). At both sites a very long normal polarity interval identified as the Brunhes Chron was observed in the trench turbidites.

Site 1174 magnetostratigraphy around the décollement shows the décollement occurring within time-equivalent sedimentary horizons from 5.894 to 6.567 Ma (Chron C3An). The magnetostratigraphic comparison of Sites 1174 and 808 suggests that the décollement zone at both sites represents the same horizon.

INORGANIC GEOCHEMISTRY

From Holes 1174A and 1174BA, 127 interstitial water samples were squeezed from selected 10- to 50-cm-long whole-round samples for chemical and isotopic analyses. Sample depths ranged from 1.4 to 66.5 mbsf at Hole 1174A and from 150 to 1110.25 mbsf at Hole 1174B. Samples were collected from every section in Cores 190-1174A-1H and 2H, from three sections per core in Cores 190-1174A-3H and 4H, from two sections in Core 190-1174A-5H, and from every section in the remaining cores from Hole 1174A. From Hole 1174B, one section per core was sampled, except for Cores 190-1174B-71R and 72R, from which two sections were sampled, and Cores 30R, 48R, 58R, 63R, and 65R, which were not sampled because of either recovery problems or the need to squeeze a previously collected sample for a longer time in order to recover adequate volumes of pore fluid. Pore fluids from the four largest 50-cm whole rounds collected from Hole 1174B (Cores 190-1174B-23R, 34R, 43R, and 78R) were subsampled for interstitial water and He isotope analyses.

Elemental concentrations are reported in Table **T14** and plotted in Figure **F33.** For large samples, nine major and minor dissolved anions and cations that sensitively reflect microbially mediated or inorganic water-rock (sediment and oceanic basement) reactions were determined. The former include alkalinity, sulfate, and ammonium, and the latter are Cl, Ca, Mg, Na, K, and Si. On smaller samples, a subset of these elements was determined, depending on the quantity of fluid recovered. Salinity and pH were also measured.

The main characteristics of the interstitial water concentration-depth profiles at Site 1174 are similar to those at Site 808 (Leg 131). Compared to Site 1173, microbially mediated reactions at Site 1174 are more intense and are significant to greater depths. The sulfate reduction is complete by 4 mbsf at Site 1174, and peak ammonium concentrations at Site 1174 are approximately twice those at Site 1173, centered at 200 mbsf as compared to 50 mbsf. There are major changes in chemical gradients associated with both lithostratigraphic boundaries (Units II and III, the trench wedge, and Shikoku Basin facies) and subtle changes associated with tectonic features (protothrust and décollement). At the depth that corresponds to the protothrust intersection and Unit II/III

T14. Pore fluid composition, p. 133.

F33. Interstitial fluid composition as a function of depth, p. 70.

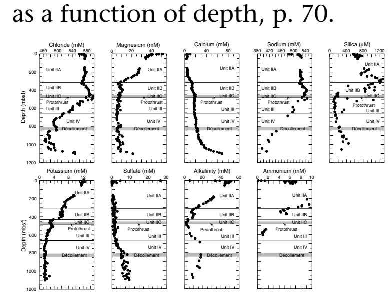

boundary, there are significant excursions, most distinctly exhibited in the Cl and Si concentrations, that may indicate hydrologic activity. A high-resolution record of pore fluid chemistry was recovered across and within the Nankai Trough décollement for the first time. The chemical changes across the décollement are subtle despite significant changes in physical properties there. Steep concentration gradients, particularly in Cl, Na, and Ca, are observed in the deepest ~50 m of the site, between 1060 and 1110 mbsf, caused by either diagenetic reactions involving hydration in the basal volcaniclastic section or by diffusional communication with an upper basement fluid flow system.

Geochemistry Controlled by Inorganic Reactions

Chloride

Cl concentrations were all determined in duplicate resulting in a relative analytical uncertainty of 0.1%. Concentrations increase from slightly greater than bottom water concentrations (558.5 mM) to 577 mM (a 3.3% increase) at a depth of 21 mbsf. This trend is most likely due to the diffusion of lower chlorinity interglacial water into the sediments and the hydration of volcanic ash. Concentrations then decrease to a minimum value, 566 mM, at the Subunit IIA/IIB lithostratigraphic boundary (~337 mbsf) (see **"Lithostratigraphy,"** p. 7). Between 337 and 468 mbsf, concentrations increase to 597 mM, where there is both a sharp reversal in the overall gradient and localized concentration spikes. It is unclear from the data whether the reversal corresponds to the Unit II/III lithostratigraphic boundary (483.2 mbsf) or to the protothrust intersection (~470 ± 5 mbsf). This gradient reversal and the localized spikes could be maintained by any combination of (1) ongoing dehydration reactions in compositionally distinct layers, (2) sustained flow of freshened fluid from depth, or (3) episodic flow of freshened fluids from depth. Below ~500 mbsf, concentrations smoothly decrease for ~230 m, consistent with this interval being dominated by diffusive transport. Assuming one-dimensional vertical diffusion, an average porosity of ~45%, a formation factor of 10 (see **"Physical Properties,"** p. 29), and molecular diffusion of 5.74×10^{-5} cm^2/s corrected for an in situ temperature of ~90°C, it would take on the order of 650 k.y. to establish this diffusion profile.

Within the décollement (808–840 mbsf) (see **"Structural Geology,"** p. 10), there is a local Cl maximum (496 mM). Cl concentrations smoothly increase to the maximum value for ~50 m above the upper boundary of the décollement. In contrast, at the lower boundary of the décollement, there is a very sharp decrease of ~10 mM over 10 m. The cause of the Cl maximum in the décollement is as yet unclear.

At greater depth, there is a low-Cl zone in the 200 m interval below the décollement, with minimum concentrations that are ~17% diluted relative to seawater. The Cl minimum is found at an almost identical distance below the décollement at adjacent Site 808. Note, however, that the dilution is ~21% at Site 808, whereas at the reference Site 1173A it is considerably less, close to 9%. Below the Cl minimum, in a 100-m interval (~950 to 1050 mbsf), concentrations slightly increase with depth, with minor discontinuities superimposed on the general gradient. In the lowermost ~100 m of the underthrust section, Cl concentrations increase monotonically, approaching seawater concentrations at 1110 mbsf. Hydration reactions in the lower volcaniclastic or an underlying upper basement fluid flow system may be responsible for the increase in the Cl concentrations.

Sodium

Na concentrations increase from a near-seawater value to a broad maximum, an 8.5% increase, between ~30 and 300 mbsf. This increase is due to a combination of processes: diffusion of low-salinity interglacial water, ion exchange driven by ammonium production, and ash alteration. Except for the discontinuity at the depth of the protothrust (between ~450 mbsf and basement), concentrations decrease, generally following the Cl trend, except in the deepest samples, where Na does not follow the Cl increase, indicating the uptake of Na into the basement.

Potassium

K concentrations decrease smoothly from slightly greater than seawater concentrations to approximately half seawater concentrations at 414 mbsf, where there is a sharp discontinuity associated with the Subunit IIB/IIC boundary. Concentrations decrease by ~30% in 16 m. This is a large decrease, especially in the depth interval of high ammonium concentrations, where K is being expelled by ammonium into the pore fluid from clay ion exchange sites. This decrease suggests that K is being incorporated into authigenic zeolite. Below this depth, concentrations asymptotically approach a nearly constant value of ~1.5 mM.

The higher than seawater concentrations are caused by K expulsion from clay mineral ion exchange sites, partial dissolution of volcanic ash, and slightly elevated concentrations in the glacial ocean. The nearly constant concentrations at depth are consistent with equilibrium control by potassium-containing silicate phase, primarily K zeolites.

Silica

Dissolved Si concentrations increase from ~600 to 1250 mM between 275 and 315 mbsf, corresponding to the Subunit IIA/IIB boundary. There is a small decrease to ~1000 µM at the Subunit IIB/IIC boundary, across which concentrations drop to ~200 µM. Below this depth, concentrations generally increase, approximately doubling by 1050 mbsf. This general trend is interrupted by a few discrete maxima that correspond to velocity maxima (see **"Physical Properties,"** p. 29) that are most likely caused by diagenetic reactions associated with ash layers, leading to some cementation. Thus throughout the section, the Si concentration-depth profile reflects the varying dominant silicate diagenetic reactions. The key reaction in Subunits IIB and IIC is the dissolution of siliceous biogenic material that rapidly diminishes in abundance and eventually disappears at the base of Subunit IIC (see **"Biostratigraphy,"** p. 14). This is consistent with a shift in grain density at the Unit II/III boundary (see **"Physical Properties,"** p. 29). In Unit III and through the décollement in Unit IV, the control seems to be quartz solubility, and the few maxima are most likely related to ash alteration. Diagenesis of the basal silicoclastics is responsible for the doubling of the silica concentrations below the décollement.

Magnesium and Calcium

Mg concentrations generally decrease with depth, whereas calcium concentrations generally increase. There are, however, significant changes in their concentration gradients that indicate the occurrence of a variety of distinct reactions. Mg and Ca concentrations decrease sharply in the uppermost 50 m. This decrease may be due to the formation of dolomite. Mg concentrations then decrease to a minimum at the Subunit IIA/IIB boundary depth. At greater depth, Mg concentrations only vary within a narrow range. There appears to be an increase in Mg in the two deepest samples, but this may be an artifact of the high Ca concentrations on the Mg determination.

Ca concentrations increase smoothly below the shallow minimum until ~50 m above the Subunit IIA/IIB boundary. At this depth, concentrations increase up to the boundary. There is another sharp increase at the Subunit IIB/IIC boundary. Below this they are relatively constant through the décollement. Below the décollement, concentrations increase, indicating a possible source of Ca from the volcaniclastic section and/or oceanic basement.

Geochemistry Controlled by Microbially Mediated Reactions

Sulfate

Sulfate concentrations decrease extremely rapidly with depth and reach zero in Core 190-1174A-1H between 2.9 and 4.4 mbsf. Because of the very few data points available for this narrow sulfate reduction zone, it is difficult to distinguish between reduction resulting from local organic matter oxidation and reduction resulting from methane oxidation at the bottom of this zone. From 4 to ~640 mbsf, close to the base of Unit III, the sulfate concentrations vary between 0 and 1.5 mM. Most of these very low concentrations are probably related to small amounts of postsampling sulfide oxidation. Dissolved sulfate concentrations increase with depth in the lower Shikoku Basin section, reaching 8–10 mM below the depth interval of the Cl minimum and remaining constant to the bottom of the section. The same pattern of sulfate reappearance below the sulfate reduction zone has been documented at the reference Site 1173 and at Site 808. At Site 1173, the reappearance is found at ~240 mbsf, whereas at this site it is found at ~660 mbsf, 400 m deeper. Interestingly, the décollement is also ~400 m deeper than the proto-décollement at the reference site. At Site 808, as at this site, sulfate reappears at ~140 m above the décollement. The presence of dissolved sulfate at such great burial depths and at temperatures that range from being within the limits of biological activity to those that are above this limit may have important consequences for microbiology. The systematics of the sulfate distributions at these sites may reflect a dynamic relationship between sedimentation rates, temperature, and microbial sulfate reduction rates.

Ammonium

An ammonium concentration maximum of ~7 mM is found at ~13.6 mbsf; at Site 1173 it is at twice this depth. In Hole 1174B, ammonium concentrations continue to increase to 12.4 mM at ~170 mbsf. It is produced by the microbially mediated decomposition of organic matter. At such high concentrations, ammonium occupies clay ion exchange sites, expelling K and Mg into the pore fluid. Concentrations then decrease to <1 mM at ~600 mbsf. The deeper samples at Site 1174 were not analyzed for ammonium because of the very small recovery of pore fluids from the whole-round core samples. The deep sink for ammonium is as yet unidentified.

Alkalinity

Alkalinity has a concentration maximum of 50 mM at ~6 mbsf in Hole 1174A. Its production is primarily driven by the microbial decomposition of organic matter. Alkalinity decreases monotonically to ~7 mM at 353 mbsf. At the depths of Ca and Mg concentration maxima, alkalinity concentrations sharply decrease, indicating authigenic carbonate (most likely dolomite) precipitation. At the alkalinity minimum, however, Mg decreases but Ca increases, suggesting either dolomitization of a precursor Ca carbonate or the flow of a low-alkalinity, low-Mg, high-Ca fluid. The latter is supported by the minimum Cl concentration at this same depth. The second and strongest minimum in alkalinity, 2.3 mM, is at the approximate depth of the protothrust and the Unit II/III boundary. The increase in alkalinity in Unit III toward the décollement is unusual and may be related to the increase in sulfate at this depth interval. The decrease in alkalinity below the décollement is caused by carbonate precipitation in this volcaniclastic high-Ca zone at the base of the section and/or in the upper basement.

Summary

In summary, the highly modified seawater pore fluid chemistry indicates that at this site fluid flow may occur or may have occurred in the recent past at three horizons: at the boundary between Subunits IIA and IIB, along the protothrust, and below the décollement. The basic shipboard geochemical analyses indicate similar pore water characteristics at all three depths: mostly $CaCl_2$-type fluid, depleted in Cl, Na, Mg, alkalinity, and, possibly, K and enriched in Ca and Si relative to seawater. Additional shore-based geochemical analyses, mineralogical analyses, and hydrologic studies will be important in distinguishing between in situ pore-water modification, advection of modified fluids from greater depth, and some combination of the two. Furthermore, both carbonate and silicate diagenesis are widespread in a hierarchy of reactions, which may affect some of the measured physical properties. Microbially mediated reactions are most intense in the top 200 m of the section. The products are involved in some of the diagenetic reactions mentioned above.

Because this site is situated along a transect between the arcward Site 808 and the reference Site 1173, it plays an important role in understanding the evolution of the geodynamics, hydrogeology, and geochemistry of this subduction zone.

ORGANIC GEOCHEMISTRY

At Site 1174, real-time monitoring of volatile hydrocarbons was carried out for safety reasons and organic, petrological, and geochemical studies were conducted to (1) determine the amount and type of organic matter preserved in the sediments; (2) characterize the light hydrocarbons generated by biogenic, thermogenic, and categenic processes; and (3) further relate hydrocarbon distributions to the thermal evolution and structural properties of the Nankai accretionary prism.

Eight sediment samples and two vacutainer samples were collected from Hole 1174A from 1.35 to 65.13 mbsf, and 102 sediment samples were collected from Hole 1174B (~10-m intervals) from 148.63 to 1110.25 mbsf. All sediments were analyzed for methane concentration and light hydrocarbon composition during headspace analyses (Fig. **F34;** Table **T15**). In addition, molecular gas composition, total carbon, and inorganic carbon (carbonate) analyses were performed, and carbon/nitrogen (C/N) ratios were determined (Fig. **F35;** Table **T16**).

The total carbon content for the sediment samples examined is relatively low, ranging from 0.03 to 1.6 wt% and averaging 0.74 wt% (Fig. **F35A**). The highest carbon values are found in the upper 171 mbsf (0.8–1.6 wt% at 171.33 mbsf), followed by a decrease in carbon content (0.8–4 wt%) between 350 mbsf and just below the décollement at 807.60 mbsf. Carbon contents slightly increase between 1000 and 1100 mbsf and then drop abruptly to 0.2 wt% at greater depth. Variations in the carbon content (Fig. **F35A**) are correlated with changes in lithostratigraphy. For example, a steady decrease in the amount of carbon was observed in the transition from the upper to lower Shikoku Basin facies and continues to the décollement. Below the décollement, higher carbon values are observed (0.50–0.85 wt%) in some thin layers that also coincide with an increase in ethane and propane hydrocarbons (Fig. **F34B, F34C**). The inorganic carbon (carbonate) concentrations are generally low (average = ~5 wt%) with several maxima of >40 wt% below ~900 mbsf (Fig. **F35C**). High concentrations of carbonate nodules were seen in some calcareous claystones (~700 mbsf) in the lower Shikoku Basin section (also observed in sediments of Hole 1173A).

Nitrogen contents of the sediments are also low (~0.1 wt%) with one minimum dropping to zero at ~1020 mbsf (Fig. **F35B**). The C/N ratios are consistent with a marine origin. At Site 808 (Leg 131), however, the upper Shikoku Basin sediments likely contain a significant terrigenous component as a result of the flux of terrestrial organic matter to these sediments (Berner and Faber, 1993). At greater depths the ratios drop abruptly (<5), consistent with carbon loss due to thermogenic or catagenic C_2 and C_3 hydrocarbon generation. As at Site 808, the generation of light hydrocarbons is relatively low (10–70 ppm) and is attributed to the low TOC and very high temperatures (up to 120°C) (see **"In Situ Temperature and Pressure Measurements,"** p. 34), which is in the range of categenic or "thermal cracking" of organic matter (Tissot and Welte, 1984).

Hydrocarbon Gases

Headspace gas concentrations of methane in Hole 1174A are low (~2.5 ppm) in the first core (1.5 mbsf) within the sulfate reduction zone (Fig. **F34A**). However, a significant increase in methane concentrations is observed just below this zone (~20,000 ppm in sediment samples and 940,000 ppm in vacutainer samples) in the first 65 mbsf of Hole 1174A. Methane concentrations are also high from 300 to 550 mbsf in Hole 1174B (up to ~40,000 ppm). As was observed at Site 808 and in other previous legs, an increase in methane in sediments below the sulfate reduction zone is indicative of bacterial origin (Claypool and Kvenvolden, 1983). The presence of small concentrations of methane in the sulfate reduction zone, however, may be due to migration from below.

F34. Molecular compositions and concentrations of headspace gases, p. 71.

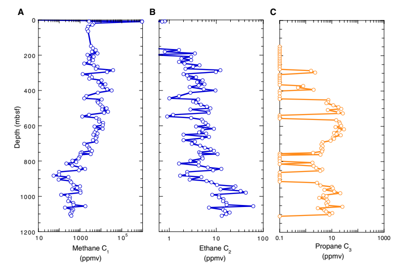

T15. Headspace and vacutainer gas analyses, Hole 1174, p. 135.

F35. Total carbon and nitrogen contents and the percentage of inorganic carbon in sediments, p. 72.

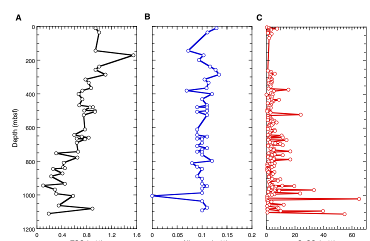

T16. Carbon, nitrogen, sulfur, and hydrogen analyses, Hole 1174, p. 137.

Ethane and propane are also present in sediments below 300 mbsf, with a sharp increase in propane from 550 to 700 mbsf (10–30 ppm). The atypical predominance of propane over ethane suggests that fermenting bacteria are preferentially utilizing ethane to produce acetate and H_2 (King and Blackburn, 1998), whereas propane remains unaffected (see **"Microbiology,"** p. 27, for microbial counts in these sediments). Interestingly, the ratios of ethane to propane in sediments at Site 808 show the same trend. The concentrations of ethane and propane in both Sites 1174 and 808 are proportional at depth and consistent with sediments of higher maturity.

The Bernard gas ratio $C_1/(C_2+C_3)$ shows that the hydrocarbons above ~900 mbsf are mixtures of biogenic and thermogenic components (Fig. **F36**). At depths >900 mbsf, the activity of methane-producing archae bacteria has ceased and only thermogenic hydrocarbons are present. Two hydrocarbon mixing zones (biogenic and thermogenic) are observed between 400 and 900 mbsf (Fig. **F36**). The increase in $C_1/(C_2+C_3)$ ratios below 900 mbsf may suggest that at this depth cracking of longer chain and less thermally stable hydrocarbons occurs rather than in situ thermal generation of these components. The higher concentrations of propane observed in the upper zone, where maturities of organic matter and temperatures are lower, implicitly suggests that these hydrocarbons were migrated from deeper sections of the accretionary prism. A previously proposed interpretation is that hot fluids moving along the décollement caused extensive heating and cracking of kerogenous organic matter, generating light hydrocarbons that may slowly leak out of the décollement, (Taira et al., 1991). The shipboard geochemical data for Site 1174, however, indicate that there is presently no active advection of light hydrocarbons occurring along the protothrust or the décollement.

F36. Ratio of $C_1/(C_2+C_3)$ with increasing depth and present-day temperature, p. 73.

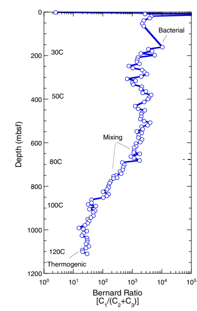

A Reexamination of Migration

One of the more interesting results from the organic geochemistry shipboard measurements for Site 1174 is the distribution of hydrocarbons within discrete sedimentary zones, suggestive of migration along the frontal and protothrusts, to stratigraphically or structurally controlled areas within the prism. Although it is difficult to reconcile the containment of light hydrocarbons such as methane, the presence of propane and higher hydrocarbons in the trench to basin transition facies and the upper Shikoku Basin strongly suggests that the physical properties of the accretionary prism are influencing the distributions of these components.

A reassessment of the organic geochemical data for Site 808 also revealed some striking similarities to Site 1174 in the distributions of hydrocarbons. As stated earlier in the hydrocarbon section, both propane and ethane show identical profiles in sediments above and below the décollement (Berner and Faber, 1993). A predominance of propane over ethane (Fig. **F34**) is unusual and was first interpreted by Berner and Faber (1993) as evidence for fluid migration along the frontal thrust from below the décollement. The lack of supportive data for vertical fluid movement in the pore-water chemistry, however, led to a reassessment of these findings (Kastner et al., 1993) and the suggestion that both ethane and propane formed from isotopically different precursor kerogens (terrigenous vs. marine) in situ at low temperature (Taira et al., 1991).

In a more detailed study of the origin of light hydrocarbons at Site 808, carbon isotopic ratios for propane in gas samples collected from the frontal thrust showed similar values to those measured below the décollement (Berner and Faber, 1993). These data are the first indication that hydrocarbons from beneath the décollement are indeed related to those at shallower depth and that migration of fluids along the frontal thrust has occurred (Berner and Faber, 1993). The observation of the same high ratios of propane over ethane in the sediments at Site 1174, coupled with the isotope data for Site 808, strengthens the evidence for migration. Future investigations of the nature of the organic matter in sediments collected at Site 1174 will allow for a more detailed assessment of the organic matter and the biological and physical properties that are found within the Nankai accretionary prism.

Conclusions

Organic geochemical analysis at Site 1174 leads to the following conclusions:

1. At Site 1174 the total carbon content decreases with depth (1.6–0.3 wt%; average = ~0.37) as indicated by the values throughout the hole.
2. C/N ratios indicate that marine organic matter is abundant in all of the sediment samples.
3. The low sulfate and high methane concentrations in the upper section below the sulfate reduction zone are consistent with a bacterial origin. At depths >900 mbsf, the activity of methane-producing archae bacteria has ceased and only thermogenic hydrocarbons are present.
4. The Bernard gas ratio $C_1/(C_2+C_3)$ shows that the hydrocarbons above ~900 mbsf are mixtures of biogenic and thermogenic components. Below 900 mbsf, cracking of longer chain and thermally less stable hydrocarbons occurs rather than thermal generation of these components.
5. Geochemical data indicate that the flux of hydrocarbons is presently negligible across the décollement.
6. The organic matter and hydrocarbon geochemical data from Site 808 are in agreement with those from Site 1174. This suggests that lighter hydrocarbons migrated from deeper sediments of a higher maturity into shallower, more immature sediments (450 and 650 mbsf) through the frontal and protothrusts.

MICROBIOLOGY

Thirty-seven samples for microbiological analysis were obtained from Holes 1174A and 1174B for direct microscopic enumeration on board ship. Fourteen whole-round cores were taken for shipboard enrichment cultures at in situ temperature and pressure, cell viability, and shore-based microbiological analysis to measure potential bacterial activities, culture microorganisms, characterize nucleic acids, and investigate fatty acid biomarkers.

Total Bacterial Enumeration

Bacteria are present in 24 of the 37 samples examined (Table T17; Fig. F37). The near-surface sample (Sample 190-1174A-1H-2, 99–100 cm) contains 1.47 × 10^8 cells/cm^3, which follows a trend observed at other ODP sites where near-surface bacterial populations decrease as overlying water depths increase (Table T18).

The deepest sample in which bacteria were observed is at 796.5 mbsf (Sample 190-1174B-69R-3, 105–106 cm) with 7.95 × 10^5 cells/cm^3, some 0.5% of the near-surface population. Prior to this depth, however, cells are not present at 578 mbsf (Sample 190-1174B-46R-4, 119–120 cm) or in five samples between 623.5 and 743.6 mbsf (Samples 190-1174B-51R-2, 149–150 cm, to 63R-5, 149–150 cm). Below 796.5 mbsf to the deepest sample at 1091.3 mbsf (Sample 190-1174B-100R-1, 11–12 cm), no bacterial cells were detected (detection limit = 6 × 10^4 cells/cm^3).

The depth distribution of total bacterial numbers in sediments from Site 1174 conforms to the general model for bacterial populations in deep-sea sediments (Parkes et al., 1994) from the surface to ~290 mbsf (Fig. F37). Two significantly low populations are found at 26.2 and 66.5 mbsf (Samples 190-1174A-4H-2, 139–140 cm, and 8H-4, 134–135 cm), and these are both samples with substantial proportions of sand. Below 370 mbsf, rising temperatures affect interpretation of the data. The temperature at 370 mbsf was ~45°–50°C (see **"In Situ Temperature and Pressure Measurements,"** p. 34), which is the boundary between mesophilic (medium temperature) and thermophilic (high temperature) bacteria. From this depth downward, bacterial population sizes decrease to zero by 575 mbsf. There is one further occurrence of bacteria (4.76 × 10^4 cells/cm^3) at 598.5 mbsf (Sample 190-1174B-48R-5, 104–105 cm) before 690 mbsf. At this depth the temperature is estimated to be 80°C, which represents the microbiological boundary where hyperthermophilic bacteria are found. There are two occurrences of bacterial populations within this zone, at 778.6 and 796.5 mbsf (Samples 190-1174B-67R-4, 120–121 cm, and 190-1174A-69R-3, 105–106 cm). The deepest of these is estimated to be at 90°C. The possibility that these were contaminated samples was examined; however, the large populations enumerated meant that they could not be the result of contamination from either seawater or drilling muds. Additionally, zero counts were obtained from both above and below these intervals, and the counting procedure was checked with blanks to confirm absence of counting procedure errors. No bacteria were detected within the décollement zone (~810–840 mbsf) or at any greater depths, despite temperature not being a limiting factor until ~875 mbsf.

Contamination Tests

Tracer tests were conducted while coring with APC (Core 190-1174A-4H) and RCB (Cores 190-1174B-4R, 5R, 31R, and 32R) at this site. In order to estimate the amount of drilling fluid intrusion into the recovered cores, chemical and particulate tracers were deployed as previously described (Smith et al., 2000).

Chemical Tracer

Perfluoro(methylcyclohexane) was used as the perfluorocarbon tracer (PFT). Calibration of the gas chromatograph (HP 5890) with standard solutions yielded a slope of 9.2 × 10^{11} area units/gram of PFT. The

T17. Total bacterial populations in sediments, p. 141.

F37. Depth and temperature distribution of total bacterial populations, p. 74.

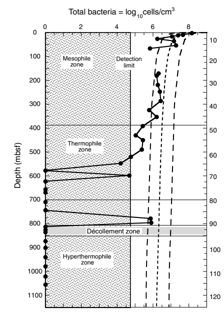

T18. Comparison of near-surface sediment bacterial populations at Site 1174 with data from nine other ODP sites, p. 142.

detection limit for these samples is equivalent to 0.01 µL of drilling fluid. The tracer was detected on the outer edge of each core, indicating a successful delivery (Table T19). Estimates of drilling fluid intrusion in these samples range from below detection to 57.9 µL/g. As expected, the intrusion of drilling fluid into the centers of Cores 190-1174B-4R and 5R (57.9 and 14.3 µL/g, respectively) was substantial. This was due to the use of the RCB in the relatively soft sediment. Visual inspection of the split cores confirmed the disturbance. No PFT was detected in the center samples from Sections 190-1174B-31R-1 and 31R-2. The chemical tracer was found throughout the Core 190-1174B-32R. It is believed that the high values are due to sample handling on the catwalk. Instead of breaking the sections after the core liner is cut, as recommended (Smith et al., 2000), the sections were separated with a knife. It is likely that the tracer was dragged through the core with the blade.

T19. Drilling fluid intrusion estimated based on PFT experiments, p. 143.

Particulate Tracer

Fluorescent microspheres were detected on the outside of four cores (Table T20); the outside sample of one of the eight samples was lost before analysis. The absence of microspheres in the samples from the outside edge of the core suggests problems with the delivery of the microspheres. No microspheres were detected in the interiors of Sections 190-1174B-4H-2, 5R-1, 31R-1, or 32R-1. As with the PFT, microspheres were found throughout Section 190-1174B-4R-1, again confirming the disturbance while coring. Microspheres were not observed in the interior of the other disturbed core (Section 190-1174B-5R-1), but the very low abundance on the outside of this core (13 microspheres/g) may explain this observation. Microspheres in the interiors of Sections 190-1174B-32R-2 and 32R-3 are consistent with the PFT data from these sections.

T20. Fluorescent microsphere tracer experiments, p. 144.

PHYSICAL PROPERTIES

Introduction

At Site 1174, laboratory measurements were made to provide a downhole profile of physical properties at a site within the protothrust zone, landward of reference Site 1173 and seaward of Site 808. With the exception of some extremely short (<50 cm), small diameter (<4 cm), and intensely fractured sections, all cores were initially passed through the MST before splitting. Gamma-ray attentuation (GRA) and magnetic susceptibility measurements were taken at 4-cm intervals with 2-s acquisition times for all cores. Natural gamma ray (NGR) was counted every 30 cm for 30-s intervals. Voids and cracking caused by gas expansion were noted in cores between 0 and 67 mbsf and degraded MST measurements. Biscuiting and reduced core diameter in RCB cores also degraded measurements. Data are not available between 74.1 and 143.70 mbsf because this interval was not cored.

Moisture and density samples were selected from undisturbed core at regularly spaced intervals of at least one per section. Additional samples were taken within the décollement zone. Measurements of dry volume and wet and dry mass were uploaded to the ODP (Janus) database and were used to calculate water content, bulk density, grain density, porosity, void ratio, and dry bulk density. During moisture and density measurements for Hole 1174B, a calibration problem was noted for the pycnometer. After recalibration, a linear correction was applied to samples that had been run with the incorrect calibration. This correction affected Cores 190-1174B-1R through 42R and Section 43R-3. The dry volumes and calculated parameters reported in the database have been updated to incorporate this correction.

P-wave velocities were measured on split cores or discrete samples at a frequency of two to three per core. Measurements were taken in three directions when core conditions permitted. Electrical conductivity measurements were taken at a frequency of two to three per core. Raw data and calculated physical properties are available from the Janus database for all MST, moisture and density, velocity, and thermal conductivity measurements (see the **"Related Leg Data"** contents list). Because electrical conductivity data are not currently available from the Janus database, they are included in Tables **T21** and Table **T22,** respectively.

T21. Formation factors for Hole 1174A by the needle-probe method, p. 145.

T22. Electrical conductivity and formation factor for sample cubes, p. 146.

Density and Porosity

Sediment bulk density was determined by both the GRA method on unsplit cores and the mass/volume method ("index properties") on discrete samples (see **"Physical Properties,"** p. 19, in the "Explanatory Notes" chapter). The GRA density data and the bulk densities determined by the mass/volume method show similar downhole trends, but density values from the two methods are significantly different (Fig. **F38A, F38B**). The GRA density values exhibit considerable scatter at all depths and are generally 0.2 g/cm³ lower than the moisture and density measurements. This may be caused by the small and variable diameter and the biscuited nature of RCB cores.

F38. Bulk density, grain density, and porosity, p. 75.

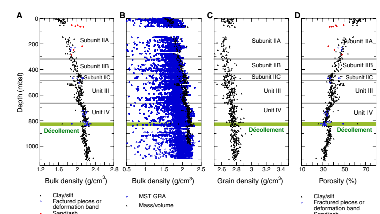

Grain densities determined from dry mass and volume measurements increase from ~2.64 g/cm³ at ~144 mbsf (start of coring in Hole 1174B) to ~2.79 g/cm³ at ~1000 mbsf (Fig. **F38C**). A shift occurs between Units III and IV; the average grain density within Unit III is 2.71 g/cm³, whereas the average for Unit IV is 2.77 g/cm³.

The calculated porosity profile is shown in Figure **F38D.** Porosities from silty clays within lithostratigraphic Unit II (trench-wedge facies) are characterized by a general decrease with depth, from 58%–72% at the seafloor to 36%–42% by 480 mbsf (Fig. **F38D**). Typically, the lower porosity values represent sands and silty sands. Scatter within the silty clay samples may reflect subtle differences in grain size and composition that were not distinguishable in hand specimen. Porosities decrease slightly from ~38% to 35% at the top of Subunit IIC (trench to basin transition facies), and this transitional unit is not readily distinguished from Unit III (upper Shikoku Basin facies) solely on the basis of moisture and density.

With the exception of two zones of scattered, elevated porosities (at 500–550 and 600–650 mbsf), the shipboard data show essentially constant porosity of 35%–42% throughout lithostratigraphic Unit III (upper Shikoku Basin facies; 480–661 mbsf). This is a significant deviation from both normal compaction trends for silty clays (e.g., Hamilton, 1976; Athy, 1930) and the decrease of porosity with depth observed within Units II and IV above and below (Fig. **F38D**).

Porosities drop slightly to 34%–40% at the top of lithostratigraphic Unit IV (lower Shikoku Basin facies; 661 to 1102 mbsf). The change in porosity at the boundary between the upper and lower Shikoku Basin facies is similar to the pattern observed at Site 1173. The correlation between the discontinuity in porosity at ~661 mbsf and the boundary between Units III and IV suggests that the character of porosity change with depth is controlled, at least in part, by lithology. Porosities resume a compaction trend from 661 to 807 mbsf, decreasing to 30%–35% by the top of the décollement zone (807.6–840 mbsf; see **"Structural Geology,"** p. 10). Within the décollement interval, porosity continues this compaction trend but exhibits somewhat greater scatter (perhaps due to increased sampling). Porosity increases sharply to 33%–38% directly below the décollement zone. In the underthrust section (below 840 mbsf), porosities remain relatively constant to 985 mbsf then decrease slightly with depth from 33%–38% at 985 mbrf to 32%–37% at the bottom of the hole. Overall, the rate of porosity decreases with depth is comparable to the porosity decrease with depth in the underthrust sequence (below 965 mbsf) at Site 808 and the age-equivalent sequence (below 390 mbsf) at Site 1173 (Fig. **F39**).

F39. Porosities below the décollement or age-equivalent horizon, p. 76.

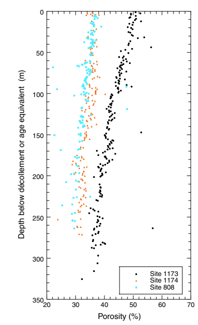

Thermal Conductivity and Projected Temperatures

Thermal conductivity was measured using one of two methods depending on core condition. For shallow, nonindurated samples, a needle probe was inserted into the unsplit core for a full-space conductivity measurement. For samples from below 67 mbsf, insertion of the needle caused fracturing, so a half-space method was used on split cores. Between the mudline and ~815 mbsf, thermal conductivities increase gradually with depth from ~0.74 to 1.8 W/(m·°C) (Fig. **F40A**). Thermal conductivities decrease slightly below the décollement zone at ~840 mbsf, and range from 1.62 to 1.81 W/(m·°C) within the underthrust sediments. The change in thermal conductivity across the décollement zone correlates with the abrupt increase in porosity (Fig. **F38D**). This relationship is expected because the thermal conductivity of sediment grains is higher than that of pore fluid.

Shipboard thermal conductivities and downhole temperature measurements to 65.5 mbsf (see **"In Situ Temperature and Pressure Measurements,"** p. 34) define a near-surface heat flow of 180 mW/m². Using this estimated heat flow and measured thermal conductivities, and assuming steady-state vertical conductive heat flow, projected downhole temperatures reach ~110°C at the top of the décollement zone and ~140° at 1111 mbsf (Fig. **F40B**). These estimates are highly speculative because it is likely that (1) thermal steady-state has not been reached and (2) conductive heat flow is perturbed within the toe of the accretionary complex by fluid flow.

F40. Thermal conductivity and temperature trends, p. 77.

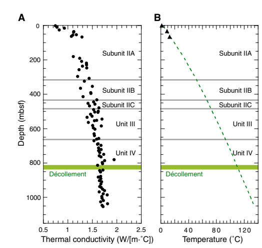

Acoustic Velocity

In APC cores from Hole 1174A, *P*-wave velocities were measured using the *P*-wave sensors 1 and 2 (PWS1 and PWS2) insertion probe system along (z-axis) and across (y-axis) the core axis, respectively. The PWS3 contact probe system was used to measure *P*-wave velocities across the liner (x-axis) (Fig. **F41A**). Because of unfavorable core conditions, measurements in more than one direction could rarely be obtained in the same interval. In RCB cores from Hole 1174B, sample cubes were cut and measurements in all three directions were performed using the PWS3 contact probe system.

The velocity-depth profile at this site displays important deviations from a smooth compaction curve. Between 200 mbsf and the décollement zone, three zones with higher velocities are identified: (1) between 360 and 420 mbsf, near the base of the outer trench wedge (Subunit IIB); (2) ~520 mbsf, near the top of the upper Shikoku Basin facies (Unit III); and (3) ~660 mbsf, across the transition from upper to lower

F41. *P*-wave velocity and bulk density, p. 78.

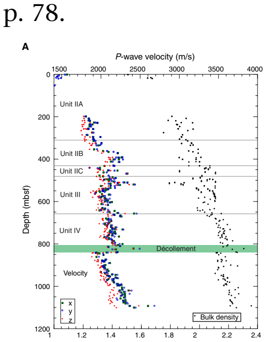

Shikoku Basin facies (Unit III/IV boundary). Of these anomalies, only the deepest one is well defined in Site 808 data, where it is also found at the same Unit III/IV boundary. Surprisingly, the two lower zones correspond to zones of lower, not higher, bulk density (Fig. **F41A**).

This anomalous behavior also appears on the porosity-velocity crossplot (Fig. **F41B**) and suggests cementation. This behavior is similar to the relatively high velocities and high porosities in the upper Shikoku Basin facies at reference Site 1173. The two zones at 520 and 660 mbsf still retain unaltered volcanic glass, and there is a correlation between these two zones in high velocity and high silica content in the pore fluid (see **"Inorganic Geochemistry,"** p. 20). The upper zone of high velocities (360–420 mbsf) is not ash rich, as it lays within the turbidite wedge, but is characterized by a higher than average cristobalite/quartz ratio (see **"Lithostratigraphy,"** p. 7). This observation suggests that (probably biogenic) recrystallization of amorphous silica is taking place in this interval as well. Velocity drops across the décollement zone by ~300 m/s and then increases regularly down to the base of the hole. The velocity decrease across the décollement zone correlates with the increase in porosity over the same interval.

Velocity anisotropy results (Fig. **F41C**) are similar to those obtained at Site 808. In Unit II, anisotropy averages 3% and decreases very slightly with depth. Varying bedding dips in a 100-m-thick zone around the décollement zone and between 400 and 450 mbsf (see **"Structural Geology,"** p. 10) may contribute to scatter of both vertical and horizontal anisotropy. Below the décollement zone, anisotropy increases with depth, reaching ~10% at the base of the hole.

Part of the anisotropy in this shallow part is attributed to the well-developed lamination in some samples, which increased attenuation along the core axis and made measurements along this direction more difficult. Lamination tends to decrease downhole, occurs only as occasional bedding-parallel cracks in samples from Units III and IV, and is absent in the zones of abnormally high velocity around 400, 540, and 660 mbsf. The effect of discrete cracks on the velocity measurements is not obvious.

Electrical Conductivity

Measurements were made on APC cores with a four-needle, 30-kHz electrode array. On RCB cores, conductivity was measured on the same sample cubes used for *P*-wave measurements with a 30-kHz two-electrode system.

Electrical conductivity and formation factor (see **"Physical Properties,"** p. 19, in the "Explanatory Notes" chapter) measured on sample cubes are given in Table **T22.** For the needle-probe measurements, only the apparent formation factor is given. Needle-probe measurements for Hole 1174A yield formation factors mostly between 2.5 and 6 (Fig. **F42A**). As at Site 1173, coarser lithologies, which include silty and sandy turbidites, appear more resistive, and formation factor measured perpendicular to the core axis (x- and y-direction) is lower than that along the core axis. Data acquired in the horizontal plane closely follow the variation in porosity and display reversals of the compaction trend with distinctive decreases of the formation factor at ~520 mbsf, 600–630 mbsf, and across the décollement zone (Fig. **F42B**). Formation factor measured along the z-axis displays stronger variations than the horizontal components at the two upper reversals (Fig. **F42C**). These rever-

F42. Formation factor and anisotropy of electrical conductivity, p. 80.

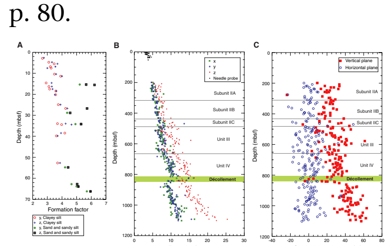

sals correlate with the zones of high porosity and anomalous *P*-wave velocity identified earlier.

Conductivity anisotropy (Fig. **F42C**) is generally higher than at the reference site. Conductivity anisotropy generally increases with depth and appears higher beneath the décollement zone than above. The anomalous high-porosity and high-velocity zones around 520 and 660 mbsf have a lower anisotropy than the formation above and below. Samples from coherent fragments within the décollement zone all have low apparent vertical anisotropy. Variations of bedding dip may not entirely explain this feature as bedding dip is <20° at most of the intervals sampled within the décollement zone (see **"Structural Geology,"** p. 10).

Although conductivity is theoretically less sensitive than *P*-wave velocity to cracks orthogonal to the direction of the measurement, bedding-parallel lamination in the upper part of Hole 1174B appeared to influence conductivity along the core axis. Conductivity along the z-axis increased by 5% or more in laminated samples when a pressure of ~2–3 bars was applied on the sample by pressing the electrode by hand. Measurements along the x- and y-axes were not as pressure sensitive. The conductivity increase from applying the same hand pressure was typically <2% for measurements along the x- and y-axes, as well as for measurements made along the z-axis on samples without lamination. Small gas bubbles were also observed escaping from the larger cracks when pressure was applied. Thus, we suspect that partial desaturation of these cracks contributed to the anomalous increase of conductivity across the cracks in the most laminated samples. This effect can probably be neglected below 500 mbsf. To limit this effect, measurements below 730 mbsf in Hole 1174B (and at later sites) were made applying a pressure of ~1 bar on the sample with a 10-lb weight.

Magnetic Susceptibility

Volumetric magnetic susceptibilities were measured in all recovered cores from Site 1174 (Fig. **F43**). Uncorrected values of magnetic susceptibility from the Janus database were used. Large magnetic susceptibility values and large scatter between 0 and 280 mbsf are correlated with the occurrence of sand-rich turbidites. Less scatter occurs below 280 mbsf, and susceptibility reaches a minimum between 570 and 640 mbsf. Below 640 mbsf, magnetic susceptibility increases to 820 mbsf. The hemipelagic mudstones between 820 and 950 mbsf are characterized by three peaks of up to 200 × 10^{-5} SI. These peaks can be correlated with magnetic susceptibility peaks at Sites 1173 and 808. Magnetic susceptibility data show a slight decrease from 950 to 1100 mbsf.

F43. Magnetic susceptibility, p. 81.

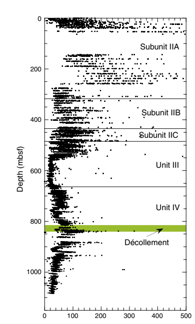

Summary and Discussion

As seen at Site 1173, porosities within the trench-wedge facies (Unit II at Site 1174, Unit I at Site 1173) are characterized by high variability and a general decrease with depth. From the top of Subunit IIC and throughout the upper Shikoku Basin facies, porosities remain nearly constant with depth. These constant porosities deviate from a typical compaction profile for silty clays. The porosities within Unit III at Site 1174 are ~20% less than porosities within this unit at Site 1173 and show considerably smaller deviation from a normal compaction trend than observed at Site 1173. At the boundary between the upper and lower Shikoku Basin facies (Units III and IV), porosity decreases slightly and resumes a trend of gradually decreasing porosity with depth. An increase in porosity across the base of the décollement zone is accompanied by decreases in thermal conductivity, velocity, and formation factor.

The physical properties of sediments drilled at Site 1174 are generally consistent with results from Site 1173 and previous DSDP and ODP sites in the region (Sites 582 and 808). Site 582, located in the Nankai Trough southwest of Site 1174, penetrated the outer trench–wedge and the upper Shikoku Basin facies. Data from Site 582 show the same pattern of decreasing porosity with depth in the trench wedge (Kagami et al., 1986). However, a change in the porosity-depth profile is noted at the top of the upper Shikoku Basin facies at Sites 1173 and 582, whereas a change occurs at the top of the trench to basin transition facies at Site 1174.

Site 808, located ~2 km landward of Site 1174 and ~3 km landward of the deformation front, penetrated the outer trench–wedge and the upper and lower Shikoku Basin facies (Taira, Hill, Firth, et al., 1991). At both Sites 1174 and 808, a slight decrease in porosity was observed at the top of the lower Shikoku Basin facies and porosities increase abruptly across the décollement zone. The porosity increase across the décollement zone at Site 1174 is 2%–4%, whereas the porosity shift at Site 808 is 5%–6%. Porosities within the underthrust sediments at Site 1174 decrease more slowly with depth than at Site 808, reaching 34%–36% at the base of Unit IV, compared to 31%–33% at Site 808 (Fig. F39). This difference in porosity of the underthrust section may reflect progressive compaction and dewatering between the two sites. Alternatively, it may be a consequence of slight variations in initial porosity, cementation, or loading history of the two sites.

IN SITU TEMPERATURE AND PRESSURE MEASUREMENTS

Two reliable determinations of downhole temperatures were made at depths of 32.9 and 65.5 mbsf at Site 1174 using the Adara temperature tool and the Davis-Villinger temperature probe (DVTP). Table T23 summarizes the deployments, and the station data are shown in Figures F44 and F45. A DVTP measurement at 165.5 mbsf was considered unreliable because of a faulty thermistor. A measurement attempt at 209.1 mbsf was not successful because the temperature record indicated invasion of seawater. No deeper penetrations were attempted.

In situ temperatures were estimated by extrapolation of the station data to correct for the frictional heating on penetration using an average thermal conductivity of 1.0 W/(m·°C). The estimated in situ temperatures from the mudline temperature and the two measurements suggest a linear gradient of 0.183°C/m in the upper 65.5 m (Fig. F46). For thermal conductivities of 1.0 W/(m·°C), conductive near-surface heat flow at Hole 1174A would be 183 mW/m². This value is considerably higher than estimated for ODP Site 808, located 3 km arcward (130 mW/m²; Taira et al., 1991). However, seafloor heat flow data show considerable variability near the deformation front (Yamano et al., 1992).

Assuming purely vertical conductive and steady state heat flow, in situ temperatures of ~140°C are projected at the bottom of the hole (see "Physical Properties," p. 29). However, because this site is located near the deformation front, it may have experienced input of warm fluids or

T23. Summary of downhole temperature measurements, Hole 1174A, p. 149.

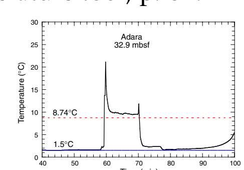

F44. Temperatures measured during the deployment of the Adara temperature tool, p. 82.

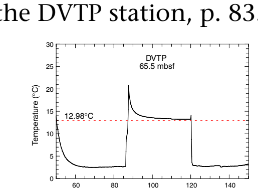

F45. Temperatures measured during the DVTP station, p. 83.

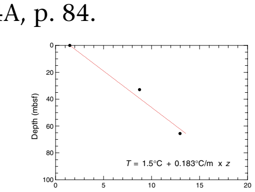

F46. Measured temperatures, Hole 1174A, p. 84.

faulting that would render this assumption invalid. Because both influx of warm fluids and thrust faulting would cause near-surface heat-flow measurements to overestimate heat flow from basement, 140°C should be considered a maximum value.

Pressures were also recorded during a DVTP-P deployment at 65.5 msbf (Fig. F47). As noted in "In Situ Temperature and Pressure Measurements," p. 26, in the "Explanatory Notes" chapter, postcruise modeling and processing is required to estimate in situ pressures, but preliminary interpretation of the raw data indicates a near-hydrostatic pressure, which is not unexpected at this relatively shallow depth.

F47. Pressures measured during the DVTP-P station, p. 85.

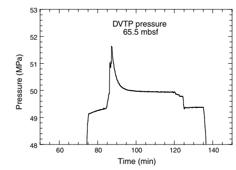

SEISMIC STRATIGRAPHY

Reflections on three-dimensional (3-D) seismic line 281 can be correlated with lithostratigraphic boundaries at Site 1174 (Fig. F48). Specific correlations should be considered preliminary at this time because the velocity structure at this site is not well known. Any inaccuracies in velocity will produce errors in depth conversion. Additional velocity work will be carried out postcruise to improve depth conversions and stratigraphic correlations.

F48. Three-dimensional seismic reflection line 281 across Site 1174, p. 86.

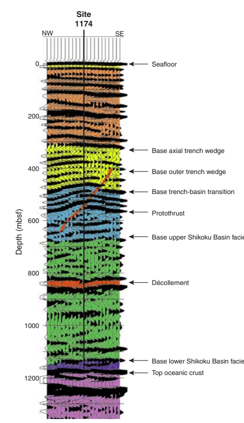

Unit I (slope-apron facies) is a very thin interval (<10 mbsf) just below the seafloor reflection. The axial trench–wedge facies (Unit II) extends to the strong reflection just below 300 mbsf (core depth of 314.55 mbsf) and is characterized by high-amplitude, laterally continuous reflections. Subunits IIB and IIC (outer trench–wedge facies and trench to basin transition facies) cannot be easily distinguished in the seismic data as there is not a distinct change in reflection character between them. The base of Subunit IIC is the top of a strong reflection representing the top of Unit III (upper Shikoku Basin facies) at ~485 mbsf. Unit III consists of a series of three strong reflections that are offset by a protothrust at ~540 mbsf at Site 1174. Note that the depth of the seismically defined protothrust does not match the depth of the thrust identified in the cores between 467.10 and 469.95 mbsf, possibly due to either a mismatch between navigation from the 1999 3-D seismic cruise and Leg 190 or incorrect velocities. The lower part of this unit has less distinct reflections. The transition between Units III and IV (lower Shikoku Basin facies) is marked by the last laterally continuous reflection at ~660 mbsf. Unit IV is characterized by indistinct, noncontinuous reflections in the upper part and stronger, more continuous reflections in its lower part. The structurally defined décollement is represented by a strong negative-polarity reflection at ~820–860 mbsf. Unit V (volcaniclastic facies) is represented by an indistinct reflection at ~1120 mbsf that overlies the strong basement reflection at ~1170 mbsf.

REFERENCES

Athy, L.F., 1930. Density, porosity, and compaction of sedimentary rocks. *AAPG Bull.,* 14:1–24.

Berner, U., and Faber, E., 1993. Light hydrocarbons in sediments of the Nankai Accretionary Prism (Leg 131, Site 808). *In* Hill, I.A., Taira, A., Firth, J.V., et al., *Proc. ODP, Sci. Results,* 131: College Station, TX (Ocean Drilling Program), 185–195.

Blöchl, E., Rachel, R., Burggraf, S., Hafenbradl, D., Jannasch, H.W., and Stetter, K.O., 1997. *Pyrolobus fumarii,* gen. and sp. nov., represents a novel group of archaea, extending the upper temperature limit for life to 113°C. *Extremophiles,* 1:14–21.

Cande, S.C., and Kent, D.V., 1995. Revised calibration of the geomagnetic polarity timescale for the Late Cretaceous and Cenozoic. *J. Geophys. Res.,* 100:6093–6095.

Claypool, G.E., and Kvenvolden, K.A., 1983. Methane and other hydrocarbon gases in marine sediment. *Annu. Rev. Earth Planet. Sci.,* 11:299–327.

Gartner, S., 1977. Calcareous nannofossil biostratigraphy and revised zonation of the Pleistocene. *Mar. Micropaleontol.,* 2:1–25.

Hamilton, E.L., 1976. Variations of density and porosity with depth in deep-sea sediments. *J. Sediment. Petrol.,* 46:280–300.

Kagami, H., Karig, D.E., Coulbourn, W.T., et al., 1986. *Init. Repts. DSDP,* 87: Washington (U.S. Govt. Printing Office).

Kastner, M., Elderfield, H., Jenkins, W.J., Gieskes, J.M., and Gamo, T., 1993. Geochemical and isotopic evidence for fluid flow in the western Nankai subduction zone, Japan. *In* Hill, I.A., Taira, A., Firth, J.V., et al., *Proc. ODP, Sci. Results,* 131: College Station, TX (Ocean Drilling Program), 397–413.

King, G.M., and Blackburn, T.H., 1998. *Bacterial Biogeochemistry* (1st ed.): San Diego (Academic Press).

Lee, M.W., Hutchinson, D.R., Collett, T.S., and Dillon, W.P., 1996. Seismic velocities for hydrate-bearing sediments using weighted equation. *J. Geophys. Res.,* 101:20347–20358.

Lowrie, W., 1990. Identification of ferromagnetic minerals in a rock by coercivity and unblocking temperature properties. *Geophys. Res. Lett.,* 17:159–162.

Maltman, A., Labaume, P., and Housen, B., 1997. Structural geology of the décollement at the toe of the Barbados accretionary prism. *In* Shipley, T.H., Ogawa, Y., Blum, P., and Bahr, J.M. (Eds.), *Proc. ODP, Sci. Results,* 156: College Station, TX (Ocean Drilling Program), 279–292.

Maltman, A.J., Byrne, T., Karig, D.E., Lallemant, S., Knipe, R., and Prior, D., 1993. Deformation structures at Site 808, Nankai accretionary prism, Japan. *In* Hill, I.A., Taira, A., Firth, J.V., et al., *Proc. ODP, Sci. Results,* 131: College Station, TX (Ocean Drilling Program), 123–133.

Martini, E., 1971. Standard Tertiary and Quaternary calcareous nannoplankton zonation. *In* Farinacci, A. (Ed.), *Proc. 2nd Int. Conf. Planktonic Microfossils Roma:* Rome (Ed. Tecnosci.), 2:739–785.

Parkes, R.J., Cragg, B.A., Bale, S.J., Getliff, J.M., Goodman, K., Rochelle, P.A., Fry, J.C., Weightman, A.J., and Harvey, S.M., 1994. A deep bacterial biosphere in Pacific Ocean sediments. *Nature,* 371:410–413.

Shipboard Scientific Party, 1986. Site 582. *In* Kagami, H., Karig, D.E., Coulbourn, W.T., et al., *Init. Repts. DSDP,* 87: Washington (U.S. Govt. Printing Office), 35–122.

————, 1991. Site 808. *In* Taira, A., Hill, I., Firth, J.V., et al., *Proc. ODP, Init. Repts.,* 131: College Station, TX (Ocean Drilling Program), 71–269.

Smith, D.C., Spivack, A.J., Fisk, M.R., Haveman, S.A., Staudigel, H., and ODP Leg 185 Scientific Party, 2000. Methods for quantifying potential microbial contamination during deep ocean coring. *ODP Tech. Note,* 28 [Online]. Available from World Wide Web: <http://www-odp.tamu.edu/publications/tnotes/tn28/INDEX.HTM>.

Taira, A., Hill, I., Firth, J.V., et al., 1991. *Proc. ODP, Init. Repts.,* 131: College Station, TX (Ocean Drilling Program).

Tissot, B.P., and Welte, D.H., 1984. *Petroleum Formation and Occurrence* (2nd ed.): Heidelberg (Springer-Verlag).

Yamano, M., Foucher, J.-P., Kinoshita, M., Fisher, A., Hyndman, R.D., and ODP Leg 131 Shipboard Scientific Party, 1992. Heat flow and fluid flow regime in the western Nankai accretionary prism. *Earth Planet. Sci. Lett.,* 109:451–462.

Young, J.R., 1998. Neogene. *In* Bown, P.R. (Ed.), *Calcareous Nannofossil Biostratigraphy* (Vol. 8): Dordrecht (Kluwer Academic), 225–265.

Figure F1. Stratigraphic column for Site 1174, showing lithostratigraphic units, ages, and characteristic lithologies.

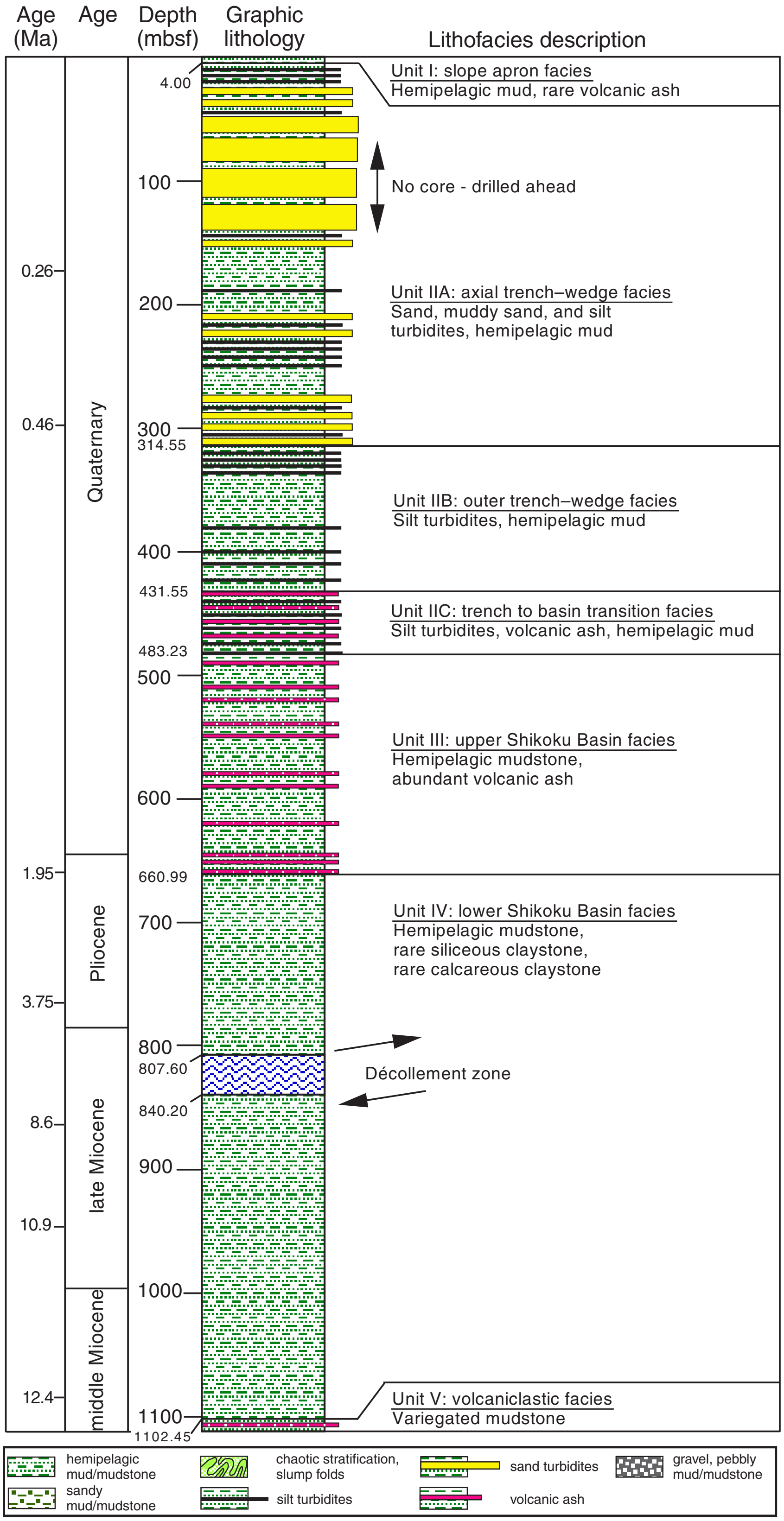

Figure F2. Medium- to fine-grained graded sand with mud chips in the upper part of Subunit IIA (intervals 190-1174A-8H, 0–40 and 40–80 cm).

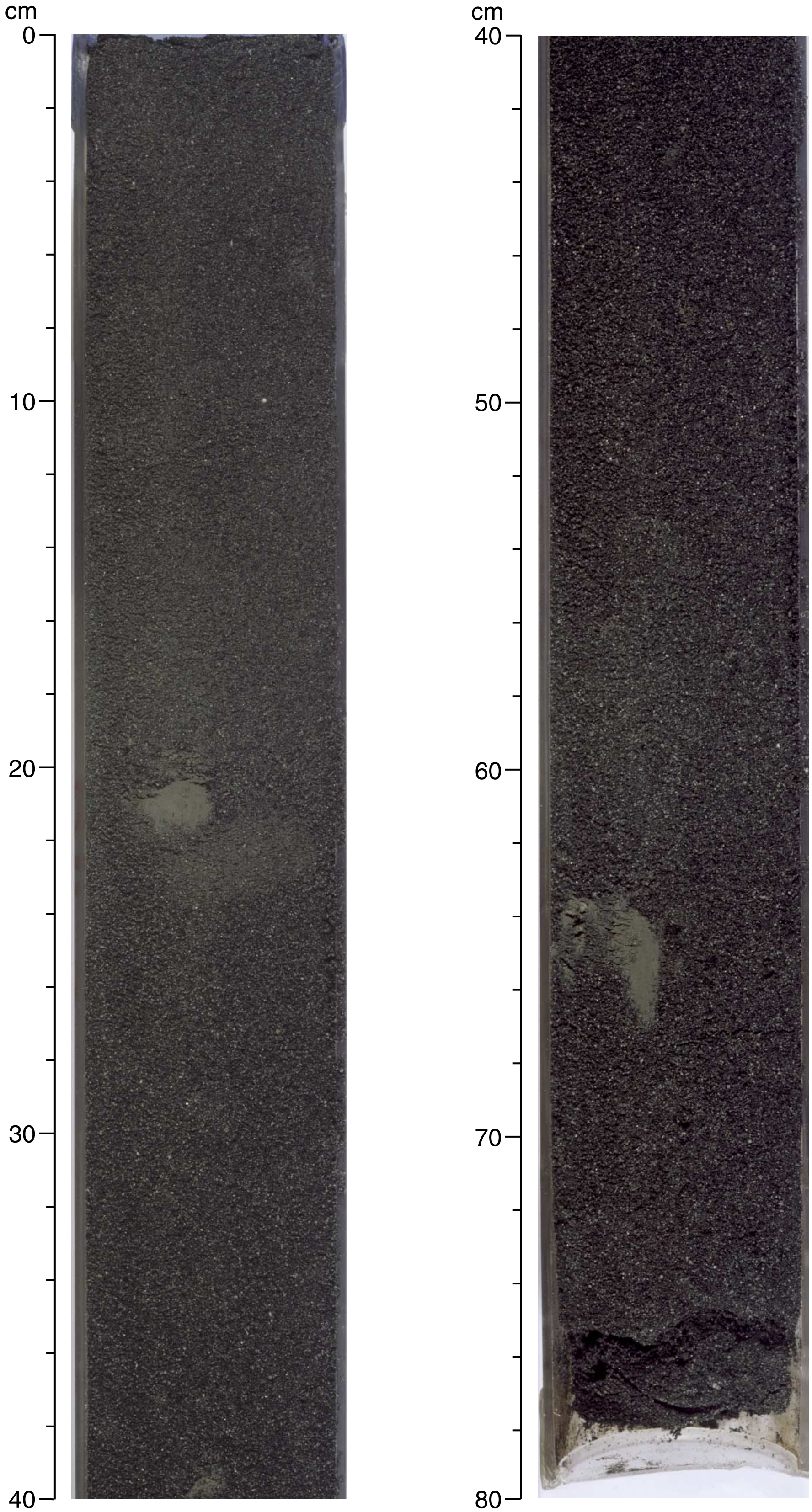

Figure F3. Granule fragments in sand from Subunit IIA (interval 190-1174B-18R-3, 70–86 cm). Granule fragments are white glassy volcanic rock fragments derived from the Honshu arc. They are present in coarse sand intermixed with silty claystone with some convoluted bedding.

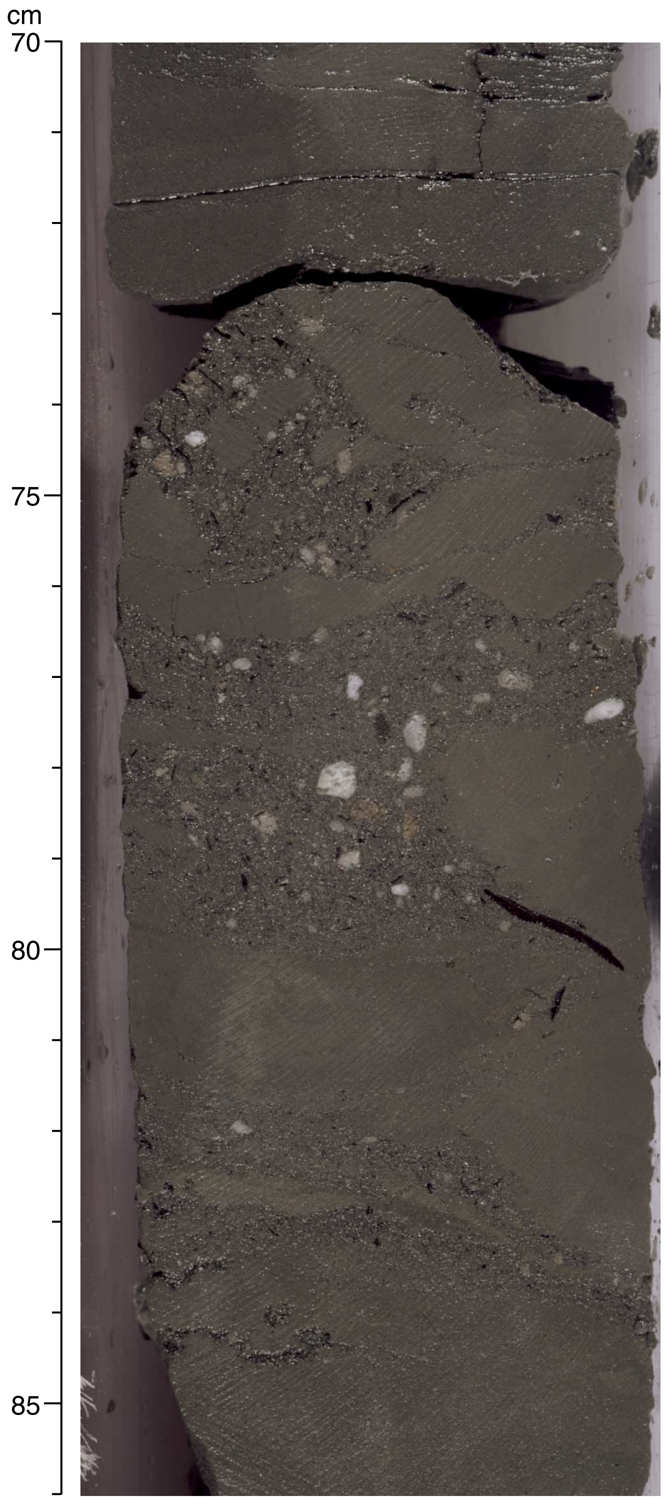

Figure F4. Silty claystone from Subunit IIB containing the trace fossil *Chondrites* (interval 190-1174B-27R-1, 80–89 cm).

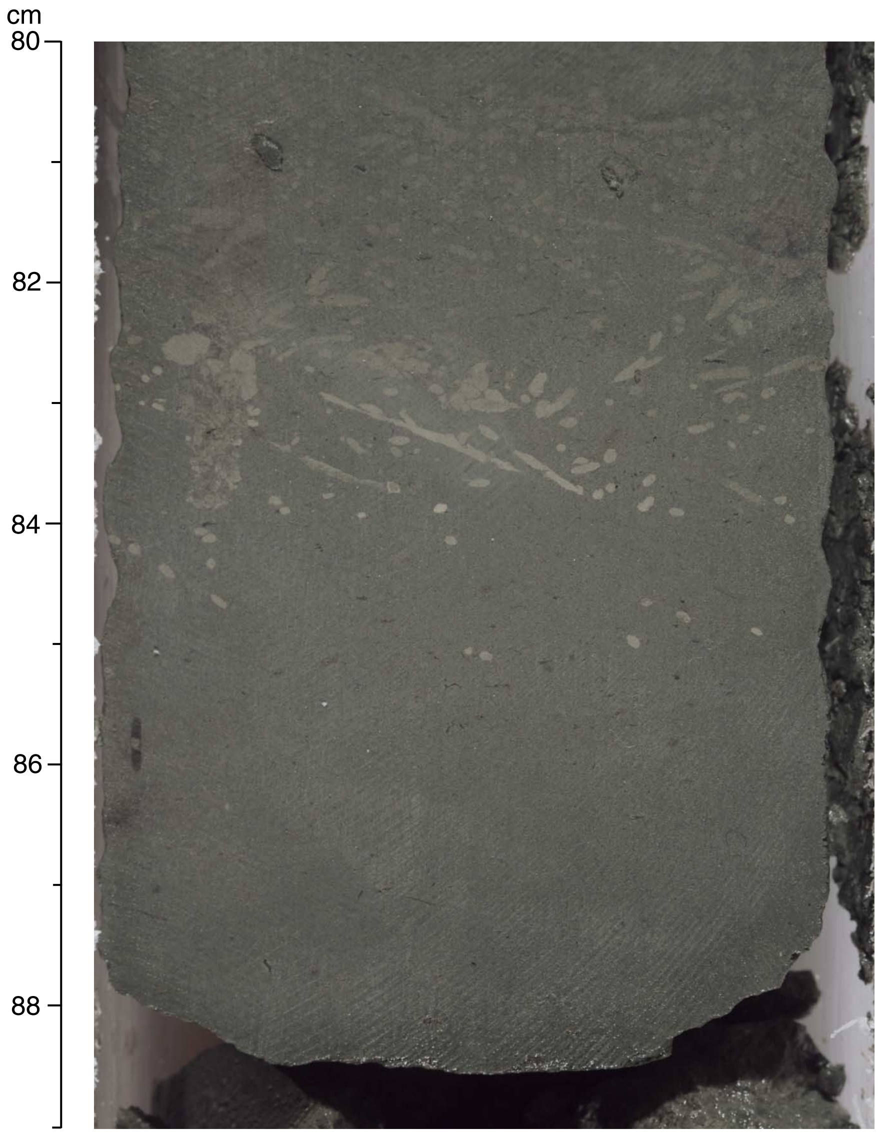

Figure F5. Two volcanic ash layers from the upper Shikoku Basin facies (interval 190-1174B-37R-2, 111–135 cm). Both ash layers have sharp lower contacts and gradational upper contacts with overlying silty clay.

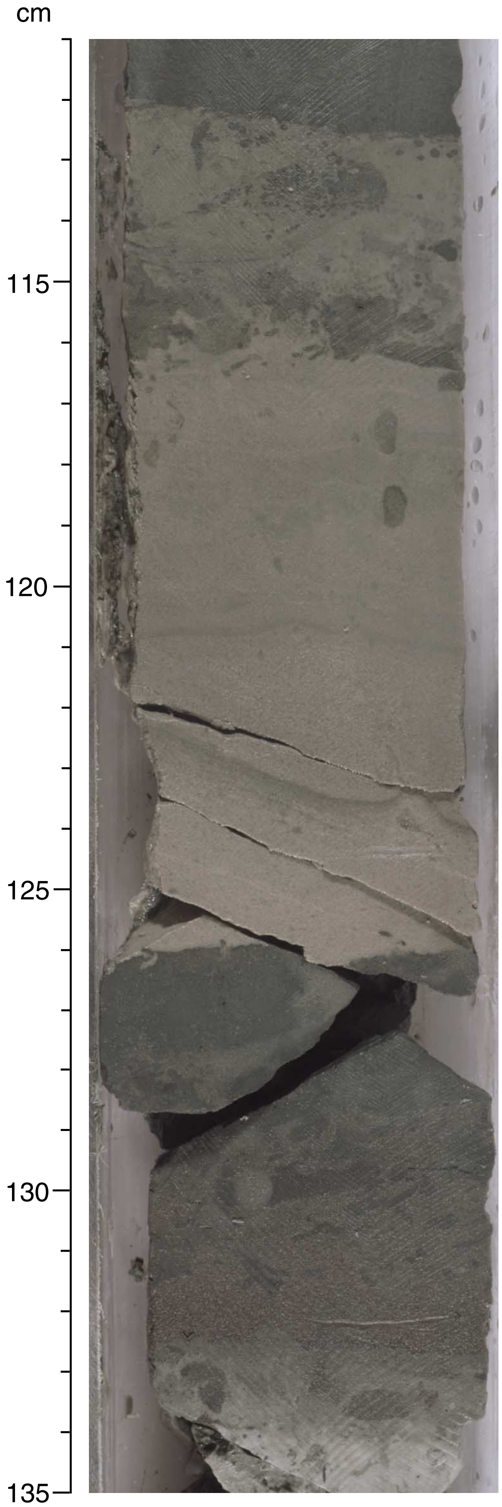

Figure F6. Silty claystone with foraminifers from the lower Shikoku Basin facies (interval 190-1174B-62R-3, 88–92 cm).

Figure F7. Silty claystone with the trace fossil *Zoophycos* from the lower Shikoku Basin facies (interval 190-1174B-74R-1, 65–75 cm).

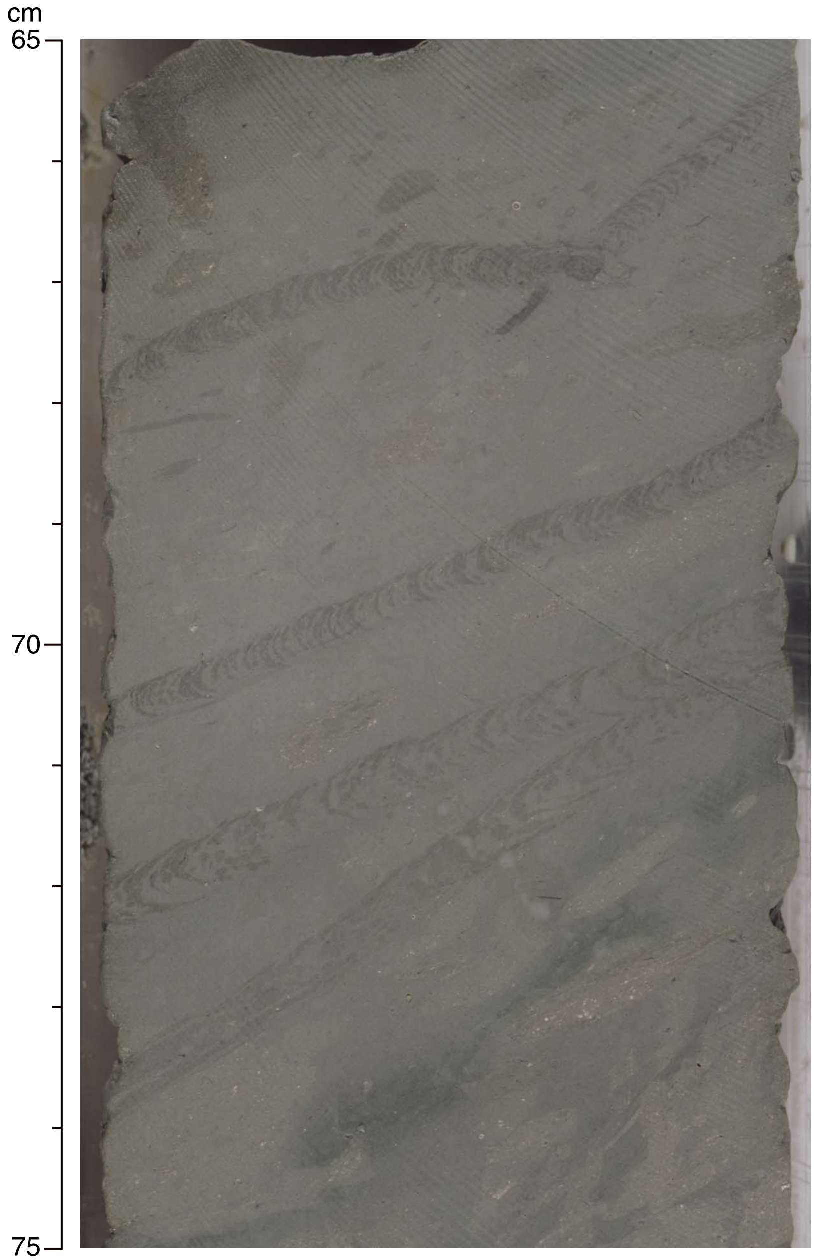

Figure F8. Distribution and thickness of volcanic ash layers at Sites 1173 and 1174. The Bruhnes-Matuyama magnetic reversal provides a stratigraphic tie line.

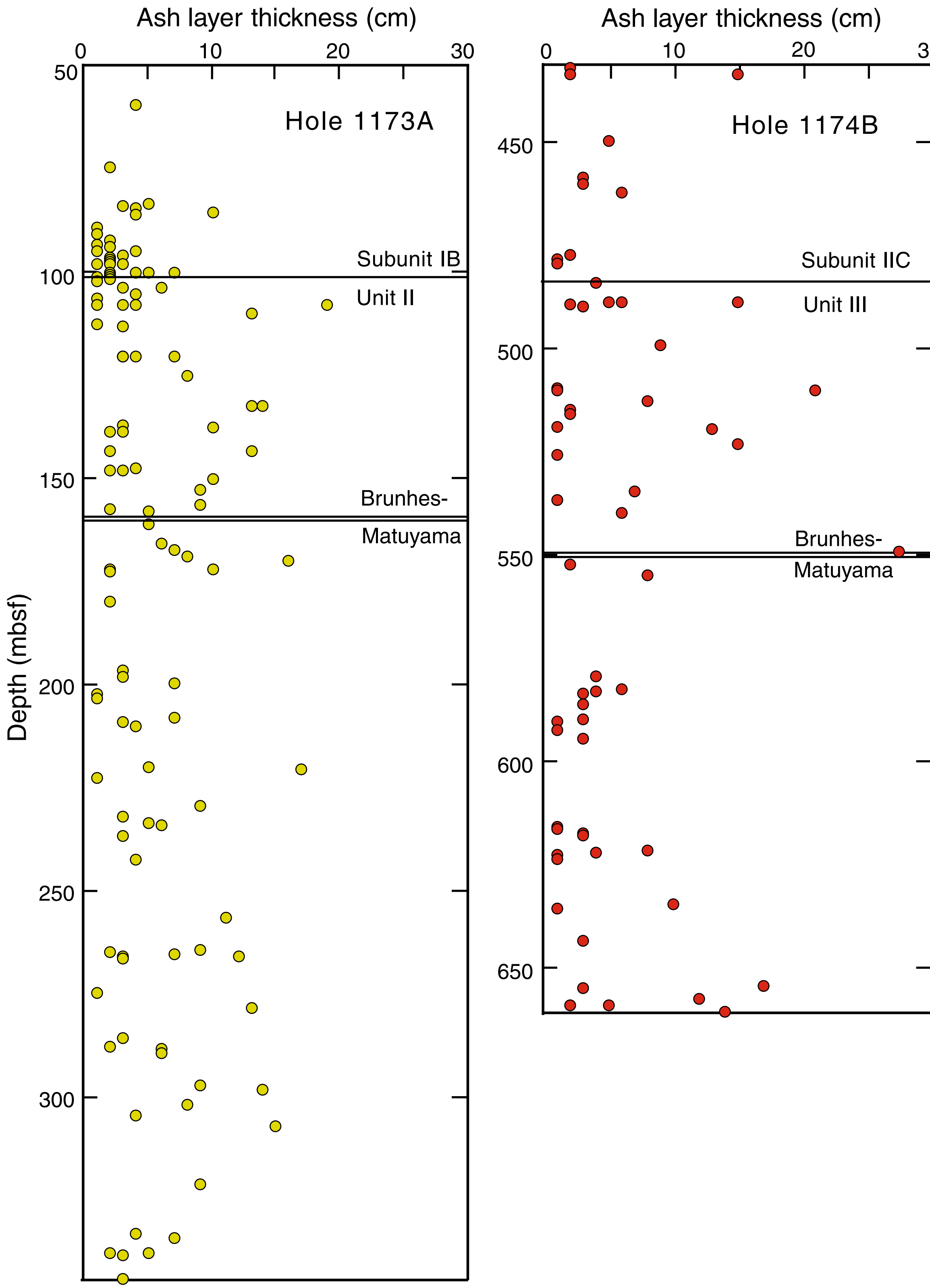

Figure F9. Relative abundances of total clay minerals, quartz, plagioclase, and calcite at Site 1174 based on X-ray diffraction analyses of random bulk powders. Also shown is the ratio of peak areas for (101) cristobalite to (100) quartz.

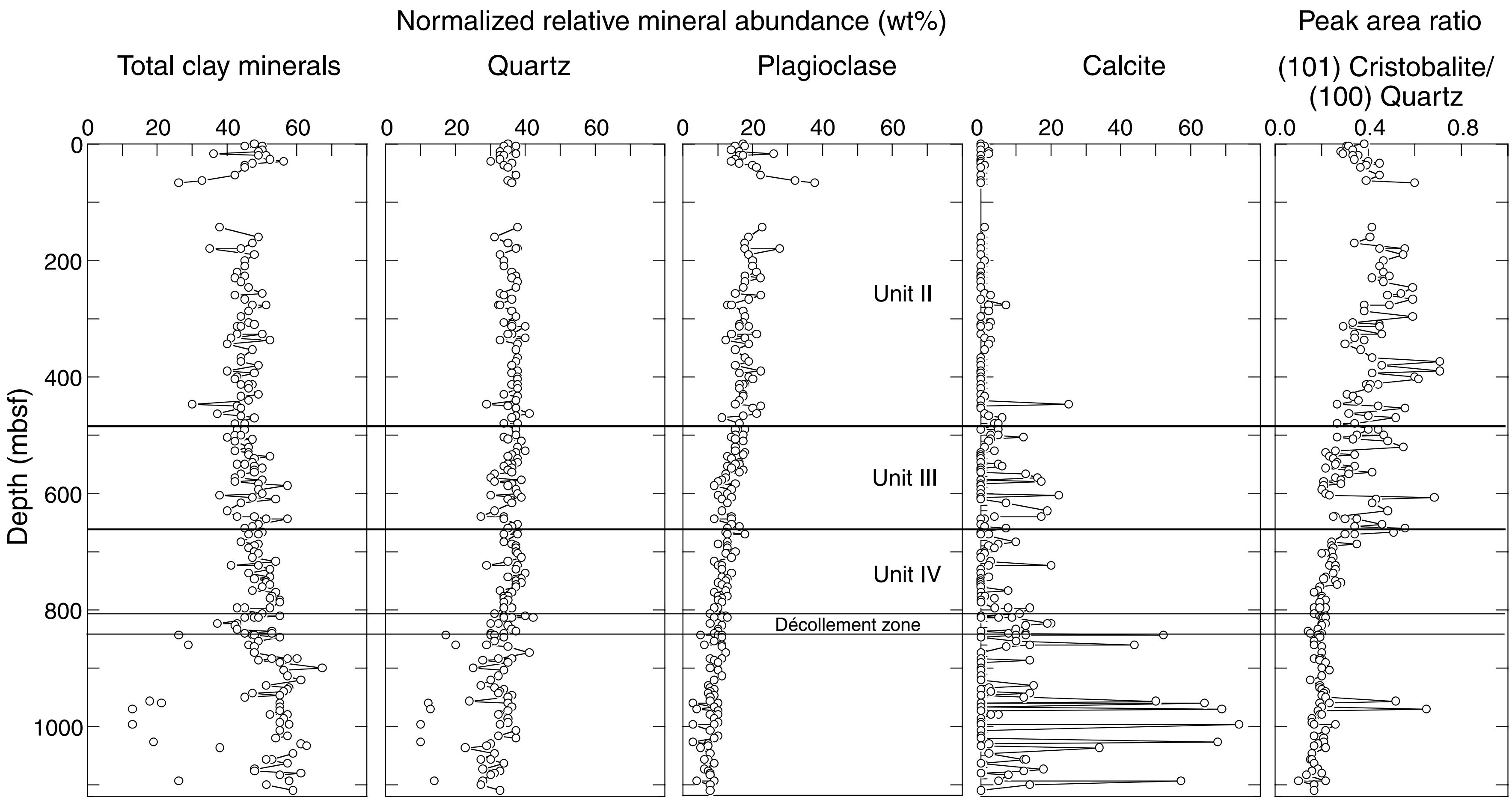

Figure F10. Representative X-ray diffractograms showing unaltered and altered volcanic ash at Site 1174. The unaltered ash sample displays a highly elevated baseline due to amorphous glass shards and minor amounts of quartz, plagioclase, and halite (Sample 190-1174B-37R-2, 131–137 cm). Common alteration products with deeper burial of the ash include smectite (e.g., Sample 190-1174B-84R-5, 77–78 cm) and undifferentiated clinoptilolite/heulandite (e.g., Sample 190-1174B-54R-7, 27–28 cm).

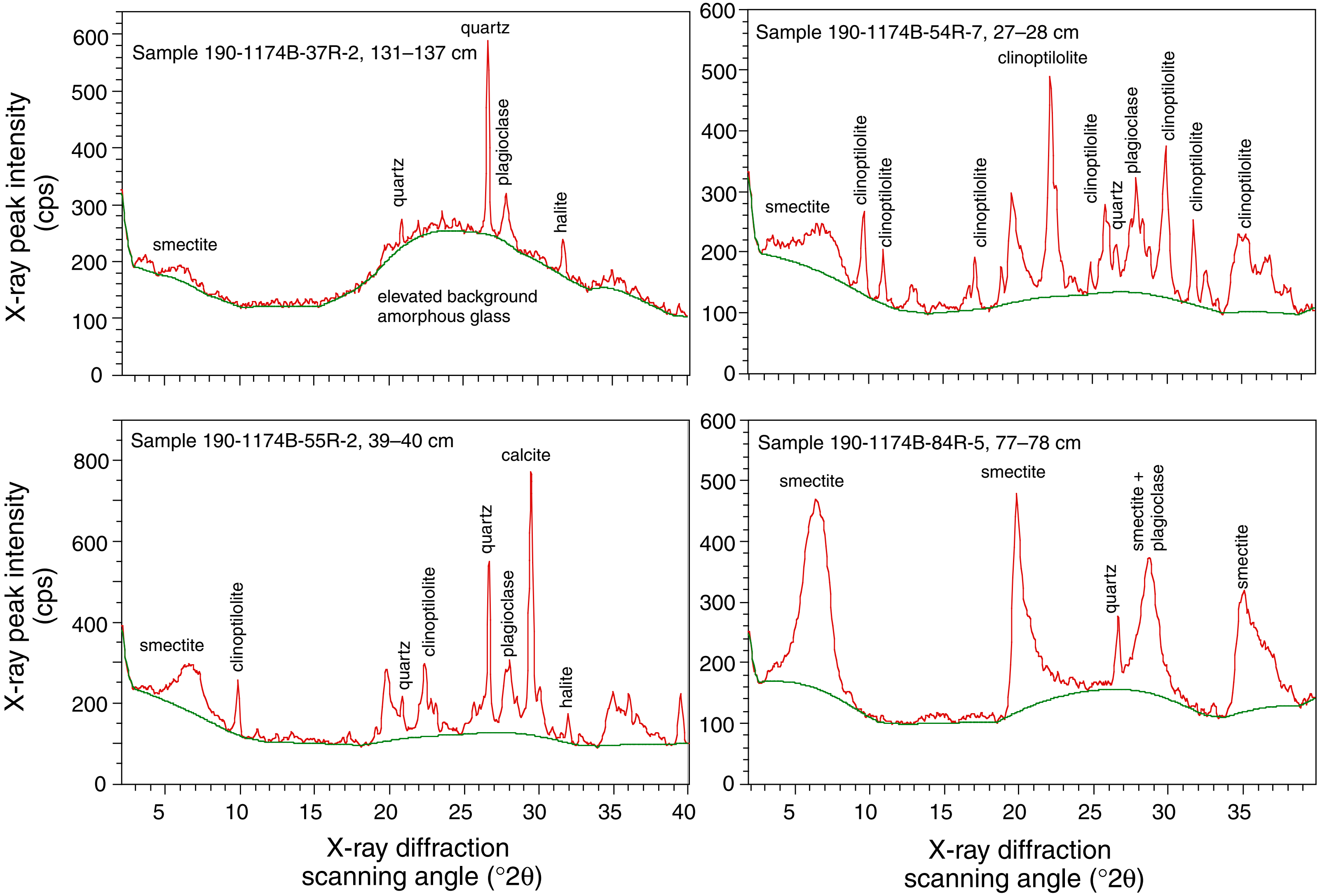

Figure F11. Overall distribution of deformation structures with depth compared with lithostratigraphic divisions. The shaded bands indicate possible fault zones.

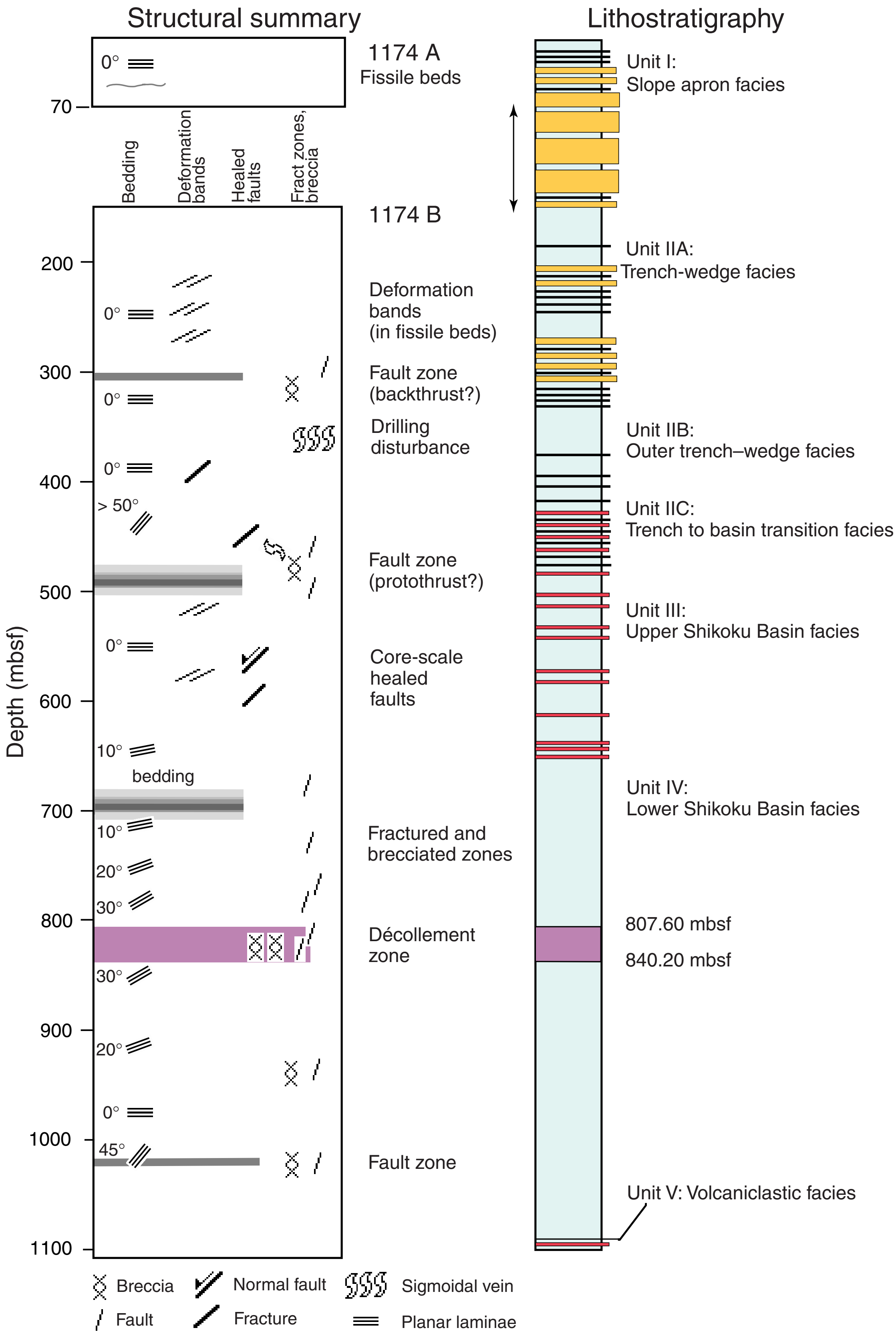

Figure F12. Distribution of bedding dips (circles) and deformation structures with depth in Hole 1174B. The numbers of deformation bands (diamonds), core-scale healed faults (shaded squares), and fractures (lines) are shown per meter. Fractures are open breaks in the core that are thought to be natural (see **"Deeper Fractured and Brecciated Zones,"** p. 12, in "Structural Geology"). The shaded bands indicate zones of steepened bedding and/or intensified fracturing.

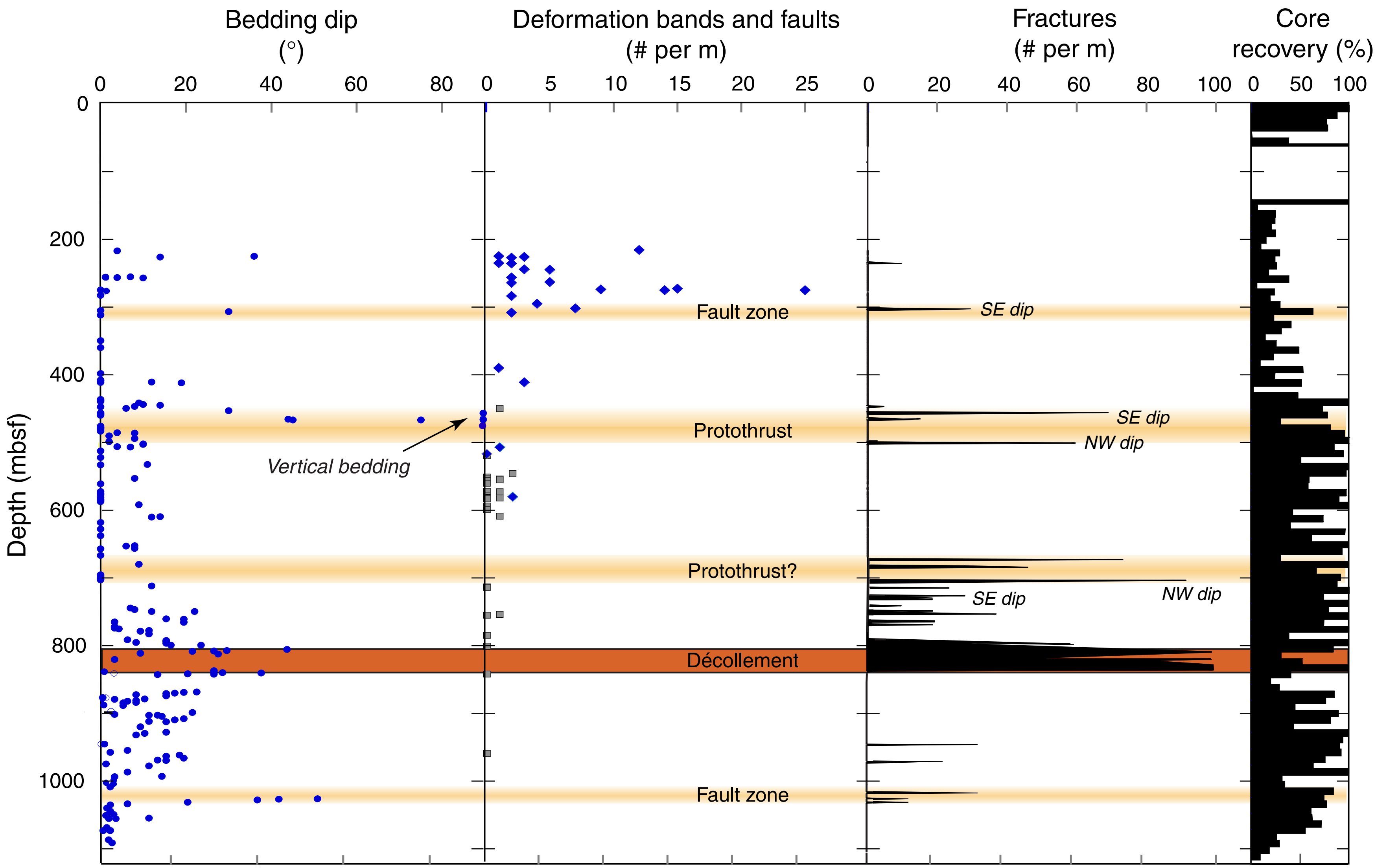

Figure F13. Deformation bands. A. Interval 190-1174B-17R-2, 103–112 cm. Note the varying width and the tendency of the bands to bifurcate. B. Interval 190-1174B-15R-2, 19–24 cm. Note the variation in width of the more shallowly inclined set.

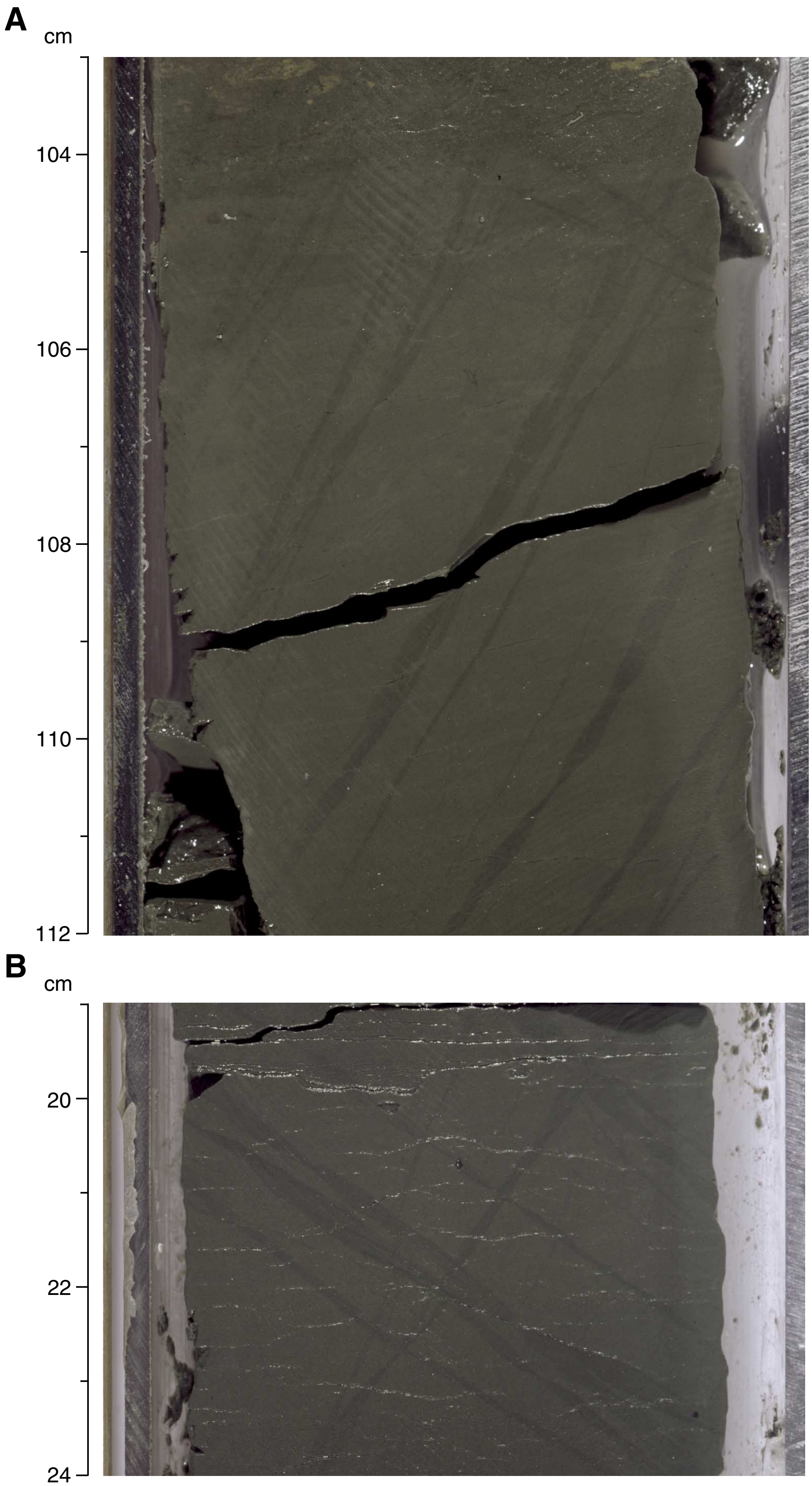

Figure F14. Equal-area lower-hemisphere stereographic projections of deformation bands illustrating the effectiveness of paleomagnetic reorientation. A. Deformation bands in the core-liner reference frame before paleomagnetic reorientation. B. Data in A after paleomagnetic correction to real geographic coordinates (excluding some planes for which the paleomagnetic information was not available). Note the concentration into two oppositely dipping sets. C. Poles to the planes shown in B. D. Average of the two sets of deformation bands showing the dihedral angle and the inclination from vertical of the acute bisectrix.

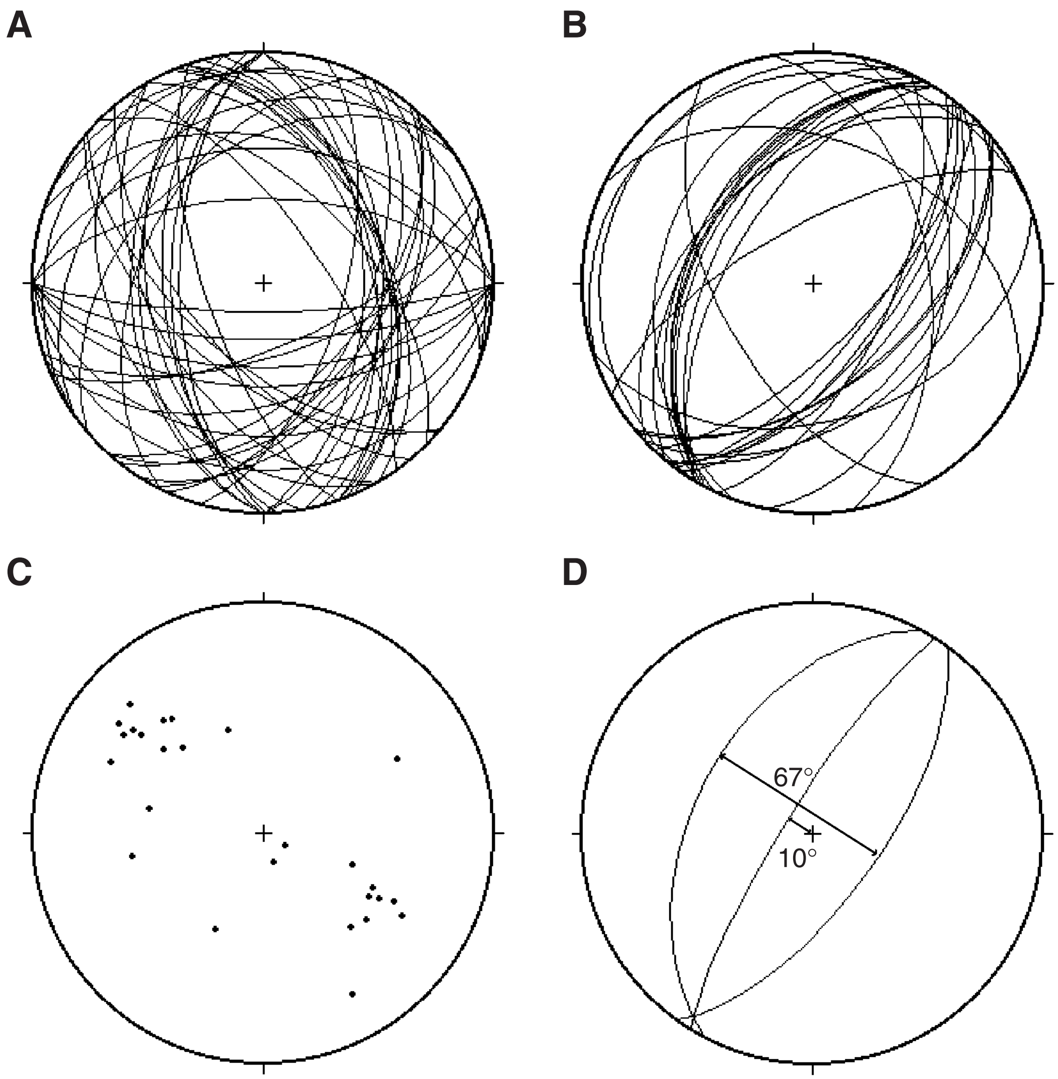

Figure F15. Inclined fractures, part of a deformed horizon that may represent a prism backthrust (interval 190-1174B-18R-2, 0–35 cm).

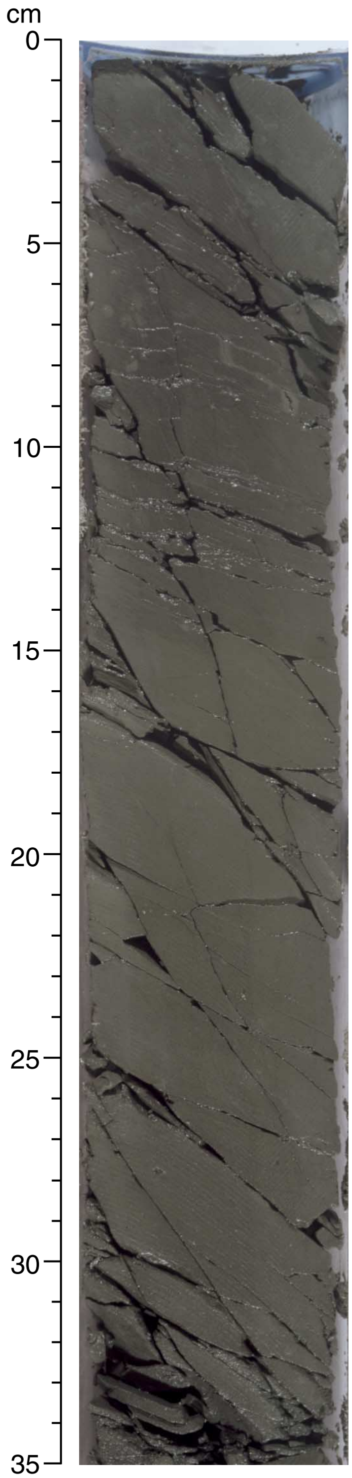

Figure F16. Equal-area lower-hemisphere stereographic projections of fractures related to prism faults in the interval 200–525 mbsf after paleomagnetic reorientation. **A.** Representative planes for the entire interval. The bold great circle labeled 1 represents narrow fractures that are axial-planar to small asymmetric folds in the fault zone at 306 mbsf (the base of the deformation band domain), and the circle labeled 2 represents the main fracture set in the same horizon. These southeast dips suggest the fault may be a prism backthrust. Note the similarity in orientation of the axial-planar fractures with the southeast-dipping set of deformation bands shown in Figure F14D, p. 51. **B.** Poles to the planes shown in A. **C.** Slickensided surfaces from the fault zone at 504 mbsf, thought to be part of a northwest-dipping protothrust.

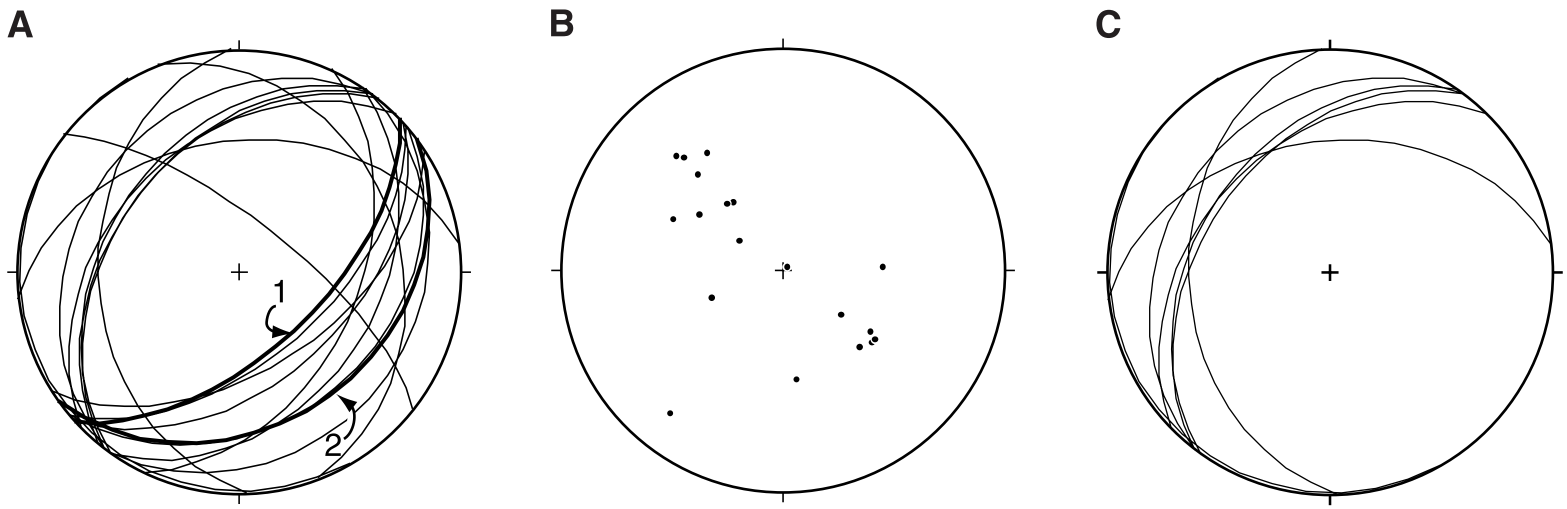

Figure F17. Steepened bedding and inclined fractures, part of a deformed interval that may represent a protothrust horizon (interval 190-1174B-35R-1, 30–63 cm).

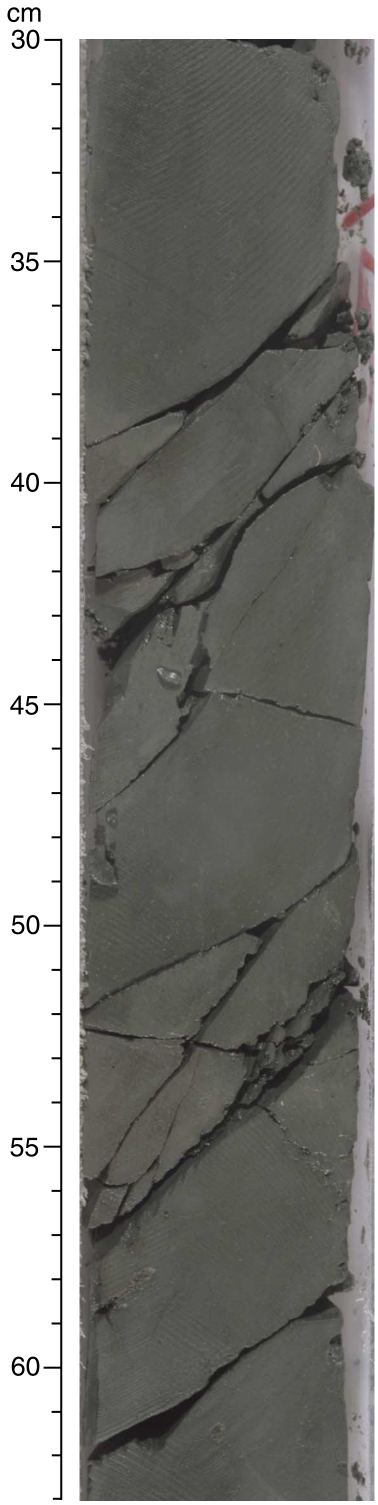

Figure F18. Bifurcating, healed normal fault (interval 190-1174B-43R-6, 79–94 cm).

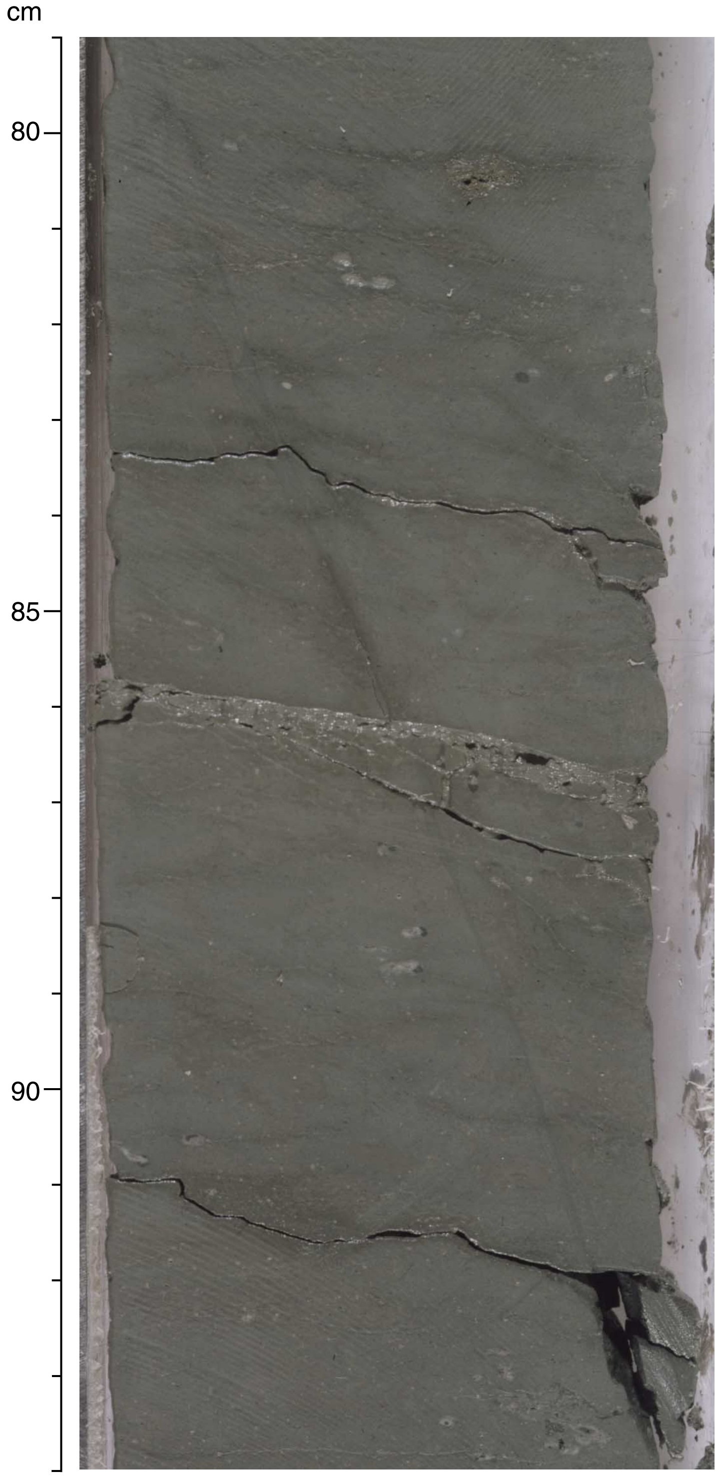

Figure F19. Equal-area lower-hemisphere stereographic projections of core-scale healed faults throughout Site 1174 based on paleomagnetically restored data. **A.** Fault planes. **B.** Contoured poles to fault planes. Number of points = 26, contour interval = 2.0%/1% area. Note that unlike the data on other structures, there is no dominant orientation even after paleomagnetic restoration, suggesting that the faults may be due to compactional processes rather than tectonic stress.

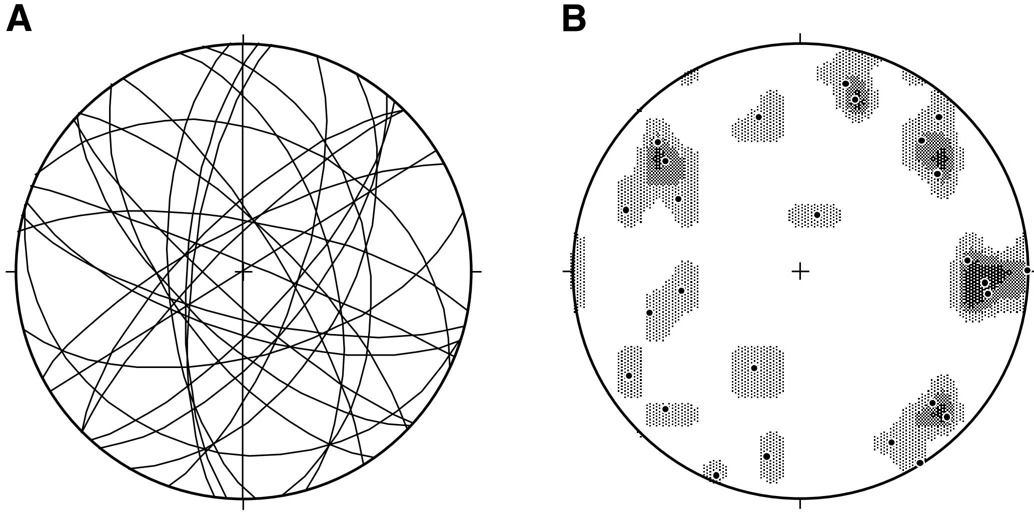

Figure F20. A. Detail of the upper part of the décollement zone showing breakage into angular blocks along inclined fractures (interval 190-1174B-71R-2, 48–79 cm). **B.** Detail of lower part of décollement zone showing comminution of sediments (interval 190-1174B-73R-1, 96–118 cm) (also see the photograph of Core 190-1174B-73R in the "Site 1174 Core Descriptions," p. 80).

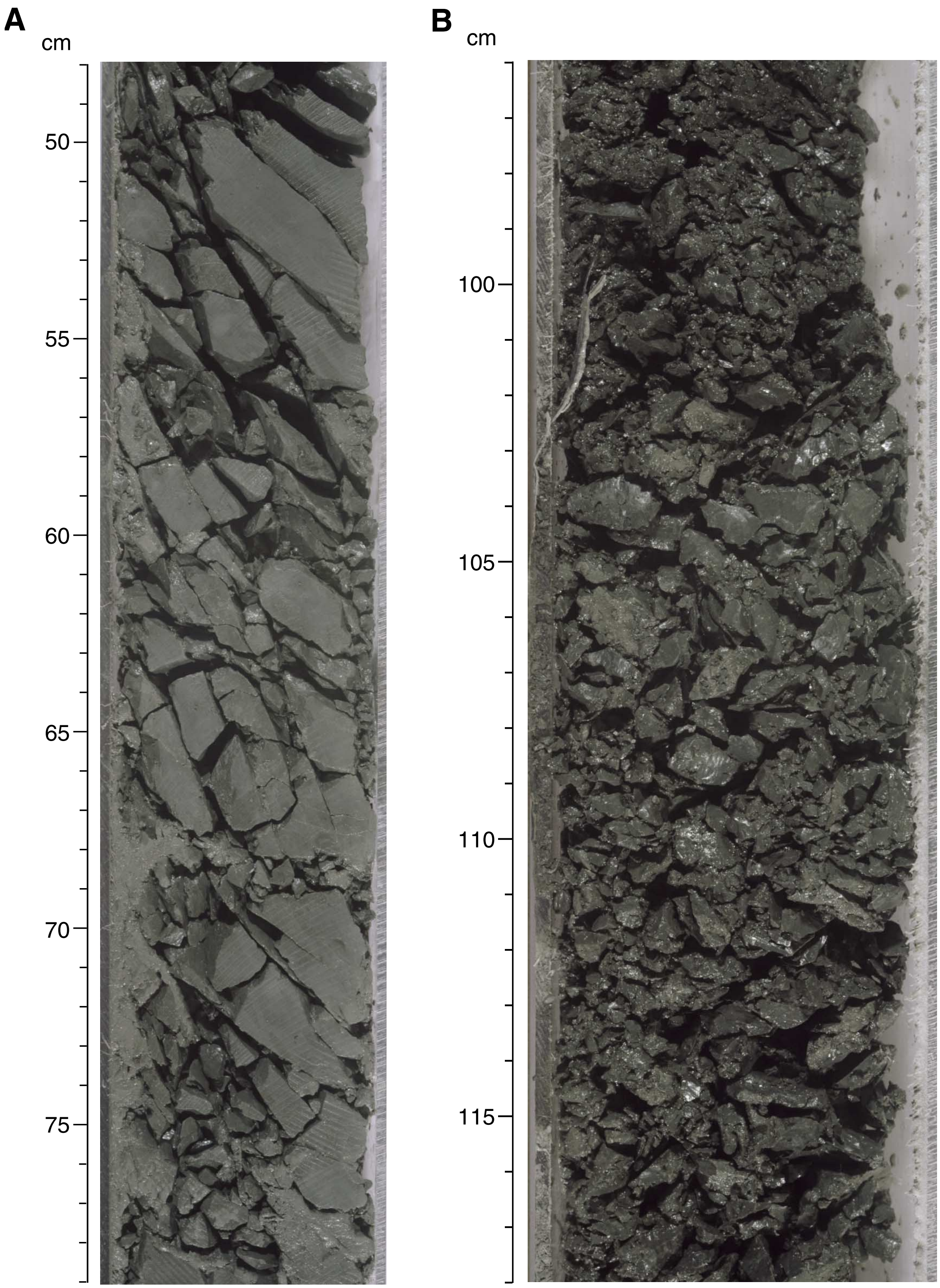

Figure F21. Equal-area lower-hemisphere stereographic projections of structures related to the décollement after paleomagnetic reorientation. **A.** Slickensided and slickenlined planes (650–840 mbsf), including the décollement zone. **B.** Contoured poles to the planes shown in A. Number of points = 26, contour interval = 2.0%/1% area. **C.** Bedding planes with poles (746–840 mbsf).

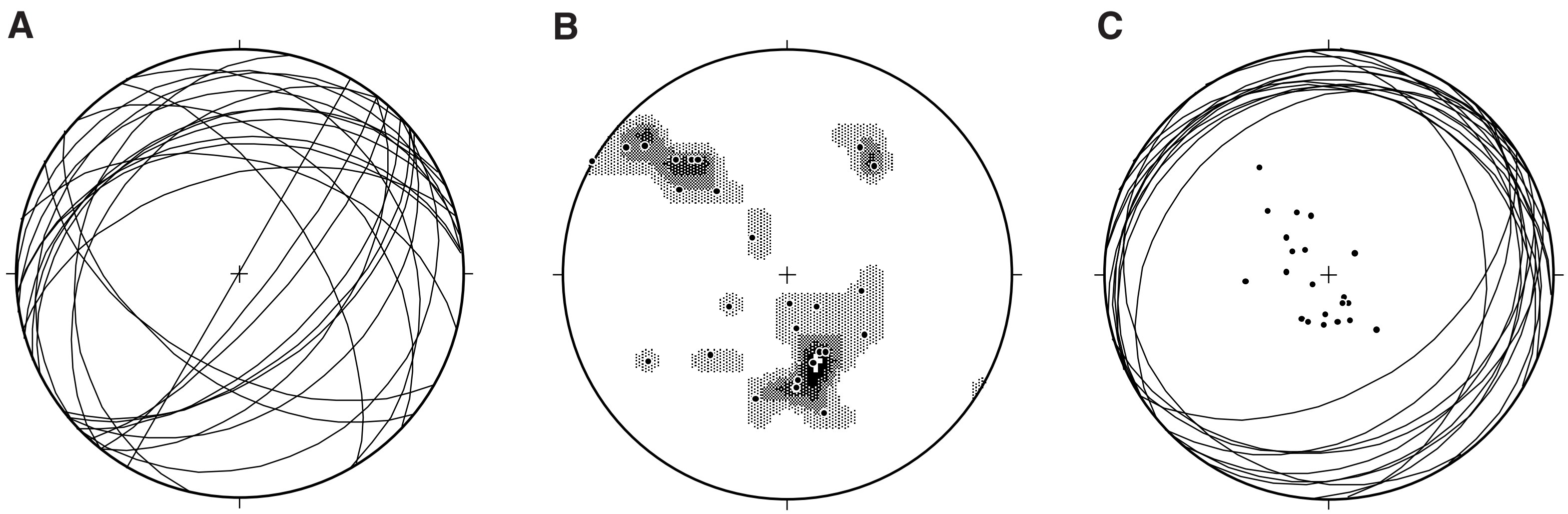

Figure F22. Details of fracturing across the décollement zone. The density of fracturing is expressed by the nature and size of the brecciated fragments. Most of the fracture surfaces are slickensided and slickenlined. Note the trend of increasing fracturing downward through the zone, peaking a few meters above a sharply defined base.

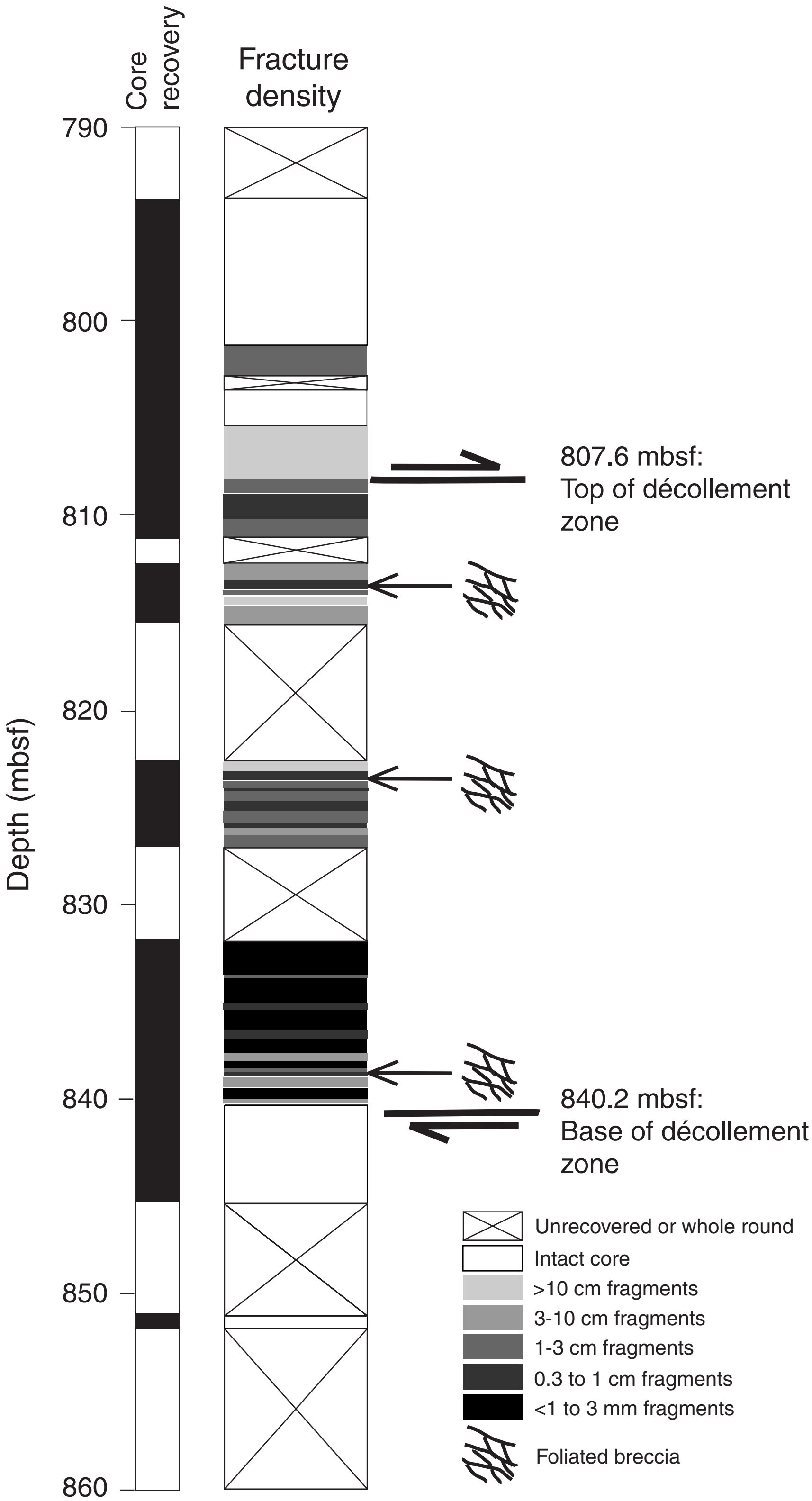

Figure F23. Example of a dewatering structure in the underthrust sediments (interval 190-1174B-84R-3, 23–44 cm).

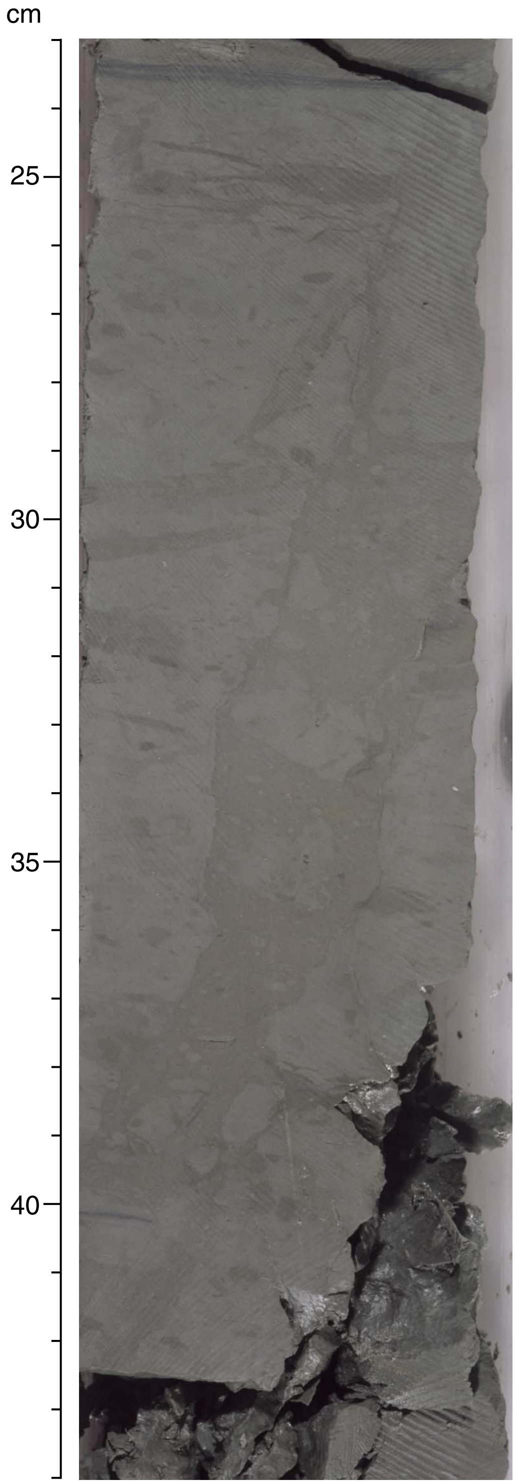

Figure F24. Variation of uncalibrated gas-permeameter measurements with depth at Site 1174.

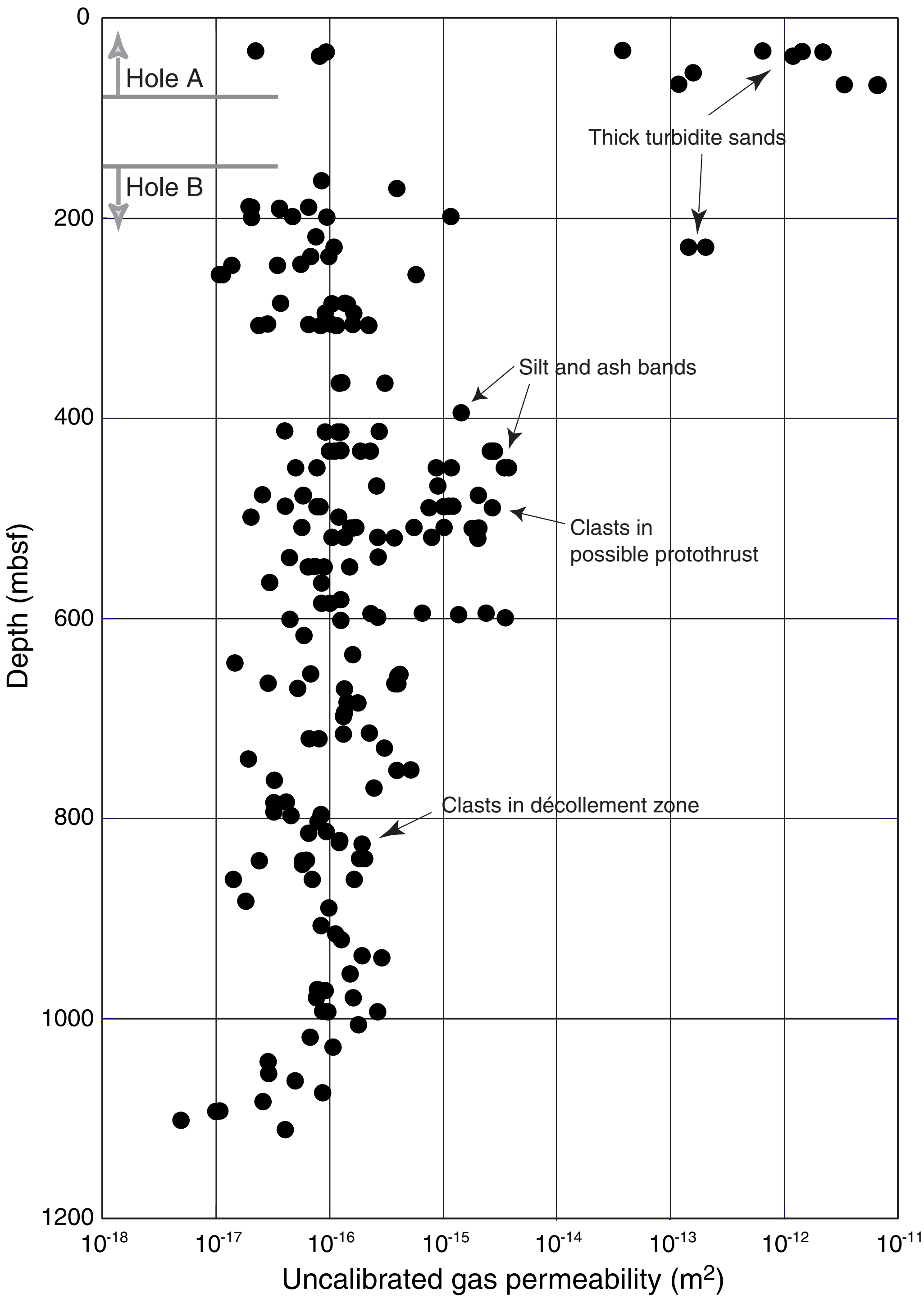

Figure F25. Detail of uncalibrated gas-permeameter measurements within a reworked layer of volcanic ash to illustrate fine-scale variations (interval 190-1174B-31R-3, 115–133 cm; 432 mbsf).

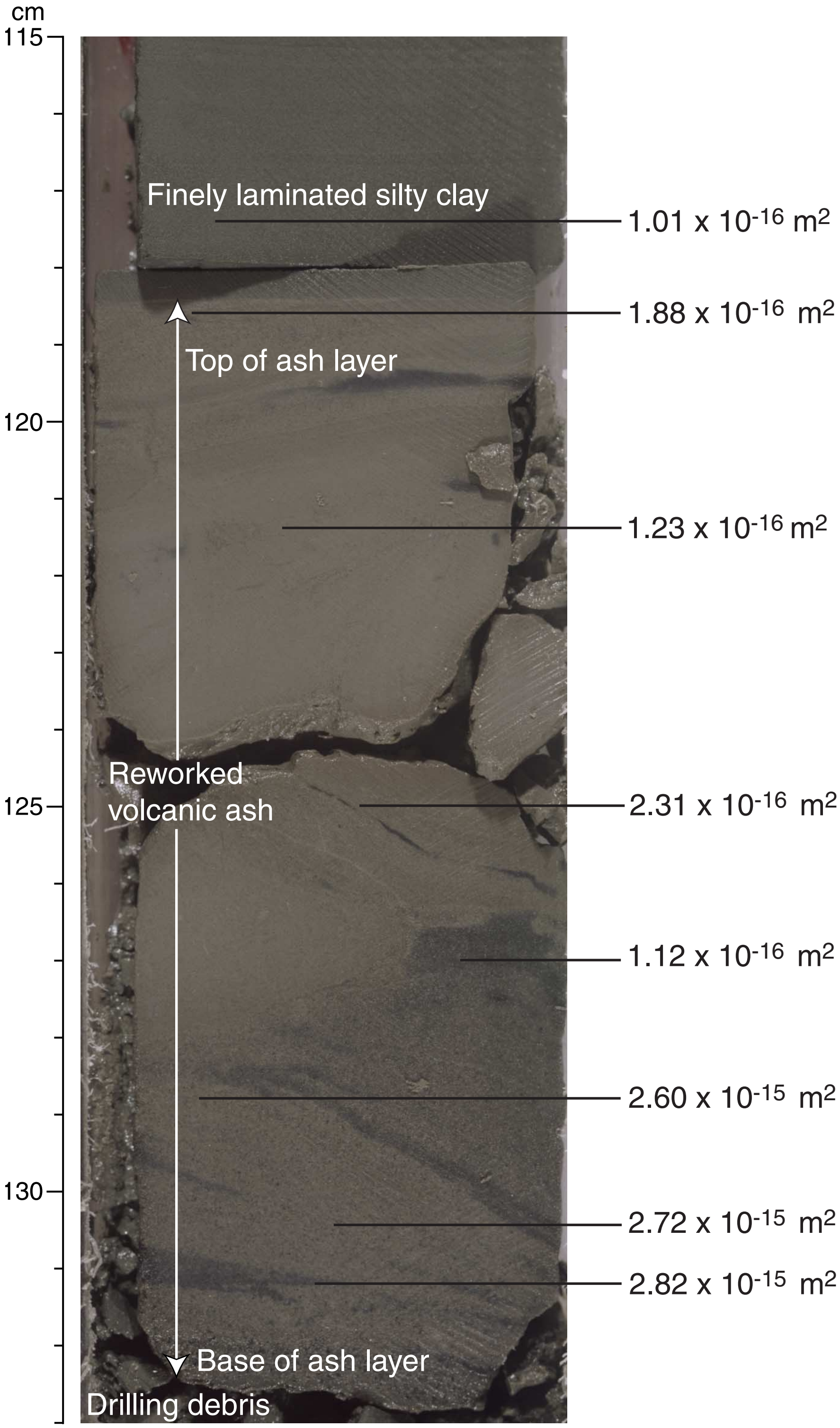

Figure F26. Paleomagnetic inclination, declination, and intensity after AF demagnetization at 30 mT for Hole 1174A. Marked reversed polarity inclinations are identified as magnetic excursions. Declinations were corrected using Tensor tool orientation data.

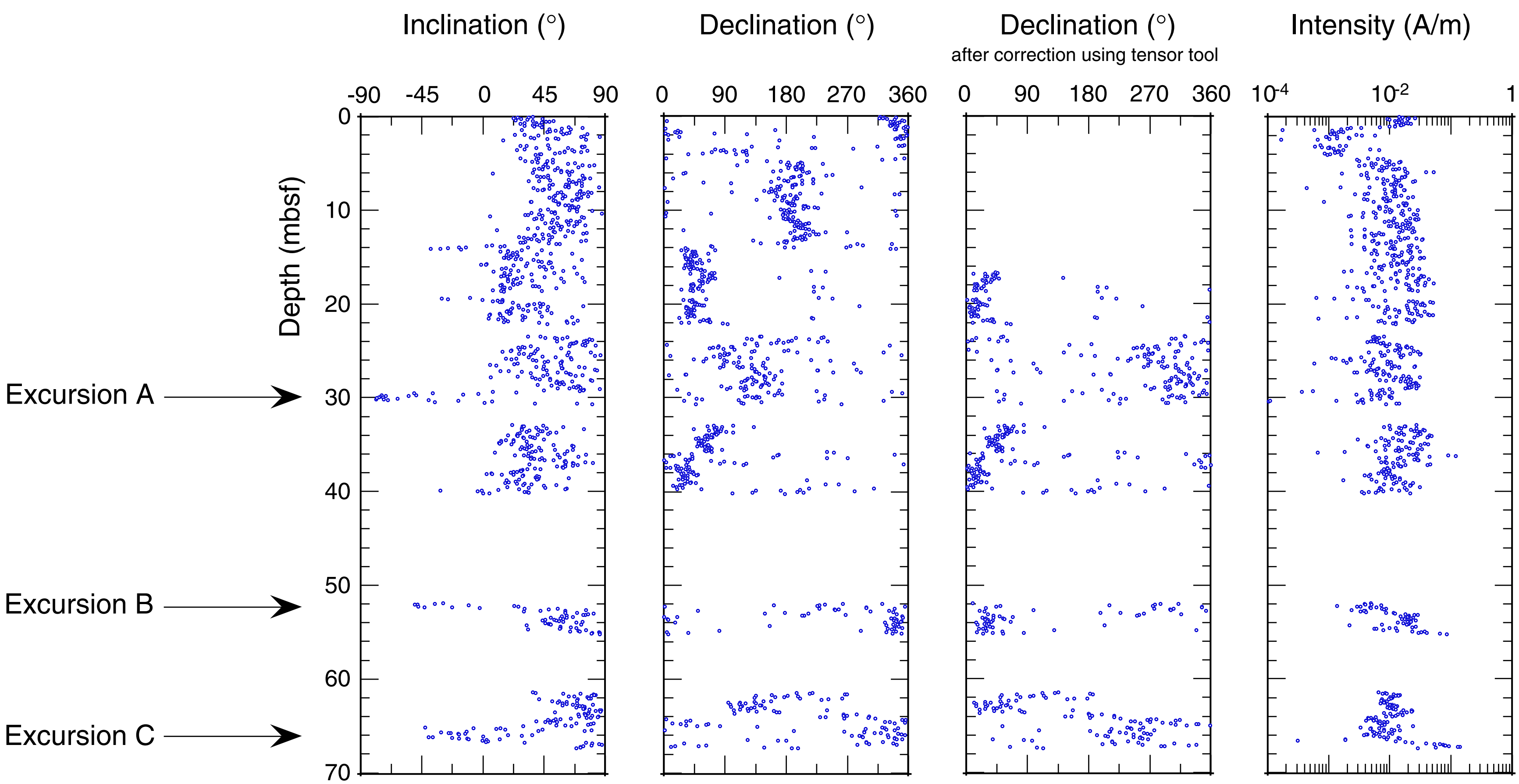

Figure F27. Typical Zijderveld diagrams of Hole 1174A interpreted excursions. A stable reversed polarity magnetization was identified after AF demagnetization at 30 mT.

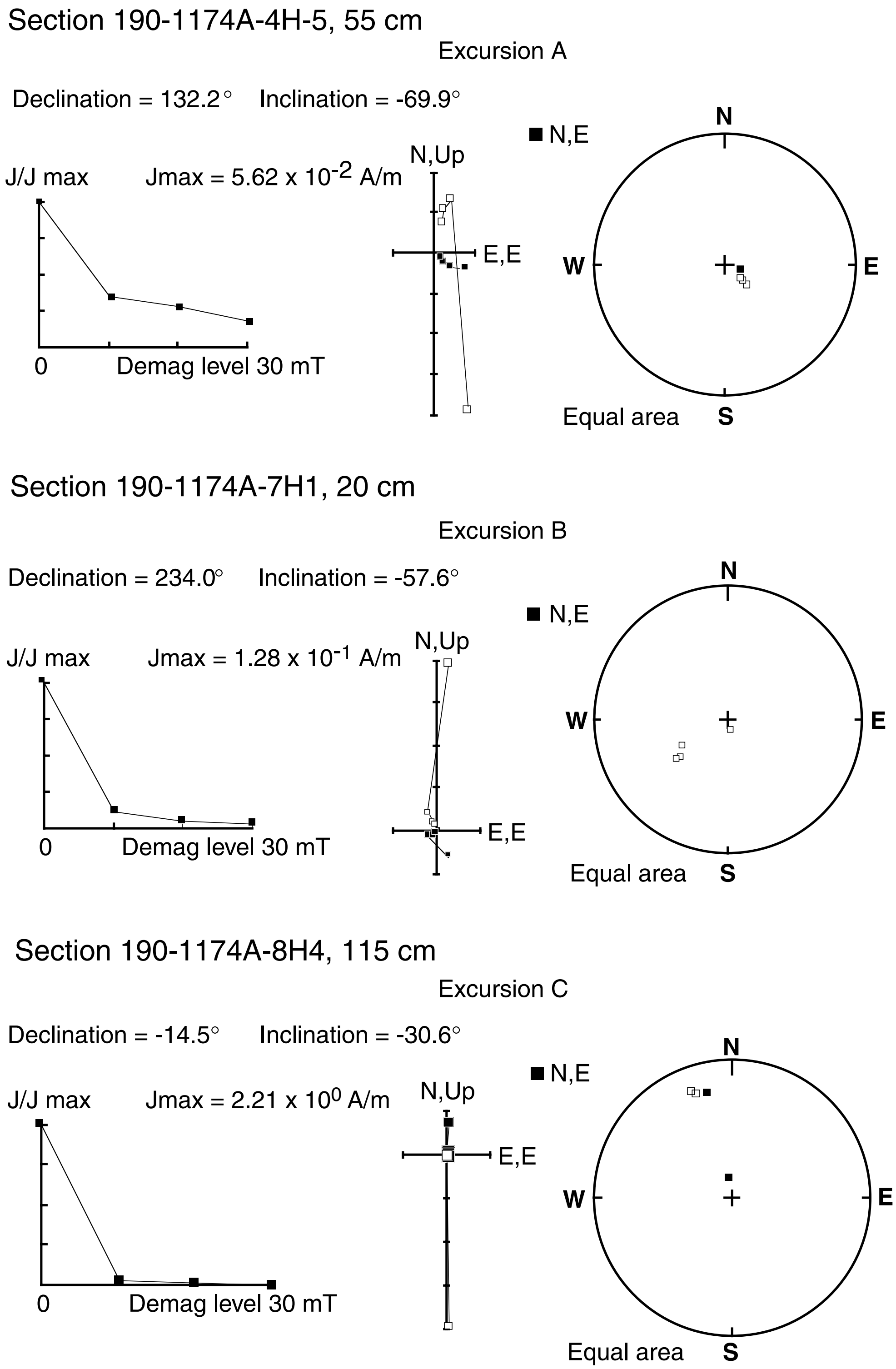

Figure F28. Comparison of magnetic intensity zones at Sites 1174 and 1173 based on magnetostratigraphic interpretations. The characteristic intensity values were identified as high-intensity Zone 1, low-intensity Zone 2, slightly high intensity Zone 3, and a second low-intensity Zone 4. An increase of intensity within Zone 2 was identified as Zone 2′.

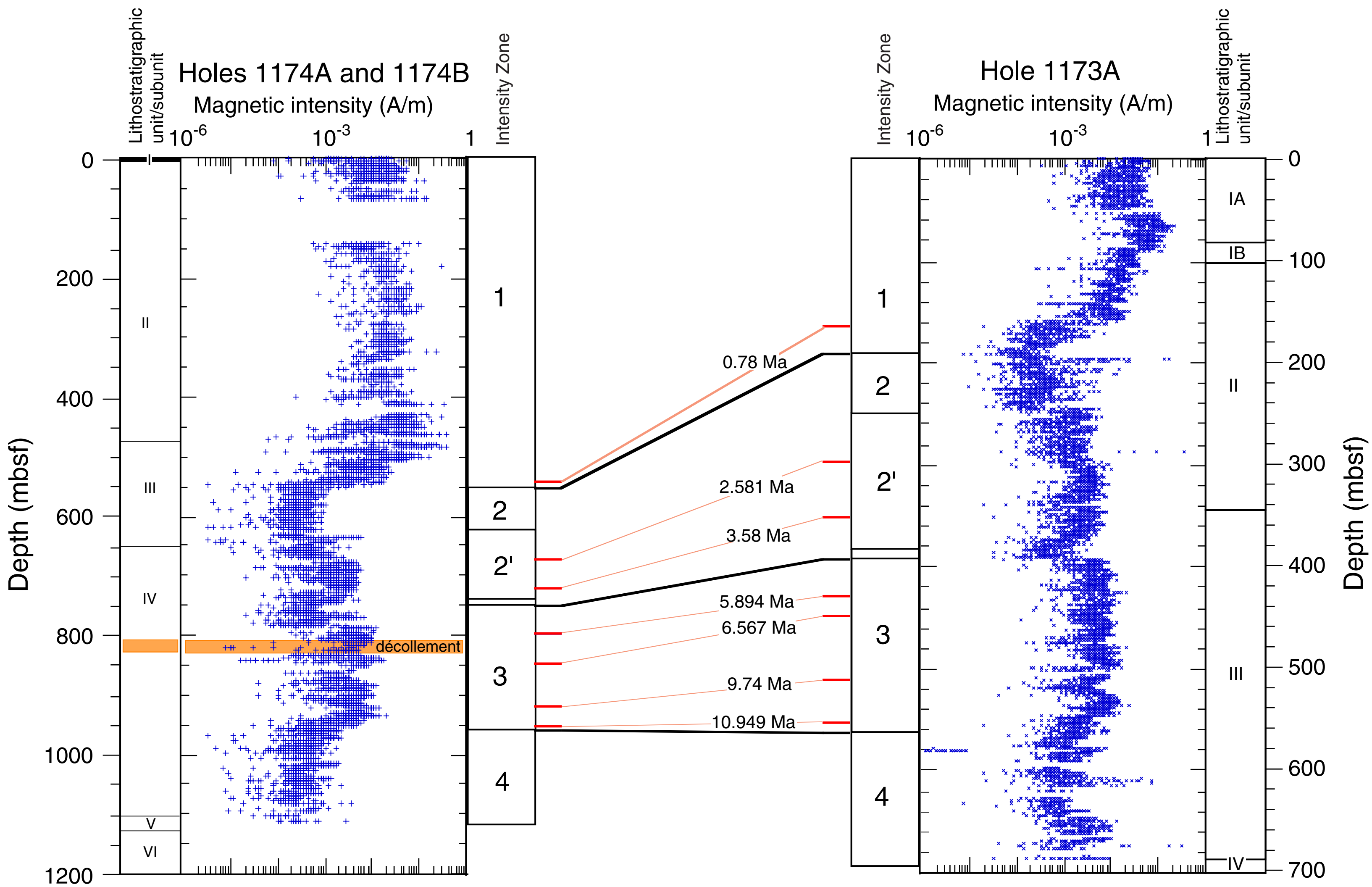

Figure F29. Multicomponent isothermal remanent magnetization (mIRM) and thermal demagnetization experiments at Hole 1174B. Discrete samples were selected from the four major intensity zones (see "Hole 1174B," p. 18, in "Paleomagnetic Results" and Fig. F28, p. 65). The three fields used to generate the IRM components are shown by the x, y, and z curves.

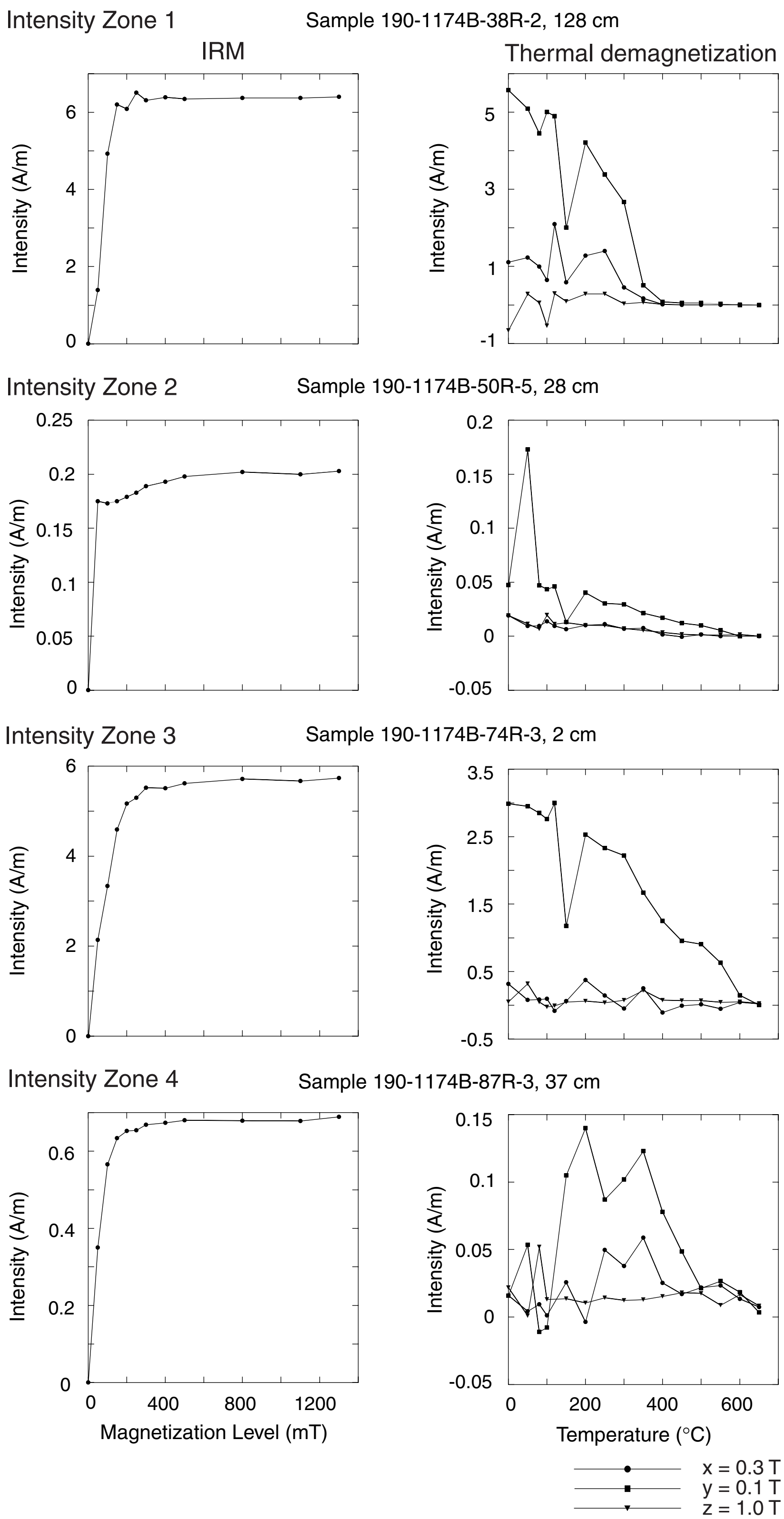

Figure F30. Site 1174 magnetostratigraphy. Solid lines indicate correspondence to the magnetic polarity time scale of Cande and Kent (1995). Black = normal polarity, white = reversed polarity, gray = unknown polarity, ? = questionable correlation.

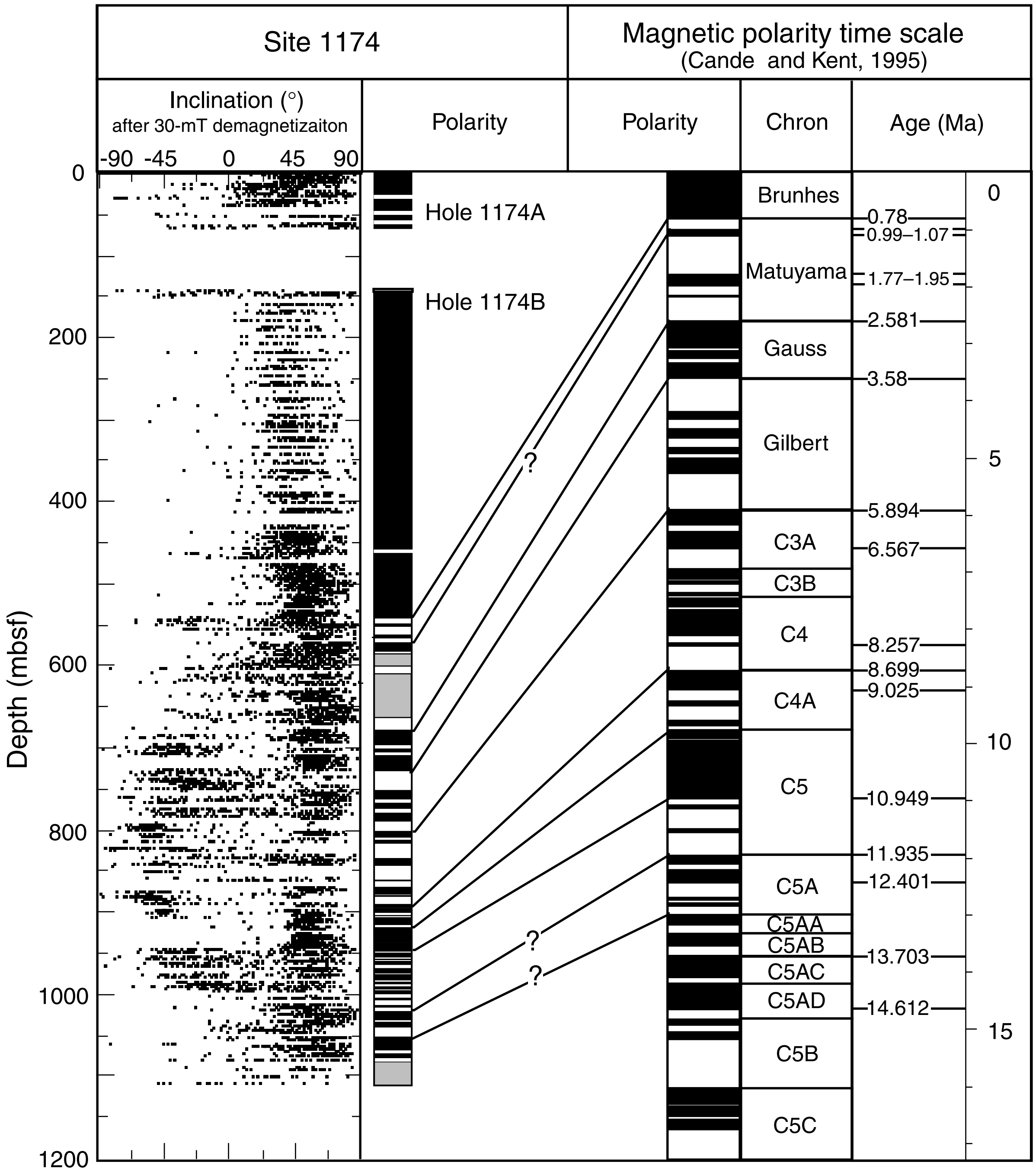

Figure F31. Site 1174 age-depth plot obtained by magnetostratigraphy and biostratigraphy. Black = normal polarity, white = reversed polarity.

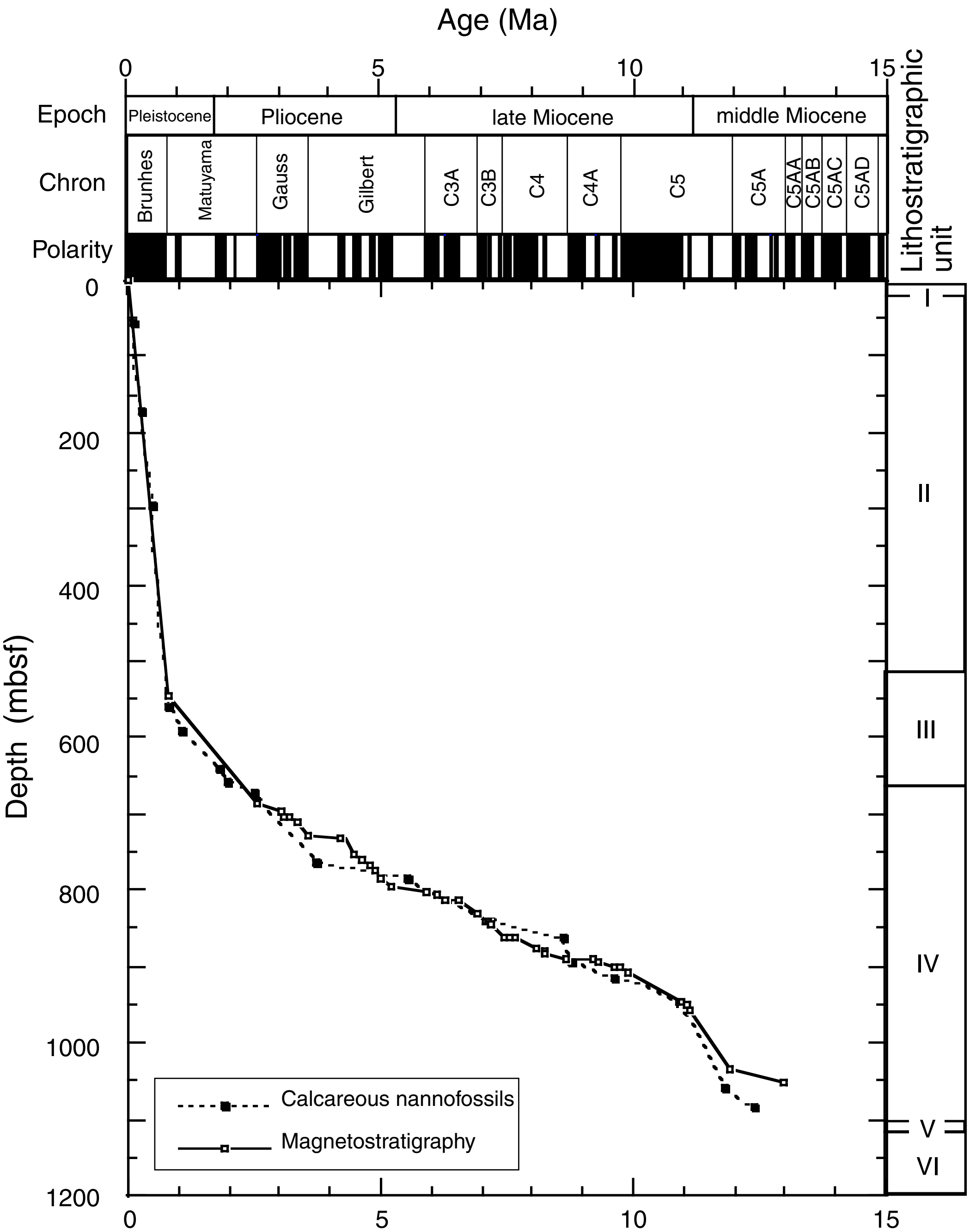

Figure F32. Correlation of magnetic polarity reversals between Sites 1173, 1174, and 808. Black = normal polarity, white = reversed polarity, gray = unknown polarity.

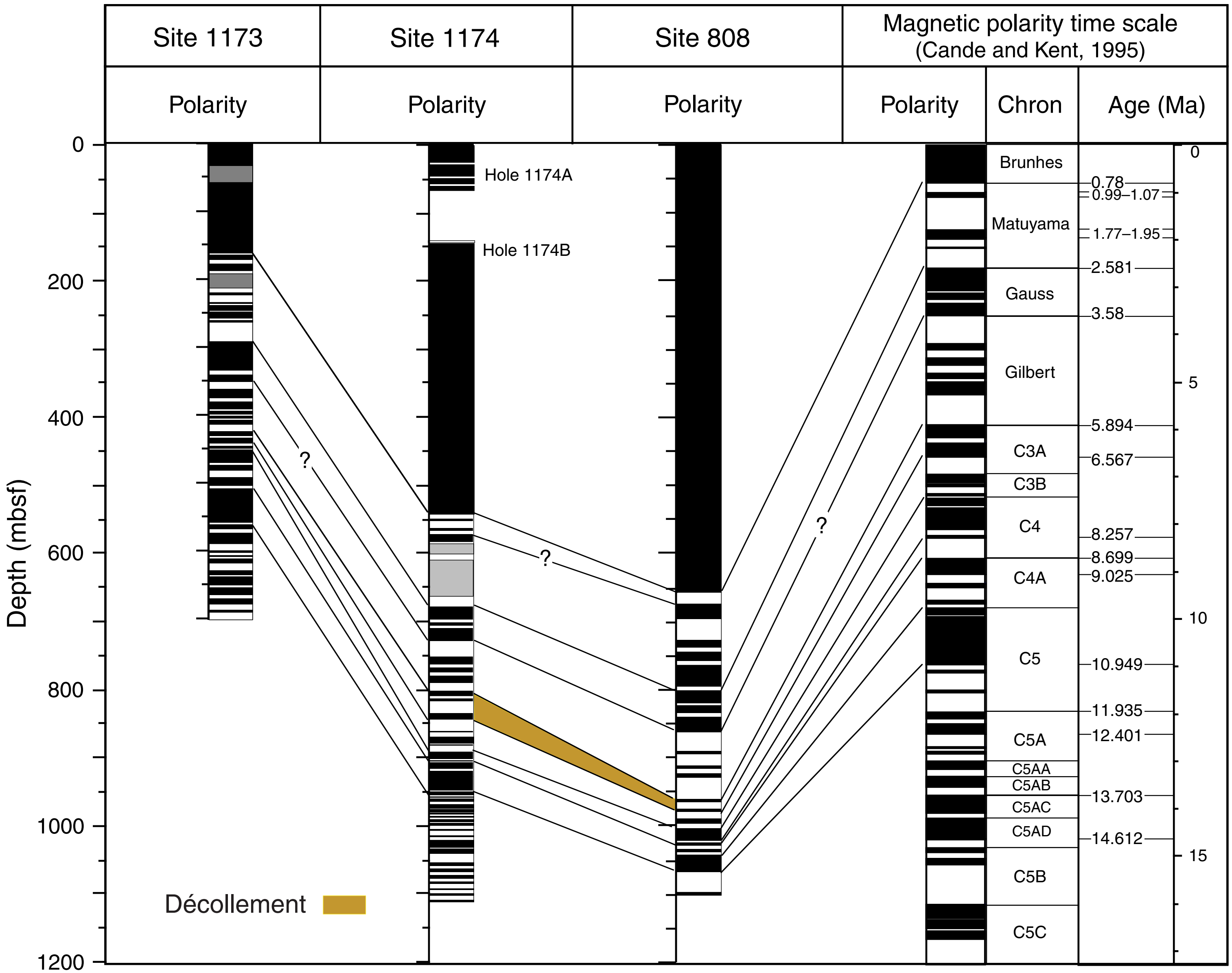

Figure F33. Pore fluid composition as a function of depth at Site 1174. Solid horizontal lines indicate lithostratigraphic boundaries.

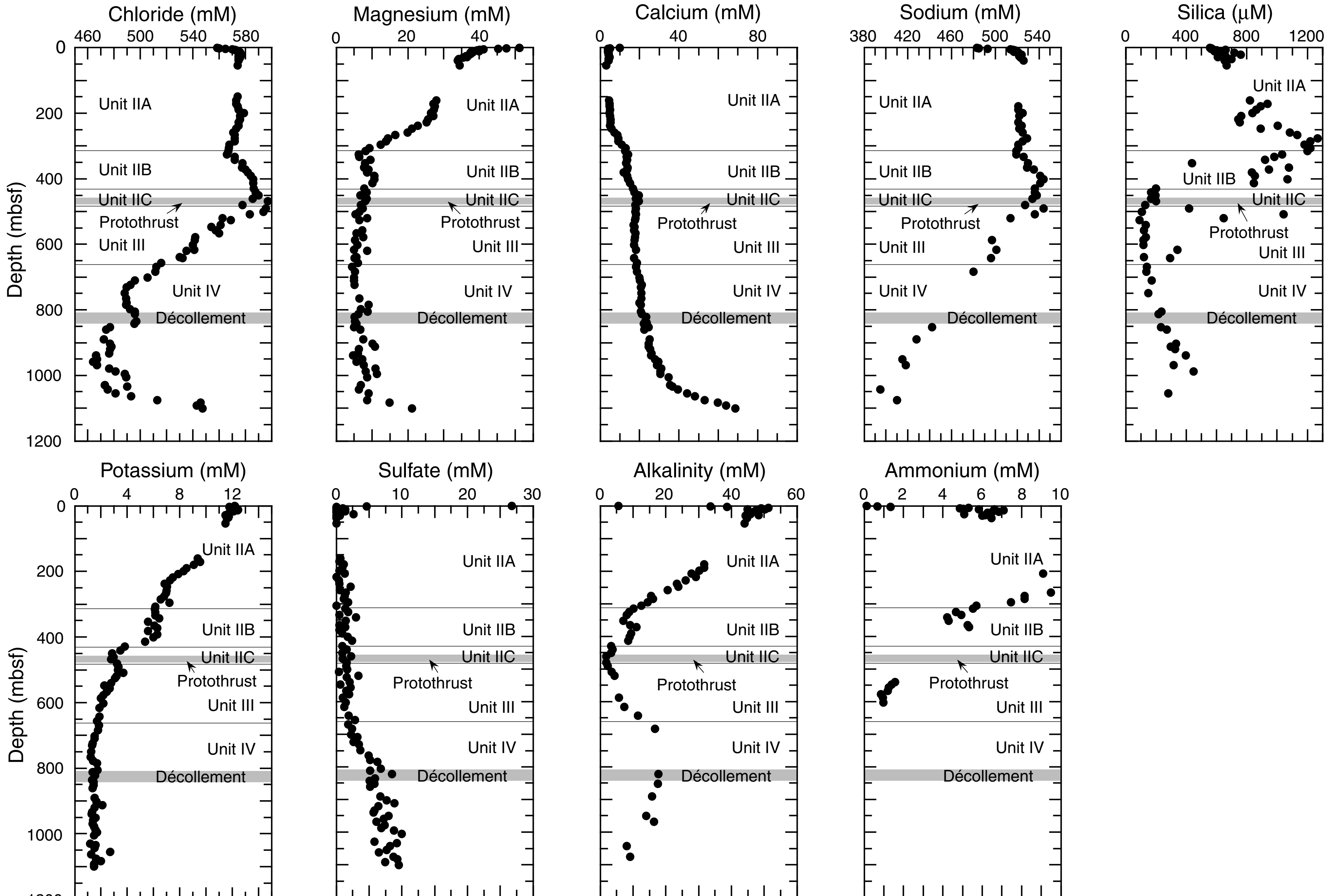

Figure F34. Molecular compositions and concentrations of headspace gases at Site 1174. **A.** Methane concentrations. **B.** Ethane concentrations. **C.** Propane concentrations. Gas concentrations are given in parts per million.

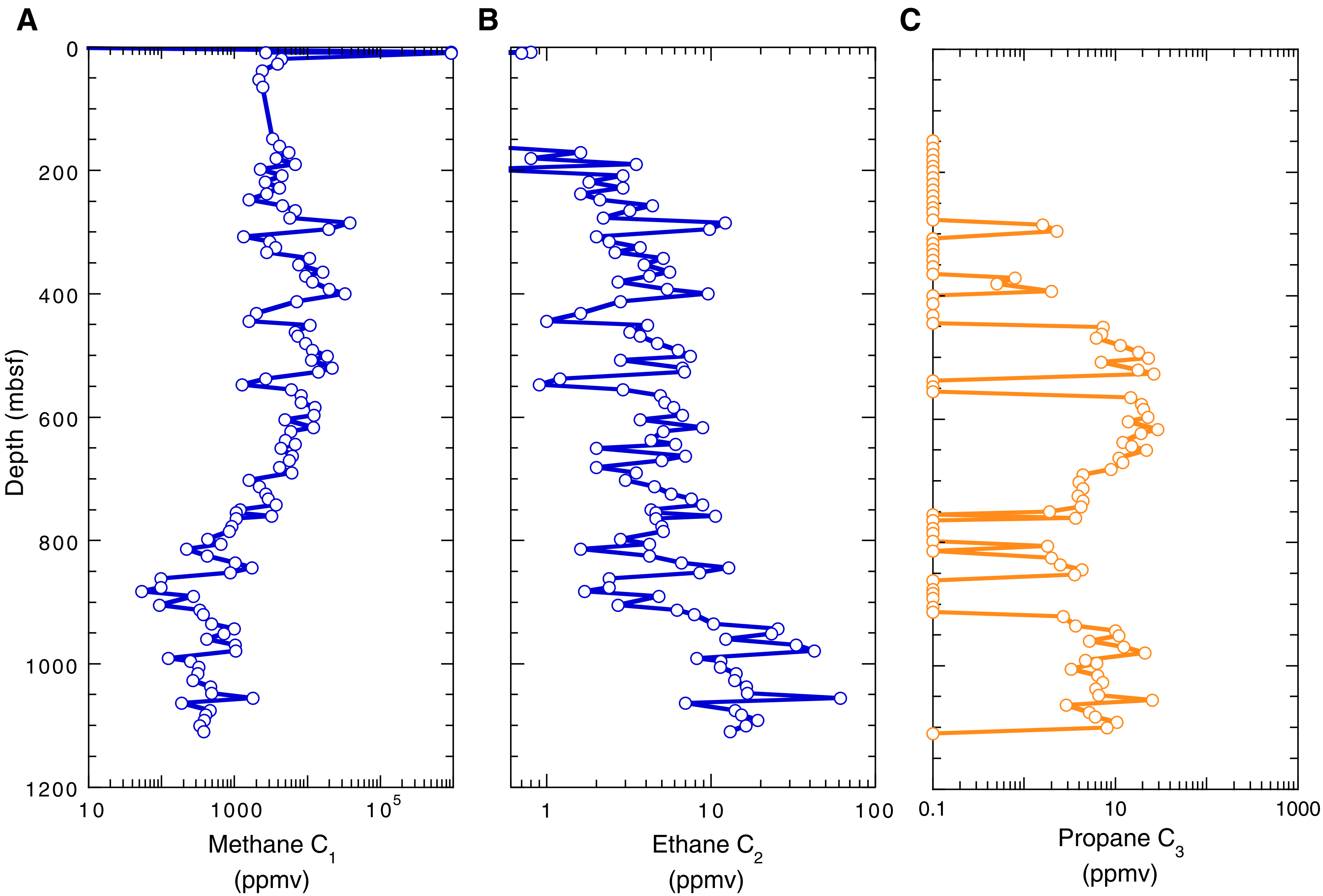

Figure F35. Total carbon and nitrogen contents in sediments from Site 1174 and the percentage of inorganic carbon (carbonate) in sediments. **A.** Total organic carbon (TOC) ranges from 0.2 to 1.5 wt% in Hole 1174A. **B.** Nitrogen contents are low, reaching zero at 1020 mbsf. **C.** Carbonate concentrations are low but increase sharply below 900 mbsf, consistent with the observation of carbonate nodules in the cores.

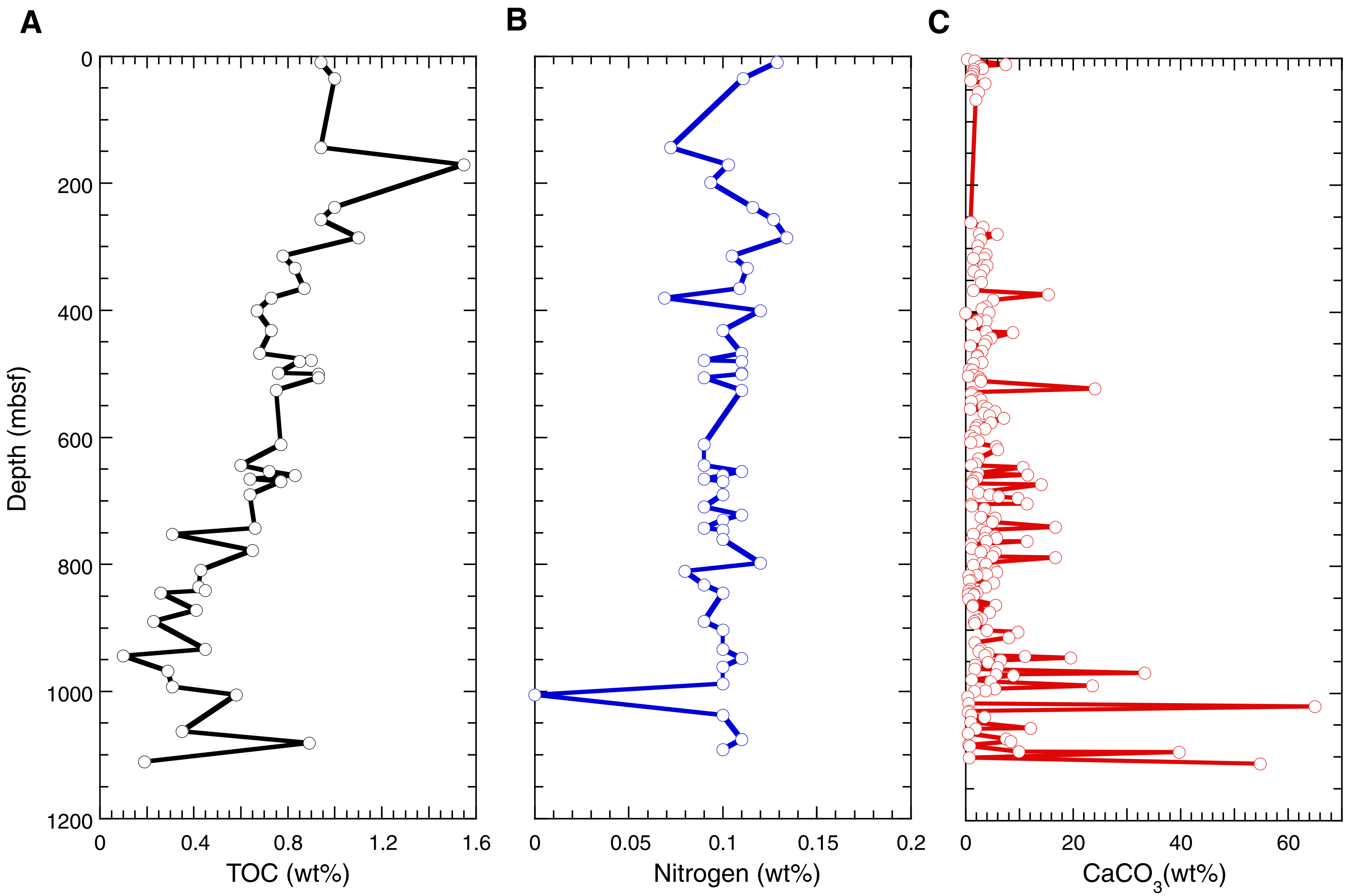

Figure F36. Bernard ratio for $C_1/(C_2+C_3)$ with increasing depth and present-day temperature (inferred temperature from in situ measurements) at Site 1174.

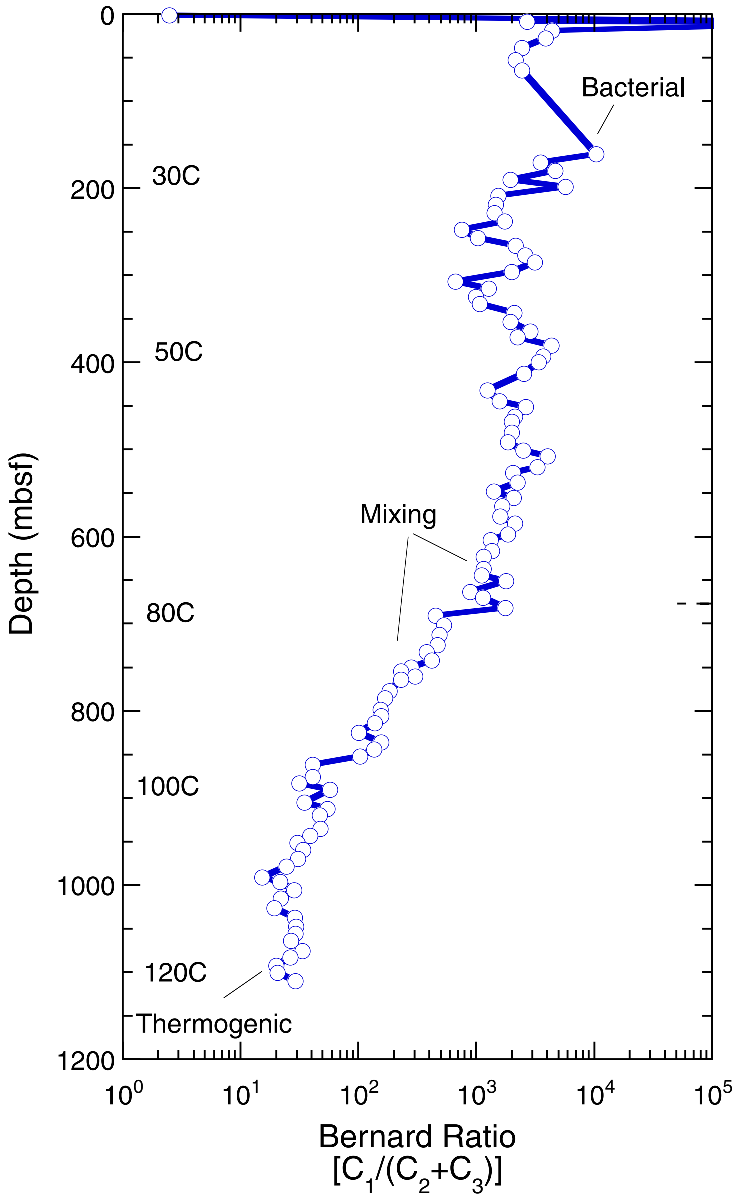

Figure F37. Depth and temperature distribution of total bacterial populations in sediment samples from Holes 1174A and 1174B. The curved dashed line represents a general regression line of bacterial numbers vs. depth in deep-sea sediments (Parkes et al., 1994), with 95% upper and lower prediction limits shown by the curved lines of longer dashes. The shaded area to the left of the figure indicates levels where bacterial populations are too low to be detected with the acridine orange direct counts technique; the detection limit was 6 × 10^4 cells/cm^3 (any values within this area are constructed from sums of three enumerations and have no measure of error). The two horizontal lines separate bacterial groups with different temperature ranges for growth.

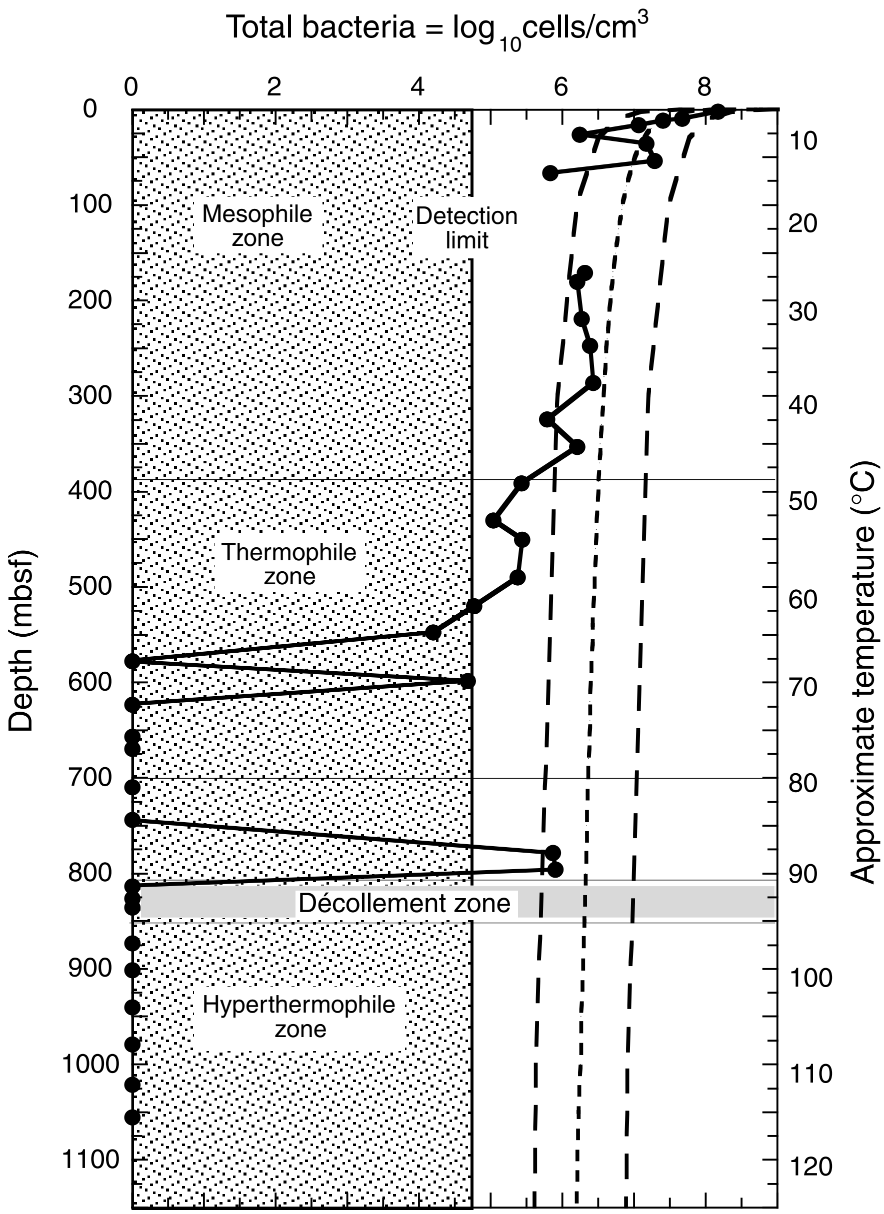

Figure F38. **A.** Site 1174 bulk-density measurements. Lithostratigraphic Units II (outer trench wedge), III (upper Shikoku Basin), and IV (lower Shikoku Basin) are indicated. **B.** MST GRA and mass/volume bulk density. **C.** Grain density. **D.** Porosity.

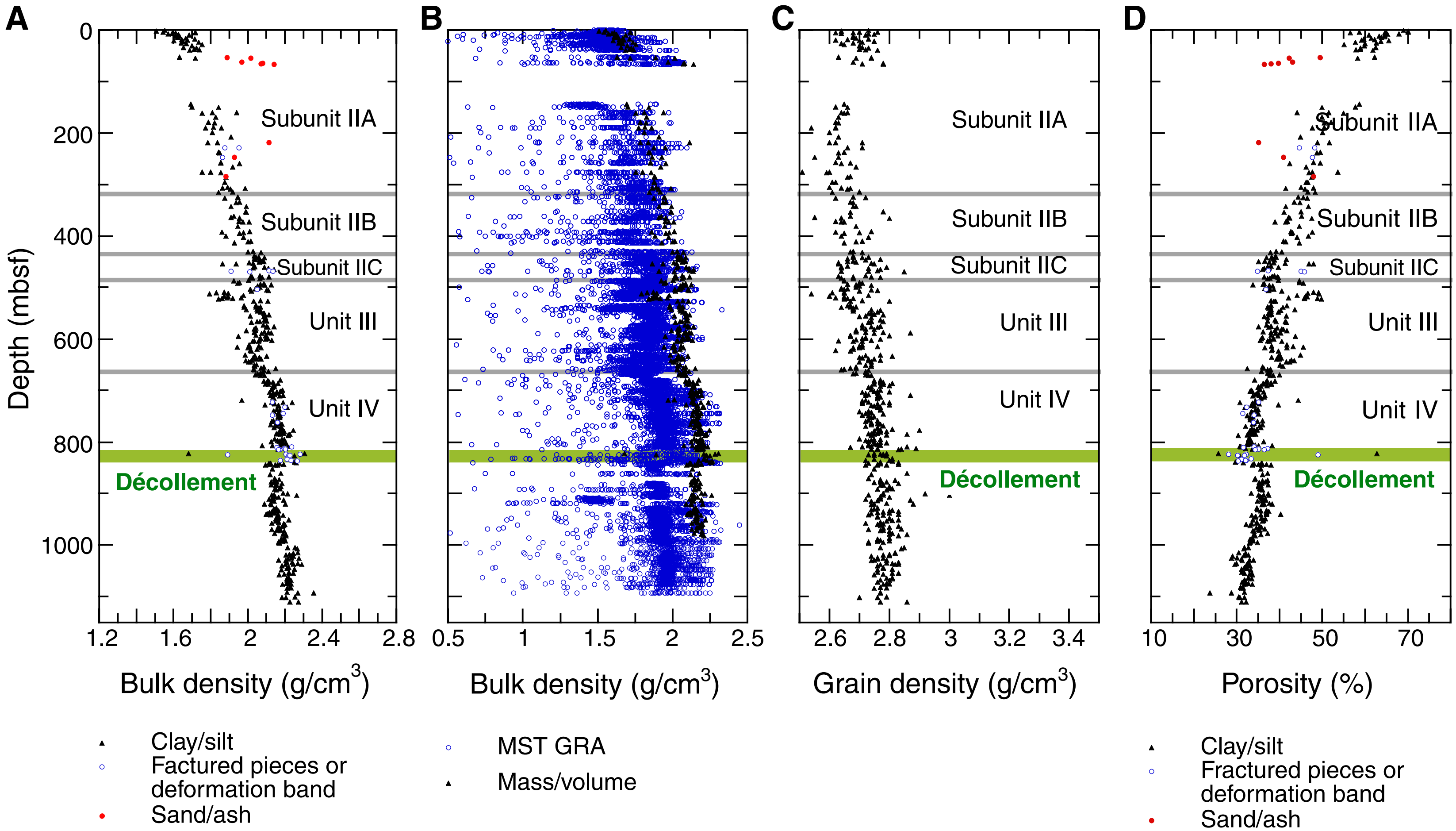

Figure F39. Porosities below the décollement zone at Sites 1174 and 808 and below the age equivalent of the décollement zone at Site 1173.

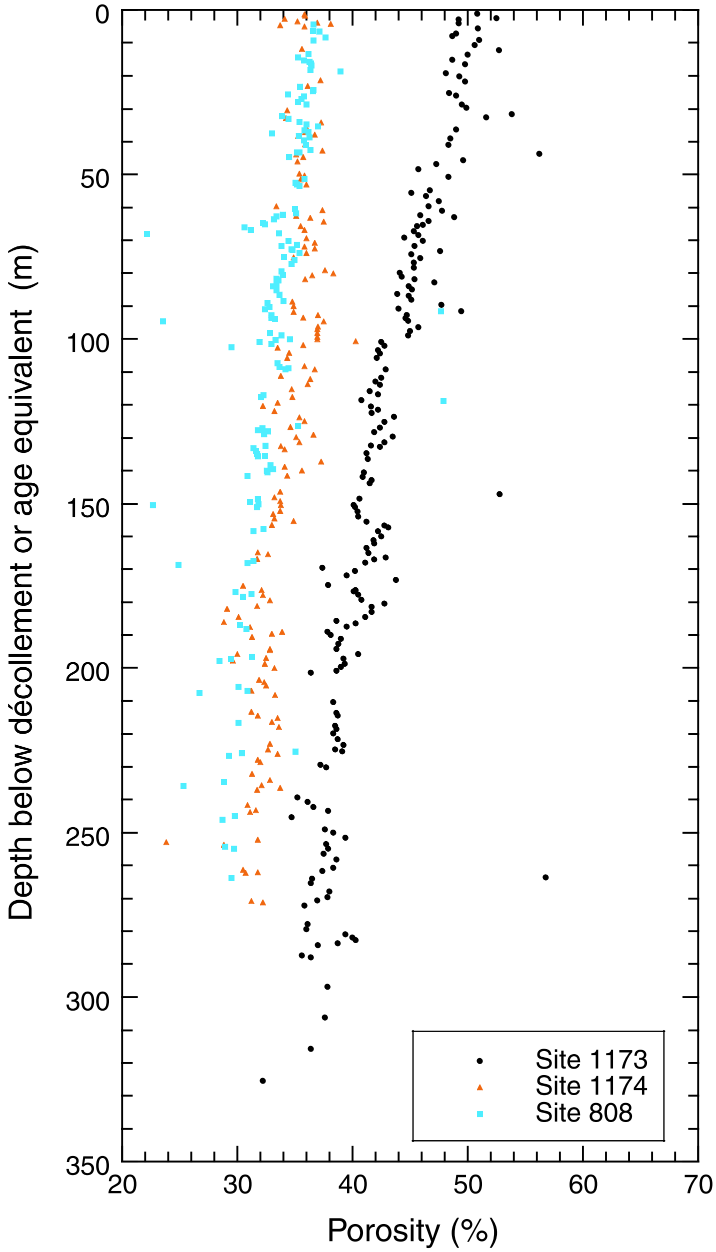

Figure F40. A. Site 1174 thermal conductivity. **B.** Observed (triangles) and projected (dashed line) temperatures.

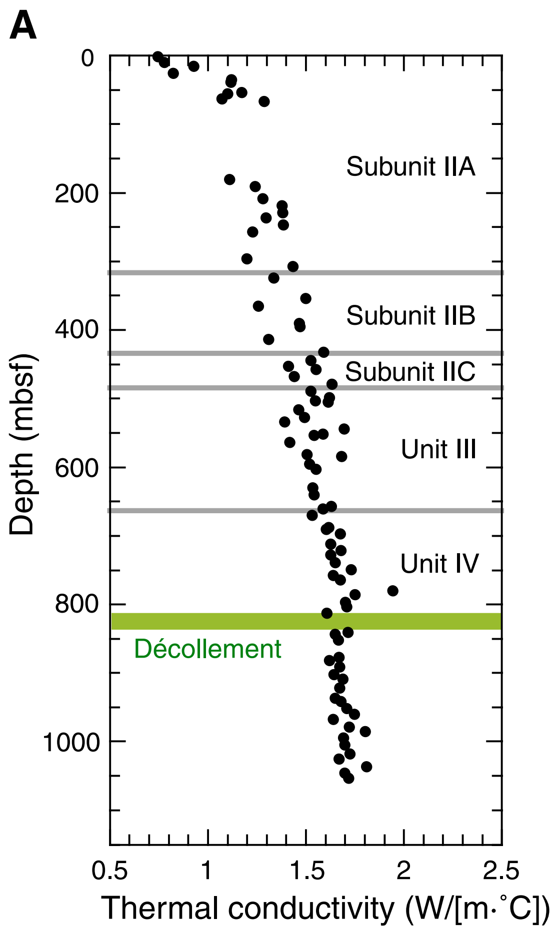

Figure F41. **A.** *P*-wave velocity and bulk density at Site 1174. (Continued on next page.)

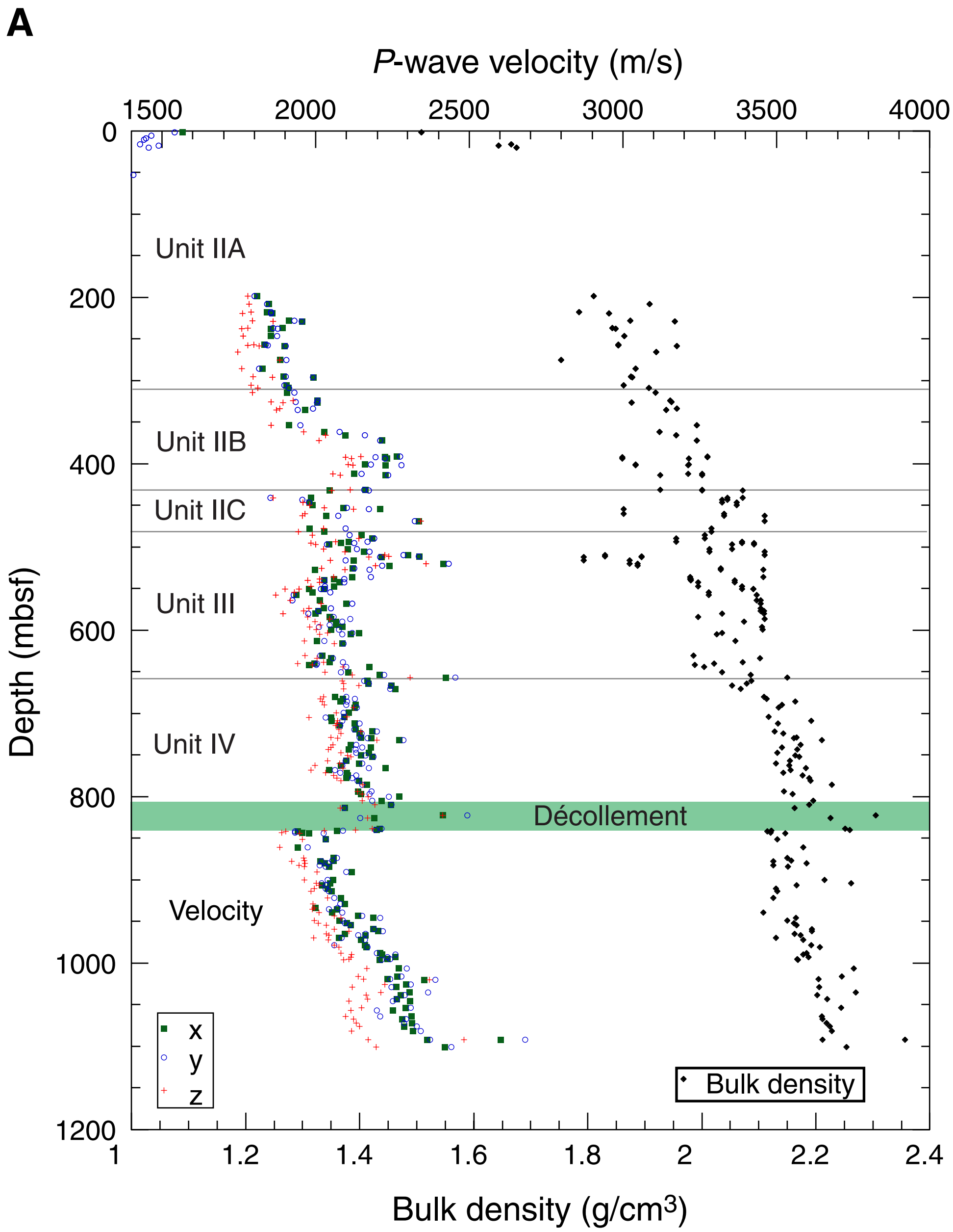

Figure F41 (continued). B. Horizontal and vertical *P*-wave velocity as a function of porosity. The line represents a typical relationship for clayey silt computed from a weighted average equation using a matrix velocity of 4500 m/s and a weighting parameter of 1.1 (Lee et al., 1996). **C.** *P*-wave velocity anisotropy. The vertical plane anisotropy compares velocity along the two transverse axes (x and y) to that parallel to the core (z), whereas the horizontal plane anisotropy compares velocity of the x- and y-axes. Because cores are randomly rotated, horizontal plane anisotropy should average zero.

B

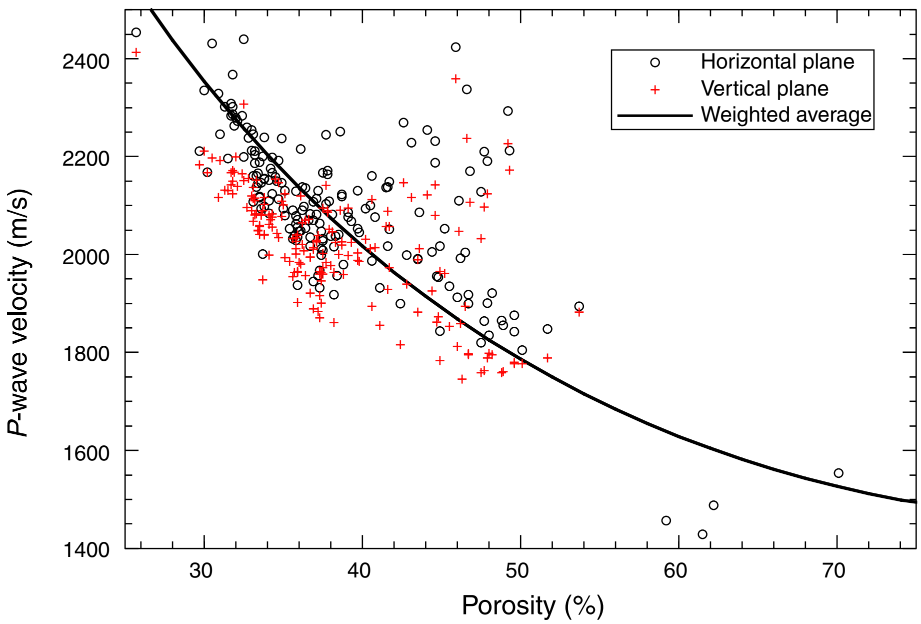

C

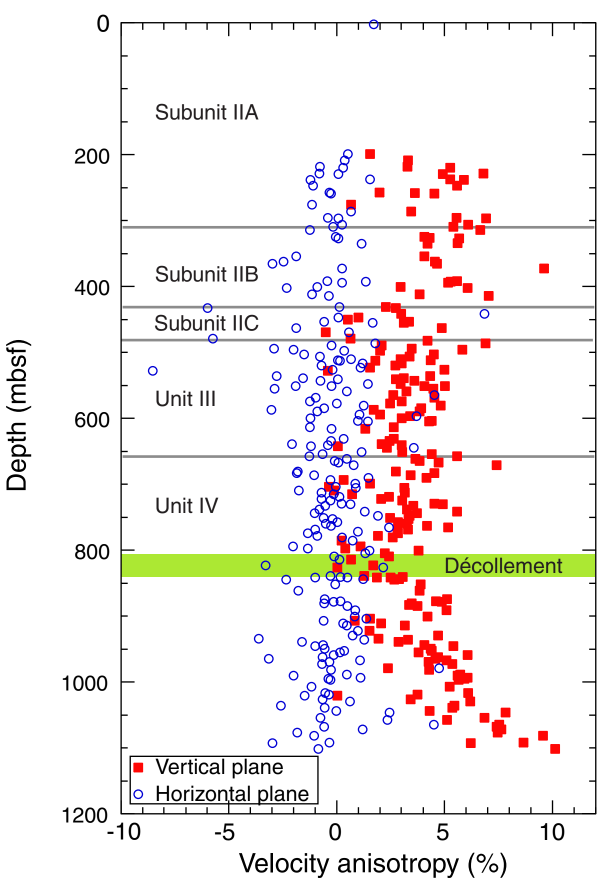

Figure F42. A. Formation factor measured with the needle-probe method on APC cores at Site 1174. **B.** All measurements. Measurements on cut samples were performed in the x- and y- (orthogonal to core) and z- (parallel to core) directions. **C.** Anisotropy of electrical conductivity in the horizontal (x- and y-axes) and vertical (z-axis) planes.

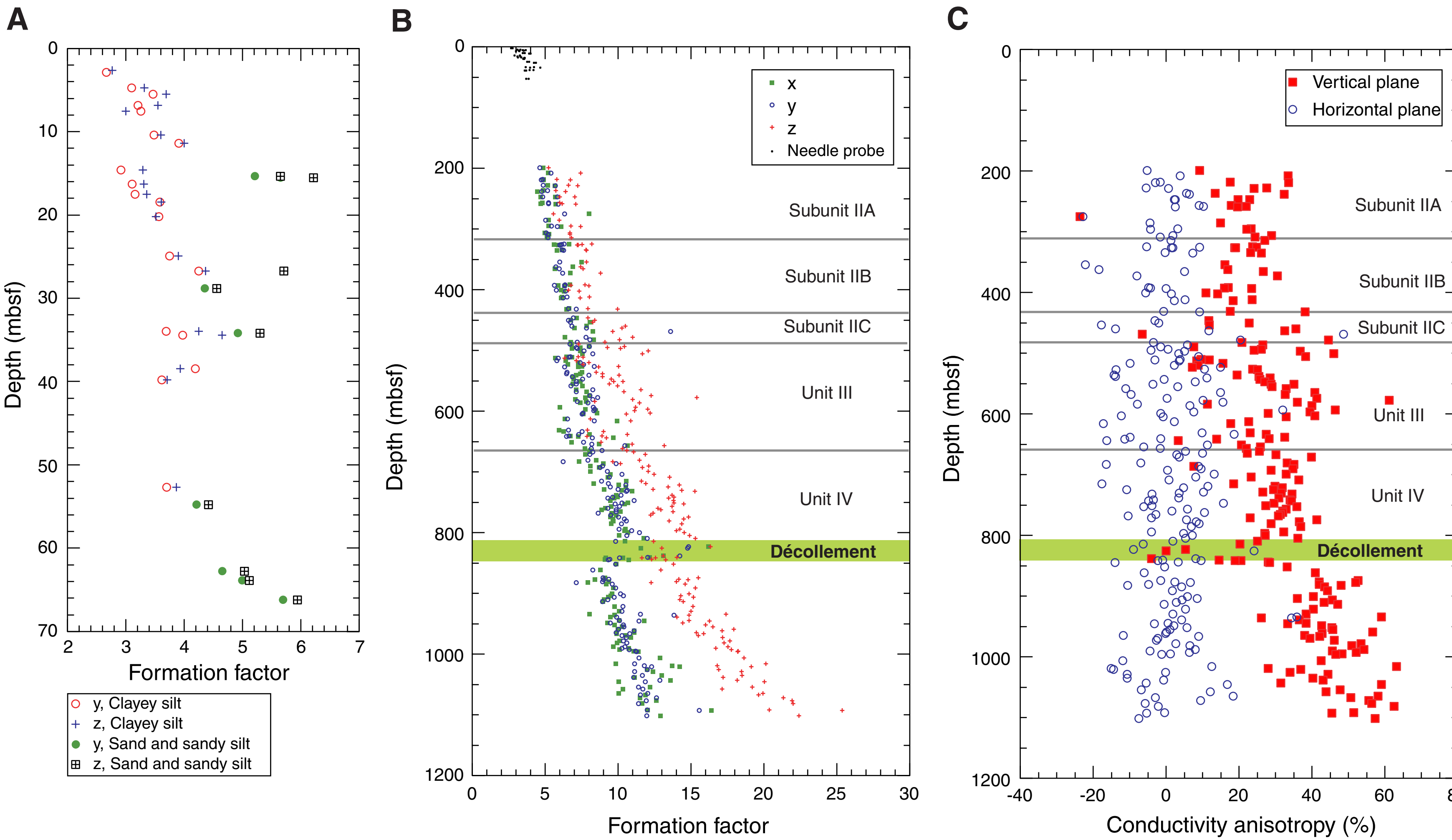

Figure F43. Site 1174 magnetic susceptibility.

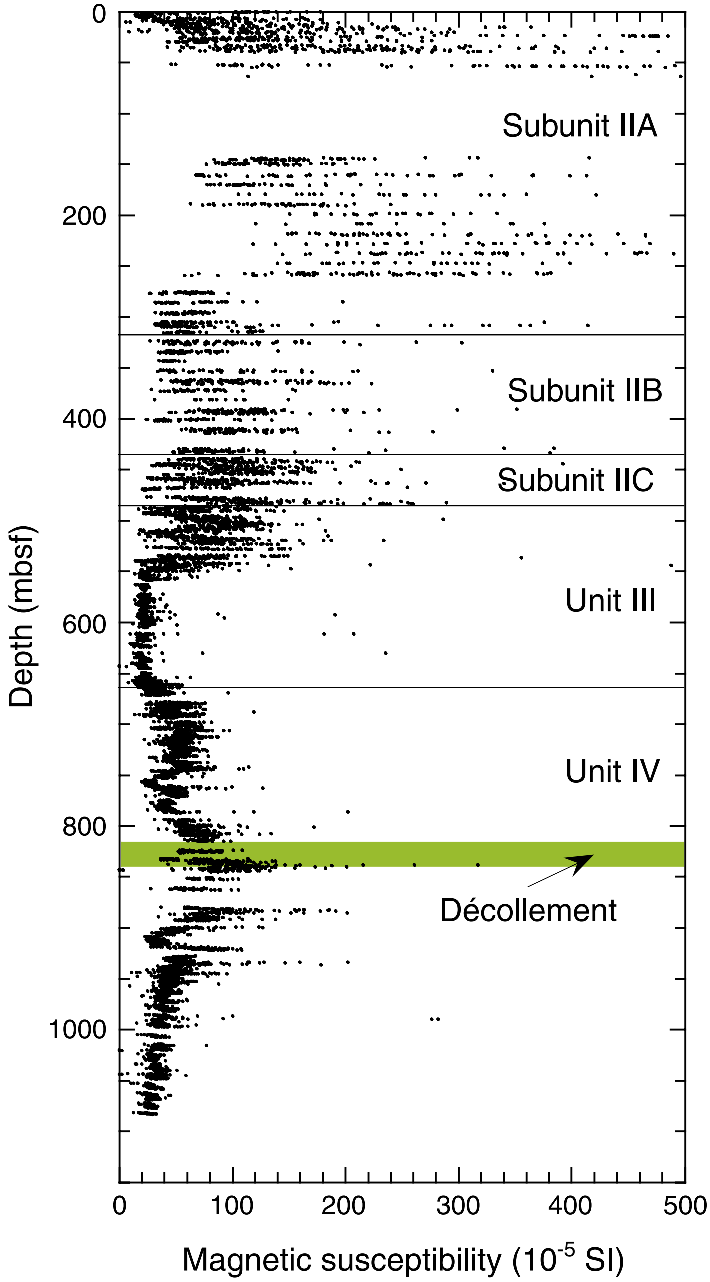

Figure F44. Temperatures measured during the deployment of the Adara temperature tool in Hole 1174A. The dashed line indicates extrapolated in situ temperature. Note that values after 64 min were not used for the extrapolation because of noise. The solid line indicates the mudline temperature.

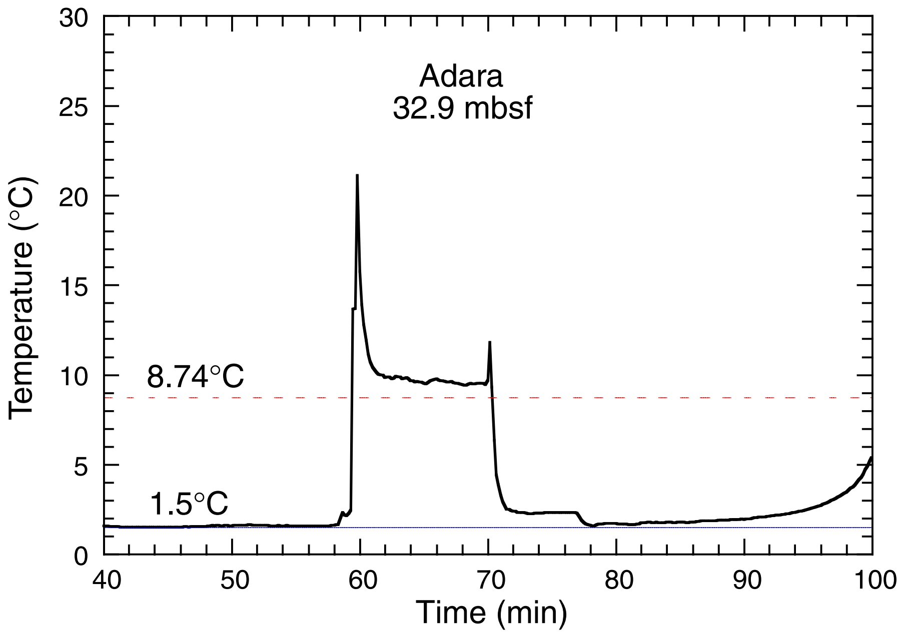

Figure F45. Temperatures measured during the DVTP station below Core 190-1174A-8H. The dashed line indicates extrapolated in situ temperature.

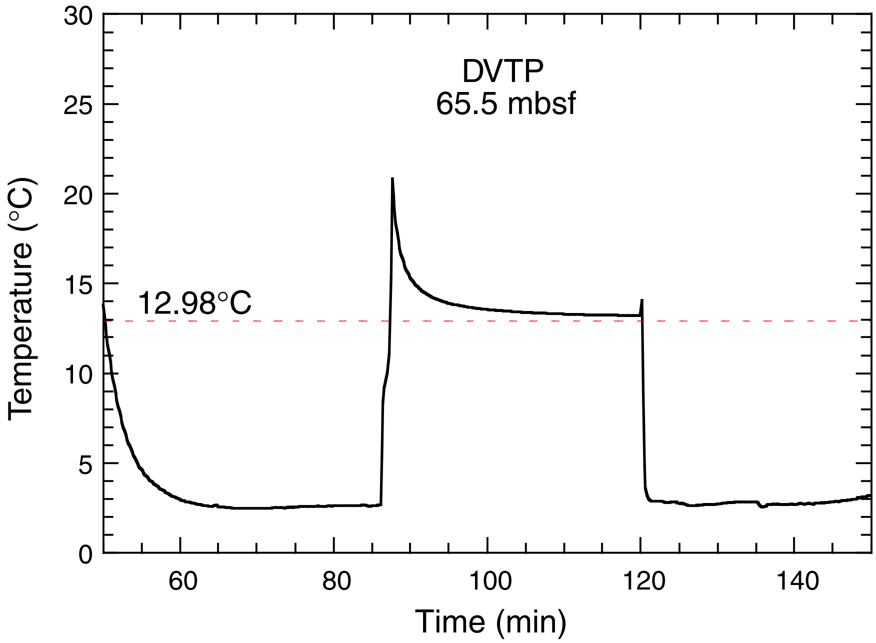

Figure F46. Measured temperatures at Hole 1174A.

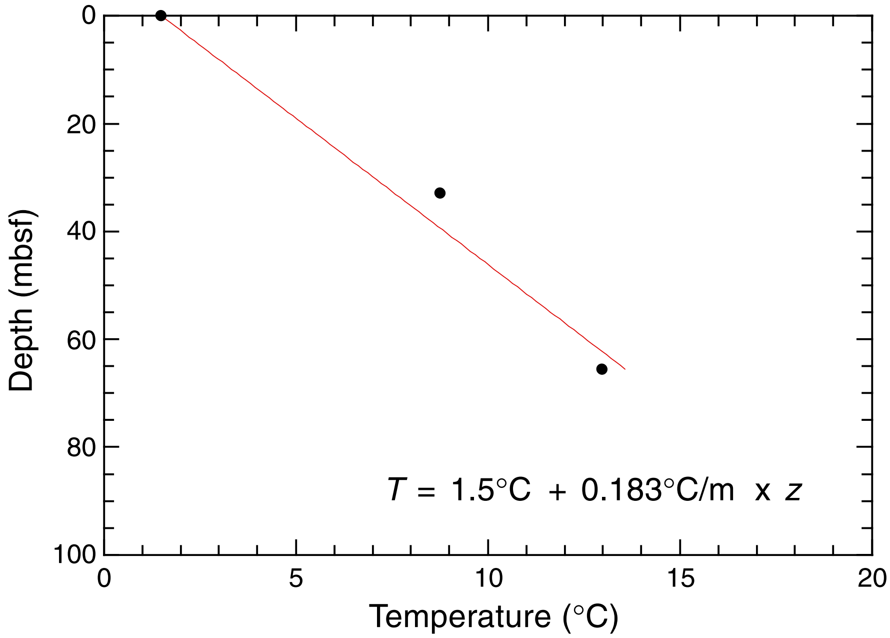

Figure F47. Pressures measured during the DVTP-P station after Core 190-1174A-8H.

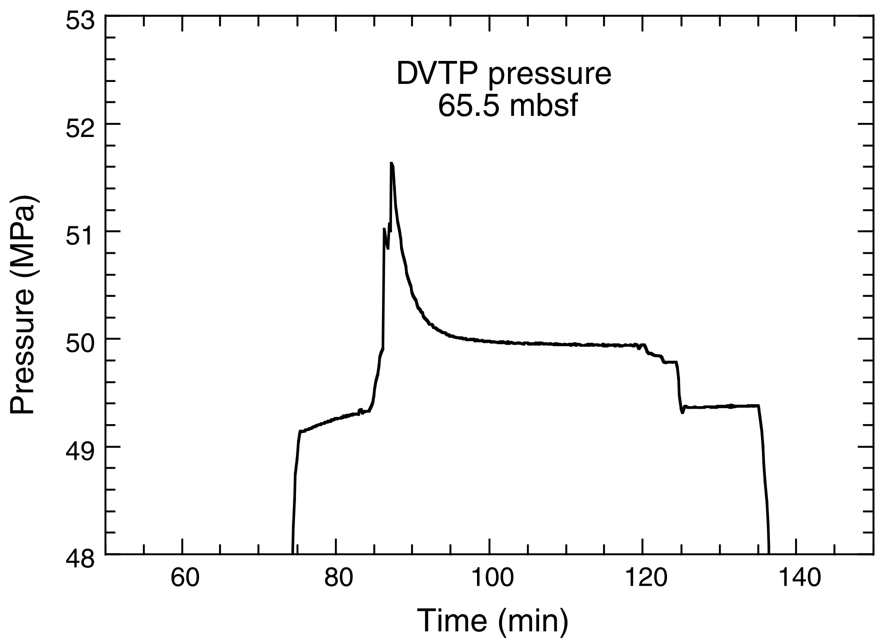

Figure F48. Three-dimensional seismic reflection line 281 across Site 1174. This line has been 3-D stacked and migrated.

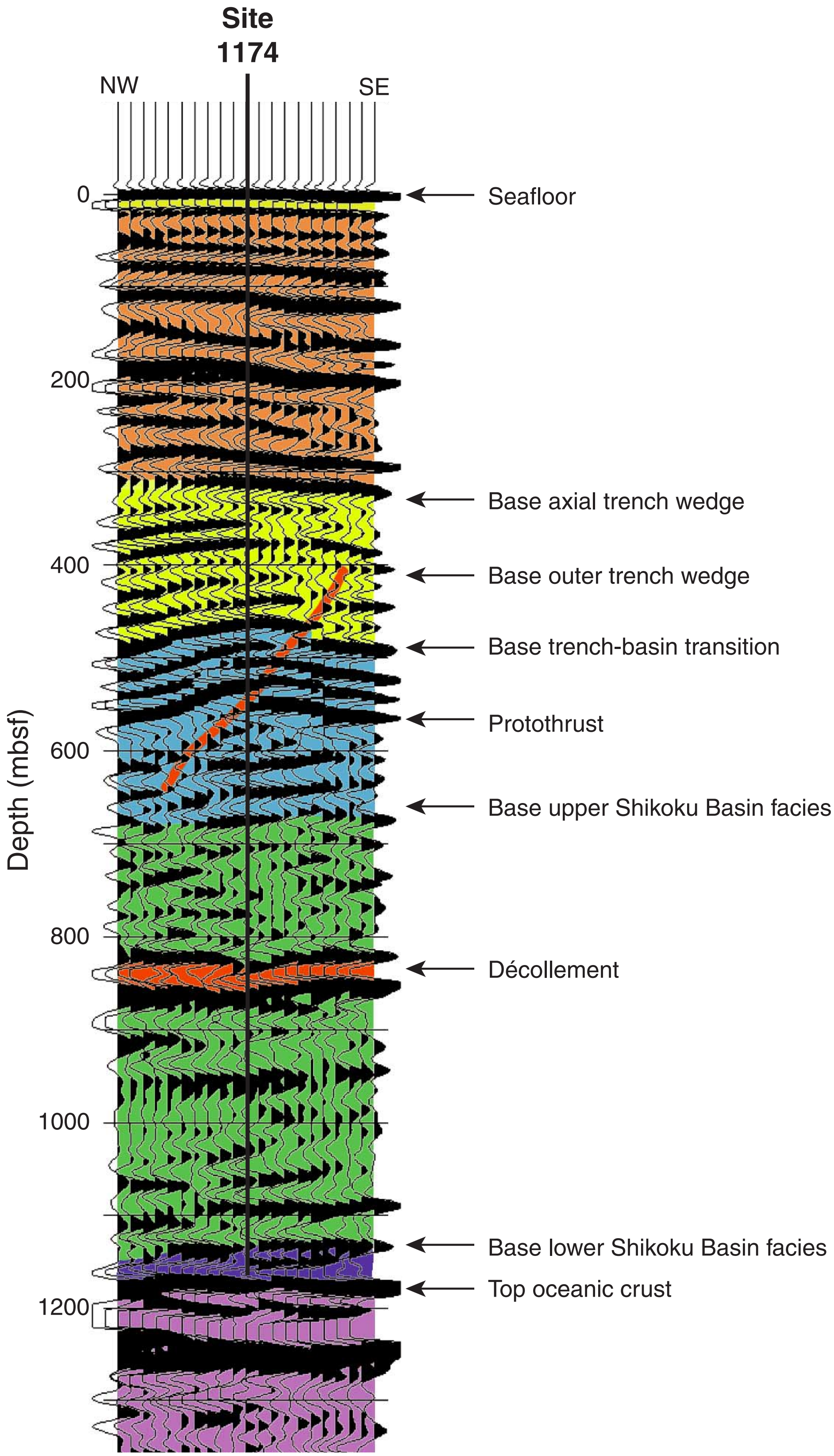

Table T1. Coring summary, Site 1174. (See table note. Continued on next page.)

Core	Date (June 2000)	Time (local)	Depth (mbsf) Top	Depth (mbsf) Bottom	Length (m) Cored	Length (m) Recovered	Recovery (%)	Comments
190-1174A-								
1H	7	1800	0.0	4.4	4.4	4.40	100.0	
2H	7	1925	4.4	13.9	9.5	9.59	100.9	
3H	7	2040	13.9	23.4	9.5	8.44	88.8	Tensor at 19:20. Expanding core: gassy voids throughout
4H	7	2225	23.4	32.9	9.5	7.38	77.7	
5H	7	2340	32.9	42.4	9.5	7.43	78.2	
6H	8	0100	42.4	51.9	9.5	0.00	0.0	Whirl-Pak, tracer
7H	8	0220	51.9	61.4	9.5	3.59	37.8	Whirl-Pak, tracer
8H	8	0415	61.4	64.4	3.0	6.21	207.0	DVTP at 4826.9 m
9X	9	0045	64.4	74.1	9.7	0.00	0.0	Core barrel jammed; end hole
				Totals:	74.1	47.04	63.4	
190-1174B-								
10	10	1830	0.0	143.7	0.0	0.00	N/A	Drill-in casing to 4906.17 m
1R	12	0730	143.7	150.1	6.4	9.62	150.3	AHC on
2R	12	1005	150.1	159.7	9.6	0.60	6.2	Run DVPT sample at 4922.17 m; AHC on
3R	12	1415	159.7	169.4	9.7	2.39	24.6	AHC on
4R	12	1630	169.4	179.0	9.6	2.31	24.1	Whirl-Pak, tracer, AHC on
5R	12	1820	179.0	188.7	9.7	1.97	20.3	Whirl-Pak, tracer, AHC on
6R	12	1945	188.7	198.4	9.7	2.39	24.6	AHC on
7R	12	2130	198.4	208.0	9.6	1.47	15.3	DVTP at 4970.5 m; AHC on
8R	13	0030	208.0	217.7	9.7	0.95	9.8	AHC on
9R	13	0210	217.7	227.2	9.5	2.79	29.4	AHC on
10R	13	0400	227.2	236.8	9.6	2.30	24.0	AHC on
11R	13	0520	236.8	246.5	9.7	2.53	26.1	AHC on
12R	13	0705	246.5	256.2	9.7	1.74	17.9	AHC on
13R	13	0900	256.2	265.8	9.6	3.69	38.4	AHC on
14R	13	1710	265.8	275.5	9.7	0.50	5.2	AHC on
15R	13	1925	275.5	285.1	9.6	2.28	23.7	AHC on
16R	13	2130	285.1	294.6	9.5	1.80	18.9	AHC on
17R	13	2350	294.6	304.3	9.7	2.88	29.7	AHC on
18R	14	0205	304.3	314.0	9.7	6.17	63.6	AHC on
19R	14	0410	314.0	323.5	9.5	2.22	23.4	AHC on
20R	14	0625	323.5	333.1	9.6	3.89	40.5	AHC on
21R	14	0830	333.1	342.4	9.3	2.85	30.6	AHC on
22R	14	1045	342.4	352.0	9.6	1.34	14.0	AHC on
23R	14	1245	352.0	361.7	9.7	2.49	25.7	AHC on
24R	14	1455	361.7	371.3	9.6	4.72	49.2	AHC on
25R	14	1655	371.3	380.9	9.6	2.20	22.9	AHC on
26R	14	1910	380.9	390.5	9.6	0.84	8.7	AHC on
27R	14	2120	390.5	400.2	9.7	5.12	52.8	AHC on
28R	14	2345	400.2	409.8	9.6	2.32	24.2	AHC on
29R	15	200	409.8	419.4	9.6	4.94	51.5	AHC on
30R	15	415	419.4	429.0	9.6	0.18	1.9	AHC on
31R	15	630	429.0	438.6	9.6	4.62	48.1	Whirl-Pak, tracer, AHC on
32R	15	920	438.6	448.2	9.6	9.55	99.5	Whirl-Pak, tracer, AHC on
33R	15	1150	448.2	457.9	9.7	7.16	73.8	AHC on
34R	15	1420	457.9	467.1	9.2	7.25	78.8	AHC on
35R	15	1645	467.1	476.5	9.4	2.85	30.3	AHC on
36R	15	1850	476.5	485.7	9.2	7.49	81.4	AHC on
37R	15	2050	485.7	495.3	9.6	9.21	95.9	AHC on
38R	15	2310	495.3	504.9	9.6	9.73	101.4	AHC on
39R	16	0125	504.9	514.6	9.7	8.31	85.7	AHC on
40R	16	1305	514.6	524.3	9.7	9.21	94.9	
41R	16	2200	524.3	533.9	9.6	4.89	50.9	
42R	17	0105	533.9	543.6	9.7	9.76	100.6	
43R	17	0315	543.6	552.9	9.3	9.13	98.2	
44R	17	0525	552.9	562.6	9.7	5.79	59.7	
45R	17	0715	562.6	572.3	9.7	5.75	59.3	
46R	17	0920	572.3	581.9	9.6	9.44	98.3	
47R	17	1115	581.9	591.6	9.7	8.79	90.6	
48R	17	1325	591.6	601.2	9.6	9.98	104.0	
49R	17	1510	601.2	610.9	9.7	4.14	42.7	
50R	17	1705	610.9	620.5	9.6	7.19	74.9	
51R	17	1850	620.5	630.1	9.6	3.85	40.1	
52R	17	2045	630.1	639.8	9.7	9.31	96.0	
53R	17	2230	639.8	649.4	9.6	5.90	61.5	
54R	18	0030	649.4	659.0	9.6	9.84	102.5	
55R	18	0230	659.0	668.7	9.7	9.08	93.6	

Table T1 (continued).

Core	Date (June 2000)	Time (local)	Depth (mbsf) Top	Depth (mbsf) Bottom	Length (m) Cored	Length (m) Recovered	Recovery (%)	Comments
56R	18	0435	668.7	678.3	9.6	2.91	30.3	
57R	18	0640	678.3	688.0	9.7	9.93	102.4	
58R	18	0845	688.0	697.6	9.6	6.44	67.1	
59R	18	1050	697.6	707.2	9.6	8.85	92.2	
60R	18	1250	707.2	716.9	9.7	8.61	88.8	
61R	18	1455	716.9	726.5	9.6	9.91	103.2	
62R	18	1640	726.5	736.1	9.6	7.18	74.8	
63R	18	1835	736.1	745.7	9.6	9.97	103.9	
64R	18	2040	745.7	755.0	9.3	7.42	79.8	
65R	18	2230	755.0	764.6	9.6	9.93	103.4	
66R	19	0030	764.6	774.2	9.6	7.17	74.7	
67R	19	0240	774.2	783.9	9.7	9.96	102.7	
68R	19	0445	783.9	793.6	9.7	3.74	38.6	
69R	19	0650	793.6	803.3	9.7	9.89	102.0	
70R	19	0900	803.3	812.5	9.2	7.82	85.0	
71R	19	1135	812.5	822.2	9.7	2.99	30.8	Firm at 5578 m (815.5 mbsf)
72R	19	1415	822.2	831.8	9.6	5.05	52.6	
73R	19	1645	831.8	841.4	9.6	9.88	102.9	
74R	19	1840	841.4	851.0	9.6	3.89	40.5	
75R	19	2025	851.0	860.7	9.7	1.91	19.7	
76R	19	2240	860.7	870.4	9.7	2.77	28.6	
77R	20	0025	870.4	880.0	9.6	8.22	85.6	
78R	20	0235	880.0	889.3	9.3	7.13	76.7	
79R	20	0450	889.3	899.0	9.7	4.38	45.2	
80R	20	0645	899.0	908.6	9.6	8.60	89.6	
81R	20	0830	908.6	918.3	9.7	7.90	81.4	
82R	20	1010	918.3	927.9	9.6	4.16	43.3	
83R	20	1220	927.9	937.5	9.6	9.93	103.4	
84R	20	1415	937.5	947.1	9.6	9.05	94.3	
85R	20	1605	947.1	956.8	9.7	8.83	91.0	
86R	20	1800	956.8	966.5	9.7	8.99	92.7	
87R	20	2010	966.5	976.1	9.6	7.30	76.0	
88R	20	2210	976.1	985.3	9.2	5.87	63.8	
89R	21	0010	985.3	994.9	9.6	9.88	102.9	AHC on
90R	21	0210	994.9	1004.6	9.7	3.06	31.5	AHC on
91R	21	0430	1004.6	1014.2	9.6	3.28	34.2	AHC on
92R	21	0640	1014.2	1023.9	9.7	8.20	84.5	AHC on
93R	21	0855	1023.9	1033.5	9.6	7.18	74.8	AHC on
94R	21	1135	1033.5	1043.1	9.6	7.43	77.4	AHC on
95R	21	1345	1043.1	1052.6	9.5	5.84	61.5	AHC on
96R	21	1540	1052.6	1062.3	9.7	6.03	62.2	AHC on
97R	21	1755	1062.3	1071.9	9.6	6.92	72.1	AHC on
98R	21	2010	1071.9	1081.5	9.6	5.37	55.9	AHC on
99R	21	2225	1081.5	1091.2	9.7	2.50	25.8	AHC on
100R	22	0045	1091.2	1100.8	9.6	2.77	28.9	AHC on
101R	22	0325	1100.8	1110.2	9.4	1.71	18.2	
102R	22	0605	1110.2	1119.8	9.6	1.11	11.6	
			**** Drilled from 0 to 143.7 mbsf ****					
				Totals:	976.1	577.57	59.2	

Note: DVTP = Davis-Villinger temperature probe, AHC = advanced hydraulic piston corer.

Table T2. Coring summary by section, Site 1174. (See table notes. Continued on next 11 pages.)

Core	Date (June 2000)	Time (local)	Core depth (mbsf) Top	Core depth (mbsf) Bottom	Length (m) Cored	Length (m) Recovered	Recovery (%)	Section	Length (m) Liner	Length (m) Curated	Section depth (mbsf) Top	Section depth (mbsf) Bottom	Catwalk samples
190-1174A-													
1H	7	1800	0.0	4.4	4.4	4.4	100						
								1	1.5	1.5	0.0	1.5	HS, IW
								2	1.5	1.5	1.5	3	IW, WRC, WRY, WRS
								3	1.19	1.19	3.0	4.19	IW, BGAS
								CC(w/3)	0.21	0.21	4.19	4.4	PAL, PAL
								Totals:	4.4	4.4			
2H	7	1925	4.4	13.9	9.5	9.59	100.9						
								1	0.29	0.29	4.4	4.69	
								2	1.5	1.5	4.69	6.19	BACT, WRY, IW
								3	1.5	1.5	6.19	7.69	IW
								4	1.5	1.5	7.69	9.19	IW, VAC
								5	1.5	1.5	9.19	10.69	HS, IW, VAC, BGAS
								6	1.5	1.5	10.69	12.19	BACT, IW, WRY
								7	1.5	1.5	12.19	13.69	IW
								CC(w/CC)	0.3	0.3	13.69	13.99	PAL
								Totals:	9.59	9.59			
3H	7	2040	13.9	23.4	9.5	8.44	88.8						
								1	1.5	1.5	13.9	15.4	
								2	1.23	1.23	15.4	16.63	BACT, IW
								3	1.21	1.21	16.63	17.84	
								4	1.5	1.5	17.84	19.34	IW
								5	1.2	1.2	19.34	20.54	HS, BGAS
								6	1.05	1.05	20.54	21.59	IW
								7	0.61	0.61	21.59	22.2	
								CC(w/7)	0.14	0.14	22.2	22.34	PAL
								Totals:	8.44	8.44			
4H	7	2225	23.4	32.9	9.5	7.38	77.7						
								1	1.5	1.5	23.4	24.9	
								2	1.5	1.5	24.9	26.4	BACT, IW
								3	1.5	1.5	26.4	27.9	
								4	1.5	1.5	27.9	29.4	IW, HS
								5	1.05	1.05	29.4	30.45	IW, BGAS
								CC(w/5)	0.33	0.33	30.45	30.78	PAL
								Totals:	7.38	7.38			
5H	7	2340	32.9	42.4	9.5	7.43	78.2						
								1	1.5	1.5	32.9	34.4	
								2	1.5	1.5	34.4	35.9	IW, BACT
								3	1.5	1.5	35.9	37.4	
								4	1.5	1.5	37.4	38.9	BGAS, IW
								5	0.59	0.59	38.9	39.49	HS
								CC(w/5)	0.84	0.84	39.49	40.33	PAL
								Totals:	7.43	7.43			
6H	8	0100	42.4	51.9	9.5	0.0	0.0						
								1	0.0	0.0			
								Totals:	0.0	0.0			
7H	8	0220	51.9	61.4	9.5	3.59	37.8						
								1	1.0	1.0	51.9	52.9	
								2	1.5	1.5	52.9	54.4	HS, IW, BGAS, SMTC
								3	0.37	0.37	54.4	54.77	
								4	0.53	0.53	54.77	55.3	
								CC(w/4)	0.19	0.19	55.3	55.49	PAL
								Totals:	3.59	3.59			
8H	8	0415	61.4	64.4	3.0	6.21	207						
								1	0.88	0.88	61.4	62.28	
								2	1.35	1.35	62.28	63.63	
								3	1.5	1.5	63.63	65.13	
								4	1.5	1.5	65.13	66.63	HS, IW, BGAS
								5	0.8	0.8	66.63	67.43	
								CC(w/5)	0.18	0.18	67.43	67.61	PAL
								Totals:	6.21	6.21			
9X	9	0045	64.4	74.1	9.7	0.0	0.0						
				Totals:	74.1	47.04	63.4						
190-1174B-													
10	10	1830	0.0	143.7	0.0	0.0	N/A						

Table T2 (continued).

Core	Date (June 2000)	Time (local)	Core depth (mbsf)		Length (m)		Recovery (%)	Section	Length (m)		Section depth (mbsf)		Catwalk samples
			Top	Bottom	Cored	Recovered			Liner	Curated	Top	Bottom	
1R	12	0730	143.7	150.1	6.4	9.62	150.3						
								1	1.5	1.5	143.7	145.2	
								2	1.26	1.26	145.2	146.46	
								3	1.5	0.0			
								4	1.5	1.5	146.46	147.96	
								5	1.5	0.67	147.96	148.63	
								6	1.5	1.5	148.63	150.13	HS, IW, BGAS
								7	0.46	0.46	150.13	150.59	PAL
								CC(w/7)	0.4	0.4	150.59	150.99	
								Totals:	9.62	7.29			
2R	12	1005	150.1	159.7	9.6	0.6	6.3						
								1	0.48	0.48	150.1	150.58	HS, BGAS
								CC(w/1)	0.12	0.12	150.58	150.7	PAL, IW
								Totals:	0.6	0.6			
3R	12	1415	159.7	169.4	9.7	2.39	24.6						
								1	1.5	1.5	159.7	161.2	IW, BGAS
								2	0.69	0.69	161.2	161.89	HS
								CC(w/2)	0.2	0.2	161.89	162.09	PAL
								Totals:	2.39	2.39			
4R	12	1630	169.4	179.0	9.6	2.31	24.1						
								1	1.5	1.5	169.4	170.9	BACT, SMTCR
								2	0.61	0.61	170.9	171.51	HS, IW
								CC(w/2)	0.2	0.2	171.51	171.71	PAL
								Totals:	2.31	2.31			
5R	12	1820	179.0	188.7	9.7	1.97	20.3						
								1	1.5	1.5	179	180.5	SMTCR, BACT, IW, I
								2	0.2	0.2	180.5	180.7	HS
								CC(w/2)	0.27	0.27	180.7	180.97	PAL
								Totals:	1.97	1.97			
6R	12	1945	188.7	198.4	9.7	2.39	24.6						
								1	1.5	1.5	188.7	190.2	IW
								2	0.71	0.71	190.2	190.91	HS
								CC(w/2)	0.18	0.18	190.91	191.09	PAL
								Totals:	2.39	2.39			
7R	12	2130	198.4	208.0	9.6	1.47	15.3						
								1	1.23	1.23	198.4	199.63	HS, IW, BGAS
								CC(w/1)	0.24	0.24	199.63	199.87	PAL
								Totals:	1.47	1.47			
8R	13	0030	208.0	217.7	9.7	0.95	9.8						
								1	0.84	0.84	208.0	208.84	HS, IW, BGAS
								CC(w/CC)	0.11	0.11	208.84	208.95	PAL
								Totals:	0.95	0.95			
9R	13	0210	217.7	227.2	9.5	2.79	29.4						
								1	1.5	1.5	217.7	219.2	IW
								2	1.14	1.14	219.2	220.34	BACT, HS, BGAS
								CC(w/2)	0.15	0.15	220.34	220.49	PAL
								Totals:	2.79	2.79			
10R	13	0400	227.2	236.8	9.6	2.3	24						
								1	1.5	1.5	227.2	228.7	IW
								2	0.62	0.62	228.7	229.32	HS, BGAS
								CC(w/2)	0.18	0.18	229.32	229.5	PAL, SFRCC
								Totals:	2.3	2.3			
11R	13	0520	236.8	246.5	9.7	2.53	26.1						
								1	1.5	1.5	236.8	238.3	
								2	0.8	0.8	238.3	239.1	HS, IW
								CC(w/2)	0.23	0.23	239.1	239.33	PAL
								Totals:	2.53	2.53			
12R	13	0705	246.5	256.2	9.7	1.74	17.9						
								1	1.5	1.5	246.5	248.0	HS, IW, BGAS
								CC(w/CC)	0.24	0.24	248.0	248.24	PAL
								Totals:	1.74	1.74			
13R	13	0900	256.2	265.8	9.6	3.69	38.4						
								1	1.5	1.5	256.2	257.7	
								2	1.5	1.5	257.7	259.2	HS, IW
								3	0.42	0.42	259.2	259.62	
								CC(w/CC)	0.27	0.27	259.62	259.89	PAL
								Totals:	3.69	3.69			

Table T2 (continued).

Core	Date (June 2000)	Time (local)	Core depth (mbsf) Top	Core depth (mbsf) Bottom	Length (m) Cored	Length (m) Recovered	Recovery (%)	Section	Length (m) Liner	Length (m) Curated	Section depth (mbsf) Top	Section depth (mbsf) Bottom	Catwalk samples
14R	13	1710	265.8	275.5	9.7	0.5	5.2						
								1	0.38	0.38	265.8	266.18	HS, IW
								CC(w/1)	0.12	0.12	266.18	266.3	PAL
								Totals:	0.5	0.5			
15R	13	1925	275.5	285.1	9.6	2.28	23.8						
								1	1.5	1.5	275.5	277.0	IW
								2	0.5	0.5	277.0	277.5	HS
								CC(w/2)	0.28	0.28	277.5	277.78	PAL
								Totals:	2.28	2.28			
16R	13	2130	285.1	294.6	9.5	1.8	18.9						
								1	1.5	1.5	285.1	286.6	BACT, HS, IW
								CC(w/CC)	0.3	0.3	286.6	286.9	PAL
								Totals:	1.8	1.8			
17R	13	2350	294.6	304.3	9.7	2.88	29.7						
								1	1.5	1.5	294.6	296.1	IW
								2	1.23	1.23	296.1	297.33	HS, BGAS
								CC(w/CC)	0.15	0.15	297.33	297.48	PAL
								Totals:	2.88	2.88			
18R	14	0205	304.3	314.0	9.7	6.17	63.6						
								1	1.5	1.5	304.3	305.8	
								2	1.5	1.5	305.8	307.3	IW, WRSF, WRC, WRY
								3	1.5	1.5	307.3	308.8	HS, BGAS
								4	1.47	1.47	308.8	310.27	
								CC(w/CC)	0.2	0.2	310.27	310.47	PAL
								Totals:	6.17	6.17			
19R	14	0410	314.0	323.5	9.5	2.22	23.4						
								1	1.5	1.5	314.0	315.5	IW
								2	0.57	0.57	315.5	316.07	HS, BGAS
								CC(w/CC)	0.15	0.15	316.07	316.22	PAL
								Totals:	2.22	2.22			
20R	14	0625	323.5	333.1	9.6	3.89	40.5						
								1	1.5	1.5	323.5	325.0	
								2	1.5	1.5	325.0	326.5	HS, IW, BGAS
								3	0.68	0.68	326.5	327.18	
								CC(w/CC)	0.21	0.21	327.18	327.39	PAL, SFRCC, WRTB
								Totals:	3.89	3.89			
21R	14	0830	333.1	342.4	9.3	2.85	30.6						
								1	1.5	1.5	333.1	334.6	HS, IW
								2	1.12	1.12	334.6	335.72	
								CC(w/2)	0.23	0.23	335.72	335.95	SFRCC, PAL
								Totals:	2.85	2.85			
22R	14	1045	342.4	352.0	9.6	1.34	14						
								1	0.51	0.51	342.4	342.91	HS, IW
								2	0.68	0.68	342.91	343.59	BGAS
								CC(w/CC)	0.15	0.15	343.59	343.74	PAL
								Totals:	1.34	1.34			
23R	14	1245	352.0	361.7	9.7	2.49	25.7						
								1	1.5	1.5	352.0	353.5	BACT, IW
								2	0.99	0.99	353.5	354.49	HS, BGAS, PAL
								Totals:	2.49	2.49			
24R	14	1455	361.7	371.3	9.6	4.72	49.2						
								1	1.5	1.5	361.7	363.2	
								2	1.5	1.5	363.2	364.7	
								3	1.46	1.46	364.7	366.16	HS, IW, BGAS
								CC(w/CC)	0.26	0.26	366.16	366.42	PAL
								Totals:	4.72	4.72			
25R	14	1655	371.3	380.9	9.6	2.2	22.9						
								1	1.5	1.5	371.3	372.8	HS, IW
								2	0.57	0.57	372.8	373.37	
								CC(w/2)	0.13	0.13	373.37	373.5	PAL
								Totals:	2.2	2.2			
26R	14	1910	380.9	390.5	9.6	0.84	8.8						
								1	0.58	0.58	380.9	381.48	HS
								CC(w/1)	0.26	0.26	381.48	381.74	PAL, IW
								Totals:	0.84	0.84			
27R	14	2120	390.5	400.2	9.7	5.12	52.8						
								1	1.5	1.5	390.5	392.0	BACT, IW
								2	1.5	1.5	392.0	393.5	

Table T2 (continued).

Core	Date (June 2000)	Time (local)	Core depth (mbsf) Top	Core depth (mbsf) Bottom	Length (m) Cored	Length (m) Recovered	Recovery (%)	Section	Length (m) Liner	Length (m) Curated	Section depth (mbsf) Top	Section depth (mbsf) Bottom	Catwalk samples
								3	1.37	1.37	393.5	394.87	HS, WRMT
								4	0.53	0.53	394.87	395.4	
								CC(w/4)	0.22	0.22	395.4	395.62	PAL
								Totals:	5.12	5.12			
28R	14	2345	400.2	409.8	9.6	2.32	24.2						
								1	1.5	1.5	400.2	401.7	HS, IW, BGAS
								2	0.56	0.56	401.7	402.26	
								CC(w/CC)	0.26	0.26	402.26	402.52	PAL
								Totals:	2.32	2.32			
29R	15	0200	409.8	419.4	9.6	4.94	51.5						
								1	1.5	1.5	409.8	411.3	
								2	1.5	1.5	411.3	412.8	WRC, WRY, WRS, PLU
								3	1.65	1.65	412.8	414.45	HS, IW, BGAS
								CC(w/CC)	0.29	0.29	414.45	414.74	PAL, WRTB
								Totals:	4.94	4.94			
30R	15	0415	419.4	429.0	9.6	0.18	1.9						
								CC(w/CC)	0.18	0.18	419.4	419.58	PAL
								Totals:	0.18	0.18			
31R	15	0630	429.0	438.6	9.6	4.62	48.1						
								1	1.5	1.5	429.0	430.5	IW
								2	1.5	1.5	430.5	432.0	
								3	1.4	1.4	432.0	433.4	HS, BGAS
								CC(w/CC)	0.22	0.22	433.4	433.62	PAL
								Totals:	4.62	4.62			
32R	15	0920	438.6	448.2	9.6	9.55	99.5						
								1	1.5	1.5	438.6	440.1	
								2	1.5	1.5	440.1	441.6	IW
								3	1.5	1.5	441.6	443.1	
								4	1.5	1.5	443.1	444.6	WRMT
								5	1.5	1.5	444.6	446.1	HS, BGAS
								6	1.5	1.5	446.1	447.6	
								7	0.25	0.25	447.6	447.85	
								CC(NS)	0.3	0.3	447.85	448.15	SFRCC, WRS, PAL
								Totals:	9.55	9.55			
33R	15	1150	448.2	457.9	9.7	7.16	73.8						
								1	1.5	1.5	448.2	449.7	
								2	1.5	1.5	449.7	451.2	IW
								3	1.5	1.5	451.2	452.7	HS
								4	1.5	1.5	452.7	454.2	
								5	0.94	0.94	454.2	455.14	
								CC(w/CC)	0.22	0.22	455.14	455.36	PAL
								Totals:	7.16	7.16			
34R	15	1420	457.9	467.1	9.2	7.25	78.8						
								1	1.5	1.5	457.9	459.4	
								2	1.5	1.5	459.4	460.9	
								3	1.5	1.5	460.9	462.4	IW, BGAS
								4	1.5	1.5	462.4	463.9	HS
								5	1.04	1.04	463.9	464.94	
								CC(w/5)	0.21	0.21	464.94	465.15	PAL
								Totals:	7.25	7.25			
35R	15	1645	467.1	476.5	9.4	2.85	30.3						
								1	1.5	1.5	467.1	468.6	IW
								2	1.1	1.1	468.6	469.7	BACT, HS, WRTB
								CC(w/2)	0.25	0.25	469.7	469.95	PAL
								Totals:	2.85	2.85			
36R	15	1850	476.5	485.7	9.2	7.49	81.4						
								1	1.5	1.5	476.5	478.0	
								2	1.5	1.5	478.0	479.5	WRTB
								3	1.5	1.5	479.5	481.0	BACT, IW
								4	1.5	1.5	481.0	482.5	HS
								5	1.49	1.49	482.5	483.99	PAL
								Totals:	7.49	7.49			
37R	15	2050	485.7	495.3	9.6	9.21	95.9						
								1	1.5	1.5	485.7	487.2	
								2	1.5	1.5	487.2	488.7	
								3	1.5	1.5	488.7	490.2	WRTB
								4	1.5	1.5	490.2	491.7	IW
								5	1.5	1.5	491.7	493.2	HS

Table T2 (continued).

Core	Date (June 2000)	Time (local)	Core depth (mbsf) Top	Core depth (mbsf) Bottom	Length (m) Cored	Length (m) Recovered	Recovery (%)	Section	Length (m) Liner	Length (m) Curated	Section depth (mbsf) Top	Section depth (mbsf) Bottom	Catwalk samples
								6	1.3	1.3	493.2	494.5	
								7	0.41	0.41	494.5	494.91	PAL
								Totals:	9.21	9.21			
38R	15	2310	495.3	504.9	9.6	9.73	101.4						
								1	1.5	1.5	495.3	496.8	
								2	1.5	1.5	496.8	498.3	BGAS
								3	1.5	1.5	498.3	499.8	WRY, WRC, WRY, WRS
								4	1.5	1.5	499.8	501.3	IW
								5	1.5	1.5	501.3	502.8	HS
								6	1.5	1.5	502.8	504.3	WRMT
								7	0.51	0.51	504.3	504.81	
								CC(w/7)	0.22	0.22	504.81	505.03	PAL
								Totals:	9.73	9.73			
39R	16	0125	504.9	514.6	9.7	8.31	85.7						
								1	1.5	1.5	504.9	506.4	HYWR
								2	1.5	1.5	506.4	507.9	
								3	1.5	1.5	507.9	509.4	HS, IW
								4	1.5	1.5	509.4	510.9	
								5	1.5	1.5	510.9	512.4	
								6	0.81	0.81	512.4	513.21	PAL
								Totals:	8.31	8.31			
40R	16	1305	514.6	524.3	9.7	9.21	94.9						
								1	1.5	1.5	514.6	516.1	
								2	1.5	1.5	516.1	517.6	
								3	1.5	1.5	517.6	519.1	
								4	1.5	1.5	519.1	520.6	BACT, IW, BGAS
								5	1.5	1.5	520.6	522.1	HS, WRTB
								6	1.46	1.46	522.1	523.56	
								CC(w/CC)	0.25	0.25	523.56	523.81	PAL
								Totals:	9.21	9.21			
41R	16	2200	524.3	533.9	9.6	4.89	50.9						
								1	1.5	1.5	524.3	525.8	
								2	1.5	1.5	525.8	527.3	IW
								3	1.5	1.5	527.3	528.8	HS, BGAS
								CC(w/CC)	0.39	0.39	528.8	529.19	PAL, WRTB
								Totals:	4.89	4.89			
42R	17	0105	533.9	543.6	9.7	9.76	100.6						
								1	1.5	1.5	533.9	535.4	
								2	1.5	1.5	535.4	536.9	
								3	1.5	1.5	536.9	538.4	WRLZ
								4	1.5	1.5	538.4	539.9	HS, BGAS
								5	1.5	1.5	539.9	541.4	IW
								6	1.5	1.5	541.4	542.9	
								7	0.56	0.56	542.9	543.46	
								CC(w/CC)	0.2	0.2	543.46	543.66	PAL, SFRCC, WRTB
								Totals:	9.76	9.76			
43R	17	0315	543.6	552.9	9.3	9.13	98.2						
								1	1.5	1.5	543.6	545.1	
								2	1.5	1.5	545.1	546.6	
								3	1.5	1.5	546.6	548.1	BACT, IW
								4	1.5	1.5	548.1	549.6	HS
								5	1.5	1.5	549.6	551.1	WRMG
								6	1.36	1.36	551.1	552.46	
								CC(w/CC)	0.27	0.27	552.46	552.73	PAL, WRTB, SFRCC
								Totals:	9.13	9.13			
44R	17	0525	552.9	562.6	9.7	5.79	59.7						
								1	1.5	1.5	552.9	554.4	
								2	1.5	1.5	554.4	555.9	
								3	1.5	1.5	555.9	557.4	HS, IW, BGAS
								4	1.29	1.29	557.4	558.69	PAL
								Totals:	5.79	5.79			
45R	17	0715	562.6	572.3	9.7	5.75	59.3						
								1	1.5	1.5	562.6	564.1	
								2	1.5	1.5	564.1	565.6	
								3	1.5	1.5	565.6	567.1	HS, IW, BGAS
								4	1.1	1.1	567.1	568.2	
								CC(w/CC)	0.15	0.15	568.2	568.35	SFRCC, WRTB, PAL
								Totals:	5.75	5.75			

Table T2 (continued).

Core	Date (June 2000)	Time (local)	Core depth (mbsf) Top	Bottom	Length (m) Cored	Recovered	Recovery (%)	Section	Length (m) Liner	Curated	Section depth (mbsf) Top	Bottom	Catwalk samples
46R	17	0920	572.3	581.9	9.6	9.44	98.3						
								1	1.5	1.5	572.3	573.8	
								2	1.5	1.5	573.8	575.3	
								3	1.5	1.5	575.3	576.8	
								4	1.5	1.5	576.8	578.3	BACT, HS, IW, BGAS
								5	1.5	1.5	578.3	579.8	
								6	1.5	1.5	579.8	581.3	
								7	0.44	0.44	581.3	581.74	PAL
								Totals:	9.44	9.44			
47R	17	1115	581.9	591.6	9.7	8.79	90.6						
								1	1.5	1.5	581.9	583.4	
								2	1.5	1.5	583.4	584.9	
								3	1.5	1.5	584.9	586.4	HS, BGAS
								4	1.5	1.5	586.4	587.9	IW
								5	1.5	1.5	587.9	589.4	
								6	1.11	1.11	589.4	590.51	
								CC(w/CC)	0.18	0.18	590.51	590.69	PAL, WRTB
								Totals:	8.79	8.79			
48R	17	1325	591.6	601.2	9.6	9.98	104						
								1	1.5	1.5	591.6	593.1	
								2	1.5	1.5	593.1	594.6	
								3	1.5	1.5	594.6	596.1	
								4	1.5	1.5	596.1	597.6	
								5	1.5	1.5	597.6	599.1	WRY, WRC, WRY, WRS
								6	1.5	1.5	599.1	600.6	
								7	0.67	0.67	600.6	601.27	
								CC(w/7)	0.31	0.31	601.27	601.58	PAL
								Totals:	9.98	9.98			
49R	17	1510	601.2	610.9	9.7	4.14	42.7						
								1	1.5	1.5	601.2	602.7	IW
								2	1.5	1.5	602.7	604.2	
								3	1.14	1.14	604.2	605.34	PAL, HS, BGAS, WRL
								Totals:	4.14	4.14			
50R	17	1705	610.9	620.5	9.6	7.19	74.9						
								1	1.5	1.5	610.9	612.4	WRHZ
								2	1.5	1.5	612.4	613.9	
								3	1.5	1.5	613.9	615.4	
								4	1.5	1.5	615.4	616.9	IW
								5	1.19	1.19	616.9	618.09	PAL, HS
								Totals:	7.19	7.19			
51R	17	1850	620.5	630.1	9.6	3.85	40.1						
								1	1.5	1.5	620.5	622.0	IW, BGAS
								2	1.5	1.5	622.0	623.5	BACT
								3	0.56	0.56	623.5	624.06	HS
								CC(w/3)	0.29	0.29	624.06	624.35	PAL
								Totals:	3.85	3.85			
52R	17	2045	630.1	639.8	9.7	9.31	96						
								1	1.5	1.5	630.1	631.6	
								2	1.5	1.5	631.6	633.1	
								3	1.5	1.5	633.1	634.6	
								4	1.5	1.5	634.6	636.1	
								5	1.5	1.5	636.1	637.6	
								6	1.5	1.5	637.6	639.1	HS, IW
								7	0.31	0.31	639.1	639.41	PAL
								Totals:	9.31	9.31			
53R	17	2230	639.8	649.4	9.6	5.9	61.5						
								1	1.5	1.5	639.8	641.3	
								2	1.5	1.5	641.3	642.8	
								3	1.5	1.5	642.8	644.3	WRMT, IW, WRSR
								4	1.15	1.15	644.3	645.45	HS
								CC(w/4)	0.25	0.25	645.45	645.7	PAL
								Totals:	5.9	5.9			
54R	18	0030	649.4	659.0	9.6	9.84	102.5						
								1	1.5	1.5	649.4	650.9	
								2	1.5	1.5	650.9	652.4	HS, BGAS
								3	1.5	1.5	652.4	653.9	WRTB
								4	1.5	1.5	653.9	655.4	
								5	1.5	1.5	655.4	656.9	WRC, WRS, BACT, IW

Table T2 (continued).

Core	Date (June 2000)	Time (local)	Core depth (mbsf) Top	Core depth (mbsf) Bottom	Length (m) Cored	Length (m) Recovered	Recovery (%)	Section	Length (m) Liner	Length (m) Curated	Section depth (mbsf) Top	Section depth (mbsf) Bottom	Catwalk samples
								6	1.5	1.5	656.9	658.4	
								7	0.63	0.63	658.4	659.03	
								CC(w/CC)	0.21	0.21	659.03	659.24	PAL
								Totals:	9.84	9.84			
55R	18	0230	659.0	668.7	9.7	9.08	93.6						
								1	1.5	1.5	659.0	660.5	WRSF
								2	1.5	1.5	660.5	662.0	
								3	1.5	1.5	662.0	663.5	
								4	1.5	1.5	663.5	665.0	HS
								5	1.5	1.5	665.0	666.5	
								6	1.43	1.43	666.5	667.93	
								CC(w/CC)	0.15	0.15	667.93	668.08	PAL
								Totals:	9.08	9.08			
56R	18	0435	668.7	678.3	9.6	2.91	30.3						
								1	1.5	1.5	668.7	670.2	BACT, IW
								2	1.41	1.41	670.2	671.61	PAL, HS, BGAS
								Totals:	2.91	2.91			
57R	18	0640	678.3	688.0	9.7	9.93	102.4						
								1	1.5	1.5	678.3	679.8	
								2	1.5	1.5	679.8	681.3	
								3	1.5	1.5	681.3	682.8	
								4	1.5	1.5	682.8	684.3	HS, IW
								5	1.5	1.5	684.3	685.8	
								6	1.5	1.5	685.8	687.3	HYWR
								7	0.63	0.63	687.3	687.93	
								CC(w/CC)	0.3	0.3	687.93	688.23	PAL, SFRCC
								Totals:	9.93	9.93			
58R	18	0845	688.0	697.6	9.6	6.44	67.1						
								1	1.5	1.5	688.0	689.5	
								2	1.5	1.5	689.5	691.0	
								3	1.5	1.5	691.0	692.5	HS
								4	1.5	1.5	692.5	694.0	
								5	0.21	0.21	694.0	694.21	
								CC(w/CC)	0.23	0.23	694.21	694.44	PAL
								Totals:	6.44	6.44			
59R	18	1050	697.6	707.2	9.6	8.85	92.2						
								1	1.5	1.5	697.6	699.1	
								2	1.5	1.5	699.1	700.6	
								3	1.5	1.5	700.6	702.1	IW, BGAS
								4	1.5	1.5	702.1	703.6	WRSR, HS, BGAS, WR
								5	1.5	1.5	703.6	705.1	WRLZ, CRG
								6	1.35	1.35	705.1	706.45	PAL
								CC(w/6)	0.0	0.0			
								Totals:	8.85	8.85			
60R	18	1250	707.2	716.9	9.7	8.61	88.8						
								1	1.5	1.5	707.2	708.7	
								2	1.5	1.5	708.7	710.2	BACT, IW
								3	1.5	1.5	710.2	711.7	
								4	1.5	1.5	711.7	713.2	
								5	1.5	1.5	713.2	714.7	HS
								6	1.11	1.11	714.7	715.81	PAL
								Totals:	8.61	8.61			
61R	18	1455	716.9	726.5	9.6	9.91	103.2						
								1	1.5	1.5	716.9	718.4	
								2	1.5	1.5	718.4	719.9	
								3	1.5	1.5	719.9	721.4	
								4	1.5	1.5	721.4	722.9	
								5	1.5	1.5	722.9	724.4	IW
								6	1.5	1.5	724.4	725.9	HS
								7	0.55	0.55	725.9	726.45	
								CC(w/7)	0.36	0.36	726.45	726.81	PAL
								Totals:	9.91	9.91			
62R	18	1640	726.5	736.1	9.6	7.18	74.8						
								1	1.5	1.5	726.5	728.0	
								2	1.5	1.5	728.0	729.5	
								3	1.5	1.5	729.5	731.0	IW, BGAS, WRSR
								4	1.5	1.5	731.0	732.5	
								5	1.07	1.07	732.5	733.57	PAL, HS

Table T2 (continued).

Core	Date (June 2000)	Time (local)	Core depth (mbsf) Top	Core depth (mbsf) Bottom	Length (m) Cored	Length (m) Recovered	Recovery (%)	Section	Length (m) Liner	Length (m) Curated	Section depth (mbsf) Top	Section depth (mbsf) Bottom	Catwalk samples
								CC(w/5)	0.11	0.11	733.57	733.68	WRTB
								Totals:	7.18	7.18			
63R	18	1835	736.1	745.7	9.6	9.97	103.9						
								1	1.5	1.5	736.1	737.6	
								2	1.5	1.5	737.6	739.1	
								3	1.5	1.5	739.1	740.6	
								4	1.5	1.5	740.6	742.1	
								5	1.5	1.5	742.1	743.6	BACT, HS
								6	1.5	1.5	743.6	745.1	
								7	0.59	0.59	745.1	745.69	
								CC(w/7)	0.38	0.38	745.69	746.07	PAL
								Totals:	9.97	9.97			
64R	18	2040	745.7	755.0	9.3	7.42	79.8						
								1	1.5	1.5	745.7	747.2	
								2	1.5	1.5	747.2	748.7	
								3	1.5	1.5	748.7	750.2	IW
								4	1.5	1.5	750.2	751.7	HS
								5	1.42	1.42	751.7	753.12	PAL
								Totals:	7.42	7.42			
65R	18	2230	755.0	764.6	9.6	9.93	103.4						
								1	1.5	1.5	755.0	756.5	HS, BGAS
								2	1.5	1.5	756.5	758.0	
								3	1.5	1.5	758.0	759.5	
								4	1.5	1.5	759.5	761.0	
								5	1.5	1.5	761.0	762.5	HS
								6	1.5	1.5	762.5	764.0	
								7	0.57	0.57	764.0	764.57	
								CC(w/7)	0.36	0.36	764.57	764.93	PAL
								Totals:	9.93	9.93			
66R	19	0030	764.6	774.2	9.6	7.17	74.7						
								1	1.5	1.5	764.6	766.1	HS, IW, BGAS
								2	1.5	1.5	766.1	767.6	
								3	1.5	1.5	767.6	769.1	
								4	1.5	1.5	769.1	770.6	
								5	1.06	1.06	770.6	771.66	HS
								CC(NS)	0.11	0.11	771.66	771.77	PAL, WRS
								Totals:	7.17	7.17			
67R	19	0240	774.2	783.9	9.7	9.96	102.7						
								1	0.24	0.24	774.2	774.44	
								2	1.5	1.5	774.44	775.94	WRMG
								3	1.5	1.5	775.94	777.44	WRSF
								4	1.5	1.5	777.44	778.94	HS, IW
								5	1.5	1.5	778.94	780.44	
								6	1.5	1.5	780.44	781.94	
								7	1.5	1.5	781.94	783.44	
								8	0.33	0.33	783.44	783.77	
								CC(w/8)	0.39	0.39	783.77	784.16	PAL
								Totals:	9.96	9.96			
68R	19	0445	783.9	793.6	9.7	3.74	38.6						
								1	1.5	1.5	783.9	785.4	IW
								2	1.5	1.5	785.4	786.9	HS, HYWR
								3	0.43	0.43	786.9	787.33	
								CC(w/3)	0.31	0.31	787.33	787.64	PAL
								Totals:	3.74	3.74			
69R	19	0650	793.6	803.3	9.7	9.89	102						
								1	0.27	0.27	793.6	793.87	
								2	1.5	1.5	793.87	795.37	WRLZ
								3	1.5	1.5	795.37	796.87	WRC, WRY, WRS, WRC
								4	1.5	1.5	796.87	798.37	IW
								5	1.5	1.5	798.37	799.87	HS, BGAS, CRG
								6	1.5	1.5	799.87	801.37	
								7	1.5	1.5	801.37	802.87	
								8	0.41	0.41	802.87	803.28	
								CC(w/8)	0.21	0.21	803.28	803.49	PAL
								Totals:	9.89	9.89			
70R	19	0900	803.3	812.5	9.2	7.82	85						
								1	1.5	1.5	803.3	804.8	
								2	1.5	1.5	804.8	806.3	IW, WRSR

Table T2 (continued).

Core	Date (June 2000)	Time (local)	Core depth (mbsf) Top	Core depth (mbsf) Bottom	Length (m) Cored	Length (m) Recovered	Recovery (%)	Section	Length (m) Liner	Length (m) Curated	Section depth (mbsf) Top	Section depth (mbsf) Bottom	Catwalk samples
								3	1.5	1.5	806.3	807.8	HS
								4	1.5	1.5	807.8	809.3	
								5	1.5	1.5	809.3	810.8	
								CC(w/CC)	0.32	0.32	810.8	811.12	WRTB, PAL
								Totals:	7.82	7.82			
71R	19	1135	812.5	822.2	9.7	2.99	30.8						
								1	0.38	0.38	812.5	812.88	WRTB, IW
								2	1.28	1.28	812.88	814.16	IW, BACT
								3	1.01	1.01	814.16	815.17	HS, BGAS
								CC(w/3)	0.32	0.32	815.17	815.49	PAL
								Totals:	2.99	2.99			
72R	19	1415	822.2	831.8	9.6	5.05	52.6						
								1	1.5	1.5	822.2	823.7	WRSF, WRS, IW, BGA
								2	1.5	1.5	823.7	825.2	
								3	1.5	1.5	825.2	826.7	HS, IW, BACT, BGAS
								4	0.28	0.28	826.7	826.98	
								CC(w/4)	0.27	0.27	826.98	827.25	PAL
								Totals:	5.05	5.05			
73R	19	1645	831.8	841.4	9.6	9.88	102.9						
								1	1.5	1.5	831.8	833.3	
								2	1.5	1.5	833.3	834.8	
								3	1.5	1.5	834.8	836.3	BACT, IW
								4	1.5	1.5	836.3	837.8	HS
								5	1.5	1.5	837.8	839.3	
								6	1.5	1.5	839.3	840.8	IW
								7	0.67	0.67	840.8	841.47	WRTB
								CC(w/7)	0.21	0.21	841.47	841.68	PAL, SFRCC
								Totals:	9.88	9.88			
74R	19	1840	841.4	851.0	9.6	3.89	40.5						
								1	1.5	1.5	841.4	842.9	WRLZ
								2	1.5	1.5	842.9	844.4	IW, WRSR, WRSF
								3	0.57	0.57	844.4	844.97	HS
								CC(w/3)	0.32	0.32	844.97	845.29	PAL, WRTB
								Totals:	3.89	3.89			
75R	19	2025	851.0	860.7	9.7	1.91	19.7						
								1	1.5	1.5	851.0	852.5	HS
								2	0.28	0.28	852.5	852.78	IW, HS
								CC(w/2)	0.13	0.13	852.78	852.91	PAL
								Totals:	1.91	1.91			
76R	19	2240	860.7	870.4	9.7	2.77	28.6						
								1	1.5	1.5	860.7	862.2	IW
								2	0.94	0.94	862.2	863.14	HS, WRTB
								CC(w/2)	0.33	0.33	863.14	863.47	PAL
								Totals:	2.77	2.77			
77R	20	0025	870.4	880.0	9.6	8.22	85.6						
								1	1.5	1.5	870.4	871.9	
								2	1.5	1.5	871.9	873.4	
								3	1.5	1.5	873.4	874.9	BACT
								4	1.5	1.5	874.9	876.4	
								5	1.5	1.5	876.4	877.9	HS, BGAS
								6	0.6	0.6	877.9	878.5	WRTB
								CC(w/CC)	0.12	0.12	878.5	878.62	PAL, WRS
								Totals:	8.22	8.22			
78R	20	0235	880.0	889.3	9.3	7.13	76.7						
								1	1.5	1.5	880.0	881.5	WRMG
								2	1.5	1.5	881.5	883.0	HYWR
								3	1.5	1.5	883.0	884.5	HS, IW, BGAS
								4	1.5	1.5	884.5	886.0	
								5	0.99	0.99	886.0	886.99	
								CC(w/CC)	0.14	0.14	886.99	887.13	WRS, PAL
								Totals:	7.13	7.13			
79R	20	0450	889.3	899.0	9.7	4.38	45.2						
								1	1.5	1.5	889.3	890.8	IW
								2	1.5	1.5	890.8	892.3	WRS, HS
								3	1.09	1.09	892.3	893.39	
								CC(w/3)	0.29	0.29	893.39	893.68	PAL
								Totals:	4.38	4.38			

Table T2 (continued).

Core	Date (June 2000)	Time (local)	Core depth (mbsf) Top	Core depth (mbsf) Bottom	Length (m) Cored	Length (m) Recovered	Recovery (%)	Section	Length (m) Liner	Length (m) Curated	Section depth (mbsf) Top	Section depth (mbsf) Bottom	Catwalk samples
80R	20	0645	899.0	908.6	9.6	8.6	89.6						
								1	1.5	1.5	899.0	900.5	
								2	1.5	1.5	900.5	902.0	WRS, WRC, WRY, PLU
								3	1.5	1.5	902.0	903.5	IW, WRSF
								4	1.5	1.5	903.5	905.0	
								5	1.5	1.5	905.0	906.5	HS, BGAS
								6	0.84	0.84	906.5	907.34	
								CC(w/6)	0.26	0.26	907.34	907.6	PAL
								Totals:	8.6	8.6			
81R	20	0830	908.6	918.3	9.7	7.9	81.4						
								1	1.5	1.5	908.6	910.1	
								2	1.5	1.5	910.1	911.6	
								3	1.5	1.5	911.6	913.1	IW
								4	1.5	1.5	913.1	914.6	HS
								5	1.5	1.5	914.6	916.1	
								6	0.15	0.15	916.1	916.25	
								CC(w/CC)	0.25	0.25	916.25	916.5	PAL, WRS
								Totals:	7.9	7.9			
82R	20	1010	918.3	927.9	9.6	4.16	43.3						
								1	1.5	1.5	918.3	919.8	
								2	1.25	1.25	919.8	921.05	HS, IW
								3	1.12	1.12	921.05	922.17	
								CC(w/3)	0.29	0.29	922.17	922.46	PAL, WRS
								Totals:	4.16	4.16			
83R	20	1220	927.9	937.5	9.6	9.93	103.4						
								1	1.5	1.5	927.9	929.4	
								2	1.5	1.5	929.4	930.9	
								3	1.5	1.5	930.9	932.4	
								4	1.5	1.5	932.4	933.9	IW
								5	1.5	1.5	933.9	935.4	
								6	1.5	1.5	935.4	936.9	HS, BGAS
								7	0.65	0.65	936.9	937.55	WRHZ
								CC(w/7)	0.28	0.28	937.55	937.83	PAL, WRS
								Totals:	9.93	9.93			
84R	20	1415	937.5	947.1	9.6	9.05	94.3						
								1	1.5	1.5	937.5	939.0	
								2	1.5	1.5	939.0	940.5	BACT, IW
								3	1.5	1.5	940.5	942.0	WRLZ
								4	1.5	1.5	942.0	943.5	
								5	1.5	1.5	943.5	945.0	HS
								6	1.2	1.2	945.0	946.2	
								CC(w/CC)	0.35	0.35	946.2	946.55	PAL, WRS
								Totals:	9.05	9.05			
85R	20	1605	947.1	956.8	9.7	8.83	91						
								1	1.5	1.5	947.1	948.6	WRTB
								2	1.5	1.5	948.6	950.1	
								3	1.5	1.5	950.1	951.6	IW
								4	1.5	1.5	951.6	953.1	HS
								5	1.5	1.5	953.1	954.6	
								6	1.17	1.17	954.6	955.77	
								CC(w/6)	0.16	0.16	955.77	955.93	PAL
								Totals:	8.83	8.83			
86R	20	1800	956.8	966.5	9.7	8.99	92.7						
								1	1.5	1.5	956.8	958.3	
								2	1.5	1.5	958.3	959.8	IW, BGAS
								3	1.5	1.5	959.8	961.3	HS
								4	1.5	1.5	961.3	962.8	
								5	1.5	1.5	962.8	964.3	
								6	1.12	1.12	964.3	965.42	
								CC(w/6)	0.37	0.37	965.42	965.79	PAL
								Totals:	8.99	8.99			
87R	20	2010	966.5	976.1	9.6	7.3	76						
								1	1.5	1.5	966.5	968.0	WRSR
								2	1.5	1.5	968.0	969.5	IW
								3	1.5	1.5	969.5	971.0	HS
								4	1.5	1.5	971.0	972.5	
								5	0.95	0.95	972.5	973.45	
								6	0.0	0.0			

Table T2 (continued).

Core	Date (June 2000)	Time (local)	Core depth (mbsf) Top	Core depth (mbsf) Bottom	Length (m) Cored	Length (m) Recovered	Recovery (%)	Section	Length (m) Liner	Length (m) Curated	Section depth (mbsf) Top	Section depth (mbsf) Bottom	Catwalk samples
								CC(w/6)	0.35	0.35	973.45	973.8	PAL
								Totals:	7.3	7.3			
88R	20	2210	976.1	985.3	9.2	5.87	63.8						
								1	1.5	1.5	976.1	977.6	
								2	1.5	1.5	977.6	979.1	IW, BACT
								3	1.5	1.5	979.1	980.6	HS
								4	1.37	1.37	980.6	981.97	PAL
								Totals:	5.87	5.87			
89R	21	0010	985.3	994.9	9.6	9.88	102.9						
								1	1.5	1.5	985.3	986.8	
								2	1.5	1.5	986.8	988.3	
								3	1.5	1.5	988.3	989.8	IW
								4	1.5	1.5	989.8	991.3	
								5	1.5	1.5	991.3	992.8	HS, BGAS
								6	1.5	1.5	992.8	994.3	WRMT
								7	0.56	0.56	994.3	994.86	
								CC(w/CC)	0.32	0.32	994.86	995.18	PAL
								Totals:	9.88	9.88			
90R	21	0210	994.9	1004.6	9.7	3.06	31.5						
								1	1.5	1.5	994.9	996.4	IW
								2	1.31	1.31	996.4	997.71	HS
								CC(w/CC)	0.25	0.25	997.71	997.96	PAL
								Totals:	3.06	3.06			
91R	21	0430	1004.6	1014.2	9.6	3.28	34.2						
								1	1.5	1.5	1004.6	1006.1	IW, IW
								2	1.54	1.54	1006.1	1007.64	HS
								CC(w/CC)	0.24	0.24	1007.64	1007.88	PAL
								Totals:	3.28	3.28			
92R	21	0640	1014.2	1023.9	9.7	8.2	84.5						
								1	1.5	1.5	1014.2	1015.7	
								2	1.5	1.5	1015.7	1017.2	HS, BGAS
								3	1.5	1.5	1017.2	1018.7	WRMG
								4	1.5	1.5	1018.7	1020.2	
								5	1.5	1.5	1020.2	1021.7	WRS, WRY, WRC, BAC
								6	0.48	0.48	1021.7	1022.18	IW
								CC(w/CC)	0.22	0.22	1022.18	1022.4	PAL, SFRCC
								Totals:	8.2	8.2			
93R	21	0855	1023.9	1033.5	9.6	7.18	74.8						
								1	1.5	1.5	1023.9	1025.4	
								2	1.5	1.5	1025.4	1026.9	
								3	1.5	1.5	1026.9	1028.4	HS
								4	1.5	1.5	1028.4	1029.9	IW
								5	0.89	0.89	1029.9	1030.79	
								CC(w/5)	0.29	0.29	1030.79	1031.08	PAL
								Totals:	7.18	7.18			
94R	21	1135	1033.5	1043.1	9.6	7.43	77.4						
								1	1.5	1.5	1033.5	1035.0	IW, IW
								2	1.5	1.5	1035.0	1036.5	
								3	1.5	1.5	1036.5	1038.0	WRLZ
								4	1.5	1.5	1038.0	1039.5	HS
								5	1.16	1.16	1039.5	1040.66	
								CC(w/5)	0.27	0.27	1040.66	1040.93	PAL
								Totals:	7.43	7.43			
95R	21	1345	1043.1	1052.6	9.5	5.84	61.5						
								1	1.5	1.5	1043.1	1044.6	IW
								2	1.5	1.5	1044.6	1046.1	
								3	1.5	1.5	1046.1	1047.6	
								4	0.97	0.97	1047.6	1048.57	HS, BGAS
								CC(w/4)	0.37	0.37	1048.57	1048.94	
								Totals:	5.84	5.84			
96R	21	1540	1052.6	1062.3	9.7	6.03	62.2						
								1	1.5	1.5	1052.6	1054.1	
								2	1.5	1.5	1054.1	1055.6	IW
								3	1.5	1.5	1055.6	1057.1	HS, BACT, WRSR
								4	1.35	1.35	1057.1	1058.45	
								CC(w/CC)	0.18	0.18	1058.45	1058.63	PAL
								Totals:	6.03	6.03			

Table T2 (continued).

Core	Date (June 2000)	Time (local)	Core depth (mbsf) Top	Core depth (mbsf) Bottom	Length (m) Cored	Length (m) Recovered	Recovery (%)	Section	Length (m) Liner	Length (m) Curated	Section depth (mbsf) Top	Section depth (mbsf) Bottom	Catwalk samples
97R	21	1755	1062.3	1071.9	9.6	6.92	72.1						
								1	1.5	1.5	1062.3	1063.8	IW, WRTB
								2	1.5	1.5	1063.8	1065.3	HS, HYWR
								3	1.5	1.5	1065.3	1066.8	
								4	1.5	1.5	1066.8	1068.3	
								5	0.68	0.68	1068.3	1068.98	
								CC(w/5)	0.24	0.24	1068.98	1069.22	PAL
								Totals:	6.92	6.92			
98R	21	2010	1071.9	1081.5	9.6	5.37	55.9						
								1	1.5	1.5	1071.9	1073.4	WRSF
								2	1.5	1.5	1073.4	1074.9	
								3	1.06	1.06	1074.9	1075.96	IW, BGAS
								4	0.46	0.46	1075.96	1076.42	HS
								5	0.85	0.85	1076.42	1077.27	PAL
								Totals:	5.37	5.37			
99R	21	2225	1081.5	1091.2	9.7	2.5	25.8						
								1	1.5	1.5	1081.5	1083.0	
								2	0.69	0.69	1083.0	1083.69	HS, IW
								CC(w/2)	0.31	0.31	1083.69	1084	
								Totals:	2.5	2.5			
100R	21	0045	1091.2	1100.8	9.6	2.77	28.9						
								1	1.36	1.36	1091.2	1092.56	HS, IW, BGAS, WRS
								2	1.13	1.13	1092.56	1093.69	
								CC(w/2)	0.28	0.28	1093.69	1093.97	
								Totals:	2.77	2.77			
101R	21	0325	1100.8	1110.2	9.4	1.71	18.2						
								1	0.64	0.64	1100.8	1101.44	HS, IW, IW
								2	0.8	0.8	1101.44	1102.24	
								CC(w/2)	0.27	0.27	1102.24	1102.51	PAL
								Totals:	1.71	1.71			
102R	21	0605	1110.2	1119.8	9.6	1.11	11.6						
								1	0.85	0.85	1110.2	1111.05	HS, IW
								CC(w/1)	0.26	0.26	1111.05	1111.31	PAL
								Totals:	1.11	1.11			
				Totals:	976.1	577.57	59.20						

Notes: Catwalk samples: IW = interstitial water, HS = headspace, PAL = paleontology, VAC = vacutainer. All other abbreviations are sample codes for postcruise research (see the **"Sample Codes"** database query). CC = core catcher (number in parenthesis indicates which section the core catcher is stored with). This table is also available in **ASCII** format.

Table T3. Summary of stratigraphic relations at Site 1174 and correlation with equivalent units at Sites 808 and 1173.

Unit	Subunit	Facies name	Interval (cm) Top	Interval (cm) Bottom	Depth (mbsf) Top	Depth (mbsf) Bottom	Thickness (m)	Stratigraphic age	Lithologic description
I		Slope apron	190-1174A-1H-1, 0	190-1174A-1H-CC, 0	0.00	4.00	4.00	Quaternary	Hemipelagic mud, rare volcanic ash
II	IIA	Axial-trench wedge	190-1174A-1H-CC, 0	190-1174B-19R-1, 55	4.00	314.55	310.55	Quaternary	Sand, muddy sand, silt turbidites, hemipelagic mud
	IIB	Outer-trench wedge	190-1174B-19R-1, 55	190-1174B-31R-2, 105	314.55	431.55	117.00	Quaternary	Silt turbidites, hemipelagic mud
	IIC	Trench to basin transition	31R-2, 105	36R-5, 73	431.55	483.23	51.68	Quaternary	Silt turbidites, volcanic ash, hemipelagic mud
III		Upper Shikoku Basin	36R-5, 73	55R-2, 49	483.23	660.99	177.76	Quaternary-Pliocene	Hemipelagic mud, volcanic ash
IV		Lower Shikoku Basin	55R-2, 49	101R-CC, 21	660.99	1102.45	441.46	Pliocene-Miocene	Hemipelagic mud, siliceous claystone, calcareous claystone
V		Volcaniclastic	101R-CC, 21	102R-CC, 26	1102.45	1111.31	8.86	Miocene	Hemipelagic mud, altered volcanic ash

Table T3 (continued).

Unit	Subunit	Processes of formation	Tectonic and physiographic setting	Statigraphic correlation Site 808	Statigraphic correlation Site 1173
I		Hemipelagic settling	Lowermost trench slope	Unit I	
II	IIA	Turbidity currents in axial channel, hemipelagic settling	Axis of trench floor	Units IIA, IIB	
	IIB	Lateral margins of turbidity currents, hemipelagic settling	Seaward margin of trench floor	Unit IIC	Unit IA
	IIC	Rare turbidity currents, air-fall ash, hemipelagic settling	Transition from trench to Shikoku Basin	Unit III	Unit IB
III		Hemipelagic settling, air-fall ash	Shikoku Basin - closer to trench; volcanism in Kyushu/Honshu	Unit IVA	Unit II
IV		Hemipelagic settling, diagenetic alteration	Shikoku Basin - distal to trench	Unit IVB	Unit III
V		Acidic volcanism, hemipelagic settling	Japan Outer Zone volcanism - triggered by ridge subduction	Unit V	Unit IV

Table T4. Results of X-ray diffraction analysis of bulk-powder volcanic ash samples, Site 1174.

Core, section, interval (cm)	Depth (mbsf)	X-ray diffraction peak intensity (cps)												X-ray diffraction peak area (total counts)											
		Smectite	Illite	Chlorite	Clinoptilolite	Hornblende	Cristobalite	Quartz	Plagioclase	Calcite	Pyroxene	Halite	Pyrite	Smectite	Illite	Chlorite	Clinoptilolite	Hornblende	Cristobalite	Quartz	Plagioclase	Calcite	Pyroxene	Halite	Pyrite
190-1174A-																									
1H-3, 33-35	3.35	0	0	0	0	0	0	154	181	24	0	260	0	0	0	0	0	0	0	2,298	2,866	601	0	3,482	0
190-1174B-																									
34R-2, 34-36	459.76	111	0	28	0	60	109	608	558	39	0	38	32	12,744	0	618	0	887	1,755	8,363	13,454	924	0	921	324
37R-2, 131-137	488.55	34	0	0	0	0	60	375	108	0	0	71	0	3,045	0	0	0	0	1,172	4,997	3,699	0	0	1,060	0
39R-4, 39-43	509.83	27	27	28	0	0	50	335	100	748	0	87	0	1,109	527	659	0	0	980	5,219	3,046	14,584	0	1,967	0
43R-4, 84-85	548.95	261	0	0	0	0	76	229	146	0	0	0	0	26,660	0	0	0	0	1,826	3,246	5,933	0	0	0	0
52R-3, 118-119	634.29	154	0	0	50	0	0	72	148	0	0	0	0	17,101	0	0	682	0	0	1,483	8,925	0	0	0	0
54R-4, 21-22	654.12	41	14	0	49	0	0	76	139	0	0	0	26	4,290	215	0	897	0	0	2,240	7,893	0	0	0	553
54R-7, 27-28	658.68	85	0	0	136	0	0	78	191	0	0	0	0	12,058	0	0	2,760	0	0	1,706	6,796	0	0	0	0
55R-2, 4-5	660.55	68	0	0	76	0	0	72	964	0	0	53	0	7,239	0	0	1,376	0	0	1,071	15,972	0	0	1,082	0
55R-2, 39-40	660.90	123	24	22	138	0	0	451	182	650	0	73	0	13,131	321	336	2,001	0	0	6,621	7,532	11,009	0	1,061	0
58R-2, 129-131	690.81	74	31	32	0	0	75	1,202	239	85	0	0	0	9,200	1,130	677	0	0	1,267	16,481	9,169	1,912	0	0	0
60R-5, 57-59	713.79	120	34	44	0	0	88	752	1,918	115	0	0	221	10,783	770	961	0	0	1,586	9,548	26,022	2,142	0	0	2,798
66R-2, 92-93	767.03	67	0	0	0	0	204	125	367	0	0	0	0	5,939	0	0	0	0	3,850	2,970	13,444	0	0	0	0
67R-6, 129-131	781.75	201	0	0	0	0	0	173	779	61	0	0	38	20,075	0	0	0	0	0	3,543	15,278	1,826	0	0	611
84R-5, 77-78	944.28	318	0	0	0	0	0	123	0	0	0	0	0	33,597	0	0	0	0	0	2,219	0	0	0	0	0
89R-3, 130-131	989.61	88	12	34	0	0	143	191	652	50	119	63	80	8,728	260	793	0	0	2,892	3,548	19,797	914	3,534	1,246	1,397

Table T5. Peak intensities and peak areas from X-ray diffraction analysis of bulk-powder sediment samples, Hole 1174A. (**See table note.** Continued on next four pages.)

Core, section, interval (cm)	Depth (mbsf)	X-ray diffraction peak intensity (cps)								X-ray diffraction peak area (total counts)							
		Smectite + chlorite	Illite	Chlorite + kaolinite	(101) Quartz	Plagioclase	Calcite	(100) Quartz	(101) Cristobalite	Smectite + chlorite	Illite	Chlorite + kaolinite	(101) Quartz	Plagioclase	Calcite	(100) Quartz	(101) Cristobalite
190-1174A-																	
1H-1, 38-39	0.39	67	122	152	2,117	559	0	390	128	3,198	2,603	2,918	27,784	13,033	0	4,621	1,749
1H-2, 96-97	2.47	72	141	153	2,213	452	82	429	119	3,159	3,115	2,794	29,261	12,181	1,878	5,232	1,614
1H-3, 109-110	4.10	58	122	131	1,893	423	0	330	107	2,214	2,145	2,389	25,451	11,128	0	4,210	1,341
2H-5, 130-131	10.50	81	142	193	2,304	496	100	430	129	3,543	3,023	3,452	30,423	11,927	1,477	5,292	1,754
2H-7, 131-132	13.51	67	151	165	2,133	502	146	420	109	2,227	3,269	2,939	28,779	12,167	2,007	5,099	1,439
3H-2, 104-105	16.45	71	173	240	3,295	1,069	252	527	129	2,143	3,293	4,185	45,909	26,674	2,946	7,387	2,156
3H-4, 75-76	18.60	80	166	201	2,213	526	87	365	132	3,295	3,323	3,489	29,055	13,290	1,114	4,498	1,636
3H-6, 84-85	21.39	76	155	180	2,147	473	44	415	126	2,509	2,950	3,308	28,544	12,488	658	5,319	1,768
4H-2, 63-64	25.54	72	187	233	2,020	506	0	368	125	2,992	3,300	4,145	28,453	11,928	0	4,724	1,615
4H-4, 129-130	29.20	75	157	185	1,487	283	29	261	102	2,447	2,821	3,455	20,417	8,376	369	3,567	1,419
5H-1, 99-100	33.90	70	134	163	2,290	481	0	320	124	2,801	2,705	2,764	29,658	12,542	0	4,372	1,988
5H-2, 134-135	35.75	72	131	173	2,050	588	120	324	126	2,699	2,562	2,948	27,237	14,708	1,833	4,319	1,663
5H-CC, 40-41	39.90	70	139	165	2,275	577	76	395	144	2,309	2,740	3,134	29,391	15,147	1,142	4,975	1,850
7H-2, 132-133	54.23	50	131	145	2,803	826	68	338	136	2,238	2,861	2,594	34,310	17,807	825	4,311	1,925
8H-3, 138-139	65.02	46	129	118	2,490	983	88	445	154	1,721	2,170	2,111	31,554	24,528	1,272	5,171	2,031
8H-4, 133-134	66.47	29	60	75	2,008	800	0	354	189	1,227	1,258	1,434	25,325	22,756	0	4,365	2,622
1R-1, 71-72	144.42	60	108	161	2,113	499	107	393	162	1,914	1,799	2,490	27,656	14,438	1,657	4,885	2,047
3R-1, 125-127	160.97	65	136	140	1,889	553	39	331	127	2,424	2,978	2,622	25,122	13,771	513	4,363	1,790
4R-2, 44-45	171.35	66	126	149	1,916	446	96	350	120	2,366	2,545	2,805	26,262	11,867	1,405	4,950	1,686
5R-1, 35-36	179.36	63	103	131	1,846	448	0	294	139	2,598	1,864	2,300	24,641	11,684	0	3,852	2,156
5R-1, 122-123	180.23	51	100	110	2,140	697	63	372	149	1,641	1,737	1,881	26,650	17,209	671	4,534	2,036
6R-1, 122-123	189.93	70	107	137	1,753	466	78	287	149	2,831	2,286	2,356	22,847	12,627	1,162	3,792	2,073
7R-1, 95-96	199.36	61	138	132	2,095	506	110	306	141	1,838	2,623	2,653	26,710	12,994	1,668	3,954	1,873
8R-1, 61-62	208.62	53	114	150	1,973	471	93	333	149	2,111	2,414	2,743	24,805	13,014	1,297	4,170	1,872
9R-1, 116-117	218.87	66	99	139	2,105	566	81	373	161	2,193	2,262	2,602	27,256	14,169	1,096	4,726	2,202
10R-1, 118-119	228.39	60	100	127	1,861	416	64	299	140	2,256	1,987	2,696	23,953	10,768	903	4,060	1,980
10R-CC, 15-16	229.48	67	115	155	2,056	510	67	349	134	1,818	2,236	2,795	26,538	13,946	866	4,368	1,822
11R-2, 15-16	238.46	62	110	148	1,935	434	75	311	142	2,606	1,828	2,660	25,045	11,330	1,095	4,013	1,878
12R-1, 112-113	247.63	72	147	147	2,460	598	68	315	160	2,538	2,614	2,704	30,023	12,901	919	4,164	2,466
13R-1, 106-107	257.27	65	84	109	1,470	350	102	247	124	3,265	1,980	2,118	19,704	9,933	1,546	3,376	1,832
13R-2, 118-119	258.89	61	120	146	1,997	567	153	376	144	2,092	2,323	2,670	26,387	14,832	2,314	4,542	2,182
14R-1, 19-20	266.00	74	121	171	2,045	482	81	309	157	2,858	2,261	3,199	26,568	13,241	1,393	4,004	2,376
15R-1, 123-124	276.73	51	112	115	1,592	352	242	289	105	1,977	2,404	1,992	21,652	8,275	3,411	4,181	2,058
15R-2, 48-49	277.48	70	138	157	1,836	402	145	314	113	2,736	2,793	2,924	25,148	9,809	2,117	4,089	1,556
16R-1, 123-124	286.33	68	116	156	1,958	433	139	347	131	2,298	2,382	2,835	26,518	11,059	1,894	4,518	1,731
17R-1, 110-111	295.70	72	88	136	1,849	417	90	356	186	3,028	1,787	2,490	24,479	12,217	1,312	4,852	2,856
18R-2, 67-68	306.47	69	103	133	1,877	435	152	335	109	2,786	2,462	2,610	25,471	12,127	2,479	4,435	1,473
18R-4, 81-82	309.61	71	107	135	1,986	417	93	294	138	2,884	2,409	2,630	26,113	11,081	1,392	4,198	1,873
19R-1, 78-79	314.78	75	116	153	2,152	512	136	337	145	2,598	2,271	2,772	27,823	13,659	2,095	4,412	1,984
19R-1, 89-90	314.89	61	140	153	2,653	473	94	416	125	2,599	2,699	2,718	35,555	12,724	1,319	5,186	1,499
20R-2, 110-111	326.10	78	105	146	2,161	666	78	443	182	2,910	2,199	2,683	28,336	15,679	1,084	5,398	2,500
20R-3, 50-51	327.00	75	115	128	1,807	373	45	321	99	3,109	2,338	2,388	23,862	9,998	515	4,331	1,485
21R-1, 114-115	334.24	79	115	170	2,490	506	123	451	145	2,331	2,111	3,143	31,556	12,780	1,660	5,808	1,996
21R-CC, 3-4	335.75	64	131	135	1,774	333	166	286	98	2,731	2,801	2,731	23,668	8,360	2,387	3,841	1,449
22R-1, 25-26	342.65	71	105	140	2,165	511	126	389	117	2,072	2,051	2,591	28,712	12,875	1,998	5,167	1,556
23R-1, 96-97	352.96	76	132	161	2,094	417	102	312	128	2,484	2,531	2,930	27,811	10,781	1,632	4,142	1,531

Table T5 (continued).

Core, section, interval (cm)	Depth (mbsf)	X-ray diffraction peak intensity (cps)								X-ray diffraction peak area (total counts)							
		Smectite + chlorite	Illite	Chlorite + kaolinite	(101) Quartz	Plagioclase	Calcite	(100) Quartz	(101) Cristobalite	Smectite + chlorite	Illite	Chlorite + kaolinite	(101) Quartz	Plagioclase	Calcite	(100) Quartz	(101) Cristobalite
24R-3, 117-118	365.87	66	101	146	2,224	465	0	384	166	2,606	2,241	2,820	28,272	12,812	0	5,127	2,177
25R-1, 122-123	372.52	69	76	114	1,862	471	0	294	168	3,217	1,675	2,392	24,199	12,966	0	4,190	2,982
26R-1, 56-57	381.46	69	124	147	1,905	435	0	323	136	3,174	2,312	2,656	25,527	11,137	0	4,408	2,046
27R-1, 123-124	391.73	60	75	110	2,000	518	57	335	227	2,561	1,726	2,400	25,893	14,618	1,051	4,470	3,162
27R-3, 115-116	394.65	78	115	138	2,101	422	44	376	144	2,765	2,599	2,492	27,692	11,552	681	5,210	2,179
28R-1, 124-125	401.44	57	66	98	1,679	414	32	275	171	2,890	1,420	2,115	22,016	11,279	687	4,136	2,467
28R-2, 49-50	402.19	58	77	130	2,091	517	0	349	189	2,789	1,755	2,489	26,285	13,200	0	4,356	2,689
29R-2, 81-82	412.11	63	89	132	2,012	478	0	397	150	2,931	1,845	2,373	25,110	12,276	0	4,929	1,945
29R-3, 133-134	414.13	67	108	145	2,067	477	42	360	148	3,480	2,319	2,756	26,618	12,907	1,052	4,731	2,072
29R-CC, 18-19	414.63	72	101	132	1,960	440	23	320	132	3,305	1,792	2,436	24,901	10,933	630	4,292	1,761
30R-CC, 5-6	419.45	80	110	146	2,148	454	65	312	134	3,289	2,132	2,906	27,391	11,658	710	4,545	1,810
31R-1, 116-117	430.16	74	121	148	2,108	442	96	465	140	2,795	2,884	2,951	27,614	12,699	1,576	5,573	1,703
31R-3, 44-45	432.44	63	111	155	2,062	416	98	373	109	2,471	2,075	2,673	26,853	11,270	1,622	4,522	1,490
32R-2, 117-118	441.27	65	114	141	2,197	473	78	394	131	2,395	2,544	2,983	29,022	11,255	1,180	5,117	1,862
32R-5, 130-131	445.90	49	78	93	1,662	354	703	288	82	1,942	1,299	1,865	21,067	10,389	10,412	3,957	1,064
33R-2, 119-120	450.89	60	87	112	1,864	710	0	295	140	2,639	1,916	2,121	23,987	14,592	0	3,949	1,728
33R-4, 18-19	452.88	69	87	112	2,050	654	0	323	175	3,098	1,909	2,364	25,595	14,136	0	4,269	2,376
34R-3, 96-97	461.86	64	104	148	3,692	653	118	472	157	2,067	1,952	2,941	33,023	14,952	1,576	5,714	1,855
35R-1, 118-119	468.28	63	98	108	2,282	581	177	355	125	3,529	2,163	1,882	28,769	13,969	2,435	4,753	1,906
35R-2, 94-95	469.54	51	28	54	1,021	207	159	239	90	4,139	686	993	13,171	6,527	2,625	3,424	1,787
36R-2, 133-134	479.33	62	106	160	2,372	500	184	381	141	2,312	2,245	2,935	30,514	11,758	2,721	4,774	1,631
36R-3, 111-112	480.61	62	112	130	1,983	405	200	339	101	2,831	2,409	2,631	26,429	11,510	3,192	4,627	1,270
37R-3, 130-131	490.00	66	89	106	1,872	440	0	334	139	3,220	1,762	2,086	24,012	12,170	0	4,668	2,071
37R-4, 117-118	491.37	60	79	92	1,874	448	209	316	121	3,524	1,477	1,621	23,413	10,874	3,142	4,443	1,763
38R-3, 84-85	499.14	52	110	123	2,234	445	209	383	137	1,974	2,273	2,179	28,337	11,507	2,958	4,850	1,720
38R-4, 115-116	500.95	59	86	127	2,036	423	171	330	188	3,073	1,937	2,358	26,481	11,191	2,496	4,552	2,160
38R-6, 62-63	503.42	46	99	125	1,989	338	389	342	106	2,018	2,141	2,487	25,555	9,419	5,475	4,689	1,245
39R-1, 133-134	506.23	69	91	123	1,866	393	149	341	117	3,527	2,078	2,363	24,381	10,891	2,369	4,563	1,492
39R-3, 117-118	509.07	61	61	86	1,704	423	99	300	138	3,071	1,222	1,656	22,187	10,333	1,690	4,258	2,060
40R-4, 118-119	520.28	74	64	74	1,673	396	98	289	132	4,537	1,210	1,499	21,543	11,271	1,557	3,948	2,189
41R-2, 29-30	526.09	72	91	117	2,300	478	187	366	109	2,738	1,932	2,058	29,517	11,054	2,744	4,976	1,272
41R-CC, 20-21	529.00	66	101	120	1,993	429	42	379	91	2,164	2,376	2,267	26,681	11,708	660	5,211	1,142
42R-1, 96-97	534.86	41	88	81	1,858	412	0	326	120	2,943	2,101	1,507	24,380	12,169	0	4,252	1,458
42R-3, 125-126	538.15	58	98	105	1,770	337	0	337	87	3,100	2,545	2,005	23,807	9,544	0	4,717	1,078
42R-5, 116-117	541.06	55	93	93	2,224	374	51	405	104	2,794	2,459	2,094	27,856	10,342	723	5,345	1,352
43R-3, 99-100	547.59	61	112	105	1,939	443	35	306	91	3,203	2,046	1,782	25,649	11,362	446	4,238	1,135
43R-5, 127-128	550.87	60	116	108	2,168	412	193	336	97	2,365	2,314	2,158	28,361	11,677	3,179	4,549	1,199
43R-5, 127-128	550.87	60	116	108	2,168	412	193	336	97	2,639	2,600	2,183	28,444	11,619	3,369	4,584	1,203
43R-6, 129-130	552.39	58	111	116	1,829	336	225	336	97	2,694	2,455	1,944	24,348	9,379	3,373	4,397	1,501
44R-3, 117-118	557.07	55	118	125	2,078	406	0	375	83	2,604	2,834	2,351	27,894	9,945	0	4,730	1,021
44R-4, 125-126	558.65	67	107	129	1,968	378	0	357	132	1,967	2,682	2,361	25,667	11,043	0	4,759	1,514
45R-1, 72-73	563.32	67	70	70	1,647	410	0	271	118	4,488	1,566	1,531	21,706	12,112		3,791	1,576
45R-3, 109-110	566.69	61	77	95	1,661	347	463	292	100	4,100	1,910	2,007	21,833	10,612	7,299	4,137	1,317
46R-1, 149-150	573.79	53	86	90	1,589	283	457	274	82	2,444	2,010	1,749	20,751	8,536	6,815	3,789	983
46R-4, 118-119	577.98	60	84	79	1,943	349	94	362	138	4,576	1,903	1,556	25,604	9,607	1,434	5,221	1,474
46R-7, 42-43	581.72	74	78	83	1,611	308	571	280	70	4,247	1,506	1,693	20,775	8,522	8,792	3,685	783
47R-1, 149-150	583.39	59	77	90	1,736	354	0	284	94	3,446	1,979	1,617	22,767	10,593	0	4,170	1,188
47R-4, 119-120	587.59	77	53	65	1,068	254	82	202	57	8,283	1,183	1,178	16,307	9,349	1,721	4,334	890

Table T5 (continued).

Core, section, interval (cm)	Depth (mbsf)	X-ray diffraction peak intensity (cps)								X-ray diffraction peak area (total counts)							
		Smectite + chlorite	Illite	Chlorite + kaolinite	(101) Quartz	Plagioclase	Calcite	(100) Quartz	(101) Cristobalite	Smectite + chlorite	Illite	Chlorite + kaolinite	(101) Quartz	Plagioclase	Calcite	(100) Quartz	(101) Cristobalite
48R-2, 134-135	594.44	62	91	102	1,927	400	0	374	90	3,643	2,087	1,961	25,344	10,411	0	5,070	1,025
48R-5, 101-102	598.61	71	93	100	2,019	351	0	389	91	4,402	2,118	2,046	26,719	10,667	0	5,434	1,198
49R-1, 119-120	602.39	61	56	65	1,582	274	599	296	78	3,801	1,311	1,453	20,387	8,360	10,932	4,349	1,000
49R-3, 99-100	605.19	70	78	98	1,744	359	59	321	281	4,232	1,424	1,773	23,122	10,485	856	4,536	3,089
50R-1, 60-61	611.50	73	45	58	1,413	364	112	260	133	6,819	1,483	1,110	18,435	10,860	1,762	4,191	1,794
50R-4, 120-121	616.60	52	96	89	1,799	346	280	295	109	3,528	1,783	1,392	24,272	10,235	4,113	4,364	1,813
52R-1, 82-83	630.92	60	64	74	1,440	298	620	247	125	3,855	1,270	1,324	18,634	8,525	8,690	3,779	1,800
52R-6, 115-116	638.75	54	78	81	1,534	490	586	277	73	3,757	2,110	1,436	19,909	11,580	8,879	3,791	968
53R-1, 107-108	640.87	67	68	70	1,463	427	215	258	74	4,418	1,497	1,217	19,266	10,741	3,073	3,763	932
53R-3, 122-123	644.02	75	93	103	1,736	372	114	325	99	4,070	2,326	1,762	23,278	11,351	1,715	4,454	1,328
53R-4, 14-15	644.44	80	48	54	1,151	279	110	232	79	8,046	1,190	870	14,877	9,778	1,677	3,745	1,308
54R-3, 127-128	653.67	63	82	93	1,874	393	104	306	120	4,019	1,919	1,600	24,927	10,711	1,458	4,454	2,062
54R-5, 96-97	656.36	56	82	80	1,651	355	118	361	122	3,313	1,712	1,343	21,714	10,774	1,730	4,595	1,562
55R-1, 131-132	660.31	65	78	77	1,638	312	294	282	126	3,846	1,551	1,285	21,732	9,528	3,977	3,966	2,224
55R-5, 92-93	665.92	54	55	60	1,487	302	61	259	139	5,206	1,493	1,235	22,266	10,182	950	4,199	2,139
56R-1, 114-115	669.84	63	76	79	1,659	912	188	300	98	5,060	1,589	1,526	22,539	15,534	2,672	4,380	1,503
56R-2, 135-136	671.55	58	83	86	1,785	325	48	300	87	4,093	1,803	1,517	24,236	10,031	797	4,459	1,316
57R-4, 116-117	683.96	64	95	104	1,934	412	364	353	96	3,901	1,961	1,882	25,348	10,815	5,628	4,574	1,099
57R-6, 133-134	687.13	77	76	78	1,852	341	238	287	102	7,047	1,384	1,645	24,015	10,317	4,132	4,103	1,446
58R-2, 75-76	690.25	69	98	99	2,009	453	186	311	85	4,890	1,861	1,758	25,926	11,922	2,586	4,496	1,063
58R-4, 80-81	693.30	64	74	83	1,861	389	189	305	85	4,335	1,654	1,593	25,061	10,639	2,985	4,525	1,115
59R-3, 117-118	701.77	58	115	119	2,007	400	99	363	104	2,814	2,352	2,192	26,561	10,418	1,680	5,073	1,240
59R-4, 84-85	702.94	57	72	91	1,881	409	54	336	80	4,270	1,846	1,760	24,396	10,258	810	4,680	1,034
59R-5, 128-129	704.88	59	72	94	1,918	304	114	342	80	4,094	1,851	1,929	25,024	9,128	1,814	4,961	978
60R-2, 113-114	709.83	75	93	115	2,321	415	26	421	110	4,151	1,978	2,350	28,949	11,490	665	5,629	1,389
61R-1, 83-84	717.74	95	58	67	1,529	405	189	297	79	8,784	1,352	1,430	19,959	10,397	3,446	4,561	1,110
61R-4, 105-106	722.46	54	69	108	1,692	316	590	316	80	3,717	1,842	2,201	21,834	8,344	10,355	4,406	1,019
61R-5, 116-117	724.07	63	90	105	2,020	354	137	343	91	4,467	1,903	1,994	25,916	9,576	2,163	4,857	1,242
62R-3, 97-98	730.48	72	105	115	2,021	366	41	353	97	4,087	2,373	2,235	26,087	9,317	698	4,923	1,274
63R-2, 81-82	738.42	55	82	104	2,123	387	0	393	102	3,170	1,954	2,080	26,803	10,005	0	4,875	1,209
63R-5, 137-138	743.48	65	84	99	1,735	318	132	312	77	4,221	2,099	2,177	22,487	8,690	2,107	4,348	962
64R-1, 106-107	746.77	61	79	102	2,304	393	0	502	108	3,946	2,201	2,079	29,038	10,358	0	6,368	1,332
64R-3, 118-119	749.89	63	100	113	2,155	345	0	370	107	3,644	2,476	2,440	27,303	9,182	0	5,048	1,318
64R-5, 109-110	752.80	67	64	92	2,088	336	0	342	104	5,376	1,731	1,733	26,046	9,307	0	4,717	1,334
65R-1, 113-114	756.14	62	105	107	2,219	350	59	358	106	3,574	2,743	2,266	28,225	9,261	853	4,826	1,299
65R-4, 83-84	760.34	80	89	112	2,064	363	29	359	77	4,821	2,143	2,448	26,700	11,542	385	5,168	998
66R-1, 114-115	765.75	78	90	109	1,962	325	234	353	71	4,255	2,322	2,205	24,790	10,404	5,160	4,841	876
66R-5, 100-101	771.61	66	122	135	2,123	293	29	384	75	4,075	2,760	2,761	27,174	7,941	552	5,167	883
67R-2, 98-99	775.43	64	150	163	2,170	360	44	384	91	2,254	3,426	3,506	28,658	9,592	732	4,965	1,013
67R-3, 128-129	777.23	66	112	130	2,031	349	127	356	77	4,006	2,780	2,721	26,709	8,768	2,110	4,881	958
67R-4, 128-129	778.73	62	114	138	2,084	354	182	379	83	3,353	2,884	2,857	26,307	8,439	3,148	5,079	1,002
68R-1, 116-118	785.08	64	130	129	2,146	315	70	371	92	3,478	3,168	2,790	27,650	8,287	1,124	4,920	1,074
68R-2, 134-136	786.76	60	133	135	2,135	303	41	374	83	2,984	3,314	2,896	27,043	8,619	727	4,989	966
69R-2, 129-130	795.17	63	142	131	2,033	329	176	347	70	3,039	3,007	2,666	26,561	7,882	2,910	4,657	814
69R-3, 96-97	796.34	59	83	108	2,145	312	249	376	92	3,230	2,158	2,344	27,099	8,102	4,524	5,003	1,088
69R-4, 118-119	798.06	47	80	96	1,727	272	344	346	73	3,676	1,721	2,134	23,028	7,359	6,871	4,822	926
70R-2, 98-99	805.78	65	132	122	1,908	293	352	332	73	3,676	2,872	2,434	24,602	7,330	6,490	4,448	752
70R-4, 148-149	809.28	57	105	111	2,187	337	53	348	89	2,932	2,066	2,422	27,540	8,607	892	4,825	1,070

Table T5 (continued).

Core, section, interval (cm)	Depth (mbsf)	X-ray diffraction peak intensity (cps)								X-ray diffraction peak area (total counts)							
		Smectite + chlorite	Illite	Chlorite + kaolinite	(101) Quartz	Plagioclase	Calcite	(100) Quartz	(101) Cristobalite	Smectite + chlorite	Illite	Chlorite + kaolinite	(101) Quartz	Plagioclase	Calcite	(100) Quartz	(101) Cristobalite
70R-5, 148-149	810.78	77	113	130	1,963	366	108	364	77	5,323	2,721	2,734	25,656	10,378	1,887	5,038	956
71R-2, 0-1	812.88	53	88	90	1,925	293	192	346	77	2,761	2,261	1,904	24,845	7,610	3,079	4,907	981
71R-2, 96-97	813.84	42	73	93	2,136	299	43	365	88	1,942	1,988	1,982	26,522	7,596	621	5,369	1,123
71R-3, 80-81	814.96	54	96	103	2,001	284	295	347	89	3,224	2,654	1,976	26,139	7,160	4,930	4,800	1,032
72R-1, 45-46	822.65	38	61	75	1,753	260	471	325	77	2,030	1,667	1,814	22,123	6,449	8,017	4,269	852
72R-1, 116-117	823.36	52	70	71	1,521	250	409	263	67	3,339	1,721	1,679	19,281	6,289	8,681	3,676	793
72R-3, 106-107	826.26	49	77	89	1,906	288	339	303	74	2,563	1,925	1,733	24,109	7,481	5,719	4,445	908
73R-1, 78-79	832.58	44	86	106	1,977	285	208	365	73	2,351	2,017	2,256	25,081	6,866	4,716	4,770	867
73R-3, 118-119	835.98	50	80	95	1,775	244	0	351	60	2,914	2,235	2,038	22,724	6,617	0	4,789	689
73R-5, 114-115	838.94	49	82	98	1,911	263	368	472	71	2,669	2,187	1,911	23,975	6,483	5,921	5,605	862
73R-7, 49-50	841.29	60	117	118	1,754	279	291	330	72	3,508	3,038	2,562	23,070	7,195	4,641	4,725	954
74R-1, 128-129	842.68	41	62	60	976	134	1,128	182	37	1,822	1,180	1,282	12,236	3,211	23,521	2,369	423
74R-2, 56-57	843.46	53	89	99	1,883	298	332	348	74	1,806	2,890	2,389	24,322	7,046	5,793	4,731	903
74R-2, 123-124	844.13	62	114	124	2,049	308	255	339	70	1,967	2,990	2,580	25,553	7,593	4,758	4,414	796
74R-CC, 16-17	845.13	62	145	146	2,122	310	0	347	80	2,426	3,313	3,193	27,430	7,858	0	4,713	898
75R-1, 95-96	851.95	74	120	137	1,986	307	357	358	74	3,555	2,848	3,056	25,621	7,543	5,881	4,849	820
76R-1, 32-33	861.02	42	59	76	1,249	180	1,010	217	47	1,689	1,572	1,692	15,834	4,408	19,017	3,092	555
76R-1, 69-70	861.39	48	140	110	2,006	440	420	340	60	1,974	2,988	2,646	24,943	8,166	6,566	4,716	781
76R-2, 77-78	862.97	56	103	104	2,077	300	210	379	86	2,074	2,781	2,555	27,179	7,795	3,671	4,913	992
77R-2, 97-98	872.87	54	90	102	2,279	368	47	387	82	3,000	2,136	2,274	28,401	8,439	703	5,359	1,060
78R-2, 129-130	882.79	54	107	111	2,130	356	0	379	97	2,996	3,796	2,692	27,393	8,957	0	5,437	1,106
78R-3, 31-32	883.31	53	48	44	1,192	197	0	233	50	5,943	2,023	1,056	15,920	7,086	0	4,733	809
78R-3, 98-99	883.98	46	106	119	2,370	331	0	346	82	3,000	3,241	2,575	30,100	8,692	0	4,988	958
78R-5, 65-66	886.65	47	108	111	1,919	279	347	326	76	2,455	3,316	2,809	24,742	7,023	7,418	4,612	897
79R-1, 116-117	890.46	46	99	112	2,120	329	0	372	84	3,563	3,119	2,569	27,327	7,955	0	5,478	1,227
80R-2, 89-90	901.39	48	120	135	2,130	335	0	392	81	3,522	6,047	3,112	27,887	8,389	0	5,250	1,049
80R-3, 115-116	903.15	45	98	95	2,095	298	0	355	91	3,509	3,287	2,207	26,622	7,985	0	5,040	1,170
81R-3, 100-102	912.60	54	107	121	2,178	321	78	364	87	3,266	3,758	2,727	27,974	8,925	1,377	4,912	1,001
82R-2, 93-94	920.73	49	94	112	2,115	322	43	380	75	3,401	4,521	2,687	27,626	7,918	744	5,535	854
83R-2, 147-148	930.87	54	88	112	1,744	254	427	288	68	3,014	3,333	2,410	22,905	6,257	7,866	4,050	754
83R-4, 114-115	933.54	53	104	112	2,021	304	121	364	76	4,150	3,617	2,625	25,759	7,689	2,638	4,863	909
83R-6, 147-148	936.87	58	103	127	1,901	324	0	343	72	4,288	3,086	2,788	25,342	7,916	0	4,847	951
84R-2, 116-117	940.16	57	98	117	1,992	263	152	348	81	4,285	3,143	2,616	25,606	6,892	2,926	4,813	1,045
84R-3, 130-131	941.80	51	78	89	1,836	306	452	324	84	4,765	2,183	1,839	23,286	7,128	7,966	4,479	945
85R-1, 122-123	948.32	44	70	85	1,930	277	45	338	82	3,891	2,692	1,914	24,868	7,430	1,033	4,980	1,012
85R-3, 118-119	951.28	44	77	90	1,776	303	228	327	80	4,216	1,646	2,009	23,466	7,080	6,273	4,833	1,076
85R-6, 86-87	955.46	13	0	0	133	46	128	31	19	571	0	0	1,833	1,000	3,642	644	338
86R-2, 117-118	959.47	42	81	93	1,998	318	0	333	73	3,354	3,084	2,192	26,085	7,896	0	4,617	877
86R-4, 27-28	961.57	14	28	25	533	69	994	96	26	1,339	740	792	6,605	1,494	25,387	1,365	314
87R-1, 128-129	967.78	46	68	103	2,116	285	0	366	86	3,447	2,920	2,209	27,151	7,311	0	5,325	1,067
87R-3, 104-105	970.54	14	0	16	210	50	501	38	20	790	0	518	2,480	1,023	12,344	465	302
87R-5, 8-9	972.58	44	83	105	2,038	281	64	348	75	2,154	3,304	2,320	26,893	7,098	899	4,960	884
88R-2, 117-118	978.77	43	64	95	1,872	274	83	345	79	2,504	2,738	2,278	23,813	7,061	2,808	4,663	884
88R-4, 90-91	981.50	41	71	104	1,886	256	104	353	89	2,951	3,441	2,490	24,769	6,551	2,403	5,169	1,029
89R-2, 144-145	988.24	44	79	107	2,088	245	55	359	74	2,911	3,099	2,228	25,918	6,415	951	5,111	839
89R-6, 37-38	993.17	41	82	105	2,168	306	47	400	74	3,203	3,234	2,481	27,743	7,826	764	5,407	868
90R-2, 4-5	996.44	38	81	110	2,101	297	0	387	76	2,873	3,659	2,521	27,339	7,384	0	5,045	845
90R-2, 41-42	996.81	16	20	31	436	52	1,273	76	20	1,089	268	664	5,127	1,163	34,479	1,139	296

Table T5 (continued).

Core, section, interval (cm)	Depth (mbsf)	X-ray diffraction peak intensity (cps)								X-ray diffraction peak area (total counts)							
		Smectite + chlorite	Illite	Chlorite + kaolinite	(101) Quartz	Plagioclase	Calcite	(100) Quartz	(101) Cristobalite	Smectite + chlorite	Illite	Chlorite + kaolinite	(101) Quartz	Plagioclase	Calcite	(100) Quartz	(101) Cristobalite
91R-1, 87-88	1005.47	44	65	88	2,012	252	61	348	79	4,663	2,467	2,449	25,884	6,879	1,431	5,049	1,096
92R-2, 66-67	1016.36	41	77	100	2,076	295	35	362	68	2,651	3,658	2,291	26,325	7,848	901	5,074	875
92R-5, 91-92	1021.11	42	72	95	2,092	244	0	389	83	3,694	2,635	2,218	26,218	7,040	0	5,323	1,104
93R-3, 73-75	1027.63	21	21	34	429	58	1,187	86	20	1,001	714	694	5,132	1,147	25,546	1,084	223
93R-4, 114-116	1029.54	65	101	131	2,028	285	142	364	68	4,448	4,277	3,152	26,507	7,092	2,936	4,862	860
94R-1, 116-118	1034.66	64	102	130	2,077	276	91	336	76	3,880	4,586	2,808	26,076	6,992	1,874	4,699	800
94R-3, 130-131	1037.80	40	62	100	1,391	174	823	260	51	3,018	2,094	2,405	17,842	4,467	16,886	3,614	804
95R-2, 141-142	1046.01	62	103	135	2,067	263	111	374	64	3,930	3,904	2,982	26,733	7,264	2,550	4,993	810
96R-2, 119-120	1055.29	57	78	102	1,782	244	389	337	64	3,824	3,373	2,321	22,608	6,515	7,250	4,628	696
96R-3, 15-16	1055.75	56	78	97	1,882	223	413	322	61	4,100	2,925	2,470	23,426	5,678	7,576	4,630	740
97R-1, 65-66	1062.95	47	89	111	2,137	294	0	362	79	3,185	3,404	2,428	26,790	7,356	0	5,073	839
98R-1, 25-26	1072.15	51	97	121	1,977	253	471	328	64	3,394	3,131	2,694	24,449	5,668	9,963	4,464	796
98R-3, 72-73	1075.62	45	86	115	1,998	258	338	347	72	3,678	2,474	2,455	25,544	6,148	6,648	4,852	776
99R-1, 21-22	1081.71	54	117	138	2,069	287	53	378	77	3,705	4,008	3,193	26,444	6,906	1,099	5,017	1,001
99R-2, 24-25	1083.24	49	97	127	1,953	257	224	333	49	3,169	3,522	2,960	24,749	6,330	4,699	4,598	594
100R-1, 102-103	1092.22	44	91	125	1,887	275	82	342	79	2,445	3,990	3,192	24,750	6,824	3,268	4,706	1,028
100R-2, 24-25	1092.80	28	35	52	705	101	1,407	138	20	2,188	1,111	1,069	8,580	2,307	27,047	1,889	183
101R-1, 51-52	1101.31	40	84	92	1,705	195	264	289	58	2,156	3,226	2,138	21,708	5,532	6,481	3,886	645
102R-1, 68-69	1110.88	52	64	98	1,886	210	0	331	68	3,158	3,426	2,203	24,424	6,314	0	4,975	841

Note: This table is also available in **ASCII** format.

Table T6. Normalized relative mineral abundances based on X-ray diffraction analyses of random bulk-sediment powders, Site 1174. (**See table note.** Continued on next three pages.)

Unit	Core, section, interval (cm)	Depth (mbsf)	Normalized relative mineral abundance (wt%): Total clay minerals	Quartz	Plagioclase	Calcite	Peak area ratio: (101) Cristobalite/ (100) Quartz
	190-1174A-						
I	1H-1, 38-39	0.39	48	35	17	0	0.38
I	1H-2, 96-97	2.47	50	34	15	1	0.31
	Mean Unit I:		49	35	16	0	0.34
IIA	1H-3, 109-110	4.10	45	37	18	0	0.32
IIA	2H-5, 130-131	10.50	50	35	14	0	0.33
IIA	2H-7, 131-132	13.51	49	33	16	2	0.28
IIA	3H-2, 104-105	16.45	36	37	26	2	0.29
IIA	3H-4, 75-76	18.60	51	33	16	0	0.36
IIA	3H-6, 84-85	21.39	49	34	17	0	0.33
IIA	4H-2, 63-64	25.54	52	33	15	0	0.34
IIA	4H-4, 129-130	29.20	56	30	14	0	0.40
IIA	5H-1, 99-100	33.90	47	36	16	0	0.45
IIA	5H-2, 134-135	35.75	45	34	20	1	0.39
IIA	5H-CC, 40-41	39.90	45	35	21	0	0.37
IIA	7H-2, 132-133	54.23	42	37	22	0	0.45
IIA	8H-3, 138-139	65.02	33	35	32	0	0.39
IIA	8H-4, 133-134	66.47	26	36	38	0	0.60
IIA	1R-1, 71-72	144.42	38	38	23	1	0.42
IIA	3R-1, 125-127	160.97	49	31	19	0	0.41
IIA	4R-2, 44-45	171.35	47	35	18	0	0.34
IIA	5R-1, 35-36	179.36	44	38	18	0	0.56
IIA	5R-1, 122-123	180.23	35	37	28	0	0.45
IIA	6R-1, 122-123	189.93	48	33	19	0	0.55
IIA	7R-1, 95-96	199.36	45	34	20	1	0.47
IIA	8R-1, 61-62	208.62	45	34	20	0	0.45
IIA	9R-1, 116-117	218.87	43	36	21	0	0.47
IIA	10R-1, 118-119	228.39	45	37	18	0	0.49
IIA	10R-CC, 15-16	229.48	42	36	22	0	0.42
IIA	11R-2, 15-16	238.46	44	38	18	0	0.47
IIA	12R-1, 112-113	247.63	46	37	17	0	0.59
IIA	13R-1, 106-107	257.27	50	33	15	1	0.54
IIA	13R-2, 118-119	258.89	42	34	22	3	0.48
IIA	14R-1, 19-20	266.00	45	36	19	0	0.59
IIA	15R-1, 123-124	276.73	47	32	13	7	0.49
IIA	15R-2, 48-49	277.48	51	33	14	2	0.38
IIA	16R-1, 123-124	286.33	46	36	17	2	0.38
IIA	17R-1, 110-111	295.70	44	37	18	0	0.59
IIA	18R-2, 67-68	306.47	46	34	17	3	0.33
IIA	18R-4, 81-82	309.61	48	36	16	0	0.45
	Mean Subunit IIA:		45	35	19	1	0.43
IIB	19R-1, 78-79	314.78	43	36	19	2	0.45
IIB	19R-1, 89-90	314.89	44	40	16	0	0.29
IIB	20R-2, 110-111	326.10	43	36	21	0	0.46
IIB	20R-3, 50-51	327.00	50	35	14	0	0.34
IIB	21R-1, 114-115	334.24	41	40	18	1	0.34
IIB	21R-CC, 3-4	335.75	52	33	12	3	0.38
IIB	22R-1, 25-26	342.65	40	38	19	2	0.30
IIB	23R-1, 96-97	352.96	47	37	15	1	0.37
IIB	24R-3, 117-118	365.87	44	38	18	0	0.42
IIB	25R-1, 122-123	372.52	44	37	19	0	0.71
IIB	26R-1, 56-57	381.46	49	36	15	0	0.46
IIB	27R-1, 123-124	391.73	40	38	22	0	0.71
IIB	27R-3, 115-116	394.65	48	36	16	0	0.42
IIB	28R-1, 124-125	401.44	43	38	19	0	0.60
IIB	28R-2, 49-50	402.19	42	38	20	0	0.62
IIB	29R-2, 81-82	412.11	44	38	18	0	0.39
IIB	29R-3, 133-134	414.13	47	36	17	0	0.44
IIB	29R-CC, 18-19	414.63	46	38	16	0	0.41
IIB	30R-CC, 5-6	419.45	46	38	16	0	0.40
IIB	31R-1, 116-117	430.16	49	34	17	0	0.31
	Mean Subunit IIB:		45	37	17	0	0.44

Table T6 (continued).

Unit	Core, section, interval (cm)	Depth (mbsf)	Normalized relative mineral abundance (wt%): Total clay minerals	Quartz	Plagioclase	Calcite	Peak area ratio: (101) Cristobalite/ (100) Quartz
IIC	31R-3, 44-45	432.44	44	38	17	1	0.33
	32R-2, 117-118	441.27	46	37	16	0	0.36
	32R-5, 130-131	445.90	30	29	15	25	0.27
	33R-2, 119-120	450.89	43	35	22	0	0.44
	33R-4, 18-19	452.88	44	37	20	0	0.56
	34R-3, 96-97	461.86	37	41	21	1	0.32
	35R-1, 118-119	468.28	44	37	17	2	0.40
	35R-2, 94-95	469.54	48	36	11	6	0.52
	36R-2, 133-134	479.33	42	38	16	4	0.34
	36R-3, 111-112	480.61	45	34	16	5	0.27
	Mean Subunit IIC:		42	36	17	4	0.38
III	37R-3, 130-131	490.00	45	37	18	0	0.44
	37R-4, 117-118	491.37	43	37	15	5	0.40
	38R-3, 84-85	499.14	42	37	17	5	0.35
	38R-4, 115-116	500.95	44	37	15	3	0.47
	38R-6, 62-63	503.42	40	34	14	12	0.27
	39R-1, 133-134	506.23	47	35	15	3	0.33
	39R-3, 117-118	509.07	42	39	17	2	0.48
	40R-4, 118-119	520.28	46	38	15	1	0.55
	41R-2, 29-30	526.09	42	40	15	4	0.26
	41R-CC, 20-21	529.00	46	37	18	0	0.22
	42R-1, 96-97	534.86	46	36	17	0	0.34
	42R-3, 125-126	538.15	52	35	13	0	0.23
	42R-5, 116-117	541.06	48	38	14	0	0.25
	43R-3, 99-100	547.59	47	38	16	0	0.27
	43R-5, 127-128	550.87	43	36	16	5	0.26
	43R-5, 127-128	550.87	45	35	15	5	0.26
	43R-6, 129-130	552.39	48	34	13	6	0.34
	44R-3, 117-118	557.07	50	36	14	0	0.22
	44R-4, 125-126	558.65	48	35	17	0	0.32
	45R-1, 72-73	563.32	48	36	16	0	0.42
	45R-3, 109-110	566.69	44	31	12	13	0.32
	46R-1, 149-150	573.79	42	30	12	16	0.26
	46R-4, 118-119	577.98	50	39	11	0	0.28
	46R-7, 42-43	581.72	42	31	10	17	0.21
	47R-1, 149-150	583.39	49	36	15	0	0.28
	47R-4, 119-120	587.59	57	35	9	0	0.21
	48R-2, 134-135	594.44	49	37	14	0	0.20
	48R-5, 101-102	598.61	50	38	13	0	0.22
	49R-1, 119-120	602.39	38	30	10	22	0.23
	49R-3, 99-100	605.19	47	39	14	0	0.68
	50R-1, 60-61	611.50	54	35	11	0	0.43
	50R-4, 120-121	616.60	44	36	13	7	0.42
	52R-1, 82-83	630.92	40	31	11	19	0.48
	52R-6, 115-116	638.75	43	27	14	17	0.26
	53R-1, 107-108	640.87	48	34	14	4	0.25
	53R-3, 122-123	644.02	51	34	14	1	0.30
	53R-4, 14-15	644.44	57	34	9	0	0.35
	54R-3, 127-128	653.67	49	38	14	0	0.46
	54R-5, 96-97	656.36	47	36	16	1	0.34
	55R-1, 131-132	660.31	45	35	13	7	0.56
	Mean Unit III:		46	35	14	4	0.34
IV	55R-5, 92-93	665.92	50	38	12	0	0.51
	56R-1, 114-115	669.84	46	34	18	2	0.34
	56R-2, 135-136	671.55	49	38	13	0	0.30
	57R-4, 116-117	683.96	44	34	13	10	0.24
	57R-6, 133-134	687.13	49	36	10	5	0.35
	58R-2, 75-76	690.25	48	37	13	2	0.24
	58R-4, 80-81	693.30	46	37	13	4	0.25
	59R-3, 117-118	701.77	48	37	15	1	0.24
	59R-4, 84-85	702.94	49	38	13	0	0.22
	59R-5, 128-129	704.88	49	38	12	1	0.20
	60R-2, 113-114	709.83	47	39	14	0	0.25
	61R-1, 83-84	717.74	54	35	9	3	0.24
	61R-4, 105-106	722.46	41	29	10	20	0.23
	61R-5, 116-117	724.07	49	38	11	2	0.26

Table T6 (continued).

Unit	Core, section, interval (cm)	Depth (mbsf)	Normalized relative mineral abundance (wt%) Total clay minerals	Quartz	Plagioclase	Calcite	Peak area ratio: (101) Cristobalite/ (100) Quartz
	62R-3, 97-98	730.48	52	37	11	0	0.26
	63R-2, 81-82	738.42	46	40	14	0	0.25
	63R-5, 137-138	743.48	52	35	11	2	0.22
	64R-1, 106-107	746.77	48	39	13	0	0.21
	64R-3, 118-119	749.89	51	37	12	0	0.26
	64R-5, 109-110	752.80	51	39	10	0	0.28
	65R-1, 113-114	756.14	52	37	11	0	0.27
	65R-4, 83-84	760.34	50	37	13	0	0.19
	66R-1, 114-115	765.75	47	33	12	8	0.18
	66R-5, 100-101	771.61	54	36	9	0	0.17
	67R-2, 98-99	775.43	53	34	13	0	0.20
	67R-3, 128-129	777.23	53	35	10	1	0.20
	67R-4, 128-129	778.73	52	34	11	4	0.20
	68R-1, 116-118	785.08	55	35	10	0	0.22
	68R-2, 134-136	786.76	55	34	11	0	0.19
	69R-2, 129-130	795.17	52	34	10	4	0.17
	69R-3, 96-97	796.34	45	36	10	8	0.22
	69R-4, 118-119	798.06	43	34	9	14	0.19
	70R-2, 98-99	805.78	50	31	8	11	0.17
	70R-4, 148-149	809.28	47	40	12	0	0.22
	70R-5, 148-149	810.78	55	34	11	0	0.19
	71R-2, 0-1	812.88	48	36	11	5	0.20
	71R-2, 96-97	813.84	45	42	13	0	0.21
	71R-3, 80-81	814.96	49	34	9	9	0.22
	72R-1, 45-46	822.65	37	32	10	20	0.20
	72R-1, 116-117	823.36	43	30	8	19	0.22
	72R-3, 106-107	826.26	42	35	11	13	0.20
	73R-1, 78-79	832.58	43	36	10	10	0.18
	73R-3, 118-119	835.98	53	37	10	0	0.14
	73R-5, 114-115	838.94	45	34	9	13	0.15
	73R-7, 49-50	841.29	53	30	9	8	0.20
	74R-1, 128-129	842.68	26	17	5	52	0.18
	74R-2, 56-57	843.46	47	30	10	13	0.19
IV	74R-2, 123-124	844.13	48	31	11	10	0.18
	74R-CC, 16-17	845.13	55	34	11	0	0.19
	75R-1, 95-96	851.95	49	31	9	10	0.17
	76R-1, 32-33	861.02	29	20	6	44	0.18
	76R-1, 69-70	861.39	46	29	11	14	0.17
	76R-2, 77-78	862.97	48	35	11	7	0.20
	77R-2, 97-98	872.87	48	41	12	0	0.20
	78R-2, 129-130	882.79	57	32	11	0	0.20
	78R-3, 31-32	883.31	60	32	8	0	0.17
	78R-3, 98-99	883.98	53	36	11	0	0.19
	78R-5, 65-66	886.65	49	28	9	14	0.19
	79R-1, 116-117	890.46	55	35	10	0	0.22
	80R-2, 89-90	901.39	67	25	8	0	0.20
	80R-3, 115-116	903.15	56	34	10	0	0.23
	81R-3, 100-102	912.60	57	32	11	0	0.20
	82R-2, 93-94	920.73	61	30	9	0	0.15
	83R-2, 147-148	930.87	51	27	7	15	0.19
	83R-4, 114-115	933.54	58	31	8	2	0.19
	83R-6, 147-148	936.87	57	34	9	0	0.20
	84R-2, 116-117	940.16	56	33	8	3	0.22
	84R-3, 130-131	941.80	47	32	7	14	0.21
	85R-1, 122-123	948.32	55	36	9	0	0.20
	85R-3, 118-119	951.28	45	35	8	12	0.22
	85R-6, 86-87	955.46	18	24	8	50	0.52
	86R-2, 117-118	959.47	55	35	10	0	0.19
	86R-4, 27-28	961.57	21	12	3	64	0.23
	87R-1, 128-129	967.78	55	36	9	0	0.20
	87R-3, 104-105	970.54	13	13	4	69	0.65
	87R-5, 8-9	972.58	55	35	10	0	0.18
	88R-2, 117-118	978.77	52	33	10	5	0.19
	88R-4, 90-91	981.50	57	32	8	3	0.20
	89R-2, 144-145	988.24	56	35	9	0	0.16
	89R-6, 37-38	993.17	55	35	10	0	0.16
	90R-2, 4-5	996.44	58	33	9	0	0.17

Table T6 (continued).

Unit	Core, section, interval (cm)	Depth (mbsf)	Normalized relative mineral abundance (wt%)				Peak area ratio: (101) Cristobalite/ (100) Quartz
			Total clay minerals	Quartz	Plagioclase	Calcite	
IV	90R-2, 41-42	996.81	13	10	3	74	0.26
	91R-1, 87-88	1005.47	55	37	8	0	0.22
	92R-2, 66-67	1016.36	57	32	10	0	0.17
	92R-5, 91-92	1021.11	54	37	9	0	0.21
	93R-3, 73-75	1027.63	19	10	3	68	0.21
	93R-4, 114-116	1029.54	61	30	7	2	0.18
	94R-1, 116-118	1034.66	63	29	7	0	0.17
	94R-3, 130-131	1037.80	38	23	5	34	0.22
	95R-2, 141-142	1046.01	59	31	8	2	0.16
	96R-2, 119-120	1055.29	53	27	7	12	0.15
	96R-3, 15-16	1055.75	51	30	6	13	0.16
	97R-1, 65-66	1062.95	57	34	9	0	0.17
	98R-1, 25-26	1072.15	48	28	6	18	0.18
	98R-3, 72-73	1075.62	48	33	7	12	0.16
	99R-1, 21-22	1081.71	61	31	8	0	0.20
	99R-2, 24-25	1083.24	55	30	8	8	0.13
	100R-1, 102-103	1092.22	58	28	9	5	0.22
	100R-2, 24-25	1092.80	26	14	4	57	0.10
	101R-1, 51-52	1101.31	51	27	8	14	0.17
	Mean Unit IV:		49	32	10	9	0.21
V	102R-1, 68-69	1110.88	59	33	8	0	0.17

Note: This table is also available in **ASCII** format.

Table T7. Structural data, Hole 1174B. (See table notes. Continued on next eight pages.)

Core, section, interval (cm)	Depth (mbsf)	Cr az. (°)	Cr dip (°)	Cr line	Cr l.plunge	Pm az.	Pm dip	Identifier	Notes	Comments
190-1174B						270				
1R	143.7					191			Highly disturbed mud and sands	
2R	150.1								Highly disturbed mud and sands	
3R	159.7								Highly disturbed mud and sands	
4R	169.4								Highly disturbed mud and sands	
5R	179.0								Highly disturbed mud and sands	
6R-1	188.7							Bed	Horizontal	
6R-2	190.2							Bed	Horizontal	
6R	188.7								Planar fissility, anastomosing microlayering	
6R-1, 122-133	190.0							Slump	Or convolute lamination, 5 mm length	
7R	198.4								Highly disturbed mud and sands	
7R-1	198.4								Biscuit with deformation bands	
8R	208.0							Bed	Horizontal, silty clays and sands with planar fissile intervals	
8R-1, 54-56	208.6							Deformation bands		
9R	217.7								Planar fissility, anastomosing microlayering	
9R-2, 29-30	219.5	0	4			335	4	Bed	(84-101)	
9R-1, 30-35	218.0	90	60-90				60-90	Deformation bands	9 bands	
9R-1, 50-55	218.2	270	60				60	Deformation bands	2 bands	
9R-1, 68-72	218.4							Deformation bands	3 bands	
10R-1, 19-23	227.4	23	36				36	Bed		
10R-1, 94-101	228.2	159	14				14	Bed	Laminations	
10R-1, 94-101	228.2	341	52				52	Deformation bands		
10R-1, 94-101	228.2	345	46				46	Deformation bands		
10R-1, 94-101	228.2	330	46				46	Deformation bands		
10R-1, 42-114	228.0	90	34				34	Deformation bands		
10R-2, 56-62	229.3	341	45				45	Deformation bands		
10R-2, 59-62	229.3	207	46				46	Deformation bands		
11R-1, 21-28	237.0	90	20				20	Deformation bands	Apparent dip only	
11R-2, 13-15	238.4	161	69			241	69	Deformation bands	(5-18)	
11R-2, 13-15	238.4	325	69			44	69	Deformation bands	(5-19)	
12R-1, 76-84	247.3	90	60				60	Deformation bands	Apparent dip only, 4 bands (61,59,53,54)	
12R-1, 76-84	247.3	270	41				41	Deformation bands	Apparent dip only	
12R-1, 9-20	246.6	90	53				53	Deformation bands	Apparent dip only, 3 bands (48, 53, 60)	
13R-1, 112-125	257.4	135	7			244	7	Bed	(112-125)	
13R-2, 104-104	258.7	0	0			360	0	Bed	Horizontal	
13R-2, 75-75	258.5	27	4			280	4	Bed	(62-75)	
13R-3, 6-6	259.3	1	10			21	10	Bed	(1-10)	
13R-2, 56-58	258.3	176	54			208	54	Deformation bands	(49-60)	
13R-2, 56-58	258.3	179	60			211	60	Deformation bands	(49-61)	
14R-1, 15-20	266.0							Deformation bands	5 bands: deflection of broken edge suggests reverse movement	
14R-CC, 8-10	266.3							Deformation bands	2 bands: deflection of broken edge suggests reverse movement	
15R-1, 0-3	275.5							Deformation bands	6 bands	
15R-1, 2-4	275.5							Deformation bands	1 band	
15R-1, 15-16	275.7							Deformation bands	2 bands, 2 mm wide, dipping	
15R-1, 18-19	275.7							Deformation bands	3 bands, two shallow and one steep dipping	
15R-1, 20-27	275.7							Deformation bands	1 band, bed-deformation band angle 15	
15R-1, 38-42	275.9							Deformation bands	2 bands, 1mm wide, bed-deformation band angle 31	
15R-1, 68-73	276.2							Deformation bands	3 bands, 1-2 mm wide, bed-deformation band angle 63	
15R-1, 68-73	276.2							Deformation bands	1 band, narrow, bed-deformation band angle 50	
15R-1, 80-84	276.3							Deformation bands	1 band, 1-2 mm wide, bed-deformation band angle 45	
15R-1, 80-84	276.3							Deformation bands	2 bands, 0.5 mm wide, bed-deformation band angle 62	
15R-1, 102-107	276.5							Deformation bands	2 bands, 0.5-3 mm, bed-deformation band angle 43	
15R-2, 17-30	277.2	150	34			200	34	Deformation bands	(14-33); no: 6	
15R-2, 17-30	277.2	0	54			50	54	Deformation bands	(4-33); no: 3	
15R-2, All	277.0	0	0				0	Bed	Horizontal	
15R-CC, 2-7	277.5	25	53			51	53	Deformation bands	(2-7), average of 4 band dip, 1-3 mm thick	
15R-CC, 2-7	277.5	180	45			206	45	Deformation bands	(2-7), average of 1 band dips, <1 mm thick	
15R-CC, 7-14	277.6	150	49			317	49	Deformation bands	(7-14), average of 6 band dip, 1-3 mm thick	Probably don't trust pmag-edge effects?

Table T7 (continued).

Core, section, interval (cm)	Depth (mbsf)	Cr az. (°)	Cr dip (°)	Cr line	Cr l.plunge	Pm az.	Pm dip	Identifier	Notes	Comments
15R-CC, 16-20	277.7	180	42			47	42	Deformation bands	(16-20), average of 5 band dip, 1 mm thick	
15R-CC, 16-20	277.7	0	47			227	47	Deformation bands	(16-20), average of 5 band dip, <1 mm thick)	
15R-CC, 21-25	277.7							Deformation bands	6 bands, <1 mm thick	
15R-CC, 21-25	277.7							Deformation bands	3 bands, piece so small	
16R	285.1	0	0				0	Bed		
16R-1, 115-122	286.3	130	62			25	62	Deformation bands		
16R-1, 115-122	286.3	140	63			35	63	Deformation bands		
17R-2, 103-112	297.2	16	61			38	61	Deformation bands	(99-112)	
17R-2, 103-112	297.2	129	56			151	56	Deformation bands	(99-112)	
17R-2, 93-99	297.1	350	50			209	50	Deformation bands	(89-99)	
17R-2, 93-99	297.1	180	57			39	57	Deformation bands	(89-99)	
18R-1, 41-42	304.7	70	47			40	47	Deformation bands	(37-46)	
18R-1, 41-42	304.7	42	42			12	42	Deformation bands	(37-46)	
18R-1, 41-42	304.7	238	9			208	9	Deformation bands	(37-46)	Corrected cr az., cr dip
18R-1, 50-52	304.8	67	67			37	67	Deformation bands	(37-46)	
18R-1, 53-56	304.8	42	53				53	Deformation bands	(53-69)	
18R-1, 60-62	304.9	72	64				64	Deformation bands	(53-69)	
18R-1, 60-62	304.9	236	26				26	Deformation bands	(53-69)	
18R-2, 0-35	306.0	194	31			54	31	Fracture	Parallel to the bedding, widespread lineated	Coherent
18R-2, 0-35	306.0	187	60			47	60	Fracture	Axial cleavage? In a growing fault fold, reverse sense	Declination
18R-2, 0-35	306.0			180	0			Intersection lineation		
18R-2, 0-35	306.0			280	30			Slickenlines	Present in all the surfaces, shear sense not clear	
18R-4, 120-125	310.0	339	45			211	45	Deformation bands	(120-136)	
18R-4, 120-125	310.0	337	47			209	47	Deformation bands	(120-136)	
18R-4, 27-50	309.2	199	30				30	Bed		
18R others	307.3	0	0				0	Bed	Horizontal	
19R	314.0	0	0				0	Bed	Horizontal; coarse sand (last?), no deformation bands	
20R	323.5	0	0				0	Fissility	Up to 5° dip; no deformation bands	
21R	333.1	0	0				0		Bioturbation - bedding, fissility rarely observed	
22R	342.4	0	0				0	Fissility	Rarely observed	
23R	352.0	0	0				0	Bed		
24R	361.7	0	0				0	Bed		
25R	371.3	0	0				0	Fissility		
26R	380.9								Highly disturbed	
27R-2	392.0	230	42				42	Deformation bands		
28R	400.2	0	0				0	Bed and fissility		
29R-1	409.8	0	0				0	Bed		
29R-2	411.3	0	0				0	Bed		
29R-3, 108-111	413.9	170	48			351	48	Deformation bands	(103-116)	
29R-3, 108-111	413.9	28	48			209	48	Deformation bands	(103-116)	
29R-3, 111-113	413.9	39	48			220	48	Deformation bands	(103-116)	
29R-3, 12-16	412.9	208	12			328	12	Bed	(13-23)	
29R-3, 109-113	413.9	0	19			181	19	Bed	(109-113)	
29R-3, 107-109	413.9	158	28			339	28	Fracture zone	(107-109)	
29R-3, 55-58	413.4	267	43			219	43	Fracture zone	(48-63)	
29R-3, 55-58	413.4	180	0			132	0	Bed	(48-63)	
30R								Bed		
31R	429.0									
32R	438.6									
32R-1, 0-0	438.6	0	0				0	Bed		
32R-2, 0-0	440.1	0	0				0	Bed		
32R-3, 0-0	441.6	0	0				0	Bed		
32R-4, 59-59	443.7	35	9			18	9	Bed	(55-64)	
32R-5, 124-124	445.8	336	10			268	10	Bed	(122-132)	
32R-6, 81-81	446.9	111	14			337	14	Bed	(63-95)	
33R-1, 141-146	449.6	0	0				0	Bed		
33R-1, 65-65	448.9	240	8			10	8	Bed	(54-80)	
33R-3, 40-40	451.6	309	6			289	6	Bed	(4-45)	
33R-5, 70-72	454.9	7	30			52	30	Bed	(66-84)	
33R-3, 127-130	452.5							Fault	Normal fault 1-5 mm apparent displacement; length 3 cm	
33R-3, 140-150	452.7							Fault	Normal fault 1-5 mm apparent displacement; length 6 cm	
34R-1, 42-52	458.4	185	45			25	45	Fracture zone	Coring induced?	
34R-1, 52-down	458.4	0	0				0	Bed		
34R-2, 0-0	459.4	0	0				0	Bed		
34R-3, 0-0	460.9	0	0				0	Bed		

Table T7 (continued).

Core, section, interval (cm)	Depth (mbsf)	Cr az. (°)	Cr dip (°)	Cr line	Cr l.plunge	Pm az.	Pm dip	Identifier	Notes	Comments
34R-4, 0-0	462.4	0	0				0	Bed		
34R-5, 16-84	464.4							Rubble interval	No evidences of internal deformation	
34R-5, 84-100	464.8	0	90				90	Bed		
34R-CC, 0-20	465.0	0	90				90	Bed		
35R-1, 0-30	467.3							Rubble interval		
35R-1, 27-62	467.8	336	57			49	57	Fracture set		
35R-1, 27-62	467.8	321	37			34	37	Fracture set		
35R-1, 27-62	467.8	344	53			57	53	Fracture set		
35R-1, 27-62	467.8	335	48			48	48	Fracture set		
35R-1, 27-62	467.8	90		90	45			Slickenline		
35R-1, 30-115	467.8	346	44				44	Bed	(15-30), representative measurement	
35R-2, 15-30	468.8	270	75				75	Bed	Apparent only	
35R-2, 50-62	469.2	150	90				90	Bed		
35R-2, 35-38	469.0	134	45				45	Bed	(32-40)	
35R-CC, 0-0	469.7							Rubble interval	Coring induced?	
36R-1, 12-14	476.6	0	90				90	Bed		
36R-2	478.0	0	0				0	Bed		
36R-3	479.5	0	0				0	Bed		
36R-4	481.0	0	0				0	Bed		
36R-5	482.5	0	0				0	Bed		
37R-1	485.7	0	0				0	Bed		
37R-3, 114-116	489.9	42	32			50	32	Fracture	(85-125)	
37R-4, 38-40	490.6	273	36			358	36	Fracture	(26-63 (87?))	
37R-5, 10-12	491.8	155	32			180	32	Fracture	(0 (10)-50)	
37R-2, 112-114	488.3	194	8			354	8	Bed	(104-116 (?))	
37R-2, 88-89	488.1	270	4			70	4	Bed	(79-104)	
37R-5, 66-67	492.4	0	2			25	2	Bed	(58-69)	
38R-6, 99-105	503.8	248	71			308	71	Fracture	Fracture zone (90-150)	
38R-6, 102-104	503.8	165	41			225	41	Fracture	Fracture zone (90-150)	
38R-6, 102-104	503.8	90	2			150	2	Fracture	Fracture zone (90-150)	
38R-6, 118-124	504.0	203	41			263	41	Fracture	Fracture zone (90-150)	
38R-6, 134-137	504.2	157	27			217	27	Fracture	Fracture zone (90-150)	
38R-6, 134-137	504.2	157	43			217	43	Fracture	Fracture zone(90-150)	
38R-6, 140-143	504.2	155	40			215	40	Fracture	Fracture zone (90-150)	
38R-6, 140-143	504.2			155	40			Slickenline	Fracture zone (90-150)	
38R-6, 134-137	504.2			204	15			Slickenline	Fracture zone(90-150)	
38R-6, 140-143	504.2			230	20			Slickenline	Fracture zone (90-150)	
38R-7, 3-8	504.4	111	37			178	37	Fracture	Fracture zone	
38R-7, 3-8	504.4			212	60	67		Slickenline	Fracture zone	
38R-7, 4-5	504.3	180	10			247	10	Bed		
38R-4, 83-91	500.7	0	2			300	2	Bed	(82-92)	
38R-1, 80-81	496.1	180	8			305	8	Bed	(57-99)	
39R-1, 29-31	505.2	195	19			35	19	Fracture	(25-41)	
39R-1, 29-31	505.2			204	10	200		Slickenline	(25-41)	
39R-1, 29-29	505.2	186	10			26	10	Bed	(25-41)	
39R-3, 96-96	508.9	90	7			300	7	Bed	(92-110)	
39R-3, 32-32	508.2	117	4			317	4	Bed	(14-63)	
39R-4, 36-44	509.8	289	38			297	38	Deformation bands	Found in ash layer	
39R-4, 36-44	509.8	315	55			323	55	Deformation bands	Found in ash layer	
40R	514.6	0	0				0	Bed		
40R-4, 86-86	520.0	294	10			251	10	Deformation band	1-mm-wide deformation band associated with veins; (83-104)	
40R-4, 84-90	520.0							Veins	Curved dark veins	
40R-5, 80-85	521.4	220	39			295	39	Fault	1-2 mm wide; (50-110)	
40R-CC, 21-24	523.8							Vein	Open fracture with green transparent crystals (calcite?)	
41R	524.3	0	0				0	Bed	Horizontal	
41R-1, 7-10	524.4					200		Vein	Sediment-filled veins, perpendicular to bedding (5-15)	
41R-1, 25-31	524.6	190	55				55	Normal fault	5-mm normal displacement	
41R-2, 125-150	527.2							Breccia	Steeply inclined fractures, probably drilling induced	
41R-3, 133-150	528.7							Breccia	Steeply inclined fractures, 2 sets, interstitial mud	
42R-1, 130-132	535.2	62	21			107	21	Normal fault	2-mm offset	
42R-1, 68-68	534.6	244	11				11	Bed	(65-80)	
42R-2, All	535.4	0	0				0	Bed	Rest of core horizontal	
43R-2, 55-66	545.7	?	90				90	Vein	Subvertical, sediment-filled veins	
43R-2, 70-77	545.8	?	90				90	Vein	Subvertical, sediment-filled veins	
43R-4, 10-21	548.3							Fault	Apparent 090, 45 in core face; branching fault	

Table T7 (continued).

Core, section, interval (cm)	Depth (mbsf)	Cr az. (°)	Cr dip (°)	Cr line	Cr l.plunge	Pm az.	Pm dip	Identifier	Notes	Comments
43R-4, 27-36	548.4							Slickenline		
43R-4, 41-46	548.5	288	76				76	Reverse fault	1-mm reverse offset (21-46)	
43R-4, 53-62	548.7	0	90				90	Normal fault	<1-mm offset (47-63)	
43R-4, 68-69	548.8	280	44			350	44	Fault		
43R-4, 102-109	549.2			90	60			Slickenline		
43R-4, 102-109	549.2	274	74			314	74	Fault		
43R-5, 37-47	550.0	214	70			184	70	Normal fault	<1-mm offset (31-75)	
43R-6, 79-94	552.0	205	71			225	71	Normal fault	<1-mm offset (78-99)	
44R-1, 18-25	553.1	159	58			344	58	Fault	No clear offset (12-37)	
44R-2, 42-55	554.9	67	8			172	8	Bed	(42-55)	
44R-2, 99-106	555.4	162	63			177	63	Normal fault	1-cm apparent offset (82-114)	
44R-3, 39-46	556.3	110	72			280	72	Normal fault	Unknown amount of offset	
44R-3, 48-65	556.5	209	70			19	70	Normal fault	1- to 5-mm-wide zone (48-65)	
44R-4, 0-150	278.7	0	0				0	Bed	Horizontal	
44R-4, 0-14	557.5	154	73			104	73	Fault	Curviplanar zone of two faults (0-14)	
44R-4, 54-67	558.0	32	73			42	73	Fault	(49-71)	
45R-1, 10-14	562.7							Fault	Rounded piece, no orientation	
45R-1, 0-150	563.4		0				0	Bed	No clear bedding, but subhorizontal based on burrows	
46R-2, 63-74	574.5	315	68			108	68	Normal fault	12-mm offset (37-116)	
46R-2, 125-130	575.1	5	52			30	52	Fault	(117-144)	
46R-2, 1-150	574.6		0				0	Bed	Horizontal	
46R-3, 59-62	575.9							Fault	3-mm offset, apparent orientation 270, 80	
46R-4, 1-150	577.6		0				0	Bed	Horizontal bedding, based on bioturbation	
46R-5, 1-150	579.1		0				0	Bed	Horizontal bedding, based on bioturbation	
46R-6, 63-82	580.5	172	75			242	75	Fault	Curviplanar steep fault (63-82)	
47R-1, 49-55	582.4	32	40			72	40	Deformation bands	3 deformation bands in ash layer (48-68)	
47R-2, 52-62	584.0	198	90			238	90	Fault	Curviplanar, probably the same fault that next one (36,61)	
47R-2, 61-73	584.1	9	65			39	65	Fault	15-mm normal offset (61-98)	
47R-2, 69-91	584.2	45	59			75	59	Fault	20-mm normal offset (61-98)	
47R-2, 0-0	583.4	0	0				0	Bed	Horizontal bedding, based on bioturbation	
47R-3, 45-55	585.4	150	63			145	63	Fault	23-mm normal offset (43-57)	
47R-3, 121-130	586.2	143	67			133	67	Fault	Narrow fault (116-134)	
47R-4, 0-0	586.4	0	0				0	Bed	Horizontal bedding, based on bioturbation	
47R-5, 0-0	587.9	0	0				0	Bed	Horizontal bedding, based on bioturbation	
47R-6, 0-0	589.4	0	0				0	Bed	Horizontal bedding, based on bioturbation	
48R-2, 101-103	594.1	328	9			333	9	Bed	(99-111)	
48R-4, 4-15	596.2	302	87			292	87	Fault	5-mm normal offset, curviplanar and anastomosing (6-23)	
49R-1, 64-89	602.0	0	90				90	Fault	Anastamozing, near vertical fault; 0.5-mm normal displacement	
49R-1, All	601.2							Horizontal bedding		
49R-2, All	602.7							Horizontal bedding		
49R-3, All	604.2							Horizontal bedding		
50R-1, 66-83	611.6	188	77			328	77	Fault	(68-80)	
50R-1, 98-117	612.0	190	80			225	80	Fault	(98-115)	
50R-1, 98-117	612.0	350	60				60	Slickenline		
50R-2, 73-73	611.6	315	14				14	Bedding	(70-78)	
50R-1, 121-121	612.1	147	12			207	12	Bedding	(110-125)	
51R	620.5	0	0				0	Bed		
52R	630.1	0	0				0	Bed		
53R	639.8	0	0				0	Bed		
54R-2, 70-88	651.7	88	80			38	80	Fracture	(63-94)	
54R-2, 70-88	651.7			270	51			Slickenline	Measured on core face	
54R-3, 116-127	653.6	124	32			118	32	Fracture	(110-128)	
54R-3, 116-127	653.6	197	31			191	31	Fracture	(110-128)	
54R-3, 116-127	653.6	336	24			330	24	Fracture	(110-128)	
54R-3, 80-91	653.6							Fracture		
54R-3, 80-91	653.3			270	51			Slickenline	Measured on core face (270/20 - get az. tr)	
54R-3, 22-31	652.7	129	30			84	30	Fracture	(22-31)	
54R-3	652.4			270	35			Slickenline	Measured on core face (270/35 - get az. tr)	
54R-4, 36-36	654.3	14	8			314	8	Bed	(0-36)	
54R-4, 92-93	654.8	9	6				6	Bed	(80-98)	
54R-7, 31-31	658.7	256	8				8	Bed		
55R-1, 0-0	659.0		0				0	Bed		
56R-1, 0-0	668.7		0				0	Bed		
57R-3, 97-97	682.3	238	9			273	9	Bed		

Table T7 (continued).

Core, section, interval (cm)	Depth (mbsf)	Cr az. (°)	Cr dip (°)	Cr line	Cr l.plunge	Pm az.	Pm dip	Identifier	Notes	Comments
58R-2, 22-40	689.8							Fractures	Coring-induced? Horizontal slickenlines	
58R-2, 78-120	690.5							Fractures	Coring-disturbed interval	
59R-1, All	697.6	0	0				0	Bedding	Heavy drilling breakage	
59R-2, All	699.1	0	0				0	Bedding	Heavy drilling breakage	
59R-3, All	700.6	0	0				0	Bedding	Heavy drilling breakage	
59R-4, All	702.1	0	0				0	Bedding	Heavy drilling breakage	
59R-5, All	703.6	0	0				0	Bedding	Heavy drilling breakage	
59R-6, All	705.1	0	0				0	Bedding	Heavy drilling breakage	
60R-6, 89-96	715.6		90				90	Fault	(80-96, only apparent)	
60R-5, 58-60	713.8	301	12			279	12	Bed	(57-65)	
61R-1, 0-37	716.9	0	90(?)			180	90(?)	Fault	(0-39)	
61R-4, 133-137	722.7	270	31			247	31	Fracture zone	(130-141)	
61R-5, 19-25	723.1	218	36			218	36	Fracture zone	(14-29)	
61R-5, 19-25	723.1			37	44	360		Slickenline	(14-29)	
62R-4, 145-148	732.5	11	25			96	25	Fractures	(140-148)	
62R-5, 46-47	733.0	288	34			253	34	Fractures	(30-40)	
62R-5, 50-52	733.0	348	41			313	41	Fractures	(30-41)	
62R-5, 15-16	732.7	346	41				41	Fracture	(6-16)	
63R-6, 52-59	744.1	6	60			46	60	Fracture	(50-59)	
63R-6, 60-64	744.2	10	56			50	56	Fracture	(50-59?) Highly disturbed region	
63R-6, 60-64	744.2	358	51			38	51	Fracture	(50-59?) Highly disturbed region	
63R-6, 101-105	744.6	349	42				42	Fracture	(95-112)	
64R-1, 103-150	746.7	0	7				7	Bed		
64R-1, 44-51	746.1	12	43				43	Fracture		
64R-1, 44-51	746.1			63	15			Slickenline		
64R-2, 3-5	747.2	196	18			46	18	Fracture	(3-17)	
64R-2, 3-5	747.2	33	32			243	32	Fracture	(3-17)	
64R-2, 27-30	747.5	44	39			264	39	Fracture	(20-34)	
64R-2, 38-42	747.6	55	42			265	42	Fracture	(35-48)	
64R-2, 81-87	748.0	353	36				36	Fracture zone		
64R-2, 98-102	748.2	48	78				78	Fracture zone		
64R-2, 98-102	748.2	235	26				26	Fracture zone		
64R-2, 69-80	747.9	20	40			50	40	Fracture zone	(69-80)	
64R-2, 69-80	747.9			70	30			Slickenline		
64R-2, 69-80	747.9	198	16			228	16	Fracture zone	(69-80)	
64R-3, 37-44	749.1	0	8				8	Bed		
64R-5, 0-3	751.7	114	22			73	22	Bed	(0-9)	
64R-5, 0-3	751.7	185	12			144	12	Bed	(0-9)	
65R-1, 32-39	755.3	205	60				60	Dark seam	(27-52)	
65R-1, 124-135	756.2	90	59				59	Fault	2-mm normal displacement, apparent only	
65R-2, 22-33	756.7	152	80			132	80	Fault	1-mm displacement (0-33)	
65R-2, 106-115	757.6	142	72			187	72	Normal fault	(106-115)	
65R-4, 1-12	759.5	270	90				90	Fracture	No slickensides	
65R-5, 76-87	761.8	135	59			152	59	Fracture	Biscuit 76-87	
65R-6, 67-68	763.2	187	23				23	Bed		
65R-6, 15-35	762.7	218	19				19	Bed		
66R-1, 1-150	764.6							Bed	<10° from *Zoophycos*	
66R-2, 93-93	767.0	326	7			327	7	Bed	(85-93)	
66R-3, 1-150	767.6	234	23				23	Bed		
66R-3, 0-18	767.6	10	74			42	74	Fracture	(0-18)	
66R-3, 21-22	767.8	45	19			85	19	Fracture zone	(0-22)	
66R-4, 44-53	769.5	187	66			167	66	Fracture	(44-82); slickenlines subperpendicular to core axis	
66R-4, 93-105	770.0	172	70			120	70	Fracture	(93-105); no slickensides	
66R-4, 111-127	770.2	18	62			328	62	Fracture zone	(111-127)	
66R-5, 29-36	770.9	129	52			129	52	Fracture zone	(29-53); polished surface	
66R-5, 29-36	770.9	0	0			360	0	Fracture	(29-53)	
66R-5, 29-36	770.9			15	37			Slickenline	Slickenlines on above fracture	
66R-5, 29-36	770.9	255	53				53	Fracture	Drilling fracture	
67R-1, All	774.2	0	7				7	Bed	Subhorizontal to 5-10°	
67R-2, All	774.4	0	7				7	Bed	Subhorizontal to 5-10°	
67R-3, All	775.9	0	7				7	Bed	Subhorizontal to 5-10°	
67R-4, 22-23	777.7	180	8				8	Bed	(1-33)	
67R-5, 52-53	779.5	233	15			3	15	Bed	(35-55)	
67R-6, 72-73	781.2	216	13			236	13	Bed	(60-87)	
67R-6, 110-142	781.5					14		Fracture zone		
67R-6, 110-142	781.5	302	62				62	Fracture	Set 1	

Table T7 (continued).

Core, section, interval (cm)	Depth (mbsf)	Cr az. (°)	Cr dip (°)	Cr line	Cr l.plunge	Pm az.	Pm dip	Identifier	Notes	Comments
67R-6, 110-142	781.5	288	19				19	Fracture	Set 2	
67R-7, 35-52	782.3							Fracture zone	Octagonal set of fractures, coring induced	
67R-7, 77-100	782.7							Fracture zone	Rounded pieces at the bottom, coring induced	
67R-8, 1-18	783.5							Fracture zone	Rounded large pieces, coring induced	
68R-1, 107-108	785.0	42	15			32	15	Bed	(76-120)	
68R-3, 30-42	787.2	30	19				19	Fracture zone	Set 15-mm spacing	
68R-3, 30-42	787.2	37	46				46	Fracture zone	Set 15-mm spacing	
68R-CC, 4-6	787.4	52	85				85	Fault	5-mm normal offset, too small piece, slickenlines downdip	
69R-1, 0-26	793.6	17	10			237	10	Bed	(0-26)	
69R-2, 72-129	794.6	150	19			300	19	Bed	(72-119)	
69R-3, 33-62	795.7	15	19			245	19	Bed	(33-62)	
69R-4, 25-26	797.1	14	12			244	12	Bed	(0-65)	
69R-4, 94-104	797.8	270	90			30	90	Fracture	(68-120)	
69R-5, 53-70	798.9	120	19			275	19	Bed	(33-70)	
69R-6, 125-125	801.1	0	27			230	27	Bed	(90-127)	
69R-6, 129-135	801.2							Fractured zone	6-mm-thick polished flakes, 2-cm blocks	
69R-6, 144-149	801.3							Fissile zone	10-mm-wide zone of strong parting fissility	
69R-7, 0-38	801.4							Bed		
69R-7, 38-80	801.8	180	20			40	20	Bed	*Zoophycos* average	
69R-8, 27-36	803.1	203	71			63	71	Normal fault	(27-36)	
69R-8, 27-36	803.1			113	85			Slickenlines	Near vertical downdip	
70R-1, 30-40	803.6	90	12	300	23	45	12	*Zoophycos*	(13-143)	
70R-2, 44-46	805.2	32	19			292	19	*Zoophycos*	(10-45)	
70R-2, 62-63	805.4	40	15			275	15	*Zoophycos*	(59-73)	
70R-3, 111-111	807.4	54	18			259	18	*Zoophycos*	(55-134)	
70R-4, 17-41	808.0							Fractured zone	3- to 10-mm lenses, 1- to 4-cm blocks	
70R-4, 4-6	807.8	37	47			57	47	Bed	(0-8)	
70R-4, 56-58	808.4	36	32			46	32	*Zoophycos*	(47-64)	
70R-5, 27-29	809.6	36	33				33	Bed		
70R-5, 75-76	810.1	315	30			355	30	Bed	(73-76)	
70R-5, 130-130	810.6	43	25			63	25	Bed	(129-135)	
70R-4, 48-76	808.3							Fracture zone	4-cm spacing between fractures	
70R-4, 77-83	808.6							Fracture zone	1- to 2-cm spacing between fractures	
70R-4, 83-150	808.6							Fracture zone	3-cm blocky fracture; slickensides	
70R-5, 1-110	809.3							Fracture zone	2- to 6-cm spacing; blocky	
70R-5, 110-123	810.4							Fracture zone	2- to 5-mm scale of fragments	
70R-5, 123-152	810.5							Fracture zone	1- to 4-cm spacing	
71R-2, 19-28	813.1							Bed	Parallel bioturbation; 90, 30 in core face.	
71R-2, 30-38	813.2	41	38			1	38	Fracture	Bedding parallel, fracture set 1	
71R-2, 30-38	813.2	295	54			255	54	Fracture	Fracture set 2	
71R-2, 49-77	813.4	226	71			106	71	Fracture	Fracture set (as above, rotated)	
71R-2, 49-77	813.4	102	84			342	84	Fracture	Fracture set (as above, rotated)	
71R-2, 49-77	813.4	206	13			86	13	Fracture	Set forms lenses in core face	
71R-2, 78-96	813.7	206	13				13	Bed		
71R-3, 16-35	814.3	197	31				31	Bed?		
71R-3, 50-80	814.7							Fracture zone	Blocky fragments up to 3 cm on average, slickenlined	
71R-3, 80-94	815.0							Fracture zone		
71R-CC, 0-31	815.2							Fracture zone		
72R-1, 46-46	822.7	283	47				47	Fracture set	(46-60?) coherent hemipelagite	
72R-1, 48-55	822.7	355	58				58	Fracture set	(46-60?) coherent hemipelagite	
72R-1, 111-123	823.3	164	44				44	Fracture set	Shattered zone, with inclined fabric, fragments 5-1 cm	
72R-1, 120-130	823.4							Fracture set	Shattered zone, apparent dip in core face: 270, 14	
72R-1, 145-148	823.7	199	60				60	Fracture set	Highly fractured zone, fragments 2-5 cm	
72R-2, 0-10	823.7	193	70				70	Fracture set	(0-10)	
72R-2, 27-34	824.0	203	65				65	Fracture set		
72R-2, 27-34	824.0	328	43				43	Fracture set		
72R-2, 43-47	824.1	163	44				44	Fracture set		
72R-2, 54-57	824.2							Fracture set	Apparent dip in core face: 270, 30	
72R-2, 70-75	824.4	247	30				30	Fracture set		
72R-2, 102-110	824.7	180	51				51	Fracture set		
72R-2, 102-110	824.7							Fracture set	Apparent dip in core face: 270, 51; set 1	
72R-2, 102-110	824.7							Fracture set	Apparent dip in core face: 90, 14; set 2	
72R-2, 102-110	824.7	0	0				0	Fracture set	Horizontal fracture; set 3	
72R-3, 65-70	825.9	188	60			118	60	Fracture set		

Table T7 (continued).

Core, section, interval (cm)	Depth (mbsf)	Cr az. (°)	Cr dip (°)	Cr line	Cr l.plunge	Pm az.	Pm dip	Identifier	Notes	Comments
72R-3, 65-70	825.9	334	11			264	11	Fracture set		
72R-3, 65-70	825.9	190	55			120	55	Fracture set		
72R-3, 65-70	825.9	263	28			193	28	Fracture set		
72R-4, 5-9	826.8	354	48			284	48	Fracture set		
72R-2, 98-102	824.7	180	26				26	Fracture	Bedding parallel	
72R-2, 88-92	824.6	216	35				35	Fracture		
72R-1, 70-73	822.9	270	7				7	Bed		
73R-1, 0-7	831.8								Zone of ductile deformation - drill mud	
73R-1, 7-15	831.9								Shattered zone, mm-cm size fragments	
73R-2, 0-150	833.3								Fractured and shattered zone, fragments 2-30 mm	
73R-2, 134-140	834.6							Fractures	Inclined fabric, apparent dip in core face: 270, 45	
73R-3, 14-20	834.9	0	66				66	Fracture set	Inclined fractures, set 1, up to 3-cm spacing	
73R-3, 14-20	834.9	0	14				14	Fracture set	Inclined fractures, set 2, ~5-mm spacing	
73R-3, 47-120	835.3							Shattered zone	No fabric evident; lenticular fragments 2 mm - 1 cm size.	
73R-4, 123-130	837.5	178	49				49	Fracture	Fragments up to 4 cm across, in shattered zone	
73R-4, 123-130	837.5	135	21				21	Fracture		
73R-4, 137-150	837.7							Fold?	Typically planar features (*Zoophycos*) show subtle fold	
73R-5, 44-45	838.2	315	21				21	Fracture	Planar surfaces	
73R-5, 62-64	838.4	46	39				39	Fracture		
73R-5, 112-115	838.9	321	40				40	Fracture	Bedding parallel, incoherent hemipelagite	
73R-5, 133-145	839.1	27	45				45	Fracture	Bedding parallel, incoherent hemipelagite	
73R-5, 141-143	839.2	54	30				30	Bed	(133-147) relatively steep dips indicated by *Zoophycos*	
73R	831.8									
73R-6, 0-20	839.3								Soft drill-mud appearance, hides shattered mudstone	
73R-6, 89-92	840.2	312	54			52	54	Fracture	With slicks, at base of deformed mudstone	
73R-6, 86-151	840.2	0	0				0	Bed	Nearly horizontal	
73R-7, 1-67	840.8							Bed	Apparent dip: 90, 5	
74R-1, 19-23	841.6	224	30			54	30	Bed	(1-33) coherent bioturbated hemipelagites	
74R-1, 80-83	842.2	324	32			314	32	Bed	(65-92)	
74R-1, 83-86	842.2	270	20			260	20	Fracture	(65-92) downdip slickenlines	
74R-1, 93-98	842.3	263	41			253	41	Bed	(64-97)	
74R-2, 77-78	843.7	322	24			352	24	Bed	(62-83)	
74R-2, 107-110	844.0	348	30			18	30	Bed	(100-123)	
74R-2, 123-131	844.1	313	54			183	54	Fracture	(123-131) slickensided	
74R-3, 14-22	844.5	168	51				51	Fault	Healed, curviplanar, offset unknown	
74R-3, 44-45	844.8	305	17				17	Bed	Based on aligned *Zoophycos*	
75R-1, 33-34	851.3							Bed	Coherent mudstone, defined by aligned *Zoophycos* (16-44)	
75R-1, 135-136	852.4							Bed	Coherent mudstone, defined by aligned *Zoophycos* (127-150)	
76R-1, All	860.7							Bed	No bedding apparent; aligned *Zoophycos* suggest horizontal	
77R-1, 11-12	870.5	233	26			320	26	Bed	(0-15)	
77R-1, 92-93	871.3	131	23			313	23	Bed	(81-105)	
77R-2, 18-19	872.1	335	21			298	21	Bed	(3-28)	
77R-2, 129-30	873.2	333	19			295	19	Bed	(123-140)	
77R-3, 109-110	874.5	114	12			334	12	Bed	(103-120)	
77R-4, 134-135	876.2	139	19			334	19	Bed	(127-140)	
78R-1, 0-80	880.0	0	0				0	Bed	(0-80)	
78R-1, 102-148	881.0	204	14				14	Bed	(102-148)	
78R-2, 0-21	881.5	0	0				0	Bed		
78R-2, 21-65	881.7	207	7			232	7	Bed	(21-65)	
78R-2, 65-132	882.2	0	0				0	Bed		
78R-3, 0-100	883.0	180	12			260	12	Bed	(0-100)	
78R-4, 0-150	884.5	270	10			40	10	Bed	(0-150)	
78R-5, 6-67	886.1	180	12				12	Bed	(0-67)	
78R-5, 68-100	886.7	145	9				9	Bed	(68-100)	
79R-1, 94-94	890.2	296	9				9	Bed	(67-119)	
79R-2, 32-76	891.1	0	3				3	Bed	(32-760	
80R-1, 64-73	899.6	42	63				63	Fracture zone	(70-75); with slickenlines	
80R-1, 64-73	899.6			100	77			Slickenlines	On above fracture	
80R-1, 18-24	899.2							Normal fault	Offset 3 mm, downdip slickenlines	
80R-2, 42-44	900.9	155	25			260	25	Bed	(30-45)	
80R-4, 31-32	903.8	270	7			93	7	Bed	(8-48)	

Table T7 (continued).

Core, section, interval (cm)	Depth (mbsf)	Cr az. (°)	Cr dip (°)	Cr line	Cr l.plunge	Pm az.	Pm dip	Identifier	Notes	Comments
80R-4, 48-61	904.0	343	71			166	71	Fracture	(8-48); slickenlined	
80R-4, 48-61	904.0			12	63	183		Slickenlines	(8-48) on above fracture	
80R-4, 131-132	904.8	163	17			243	17	Bed	(123-150)	
80R-4, 131-132	904.8	80	67			160	67	Fracture	(123-150); with downdip slickenlines	
80R-5, 19-20	905.2	130	15			275	15	Bed	(10-40)	
80R-6, 33-34	906.8	147	18			257	18	Bed	(11-35)	
81R-1, 26-30	908.9							Fractures	With slickenlines	
81R-1, 123-121	909.8	49	23			294	23	Bed	(90-135)	
81R-3, 16-17	911.8	194	21			271	21	Bed	(0-17)	
81R-4, 77-78	913.9	50	15				15	Bed	(50-85)	
81R-5, 11-12	914.7	137	19			257	19	Bed	(0-27)	
82R-3, 69-70	921.7	13	13			245	13	Bed	(69-79)	
83R-2, 34-34	929.7	322	19			172	19	Bed		
83R-3, 98-98	931.9	348	14			293	14	Bed	(96-150)	
83R-5, 13-14	934.0	0	12				12	Bed	(13-17)	
84R-3, 25-44	940.8	357	75				75	Fluid escape structure	(0-45)	
84R-5, 118-125	944.7							Fracture zone	Curviplanar blocks 1-3 cm with few slickenlines	
84R-6, 31-31	945.3	0	0				0	Bed	(15-31)	
85R-1, 0-0	947.1	0	0				0	Bed	Based on aligned *Zoophycos*	
86R-1, 27-27	957.1	180	10				10	Bed	(5-54)	
86R-3, 11-11	959.9	135	6				6	Bed	(0-16)	
86R-3, 42-52	960.2	191	70			141	70	Fracture	(17-90)	
86R-3, 134-150	961.1	33	90				90	Fault	7-mm normal displacement	
86R-4, 64-74	961.9	24	60				60	Fracture zone	Drilling induced?	
86R-5, 114-114	963.9	38	22			195	22	Bed	(96-116)	
86R-6, 108-108	965.4	317	19			247	19	Bed	(58-112)	
87R-2, 21-23	968.2	185	23				23	Bed		
87R-2, 62-95	968.6	328	42				42	Fracture zone	Drilling induced?	
87R-4, 57-60	971.6	171	19				19	Bed	(48-73)	
87R-4, 5-7	971.1	317	17			67	17	Bed	(0-16)	
87R-4, 85-92	971.9	302	68				68	Fracture	(85-125) Drilling induced?	
88R-1, 94-94	977.0	270	5			360	5	Bed	(25-115)	
88R-3, 66-66	979.8	90	15			263	15	Bed	(60-80)	
89R-3, 39-40	988.7	0	10				10	Bed	(29-108)	
90R-1, 78-78	995.7	0	7				7	Bed	(65-95)	
90R-1, 43-43	995.3	331	18			351	18	Bed	(30-45)	
91R-1, 1-150	1004.6	0	0				0	Bed	No bedding apparent; aligned *Zoophycos* suggest horizontal	
91R-2, 1-150	1006.1	0	0				0	Bed	No bedding apparent; aligned *Zoophycos* suggest horizontal	
92R-1, 123-150	1015.4							Foliated breccia	40-cm-thick interval of polished fractures forming a subhorizontal set	
92R-2, 0-16	1015.7							Foliated breccia	Continutation of above (1- to 3-cm scale angular fragments)	
92R-2, 137-138	1017.1	250	47			250	47	Fracture	(97-145) downdip slickenlines	
92R-2, 145-146	1017.2	90	48			105	48	Fracture	(97-145) downdip slickenlines - conjugate to above	
92R-2, 77-97	1016.5							Fracture zone	Strongly polished, pronounced curviplanar	
92R-1, 1-150	1014.2	0	0				0	Bed	Bioturbation indicates subhorizontal	
93R-1, 33-33	1024.2	86	50				50	Fracture	(40); downdip slickenlines; single fracture, not a set	
93R-1, 67-79	1024.6							Fracture zone	8-cm-thick zone of angular polished fracture	
93R-3, 29-30	1027.2	0	16			288	16	Fracture zone	(119-135); slickenlines	
93R-3, 119-135	1028.1	322	54			250	54	Bed	(119-135) general bioturbation indication	
93R-4, 23-27	1028.6	46	45			86	45	Bed	(20-30) general bioturbation indication	
93R-4, 70-90	1029.1	116	90				90	Fracture	Highly polished open fracture surface, no slickenlines	
93R-5, 9-11	1030.0	314	40				40	Bed	(0-14)	
94R-1, 32-32	1033.8	38	24			68	24	Bed	(20-50)	
94R-2, 85-85	1035.9	180	10			150	10	Bed	(70-100)	
94R-3, 1-150	1036.5	0	0				0	Bed		
94R-4, 1-150	1038.0	0	0				0	Bed		
94R-5, 1-150	1039.5	0	0				0	Bed		
95R	1043.1	0	0				0	Bed		
96R-1, 36-37	1053.0	143	5				5	Bed	(21-77)	
96R-2	1054.1	0	0				0	Bed		
96R-3	1055.6	0	0				0	Bed		
96R-4, 4-5	1057.1	23	15			83	15	Bed	(0-30)	
97R	1062.3	0	0				0	Bed		
98R-1	1071.9	0	0				0	Bed		

Table T7 (continued).

Core, section, interval (cm)	Depth (mbsf)	Cr az. (°)	Cr dip (°)	Cr line	Cr l.plunge	Pm az.	Pm dip	Identifier	Notes	Comments
98R-2	1073.4	0	0				0	Bed		
98R-3, 9-28	1075.0	0	6				6	Bed		
98R-4	1076.0	0	0				0	Bed		
98R-5	1076.4	0	0				0	Bed		
99 All	1081.5	0	0				0	Bed		
100 All	1091.2	0	0				0	Bed		
101 All	1100.8								Highly fragmented hemipelagites and volcaniclastic (drilling induced)	
102 All	1110.2								Highly fragmented hemipelagites and volcaniclastic (drilling induced)	

Notes: Cr az. = azimuth of plane in core reference frame, Cr plunge = plunge of plane in core reference frame, Cr line = azimuth of line in core reference frame, Cr l.dip = dip of line in core reference frame, Pm az. = azimuth of plane in paleomagnetic reference frame, Pm dip = dip of plane in paleomagnetic reference frame, paired values in parentheses, in Notes column, record interval of coherent drilling biscuit used in paleomagnetic reorientation. This table is also available in **ASCII** format.

Table T8. Nannofossil events recognized, Site 1174.

Nannofossil zones	Datum events	Age (Ma)	Depth (mbsf)	Average sedimentation rate* (m/m.y.)
NN21b	FAD *Emiliania huxleyi* acme	0.085	59.25 ± 3.77	
NN21a	FAD *Emiliania huxleyi*	0.26	166.90 ± 4.81	
NN20	LAD *Pseudoemiliania lacunosa*	0.46	292.18 ± 5.29	685.4
	LAD *Reticulofenestra asanoi*	0.8	554.68 ± 1.96	
	FAD *Reticulofenestra asanoi*	1.06	596.14 ± 5.44	
	FAD *Gephyrocapsa oceanica*	1.77	641.50 ± 2.09	
NN19	LAD *Discoaster brouweri*	1.95	652.47 ± 3.00	
NN18	LAD *Discoaster pentaradiatus*	2.52	671.28 ± 0.33	
NN17	LAD *Discoaster surculus*	2.55	676.08 ± 4.47	
NN16	LAD *Reticulofenestra pseudoumbilicus* (>7 µm)	3.75	739.87 ± 6.20	
NN15	LAD *Amaurolithus* spp.	4.0	763.35 ± 15.50	
NN14	FCAD *Discoaster asymmetricus*	4.13	796.08 ± 0.73	
NN12	LAD *Discoaster quinqueramus*	5.54	779.69 ± 1.50	
NN11b	FAD *Amaurolithus* ssp.	7.2	843.24 ± 1.57	
NN11a	FAD *Discoaster quinqueramus*	8.6	871.05 ± 7.57	54.8
NN10b	LAD *Reticulofenestra pseudoumbilicus* (>7 µm)	8.8	890.41 ± 3.27	
NN10a	LAD *Discoaster hamatus*	9.63	898.96 ± 5.29	
NN9	FAD *Discoaster hamatus*	10.7	918.52 ± 2.02	
NN8	FAD *Catinaster coalitus*	10.9	954.14 ± 1.79	
NN7	FAD *Discoaster kugleri*	11.8	1067.89 ± 9.27	
	LAD *Orthorhabdus serratus*	12.3	1067.89 ± 8.27	
	LCAD *Cyclicargolithus floridanus*	13.2	1088.99 ± 4.99	
	FAD *Reticulofenestra pseudoumbilicus* (>7 µm)	13.4	1106.90 ± 4.40	

Notes: FAD = first appearance datum, LAD = last appearance datum, FCAD = first common appearance datum, LCAD = last common occurrence datum. * = uncorrected for compaction.

Table T9. Interval and depth constraints of calcareous nannofossil events, Site 1174.

Event		Interval (cm)		Depth (mbsf)	
		Top	Bottom	Top	Bottom
		190-1174A-	190-1174A-		
B	*Emiliania huxleyi* acme	7H-CC	8H-2, 74-75	55.49	63.02
		190-1174B-	190-1174B-		
B	*Emiliania huxleyi*	3R-CC	4R-CC	162.90	171.71
T	*Pseudoemiliania lacunosa*	16R-CC	17R-CC	286.90	297.48
T	*Reticulofenestra asanoi*	43R-CC	44R-3, 75-76	552.73	556.65
B	*Reticulofenestra asanoi*	47R-CC	48R-CC	590.69	601.58
B	*Gephyrocapsa oceanica*	52R-CC	53R-3, 79-80	639.41	643.59
T	*Discoaster brouweri*	53R-CC	54R-CC	645.70	659.24
T	*Discoaster pentaradiatus*	56R-2, 75-76	56R-CC	670.95	671.61
T	*Discoaster surculus*	56R-CC	57R-2, 75-76	671.61	680.55
T	*Reticulofenestra pseudoumbilicus* (>7 µm)	62R-CC	63R-CC	733.68	746.07
T	*Amaurolithus* spp.	65R-5, 74-75	65R-CC	761.94	764.93
B	*Discoaster asymmetricus* (common)	66R-3, 75-76	66R-4, 71-72	768.35	769.81
T	*Discoaster quinqueramus*	67R-4, 75-76	67R-6, 75-76	778.19	781.19
B	*Amaurolithus* ssp.	73R-CC	74R-3, 41-42	841.68	844.81
B	*Discoaster quinqueramus*	76R-CC	79R-CC	863.47	893.68
T	*Reticulofenestra pseudoumbilicus* (>7 µm)	76R-CC	79R-CC	863.47	893.68
T	*Discoaster hamatus*	79R-CC	80R-4, 75-76	893.68	904.25
B	*Discoaster hamatus*	81R-CC	82R-2, 74-75	816.50	920.54
B	*Catinaster coalitus*	85R-4, 75-76	85R-CC	952.35	955.93
B	*Discoaster kugleri*	96R-CC	98R-CC	1058.62	1077.16
T	*Orthorhabdus serratus*	96R-CC	98R-CC	1058.62	1077.16
T	*Cyclicargolithus floridanus* (common)	99R-CC	100R-CC	1084.00	1093.97
B	*Reticulofenestra pseudoumbilicus* (>7 µm)	101R-CC	102R-CC	1102.50	1111.30

Note: B = bottom occurrence, T = top occurrence.

Table T10. Epoch boundaries, Hole 1174B.

Boundary	Depth (mbsf)	Event
Pleistocene/Pliocene	641.50 ± 2.09	B *Gephyrocapsa oceanica*
late/early Pliocene	686.00	Gauss (O)
Pliocene/Miocene	779.69 ± 1.90	T *Discoaster quinqueramus*
late/middle Miocene	954.14 ± 1.79	B *Catinaster coalitus*

Notes: (O) = onset. B = bottom occurrence, T = top occurrence.

Table T11. Calcareous nannofossil range chart, Zones NN21b–NN19. (See table notes. Continued on next three pages.)

Epoch	Zones	Core, section, interval (cm)	Depth (mbsf)	Preservation	Abundance	*Braarudosphaera bigelowii*	*Calcidiscus tropicus*	*Calcidiscus leptoporus*	*Calcidiscus macintyrei*	*Ceratolithus cristatus*	*Ceratolithus cristatus* var. *telesmus*	*Coccolithus pelagicus*	*Coccolithus pelagicus* (with bar)	*Cyclolithus annulus*	*Discoaster brouweri*	*Discoaster pentaradiatus*	*Discoaster* spp.	*Discoaster variabilis*	*Discosphaera tubifera*	*Emiliania huxleyi*	*Florisphaera profunda*	*Gephyrocapsa muellerae*	*Gephyrocapsa oceanica*	*Gephyrocapsa* spp. (<2 µm)	*Hayaster perplexus*	*Helicosphaera carteri*	*Helicosphaera carteri* var. *walichii*	*Helicosphaera inversa*	*Helicosphaera sellii*	*Holodiscolithus macroporus*	*Neosphaera coccolithomorpha*	*Oolithotus fragilis*	*Pontosphaera discopora*	*Pontosphaera japonica*	*Pontosphaera multipora*	*Pseudoemiliania lacunosa*	*Pseudoemiliania ovata*	*Reticulofenestra asanoi*	*Reticulofenestra pseudoumbilicus* (>7 µm)	*Reticulofenestra pseudoumbilicus* (5–7 µm)	*Reticulofenestra* spp.	*Reticulofenestra minuta*	*Reticulofenestra minutula*	*Rhabdosphaera clavigera*	*Rhabdosphaera clavigera* var. *stylifera*
Pleistocene		190-1174A-																																											
	NN21b	1H-CC		M	C			C											F	D	C	C	A	C		F	F														F				
		2H-CC		M	F	R		R		F				R						D	C	C	A	F		F								R		F			F			C			
		3H-CC		G	C			F		R							F		F	D	C	C	A			C				F								R	R			F		F	
		4H-CC		G	C			F		R		R	R							D	C	C	A		F	C										F	F		F					F	
		5H-CC		M	C			F		R		R	R							D	C	C	A	F		F									R										
		7H-CC		P	R			C												D	C	A	A	C		C																			
	NN21a	8H-2, 74-75	63.02	P	R															A	C	A	D	A												C									
		8H-CC		P	F			C		F			C									A	A			C																C			
		1R-6, 75-76	149.38	P	F			C												A	A	A	A	A		C	C																		
		1R-CC		P	F												C			A	C	A	A	C		C	C																		
		2R-CC		M	C			C				F	R	F				F		A	A	C	A	C		F																		C	
		3R-CC		M	F			C				F								A	C	A	A	C		F									R	F	F					C			
	NN20	4R-CC		M	C	R		C		R			R				R				A	A	A	A		R	R									R									
		5R-CC		P	R								D																																
		6R-CC		P	F	F		F					F								C	C	A	D		F																			
		7R-CC		M	C			F													A	C	A	D		R		R																	
		8R-CC		P	F			F													A	C	C	D		F	R	R								F					F				
		9R-CC		P	F								C								C	A	A	A		C															C				
		10R-CC		M	F			F													C	A	C	D		F										F									
		11R-CC		M	C			F					R								A	C	C	D		F								R											
		12R-CC		M	F			F													A	C	C	D		R															F				
		13R-CC		M	F			F													A	C	C	D												R					C				
		14R-CC		M	F			F				R									A	A	C	D		F		F			F							R							
		15R-CC		M	F			F				R									A	C	C	D		F	F	F				F				R	F								
		16R-CC		M	R			F				R	R								A	C	A	D		R	R																		
	NN19	17R-CC		M	F			C		R	R	R			F						A	A	A	A		C										F		R	F						
		18R-CC		P	R			F										C			C	A	C	D		C										C	C								
		19R-CC		P	C			F	F												C	A	A	D		F	R								F	F	C				F			F	
		20R-CC		M	F			C													C	A	C	D		C	F									F	F		F						
		21R-CC		P	R			C					R	F							C	A	C	D		R	F																		
		22R-CC		M	C			C		F			R								A	A	C	D		F	F									F	R								
		23R-2, 73-74	354.23	P	F			C			R		F								C	A	C	D		R										F					F	R			
		24R-CC		M	F			F		R							R				C	C	C	D		F										R	R	R			R				
		25R-CC		M	F			F	R							R					C	A	A	D		F										C	C				F		F		
		26R-CC		P	R	F		R				F		C							A	A	C	A		R											F		F		F	F	F		
		27R-CC			B																																								

Table T11 (continued).

Epoch	Zones	Core, section, interval (cm)	Depth (mbsf)	Preservation	Abundance	*Scapholithus fossilis*	*Scyphosphaera* spp.	*Solidopons petrae*	*Sphenolithus grandis*	*Sphenolithus* spp.	*Syracosphaera pulchra*	*Syracosphaera* spp.	*Umbellosphaera irregularis*	*Umbellosphaera tenuis*	*Umbilicosphaera hulburtiana*	*Umbilicosphaera rotula*	*Umbilicosphaera sibogae* var. *foliosa*	*Umbilicosphaera sibogae* var. *sibogae*
Pleistocene		190-1174A-																
	NN21b	1H-CC		M	C						F		F	F			F	
		2H-CC		M	F					R	F	F						C
		3H-CC		G	C	F					F	F		F	F			C
		4H-CC		G	C						F	F		F	F			F
		5H-CC		M	C												F	F
		7H-CC		P	R					F		F						C
	NN21a	8H-2, 74-75	63.02	P	R													
		8H-CC		P	F													
		1R-6, 75-76	149.38	P	F													C
		1R-CC		P	F	C				C		C						
		2R-CC		M	C							C		F			F	C
		3R-CC		M	F					F							F	C
	NN20	4R-CC		M	C													F
		5R-CC		P	R													
		6R-CC		P	F													F
		7R-CC		M	C					R							F	F
		8R-CC		P	F							F						
		9R-CC		P	F													
		10R-CC		M	F								F				F	F
		11R-CC		M	C													F
		12R-CC		M	F					R					R		F	R
		13R-CC		M	F							R			F		F	
		14R-CC		M	F												F	F
		15R-CC		M	F							F		R	R			F
		16R-CC		M	R							R						
	NN19	17R-CC		M	F							F						
		18R-CC		P	R													
		19R-CC		P	C	F					F	F						C
		20R-CC		M	F					R	R			F				
		21R-CC		P	R					R				F				F
		22R-CC		M	C					F	F	F		F				
		23R-2, 73-74	354.23	P	F							F			F			
		24R-CC		M	F			R				R		R				F
		25R-CC		M	F					R		R		F				
		26R-CC		P	R							F						F
		27R-CC			B													

Table T11 (continued).

Epoch	Zones	Core, section, interval (cm)	Depth (mbsf)	Preservation	Abundance	*Braarudosphaera bigelowii*	*Calcidiscus tropicus*	*Calcidiscus leptoporus*	*Calcidiscus macintyrei*	*Ceratolithus cristatus*	*Ceratolithus cristatus* var. *telesmus*	*Coccolithus pelagicus*	*Coccolithus pelagicus* (with bar)	*Cyclolithus annulus*	*Discoaster brouweri*	*Discoaster pentaradiatus*	*Discoaster* spp.	*Discoaster variabilis*	*Discosphaera tubifera*	*Emiliania huxleyi*	*Florisphaera profunda*	*Gephyrocapsa muellerae*	*Gephyrocapsa oceanica*	*Gephyrocapsa* spp. (<2 µm)	*Hayaster perplexus*	*Helicosphaera carteri*	*Helicosphaera carteri* var. *wallichii*	*Helicosphaera inversa*	*Helicosphaera sellii*	*Holodiscolithus macroporus*	*Neosphaera coccolithomorpha*	*Oolithotus fragilis*	*Pontosphaera discopora*	*Pontosphaera japonica*	*Pontosphaera multipora*	*Pseudoemiliania lacunosa*	*Pseudoemiliania ovata*	*Reticulaofenestra asanoi*	*Reticulofenestra pseudoumbilicus* (>7 µm)	*Reticulofenestra pseudoumbilicus* (5–7 µm)	*Reticulofenestra* spp.	*Reticulofenstra minuta*	*Reticulofenstra minutula*	*Rhabdosphaera clavigera*	*Rhabdosphaera clavigera* var. *stylifera*
		28R-CC		M	F			C				R	F								C	A	A	D		F										R	R								
		29R-CC		M	F			F				F	F								C	A	A	D		R										F			R		F				
		30R-CC		P	R			C													A	A	A													C									
		31R-CC		P	R																	D	C	C												C							C		
		32R-CC		P	R			C													C	D		A												C	C								
		33R-CC		P	R																A	D	C	A												C	R	F					C		
		34R-CC		P	C			C													A	D	C			F										C	F		R						
		35R-CC		P	C			F													A	D		A												C	C								
		36R-CC		M	F			F													C	A	C	D		F			R					R		F	F								
		37R-CC		M	C			R					R									D	C	A												C	C					F			
		38R-CC		M	C			F				R									C	D	C	A												C	F					F			
		39R-CC		M	C			R						F							A	D	A	A												F	F					R			
		40R-CC		P	R			R													D	C	C	C												C	C				F	C	F		
		41R-CC		M	R																		D																						
Pleistocene	NN19	42R-CC			B																																								
		43R-CC		P	R			F													A	A	C	D						F					F	C	F	F				C			
		44R-3, 75-76	556.65	P	F			F													C	A	A	A		C										A	C	F							
		44R-CC		P	R			C						C							A	C	A	C												C	C	C				A	C		
		45R-CC		P	R			A													C	A		A												C		A			A	A			
		46R-CC		M	C			C				R	R								C	C		D		F	R						F		R	C	C	C							
		47R-4, 56-57	586.96	M	C			F				R									R	C	C	D		R	R								F	C	C	F							
		47R-CC		P	C			C													C	F	C	D						F						C	C				R	C			
		48R-CC		P	F			C				F									A	F	A	D								F			F	C	C					F			
		49R-CC			B																																								
		50R-CC		P	F			C				F									C	C	A	D										F		C	C					F			F
		51R-CC		P	F			F					F					R			A	A	C	A		R										C	F			R		R			
		52R-CC		P	C		F	C	F			R	F								A	F	C	A		F	R		F				F			A	C					A			
		53R-3, 79-80	643.59	P	F			C				F									C	A		D		C										C	A					C	C		
		53R-CC		P	R			C	F	R				F							D	C		A												C	C						C		

Notes: Abundance: D = dominant, A = abundant, C = common, F = few, R = rare. Preservation: P = poor, M = moderate, G = good. See "**Biostratigraphy**," p. 9, in the "Explanatory Notes" chapter. This table is also available in **ASCII** format.

Table T11 (continued).

Epoch	Zones	Core, section, interval (cm)	Depth (mbsf)	Preservation	Abundance	*Scapholithus fossilis*	*Scyphosphaera* spp.	*Solidopons petrae*	*Sphenolithus grandis*	*Sphenolithus* spp.	*Syracosphaera pulchra*	*Syracosphaera* spp.	*Umbellosphaera irregularis*	*Umbellosphaera tenuis*	*Umbilicosphaera hulburtiana*	*Umbilicosphaera rotula*	*Umbilicosphaera sibogae* var. *foliosa*	*Umbilicosphaera sibogae* var. *sibogae*
		28R-CC		M	F						R	F		F				R
		29R-CC		M	F									F				F
		30R-CC		P	R													
		31R-CC		P	R													
		32R-CC		P	R													F
		33R-CC		P	R													
		34R-CC		P	C													
		35R-CC		P	C													
		36R-CC		M	F						F	F					R	
		37R-CC		M	C							R						R
		38R-CC		M	C													
		39R-CC		M	C												R	
		40R-CC		P	R												F	F
		41R-CC		M	R													
Pleistocene	NN19	42R-CC			B													
		43R-CC		P	R							F						
		44R-3, 75-76	556.65	P	F													
		44R-CC		P	R													
		45R-CC		P	R													
		46R-CC		M	C													F
		47R-4, 56-57	586.96	M	C												F	
		47R-CC		P	C												F	F
		48R-CC		P	F												F	
		49R-CC			B													
		50R-CC		P	F							F						F
		51R-CC		P	F							F					F	
		52R-CC		P	C					R	F						F	F
		53R-3, 79-80	643.59	P	F													
		53R-CC		P	R													

Table T12. Calcareous nannofossil range chart, Zones NN18–NN6. (See table notes. Continued on next three pages.)

Epoch	Zone	Core, section, interval (cm)	Depth (mbsf)	Preservation	Abundance	*Amaurolithus amplificus*	*Amaurolithus delicatus*	*Amaurolithus primus*	*Amaurolithus tricorniculatus*	*Angulolithina arca*	*Calcidiscus leptoporus*	*Calcidiscus macintyrei*	*Calcidiscus premacintyrei*	*Calcidiscus tropicus*	*Catinaster calyculus*	*Catinaster coalitus*	*Catinaster* spp.	*Ceratolithus cristatus*	*Coccolithus miopelagicus*	*Coccolithus pelagicus*	*Coccolithus pelagicus* (with bar)	*Coronocyclus nitescens*	*Cryptococcolithus mediaperforatus*	*Cyclicargolithus floridanus*	*Discoaster asymmetricus*	*Discoaster bellus*	*Discoaster bergeni*	*Discoaster bollii*	*Discoaster braarudii*	*Discoaster brouweri*	*Discoaster calcaris*	*Discoaster challengeri*	*Discoaster deflandrei*	*Discoaster exilis*	*Discoaster hamatus*	*Discoaster kugleri*	*Discoaster musicus*	*Discoaster neorectus*	*Discoaster pansus*	*Discoaster pentaradiatus*	*Discoaster petaliformis*	*Discoaster prepentaradiatus*	*Discoaster quinqueramus*	*Discoaster* spp.	*Discoaster subsurculus*	*Discoaster surculus*	*Discoaster tamalis*	*Discoaster triradiatus*	*Discoaster variabilis*	*Florisphaera profunda*
		190-1174B-																																																
late Pliocene	NN18	54R-CC		P	R						C	C		C							C									C														F						A
		55R-CC		P	R							C								C										C														C						A
		56R-2, 75-76	670.95	P	F						C	C													F					C																		F	F	
	NN17	56R-CC		P	R						C	C		C																C						C										F				D
	NN16	57R-2, 75-76	680.55	P	R						C																			C										F						C				A
		57R-4, 75-76	683.55	P	R						C																													F						C	C			A
early Piocene		58R-CC		P	F						C										C									C										F							C			D
		58R-3, 75-76	691.75	P	R																				F					C										C				C			F			A
		58R-CC		P	R						C	C								F					F											C								F		C				A
		59R-CC		P	F						C	C		C						F					F					F										F						R			F	A
		60R-CC		P	R																									A														C		C			C	
		61R-CC		P	R							F		R											R					R						R								R		F			F	A
		62R-CC		P	F							F													R					R										R										A
	NN15	63R-4, 74-75	741.34		B																																													
		63R-CC		P	R						C	C						F		C					C																								C	C
		64R-2, 71-72	747.91		B																																													
		64R-4, 77-78	750.97		B																																													
		54R-CC			B																									C										A									C	A
		65R-5, 74-75	761.74	P	R																																													
	NN14	65R-CC		P	R		F				C	C													C																			C					C	C
		66R-3, 72-73	739.82	P	R																				C																								C	C
	NN13-12	66R-4, 71-72	769.81	P	R							C																												F										C
		66R-CC			B																																													
		67R-4, 75-76	778.19	P	R																																													
late Miocene	NN11b	67R-6, 75-76	781.19	P	C						C	F		F																F													F			F			R	
		67R-CC		M	C		R				R	F													R																		R			R		R	F	
		68R-CC			B																																													
		69R-CC		P	C						F	F		F																													R			R			R	C
		70R-CC		P	R																																							A					A	
		71R-CC		P	C		F		R	R	F	F		F						C													R			R							R	C		F			F	
		72R-CC		P	R																																												C	
		73R-CC		M	F	C	C		C					C																						C			F				A	C		C		F	C	
	NN11a	74R-3, 41-42	844.81	P	F									C																										F			C			C			F	
		74R-CC			B																																													
		75R-CC		P	R																						C									C			C				C	A		F			C	
		76R-CC		P	R															C							C				C					A			F				C						A	

Table T12 (continued).

Epoch	Zone	Core, section, interval (cm)	Depth (mbsf)	Preservation	Abundance	*Gephyrocapsa* spp. (<2 µm)	*Hayella challengeri*	*Helicosphaera carteri*	*Helicosphaera carteri* var. *Walichii*	*Helicosphaera granulata*	*Helicosphaera intermedia*	*Helicosphaera orientalis*	*Helicosphaera sellii*	*Helicosphaera* spp.	*Helicosphaera stalis*	*Helicosphaera vedderi*	*Helicosphaera waltrans*	*Hughesius gizoensis*	*Orthorhabdus serratus*	*Pontosphaera japonica*	*Pontosphaera multipora*	*Pseudoemiliania lacunosa*	*Pseudoemiliania ovata*	*Reticulofenestra haqii*	*Reticulofenestra minuta*	*Reticulofenestra minutula*	*Reticulofenestra pseudoumbilicus* (>7 µm)	*Reticulofenestra pseudoumbilicus* (5–7 µm)	*Reticulofenestra* spp.	*Rhabdosphaera clavigera*	*Scapholithus fossilis*	*Scyphosphaera globulata*	*Scyphosphaera pulcherrima*	*Scyphosphaera tubifera*	*Scyphosphaera ventriosa*	*Sphenolithus abies*	*Sphenolithus grandis*	*Sphenolithus heteromorphus*	*Sphenolithus moriformis*	*Sphenolithus* spp.	*Triquetrorhabdulus milowii*	*Triquetrorhabdulus rugosus*	*Umbilicosphaera jafari*	*Umbilicosphaera rotula*	*Umbilicosphaera sibogae* var. *sibogae*
		190-1174B-																																											
late Pliocene	NN18	54R-CC		P	R	A																A	C			A	F																		F
		55R-CC		P	R	C																C	C		F	A																			
		56R-2, 75-76	670.95	P	F	D																C	A		C																				
	NN17	56R-CC		P	R																	A	C			C																			
	NN16	57R-2, 75-76	680.55	P	R	A																			C	A																			
		57R-4, 75-76	683.55	P	R																	C	C			A																			
early Pliocene		58R-CC		P	F	C																A				A																			
		58R-3, 75-76	691.75	P	R	A																A	C			A																			
		58R-CC		P	R																	F			C	D																		F	
		59R-CC		P	F	A		F												R		C	F	A		A																	F	F	
		60R-CC		P	R																			D																					
		61R-CC		P	R	C																C	F		A	A																			
		62R-CC		P	F	C																C	C		A	A										R		F							
	NN15	63R-4, 74-75	741.34		B																																								
		63R-CC		P	R	A																C			A	A	A												C				C	C	
		64R-2, 71-72	747.91		B																																								
		64R-4, 77-78	750.97		B																																								
		54R-CC			B	A																																							
		65R-5, 74-75	761.74	P	R																			A			D																		
	NN14	65R-CC		P	R			C															C	D			C	C								C									
		66R-3, 72-73	739.82	P	R			R																A			A																		
	NN13-12	66R-4, 71-72	769.81	P	R																			A	D		A																		
		66R-CC			B																																								
		67R-4, 75-76	778.19	P	R																																								
late Miocene	NN11b	67R-6, 75-76	781.19	P	C																			A	D		C	F								C							F		
		67R-CC		M	C	D															F			A	C							R		R	R	F									
		68R-CC			B																																								
		69R-CC		P	C		F																	C	D		C	C								F			F						
		70R-CC		P	R																						A																		
		71R-CC		P	C																			C			A	A								C	F		C	C				F	
		72R-CC		P	R																						D																		
		73R-CC		M	F																			A	C		C	C					C			C			C					C	
	NN11a	74R-3, 41-42	844.81	P	F																			C	D		C																C		
		74R-CC			B																																								
		75R-CC		P	R																			A	A		F	A								C									
		76R-CC		P	R																			A				A																	

Table T12 (continued).

Epoch	Zone	Core, section, interval (cm)	Depth (mbsf)	Preservation	Abundance	*Amaurolithus amplificus*	*Amaurolithus delicatus*	*Amaurolithus primus*	*Amaurolithus tricorniculatus*	*Angulolithina arca*	*Calcidiscus leptoporus*	*Calcidiscus macintyrei*	*Calcidiscus premacintyrei*	*Calcidiscus tropicus*	*Catinaster calyculus*	*Catinaster coalitus*	*Catinaster* spp.	*Ceratolithus cristatus*	*Coccolithus miopelagicus*	*Coccolithus pelagicus*	*Coccolithus pelagicus* (with bar)	*Coronocyclus nitescens*	*Cryptococcolithus mediaperforatus*	*Cyclicargolithus floridanus*	*Discoaster asymmetricus*	*Discoaster bellus*	*Discoaster bergeni*	*Discoaster bollii*	*Discoaster braarudii*	*Discoaster brouweri*	*Discoaster calcaris*	*Discoaster challengeri*	*Discoaster deflandrei*	*Discoaster exilis*	*Discoaster hamatus*	*Discoaster kugleri*	*Discoaster musicus*	*Discoaster neorectus*	*Discoaster pansus*	*Discoaster pentaradiatus*	*Discoaster petaliformis*	*Discoaster prepentaradiatus*	*Discoaster quinqueramus*	*Discoaster* spp.	*Discoaster subsurculus*	*Discoaster surculus*	*Discoaster tamalis*	*Discoaster triradiatus*	*Discoaster variabilis*	*Florisphaera profunda*
	NN10b	77R-CC			B																																													
		78R-CC			B																																													
	NN10a	79R-CC		P	F											D										F										F		F	C										F	
	NN9	80R-4, 75-76	904.25	M	C										C					C						C		C			C	C			C					C		C								
		80R-CC			B																																													
late Miocene		81R-CC		P	C						F			F	F	C				C								C	C					C	R	R								F	F					
	NN8	82R-2, 74-75	920.54	P	R									C		C				C									F																					
		82R-CC		P	R											A																																		
		83R-3, 85-86	931.75	P	C						C					C															F	C																		
		83R-CC			B																																													
		84R-CC		P	R												A			C												F				F								C						
		85R-4, 75-76	952.35	P	R											A																	C																	
	NN7	85R-CC		P	R																													A		A														
		86R-CC		P	R																							F					C	C		F			C											
		87R-3, 46-47	969.96		B																																													
		87R-CC			B																																													
		88R-CC			B																																													
		89R-CC		P	F																							C	C					C		C								A						
		90R-2, 77-78	997.17	P	R																			A									A											A						
		90R-CC		P	R							C		C																				C		F														
		91R-CC		M	F						C	C							C	C													F			F								F						
middle Miocene		92R-CC		P	R															A																														
		93R-CC		P	R															C		F						F					C	A		C								A						
		94R-CC		P	C						F	C							C	C		F		F										F										F						
		95R-CC		P	C							C							C	C		C		F									F	F		F								C						
		96R-CC		P	R															F				F										C		F								C						
		97R-CC			B																																													
		98R-CC		P	R															F			F	C								F	C			R								C						
	NN6	99R-CC		M	C						F		F						R	C		F		C								C	C			R								C						
		100R-CC		P	F						F									C			R	A									C											C						
		101R-CC		P	R															A				A																				A						
		102R-CC		P	R																	A																												

Notes: D = dominant, A = abundant, C = common, F = few, R = rare, P = poor, M = moderate, G = good. See **"Biostratigraphy,"** p. 9, in the "Explanatory Notes" chapter. This table is also available in **ASCII** format.

Table T12 (continued).

Epoch	Zone	Cor	Depth (mbsf)	Preservation	Abundance	*Gephyrocapsa* spp. (<2 µm)	*Hayella challengeri*	*Helicosphaera carteri*	*Helicosphaera carteri* var. *Walichii*	*Helicosphaera granulata*	*Helicosphaera intermedia*	*Helicosphaera orientalis*	*Helicosphaera sellii*	*Helicosphaera* spp.	*Helicosphaera stalis*	*Helicosphaera vedderi*	*Helicosphaera waltrans*	*Hughesius gizoensis*	*Orthorhabdus serratus*	*Pontosphaera japonica*	*Pontosphaera multipora*	*Pseudoemiliania lacunosa*	*Pseudoemiliania ovata*	*Reticulofenestra haqii*	*Reticulofenestra minuta*	*Reticulofenestra minutula*	*Reticulofenestra pseudoumbilicus* (>7 µm)	*Reticulofenestra pseudoumbilicus* (5–7 µm)	*Reticulofenestra* spp.	*Rhabdosphaera clavigera*	*Scapholithus fossilis*	*Scyphosphaera globulata*	*Scyphosphaera pulcherrima*	*Scyphosphaera tubifera*	*Scyphosphaera ventriosa*	*Sphenolithus abies*	*Sphenolithus grandis*	*Sphenolithus heteromorphus*	*Sphenolithus moriformis*	*Sphenolithus* spp.	*Triquetrorhabdulus milowii*	*Triquetrorhabdulus rugosus*	*Umbilicosphaera jafari*	*Umbilicosphaera rotula*	*Umbilicosphaera sibogae* var. *sibogae*
	NN10b	77R-CC			B																																								
		78R-CC			B																																								
	NN10a	79R-CC		P	F			F																C			C	C								A			C						
	NN9	80R-4, 75-76	904.25	M	C			C																C	C		A	C																	
		80R-CC			B																																								
late Miocene		81R-CC		P	C																			C	A		A	C			F					F			C				C	C	
	NN8	82R-2, 74-75	920.54	P	R																				D		C									C	F							C	
		82R-CC		P	R																						D																		
		83R-3, 85-86	931.75	P	C																			A	D		C	A								F			F						
		83R-CC			B																																								
		84R-CC		P	R																						A	A																	
		85R-4, 75-76	952.35	P	R																			C	A			C											F						
middle Miocene	NN7	85R-CC		P	R																						A																		
		86R-CC		P	R														F								D	C								C	C				C		C	C	
		87R-3, 46-47	969.96		B																																								
		87R-CC			B																																								
		88R-CC			B																																								
		89R-CC		P	F																			A	C		A	A			C						C		C				C	C	
		90R-2, 77-78	997.17	P	R																							D																	
		90R-CC		P	R																			C	C		A	A								F			F				F	F	
		91R-CC		M	F									F							F			C	D		A	C								F	F		F	F			F	C	
		92R-CC		P	R																						A	A																	
		93R-CC		P	R																			C	C		C	A											A	C	C				
		94R-CC		P	C					R	F	F									C			A	A		C	A								C	C		C	F			C	C	
		95R-CC		P	C							F												A	A		A	A								F	R		C					C	
		96R-CC		P	R			F																A	A		A	A									C		C				C		
	NN6	97R-CC			B																																								
		98R-CC		P	R														F					D	A		F	C									F		C	F				F	
		99R-CC		M	C						R								R		F			A	A		C	A											C					C	
		100R-CC		P	F		F							F					F					A	A			A											C		F			F	
		101R-CC		P	R																							A											A						
		102R-CC		P	R																			A				A																	

Table T13. Depths and ages of magnetic chrons and subchrons identified, Site 1174.

Depth (mbsf)					
Top	Bottom	Polarity	Chron	Subchron	Age (Ma)
0.00	544.70	N	Brunhes		0.00
544.70	686.00	R	Matuyama		0.78
686.00	697.85	N	Gauss		2.58
697.85	702.45	R		Kaena	3.04
702.45	705.15	N		C2An.2n	3.11
705.15	710.35	R		Mammoth	3.22
710.35	727.85	N		C2An.3n	3.33
727.85	731.70	R	Gilbert		3.58
731.70	732.70	N		Cochiti (C3n.1n) ?	4.18
732.70	737.75	R		C3n.2r ?	4.29
737.75	738.55	N		Nunivak (C3n.2n) ?	4.48
738.55	738.95	N		?	
738.95	751.80	R		?	
751.80	761.55	N		Nunivak (C3n.2n) ?	4.48
761.55	767.25	R		C3n.3r ?	4.62
767.25	774.99	N		Sidufjall (C3n.3n)	4.80
774.99	784.50	R		C3n.4r ?	4.89
784.50	793.92	N		Thvera (3n.4n) ?	4.98
793.92	802.12	R		C3n.5r ?	5.23
802.12	807.25	N	C3A	C3An.1n	5.89
807.25	812.55	R		C3A.1r	6.14
812.55	814.21	N		C3An.2n	6.27
814.21	832.10	R		C3Ar	6.57
832.10	841.55	N	C3B	C3Bn	6.94
841.55	842.95	R		C3Br.1r	7.09
842.95	843.80	N		C3Br.1n	7.14
843.80	860.95	R		C3Br.2r	7.17
860.95	862.70	N	C4	C4n.1n	7.43
862.70	863.24	R		C4n.1r	7.56
863.24	875.90	N		C4n.2n	7.65
875.90	880.40	R		C4r.1r	8.07
880.40	881.75	N		C4r.2n	8.23
881.75	890.15	R		C4r.2r	8.26
890.15	892.20	N		C4An	8.70
892.20	893.59	N		C4Ar.1n	9.23
893.59	899.85	R		C4Ar.2n	9.31
899.85	901.40	R		C4Ar.3r	9.64
901.40	906.35	N	C5	C5n.1n	9.74
906.35	906.90	R		C5n.1r	9.88
906.90	947.15	N		C5n.2n	9.92
947.15	950.00	R		C5r.1r	10.95
950.00	954.55	N		C5r.1n	11.05
954.55	956.90	N		?	?
956.90	1033.60	N		C5r.2r	11.10
1033.60	1052.65	N	C5A?	C5An.1n	11.94
1052.65		N		C5AAn	12.99

Notes: N = normal, R = reversed. ? = uncertain subchron boundary.

Table T14. Pore fluid compositions, Site 1174. (**See table note.** Continued on next page.)

Hole, core, section, interval (cm)	Depth (mbsf)	pH (ISE)	Alk (T) (mM)	SAL (R) (psu)	Cl (T) (mM)	SO_4 (I) (mM)	Na (I) (mM)	Mg(T) (mM)	Ca (I) (mM)	Ca(T) (mM)	K (I) (mM)	H_4SiO_4 (S) (µM)	NH_4 (S) (mM)
190-1174A-													
1H-1, 140-150	1.40	8.08	5.59	35.0	558.5	26.72	483	51.2	10.07	9.9	12.2	559	0.14
1H-2, 140-150	2.90	8.42	33.66	34.5	560.0	4.62	485	47.6	5.07	5.1	12.2	568	0.68
1H-3, 109-119	4.09	7.96	38.72	34.5	565.0	0.00	493	45.2	4.02	3.7	11.8	566	1.34
2H-2, 135-150	6.04	8.42	51.31	35.0	570.0	0.00	514	41.2	4.13	3.9	12.1	576	5.30
2H-3, 140-150	7.59	8.18	49.06	35.0	572.0	1.00	516	40.1	4.07	4.0	12.0	662	4.85
2H-4, 140-150	9.09	8.10	49.30	35.0	573.0	0.00	518	39.4	3.94	3.9	12.3	602	5.02
2H-5, 135-150	10.54	7.97	50.31	35.0	574.0	1.34	519	40.0	4.00	3.8	12.1	588	5.82
2H-6, 135-150	12.04	7.89	44.95	35.5	574.0	1.23	517	37.8	4.00	3.7	12.4	646	6.61
2H-7, 140-150	13.59	7.91	47.62	35.5	576.0	0.00	521	38.1	3.98	3.7	12.4	623	7.08
3H-2, 108-123	16.48	8.02	47.12	35.5	576.0	1.37	521	37.5	4.40	4.0	12.1	719	6.54
3H-4, 80-150	18.64	7.89	47.67	35.5	576.0	0.00	521	37.7	4.21	4.0	11.9	647	6.83
3H-6, 95-105	21.49	7.83	47.92	35.5	577.0	0.00	524	37.2	4.32	4.1	11.8	761	6.27
4H-2, 140-150	26.30	7.97	45.76	35.0	575.0	2.63	522	36.3	4.63	4.6	11.7	662	5.08
4H-4, 135-150	29.25	8.04	48.38	35.0	575.0	0.00	523	36.6	4.80	4.8	11.5	609	6.15
4H-5, 90-105	30.30	7.49	44.27	35.0	576.0	0.58	523	35.4	4.52	4.5	11.6	645	6.01
5H-2, 135-150	35.75	8.28	44.68	35.0	575.0	0.00		34.3	4.29	4.3	11.7	700	
5H-4, 135-150	38.75	8.25	44.83	35.0	575.0	0.00	526	34.0	4.21	4.0	11.6	654	6.46
7H-2, 135-150	54.25	7.96	44.03	35.0	574.0	0.00		34.5	3.07	2.7	11.5	667	
8H-4, 135-150	66.48			35.0		14.79			6.01		11.4	387	
190-1174B-													
1R-6, 135-150	149.98	7.73	43.42	35.0		2.88		37.2	4.68	4.5	11.5	663	
2R-CC, 0-12	150.58	7.74	30.01	32.0		2.97		31.4	4.55	4.5	9.5	738	9.37
3R-1, 135-150	161.05			33.5	573.0	0.61		27.9	4.58	5.0	9.4	822	11.58
4R-2, 46-61	171.36			33.5	573.0	0.50		27.2	4.91	5.1	9.5	937	12.73
5R-1, 40-60	179.40	7.80	31.76	34.0	574.0	1.13	521	27.5	4.83	5.1	9.1	893	10.51
6R-1, 125-150	189.95	7.84	31.66	34.0	575.0	0.90	521	27.3	4.98	5.3	8.5	865	12.28
7R-1, 98-123	199.38	7.94	30.22	34.0	579.0	0.46	525	26.5	4.76	5.3	8.3	838	12.44
8R-1, 64-84	208.64	8.06	27.80	34.0	576.0	1.32	522	27.1	5.12	5.5	7.9	764	9.09
9R-1, 125-150	218.95	8.08	29.14	34.0	576.0	0.00		25.7	5.16	5.6	7.5	744	
10R-1, 120-150	228.40	8.00	26.02	33.5	575.0	0.38	521	25.2	5.20	5.5	7.2	754	11.21
11R-2, 50-80	238.80	7.87	23.45	33.0	575.0	0.46	524	22.8	5.14	5.8	6.8	1005	10.80
12R-1, 120-150	247.70	7.96	23.89	33.5	573.0	2.22	522	21.1	5.74	6.8	7.0	893	11.67
13R-2, 120-150	258.90	7.79	20.55	33.0	571.0	0.54	525	19.9	7.23	4.6	7.0	1086	10.85
14R-1, 21-38	266.01			32.5	572.0	1.48		16.5	8.77	8.2	7.0	1134	9.48
15R-1, 125-150	276.75	7.67	15.48	32.5	572.0	1.33	529	14.5	9.19	7.0	6.8	1269	8.16
16R-1, 125-150	286.35	7.87	16.16	32.0	572.0	1.14	525	13.9	9.36	10.2	6.6	1219	8.14
17R-1, 120-150	295.80	7.87	14.42	32.0	568.0	1.79	521	12.4	10.94	11.2	7.2	1183	7.47
18R-2, 120-150	307.00	7.96	12.46	32.0	567.5	0.01	521	9.3	13.00	14.1	6.1	1219	5.69
19R-1, 125-150	315.25	7.82	10.22	32.0	567.0	1.38	519	8.2	12.66	15.0	6.1	1201	5.54
20R-2, 120-150	326.20	7.90	8.81	32.0	566.0	1.85	519	6.3	14.30	16.0	6.1	1034	4.67
21R-1, 118-150	334.28	7.82	8.07	32.0	572.0	0.48	526	6.4	13.49	14.9	6.2	982	4.94
22R-1, 33-51	342.73			32.0	572.0	2.97		9.6	13.79	15.0	6.4	920	4.21
23R-1, 100-150	353.00	7.93	7.05	32.0	578.0	1.44	530	8.1	13.27	14.6	5.6	440	4.30
24R-3, 121-146	365.91	7.74	9.13	32.0	577.5	0.49	529	7.8	13.86	15.2	6.1	1080	5.25
25R-1, 125-150	372.55	7.80	11.01	32.5	580.0	1.36	535	9.0	13.64	13.3	6.3	948	5.32
26R-CC, 5-22	381.53			33.0	582.0	0.52		8.7	11.87	13.2	5.6	833	
27R-1, 125-150	391.75	8.02	9.47	33.0	584.0	0.95	541	10.7	13.66	13.6	6.3	854	
28R-1, 125-150	401.45	7.77	9.02	33.0	586.0	1.74	544	10.7	14.35	13.7	6.0	1069	
29R-3, 135-165	414.15	7.87	8.58	33.5	586.0	2.38	541	10.1	15.17	16.4	5.4	849	
31R-1, 115-150	430.15	8.07	3.31	33.5	586.5	0.89	536	7.9	16.64	18.1	3.8	200	
32R-2, 120-150	441.30	8.11	3.80	33.0	588.0	1.55	536	8.5	17.45	19.0	3.5	168	
33R-2, 120-150	450.90	8.13	3.25	33.0	590.0	0.89	538	6.7	19.74	20.6	2.8	197	
34R-3, 100-150	461.90	8.10	1.89	32.5	585.5	2.27	534	8.5	18.18	19.1	2.9	168	
35R-1, 120-150	468.30			33.0	597.0	0.99		8.1	19.59	20.8	2.8	200	
36R-3, 110-150	480.60	8.34	1.89	32.5	578.0	1.61	527	6.9	17.99	19.6	3.2	131	
37R-4, 120-150	491.40	8.25	2.28	32.5	595.5	1.51	544	7.4	18.15	19.4	3.3	418	
38R-4, 120-150	501.00			32.5	594.0	1.70		6.5	17.87	18.7	3.3	107	
39R-3, 120-150	509.10	7.72	3.43	32.5	583.5	0.43	536	5.4	18.13	18.9	3.7	1045	
40R-4, 125-150	520.35	7.85	4.44	32.0	562.5	3.40	514	8.6	17.97	19.8	3.2	648	
41R-2, 0-30	525.80			32.0	569.0	1.59		6.4	17.58	18.4	3.1	91	
42R-5, 120-150	541.10			32.0	561.0	2.04			16.90		2.7	134	1.58
43R-3, 100-150	547.60			32.0	554.0	0.61			17.45		2.2		1.40
44R-3, 120-150	557.10			31.5	557.5	2.21		7.3	17.23	18.1	2.7	120	1.25
45R-3, 120-150	566.80			31.0	560.0	1.53		5.6	17.90	19.3	2.4		1.20
46R-4, 120-150	578.00			31.0	542.0	1.95		7.5	17.76	19.3	2.2	134	0.84
47R-4, 120-150	587.60	8.38	5.69	30.5	541.5	1.00	497	5.3	17.38	19.5	2.0	117	0.95
49R-1, 120-150	602.40			30.0	540.0	1.47		5.9	17.15	18.9	2.2	117	0.97
50R-4, 120-150	616.60	8.20	7.28	30.0	541.0	1.24	501	5.0	18.12	19.1	1.9	343	

Table T14 (continued).

Hole, core, section, interval (cm)	Depth (mbsf)	pH (ISE)	Alk (T) (mM)	SAL (R) (psu)	Cl (T) (mM)	SO_4 (I) (mM)	Na (I) (mM)	Mg(T) (mM)	Ca (I) (mM)	Ca(T) (mM)	K (I) (mM)	H_4SiO_4 (S) (µM)	NH_4 (S) (mM)
51R-1, 0-31	620.50			31.5	535.0			8.6		18.3			
52R-6, 120-150	638.80			30.0	530.0			5.7		20.4		120	
53R-3, 15-45	642.95	8.03	11.53	30.0	532.0	1.90	496	5.1	17.32	19.7	1.9	295	
54R-5, 120-150	656.60			30.0	516.0	2.89		6.0	18.62	19.7	1.7		
56R-1, 120-150	669.90			30.0	512.0	1.79		4.4	18.11	19.5	1.8	141	
57R-4, 120-150	684.00	8.49	16.67	29.5	511.5	2.40	480	5.3	18.79	20.4	1.8	137	
59R-3, 120-150	701.80			29.5	505.5	2.25		5.0	19.84	20.2	1.5		
60R-2, 115-150	709.85			29.0	496.0	3.23		5.0	20.20	22.4	1.5	172	
61R-5, 120-150	724.10			30.0	492.5	2.62		5.1	21.08	23.2	1.4		
62R-3, 120-150	730.70			30.0	489.5	3.46			20.70		1.3		
64R-3, 120-150	749.90			30.0	488.0	3.64			20.93		1.3	148	
66R-1, 120-150	765.80			28.0	489.0	4.91		6.4	20.87	22.6	1.2		
67R-4, 135-150	778.79			29.0	489.5	5.13			19.96		1.4		
68R-1, 120-150	785.10			29.5	489.0	6.30		9.0	20.63	22.5	1.7		
69R-4, 120-150	798.07			28.0	492.0	0.62		6.9	2.45	22.7	0.6		
70R-2, 120-150	806.00			29.0	496.0	6.77		8.8	20.58	23.6	1.7	235	
71R-1, 1-27	812.51			28.0	496.0	5.14		6.2	21.03	24.1	1.4	218	
72R-1, 17-38	822.37		17.73	28.0		8.52		5.1	23.43	28.0	1.6		
73R-3, 120-150	836.00			28.0	497.0	5.92		5.2	22.99	27.9	1.3		
73R-6, 24-60	839.54			30.0	496.0	5.85		5.4	23.53	27.9	1.4		
74R-2, 0-40	842.90			30.0	495.5	5.07		5.6	22.11	25.5	1.4		
75R-2, 0-28	852.50	8.22	17.57	28.5	477.0	5.82	442	5.0	24.66	26.5	1.4	233	
76R-1, 38-60	861.08			28.0	474.0	5.18		6.7	22.26	26.0	1.3	271	
79R-1, 120-150	890.50	7.82	15.74	29.5	472.0	6.68	428	7.5	25.12	28.4	1.5		
80R-3, 120-150	903.20			29.5	477.0	7.67		10.1	24.58	26.8	1.7	334	
81R-3, 102-150	912.62			29.5	478.0	8.84		10.8	24.67	28.3	2.1	299	
82R-2, 98-125	920.78			28.5	477.0	6.38		6.3	25.28	29.5	1.5	328	
83R-4, 116-150	933.56			27.8	476.0	5.80		6.0	26.04	29.8	1.3		
84R-2, 120-150	940.20			28.0	466.0	5.70		4.7	25.84	30.5	1.3	397	
85R-3, 120-150	951.30	7.65	13.96	27.5	467.0	7.97	415	7.3	27.90	32.6	1.6		
86R-2, 120-150	959.50			28.5	464.0	7.23		5.6	29.52	32.9	1.4		
87R-2, 120-150	969.20	7.92	16.37	28.5	467.0	6.15	418	7.7	28.78	30.3	1.3	316	
88R-2, 120-150	978.80			28.0	476.0	7.36		10.9	30.97	28.8	1.5		
89R-3, 0-30	988.30			28.5	481.0	6.85		8.2	30.43	32.5	1.6	448	
90R-1, 120-150	996.10			29.5	488.0	8.80		11.4	30.56	32.9	1.7		
91R-1, 100-150	1005.60			30.0	489.0	10.00		8.6	34.62	37.9	1.5		
92R-6, 0-30	1021.70			29.5									
93R-4, 120-150	1029.60			28.0	473.0	5.82		6.9	35.56	38.7	1.2		
94R-1, 120-150	1034.70			30.0	490.0	9.27			36.68		1.6		
95R-1, 39-71	1043.49	7.38	8.12	29.0	475.0	8.20	395	6.3	39.40	45.4	1.5		
96R-2, 120-150	1055.30			29.0	481.0	7.71		9.1	44.11	47.1	2.7	282	
97R-1, 90-150	1063.20			29.0	493.0	6.46			48.08		1.2		
98R-3, 76-106	1075.66	7.13	9.17	31.0	513.0	8.71	410	8.6	53.00	55.3	1.6		
99R-2, 29-69	1083.29			34.5	546.0	9.34		14.9	59.73	60.1	2.0		
100R-1, 106-136	1092.26			33.0	543.0	7.46			64.01		1.5		
101R-1, 0-13	1100.80			33.0	547.5	9.54		21.2	68.63	62.2	1.5		
102R-1, 5-21	1110.25			32.0									

Note: ISE = ion selective electrode, T = titration, R = refractometry, I = ion, S = spectrophotometry.

Table T15. Headspace gas and vacutainer analysis, Site 1174. (See table note. Continued on next page.)

Core, section, interval (cm)	Depth (mbsf)	Sample method	C_1/C_2	C_1 (ppm)	C_2 (ppm)	C_2= (ppm)	C_3 (ppm)	C_3= (ppm)
190-1174A-								
1H-1, 135-140	1.35	HS		3	0.0	0.0	0.0	0.0
2H-4, 118-119	8.87	VAC	1,176,223	940,978	0.8	0.0	0.0	0.0
2H-5, 0-5	9.19	HS		2,714	0.0	0.0	0.0	0.0
2H-5, 110-111	10.29	VAC	1,341,373	938,961	0.7	0.0	0.0	0.0
3H-5, 0-5	19.34	HS		4,423	0.0	0.0	0.0	0.0
4H-4, 0-5	27.90	HS		3,915	0.0	0.0	0.0	0.0
5H-5, 0-5	38.90	HS		2,441	0.0	0.0	0.0	2.3
7H-2, 0-5	52.90	HS		2,171	0.0	0.0	0.0	0.0
8H-4, 0-5	65.13	HS		2,463	0.0	0.0	0.0	0.0
190-1174B-								
1R-6, 0-5	148.63	HS		3,342	0.0	0.0	0.0	0.0
3R-2, 0-5	161.20	HS	10,491	4,196	0.4	0.0	0.0	0.0
4R-2, 0-5	170.90	HS	3,519	5,631	1.6	0.4	0.0	0.0
5R-2, 0-5	180.50	HS	4,684	3,747	0.8	0.0	0.0	0.0
6R-2, 0-5	190.20	HS	1,962	6,867	3.5	0.5	0.0	0.0
7R-1, 0-5	198.40	HS	5,713	2,285	0.4	0.0	0.0	0.0
8R-1, 64-84	208.64	HS	1,553	4,504	2.9	0.0	0.0	0.0
9R-2, 0-5	219.20	HS	1,474	2,653	1.8	0.0	0.0	0.0
10R-2, 0-5	228.70	HS	1,435	4,161	2.9	0.0	0.0	0.0
11R-2, 0-5	238.30	HS	1,755	2,808	1.6	0.0	0.0	0.0
12R-1, 120-150	247.70	HS	759	1,594	2.1	0.0	0.0	0.0
13R-2, 0-5	257.70	HS	1,033	4,547	4.4	0.6	0.0	0.0
14R-1, 0-5	265.80	HS	2,161	6,915	3.2	0.0	0.0	0.0
15R-2, 0-5	277.00	HS	2,608	5,737	2.2	0.0	0.0	0.0
16R-1, 0-5	285.10	HS	3,134	38,229	12.2	0.0	1.6	0.0
17R-2, 0-5	296.10	HS	2,016	19,760	9.8	0.6	2.3	0.0
18R-3, 0-5	307.30	HS	668	1,335	2.0	0.0	0.0	0.0
19R-2, 0-5	315.50	HS	1,274	3,057	2.4	0.0	0.0	0.0
20R-2, 0-5	325.00	HS	1,001	3,705	3.7	0.0	0.0	0.0
21R-1, 0-5	333.10	HS	1,080	2,809	2.6	0.0	0.0	0.0
22R-1, 48-51	342.88	HS	2,101	10,714	5.1	0.0	0.0	0.0
23R-2, 0-5	353.50	HS	1,955	7,623	3.9	0.0	0.0	0.0
24R-3, 0-5	364.70	HS	2,908	16,284	5.6	0.3	0.0	0.0
25R-1, 0-5	371.30	HS	2,250	9,448	4.2	0.0	0.8	0.0
26R-1, 0-5	380.90	HS	4,357	11,764	2.7	0.0	0.5	0.0
27R-3, 0-5	393.50	HS	3,681	19,875	5.4	0.0	2.0	0.0
28R-1, 0-5	400.20	HS	3,405	32,689	9.6	0.0	0.0	0.0
29R-3, 0-5	412.80	HS	2,558	7,162	2.8	0.0	0.0	0.0
31R-3, 0-5	432.00	HS	1,252	2,002	1.6	0.0	0.0	0.0
32R-5, 0-5	444.60	HS	1,589	1,589	1.0	0.0	0.0	0.0
33R-3, 0-5	451.20	HS	2,652	10,875	4.1	0.0	7.4	0.0
34R-4, 0-5	462.40	HS	2,131	6,820	3.2	0.3	7.1	0.0
35R-2, 0-5	468.60	HS	2,003	7,409	3.7	0.0	6.2	0.0
36R-4, 0-5	481.00	HS	2,018	9,485	4.7	0.0	11.4	0.0
37R-5, 0-5	491.70	HS	1,874	11,806	6.3	0.0	17.9	0.0
38R-5, 0-5	501.30	HS	2,520	18,898	7.5	0.0	23.1	0.0
39R-3, 0-5	507.90	HS	4,074	11,406	2.8	0.0	7.0	0.0
40R-5, 0-5	520.60	HS	3,305	22,141	6.7	0.0	17.8	0.0
41R-3, 0-5	527.30	HS	2,071	14,288	6.9	0.0	26.4	0.0
42R-4, 0-5	538.40	HS	2,265	2,718	1.2	0.0	0.0	0.0
43R-4, 0-5	548.10	HS	1,412	1,271	0.9	0.0	0.0	0.0
44R-3, 0-5	555.90	HS	2,079	6,030	2.9	0.0	0.0	0.0
45R-3, 0-5	565.60	HS	1,670	8,185	4.9	0.0	14.8	0.0
46R-4, 0-5	576.80	HS	1,599	8,313	5.2	0.0	19.4	0.0
47R-3, 0-5	584.90	HS	2,141	12,629	5.9	0.0	20.3	0.0
48R-5, 0-5	597.60	HS	1,856	12,439	6.7	0.0	22.8	0.0
49R-3, 0-5	604.20	HS	1,332	4,927	3.7	0.0	13.9	0.0
50R-5, 0-5	616.90	HS	1,366	12,154	8.9	0.0	29.1	0.0
51R-3, 0-5	623.50	HS	1,163	5,931	5.1	0.0	19.2	0.0
52R-6, 0-5	637.60	HS	1,165	5,009	4.3	0.0	12.1	0.0
53R-4, 0-5	644.30	HS	1,121	6,838	6.1	0.0	15.1	0.0
55R-4, 0-5	663.50	HS	917	6,235	6.8	0.0	11.1	0.0
58R-3, 0-5	691.00	HS	457	1,598	3.5	0.0	4.4	0.0
59R-4, 0-5	702.10	HS	333	599	1.8	0.0	2.9	0.0
60R-5, 0-5	713.20	HS	488	2,198	4.5	0.0	4.4	0.0
61R-6, 0-5	724.40	HS	470	2,677	5.7	0.0	3.9	0.0

Table T15 (continued).

Core, section, interval (cm)	Depth (mbsf)	Sample method	C_1/C_2	C_1 (ppm)	C_2 (ppm)	C_2= (ppm)	C_3 (ppm)	C_3= (ppm)
62R-5, 0-5	732.50	HS	382	2,901	7.6	0.0	4.4	0.0
63R-5, 0-5	742.10	HS	422	3,756	8.9	0.0	4.2	0.0
64R-4, 0-5	750.20	HS	282	1,213	4.3	0.0	1.9	0.0
65R-1, 0-5	755.00	HS	231	1,063	4.6	0.0	0.0	0.0
65R-5, 0-5	761.00	HS	306	3,240	10.6	0.0	3.7	0.0
66R-1, 0-5	764.60	HS	231	1,063	4.6	0.0	0.0	0.0
67R-4, 0-5	777.44	HS	185	924	5.0	0.0	0.0	0.0
68R-2, 0-5	785.40	HS	169	860	5.1	0.0	0.0	0.0
69R-5, 0-5	798.37	HS	154	432	2.8	0.0	0.0	0.0
70R-3, 0-5	806.30	HS	157	657	4.2	0.0	1.8	0.0
71R-3, 0-5	814.16	HS	138	221	1.6	0.0	0.0	0.0
72R-3, 0-5	825.20	HS	101	423	4.2	0.0	2.0	0.0
73R-4, 0-5	836.30	HS	156	1,029	6.6	0.0	2.5	0.0
74R-3, 0-5	844.40	HS	137	1,750	12.8	0.0	4.3	0.0
75R-1, 145-150	852.45	HS	104	883	8.5	0.0	3.6	0.0
76R-2, 0-5	862.20	HS	41	99	2.4	0.0	0.0	0.0
77R-5, 0-5	876.40	HS	41	99	2.4	0.0	0.0	0.0
78R-3, 0-5	883.00	HS	32	54	1.7	0.0	0.0	0.0
79R-2, 0-5	890.80	HS	58	276	4.8	0.0	0.0	0.0
80R-5, 0-5	905.00	HS	35	94	2.7	0.0	0.0	0.0
81R-4, 0-5	913.10	HS	55	339	6.2	0.0	0.0	0.0
82R-2, 0-5	919.80	HS	47	375	7.9	0.0	2.7	0.0
83R-6, 0-5	935.40	HS	48	493	10.3	0.0	3.7	0.0
84R-5, 0-5	943.50	HS	39	1,002	25.5	0.0	10.0	0.0
85R-4, 0-5	951.60	HS	31	716	23.4	0.0	11.0	0.0
86R-3, 0-5	959.80	HS	34	419	12.3	0.0	5.2	0.0
87R-3, 0-5	969.50	HS	31	1,021	33.0	0.0	12.4	0.0
88R-3, 0-5	979.10	HS	25	1,049	42.6	0.0	21.1	0.0
89R-5, 0-5	991.30	HS	15	125	8.2	0.0	4.7	0.0
90R-2, 0-5	996.40	HS	22	250	11.5	0.0	6.3	0.0
91R-2, 0-5	1006.10	HS	29	328	11.4	0.0	3.3	0.0
92R-2, 0-5	1015.70	HS	22	315	14.2	0.0	6.4	0.0
93R-3, 0-5	1026.90	HS	20	272	13.9	0.0	7.3	0.0
94R-4, 0-5	1038.00	HS	29	473	16.4	0.0	6.1	0.0
95R-4, 0-5	1047.60	HS	30	492	16.6	0.0	6.6	0.0
96R-3, 0-5	1055.60	HS	29	1,805	61.4	0.0	25.5	0.0
97R-2, 0-5	1063.80	HS	27	189	7.0	0.0	2.9	0.0
98R-4, 0-5	1075.96	HS	33	469	14.0	0.0	5.2	0.0
99R-2, 0-5	1083.00	HS	27	408	15.3	0.0	6.0	0.0
100R-1, 106-126	1092.26	HS	20	385	19.2	0.0	10.4	0.0
101R-1, 0-5	1100.80	HS	21	335	16.3	0.0	8.1	0.0
102R-1, 5-21	1110.25	HS	29	382	13.1	0.0	0.0	0.0

Note: HS = headspace, VAC = vacutainer.

Table T16. Carbon, nitrogen, sulfur, and hydrogen analyses, Site 1174. (**See table note.** Continued on next three pages.)

Core, section, interval (cm)	Depth (mbsf)	Inorganic C (wt%)	$CaCO_3$ (wt%)	TOC (wt%)	Organic C (wt%)	N (wt%)	S (wt%)	H (mg HC/g of sediment)
190-1174A-								
1H-1, 38-39	0.38	0.03	0.29	NA	NA	NA	NA	NA
1H-2, 96-97	2.46	0.19	1.66	NA	NA	NA	NA	NA
1H-3, 109-110	4.09	0.89	7.43	NA	NA	NA	NA	NA
2H-5, 130-131	10.49	0.32	2.68	0.94	0.61	0.12	0.09	0.49
2H-7, 131-132	13.50	0.37	3.13	NA	NA	NA	NA	NA
3H-2, 104-105	16.44	0.18	1.55	NA	NA	NA	NA	NA
3H-4, 76-77	18.60	0.17	1.48	NA	NA	NA	NA	NA
3H-6, 85-86	21.39	0.16	1.35	NA	NA	NA	NA	NA
4H-2, 64-65	25.54	0.13	1.10	NA	NA	NA	NA	NA
4H-4, 130-131	29.20	0.13	1.10	NA	NA	NA	NA	NA
5H-1, 99-100	33.89	0.11	0.98	NA	NA	NA	NA	NA
5H-2, 134-135	35.74	0.42	3.57	1.00	0.57	0.11	0.07	0.49
5H-CC, 40-41	39.89	0.28	2.36	NA	NA	NA	NA	NA
7H-2, 131-132	54.21	0.23	1.97	NA	NA	NA	NA	NA
8H-4, 134-135	66.47	0.11	0.92	NA	NA	NA	NA	NA
190-1174B-								
1R-1, 69-70	144.39	0.38	3.23	0.94	0.55	0.07	0.09	0.48
3R-1, 125-127	160.95	0.31	2.59	NA	NA	NA	NA	NA
4R-2, 43-44	171.33	0.70	5.89	1.55	0.84	0.10	0.06	0.52
5R-1, 35-36	179.35	0.34	2.83	NA	NA	NA	NA	NA
5R-1, 122-123	180.22	0.27	2.29	NA	NA	NA	NA	NA
6R-1, 121-122	189.91	0.28	2.34	NA	NA	NA	NA	NA
7R-1, 94-95	199.34	0.45	3.80	1.08	0.62	0.09	0.09	0.52
8R-1, 60-61	208.60	0.41	3.42	NA	NA	NA	NA	NA
9R-1, 122-123	218.92	0.16	1.39	NA	NA	NA	NA	NA
10R-1, 118-119	228.38	0.41	3.42	NA	NA	NA	NA	NA
10R-CC, 17-18	229.49	0.47	3.96	NA	NA	NA	NA	NA
11R-2, 16-17	238.46	0.40	3.34	1.00	0.60	0.11	0.06	0.56
12R-1, 113-114	247.63	0.18	1.50	NA	NA	NA	NA	NA
13R-1, 105-106	257.25	0.33	2.79	0.94	0.60	0.12	0.11	0.62
13R-2, 118-119	258.88	0.35	2.95	NA	NA	NA	NA	NA
14R-1, 19-20	265.99	0.17	1.42	NA	NA	NA	NA	NA
15R-1, 123-124	276.73	1.84	15.39	NA	NA	NA	NA	NA
15R-2, 48-49	277.48	0.61	5.14	NA	NA	NA	NA	NA
16R-1, 124-125	286.34	0.45	3.81	1.10	0.64	0.13	0.09	0.60
17R-1, 111-112	295.71	0.36	3.05	NA	NA	NA	NA	NA
18R-2, 66-67	306.46	0.52	4.34	NA	NA	NA	NA	NA
18R-4, 80-81	309.60	0	0	NA	NA	NA	NA	NA
19R-1, 77-78	314.77	0.32	2.74	0.78	0.45	0.10	0.07	0.53
19R-1, 123-124	315.23	0.45	3.80	NA	NA	NA	NA	NA
20R-2, 111-112	326.11	0.25	2.11	NA	NA	NA	NA	NA
20R-3, 51-52	327.01	0.13	1.14	NA	NA	NA	NA	NA
21R-1, 115-116	334.25	0.45	3.79	0.83	0.37	0.11	0	0.47
21R-CC, 4-5	335.76	1.05	8.74	NA	NA	NA	NA	NA
22R-1, 26-27	342.66	0.57	4.79	NA	NA	NA	NA	NA
23R-1, 97-98	352.97	0.45	3.75	NA	NA	NA	NA	NA
24R-3, 117-118	365.87	0.42	3.53	0.87	0.44	0.10	0.06	0.53
25R-1, 122-123	372.52	0.10	0.88	NA	NA	NA	NA	NA
26R-1, 55-56	381.45	0.35	2.99	0.73	0.37	0.06	0	0.59
27R-1, 124-125	391.74	0.26	2.20	NA	NA	NA	NA	NA
27R-3, 116-117	394.66	0.26	2.21	NA	NA	NA	NA	NA
28R-1, 123-124	401.43	0.36	3.03	0.67	0.30	0.12	0.05	0.61
28R-2, 46-47	402.16	0.17	1.48	NA	NA	NA	NA	NA
29R-2, 80-81	412.10	0.07	0.65	NA	NA	NA	NA	NA
29R-3, 135-136	414.15	0.15	1.29	NA	NA	NA	NA	NA
29R-CC, 17-18	414.62	0.16	1.40	NA	NA	NA	NA	NA
30R-CC, 3-4	419.43	0.05	0.48	NA	NA	NA	NA	NA
31R-1, 115-116	430.15	0.30	2.55	NA	NA	NA	NA	NA
31R-3, 43-44	432.43	0.34	2.91	0.73	0.38	0.10	0.07	0.54
32R-2, 116-117	441.26	0.34	2.86	NA	NA	NA	NA	NA
32R-5, 129-130	445.89	2.88	24.06	NA	NA	NA	NA	NA
33R-2, 119-120	450.89	0.13	1.16	NA	NA	NA	NA	NA
33R-4, 18-19	452.88	0.12	1.05	NA	NA	NA	NA	NA
34R-3, 97-98	461.87	0.30	2.51	NA	NA	NA	NA	NA
35R-1, 118-119	468.28	0.33	2.80	0.68	0.34	0.11	0.19	0.58
35R-2, 94-95	469.54	0.12	1.05	NA	NA	NA	NA	NA

Table T16 (continued).

Core, section, interval (cm)	Depth (mbsf)	Inorganic C (wt%)	$CaCO_3$ (wt%)	TOC (wt%)	Organic C (wt%)	N (wt%)	S (wt%)	H (mg HC/g of sediment)
36R-2, 133-134	479.33	0.40	3.36	0.90	0.50	0.09	0.12	0.53
36R-3, 111-112	480.61	0.47	3.98	0.85	0.37	0.11	0	0.53
37R-3, 131-132	490.01	0.10	0.89	NA	NA	NA	NA	NA
37R-4, 118-119	491.38	0.66	5.52	NA	NA	NA	NA	NA
38R-3, 85-86	499.15	0.41	3.43	0.76	0.35	0.11	0	0.56
38R-4, 115-116	500.95	0.53	4.46	0.93	0.39	0.11	0.07	0.60
38R-6, 63-64	503.43	0.85	7.11	NA	NA	NA	NA	NA
39R-1, 134-135	506.24	0.57	4.75	0.93	0.36	0.09	0	0.57
39R-3, 118-119	509.08	0.25	2.16	NA	NA	NA	NA	NA
40R-4, 118-119	520.28	0.22	1.89	NA	NA	NA	NA	NA
41R-2, 28-29	526.08	0.43	3.64	0.75	0.32	0.11	0.13	0.56
41R-CC, 19-20	528.99	0.20	1.73	NA	NA	NA	NA	NA
42R-1, 97-98	534.87	0.11	0.97	NA	NA	NA	NA	NA
42R-3, 126-127	538.16	0.18	1.54	NA	NA	NA	NA	NA
42R-5, 117-118	541.07	0.28	2.34	NA	NA	NA	NA	NA
43R-3, 98-99	547.58	0.11	0.95	NA	NA	NA	NA	NA
43R-5, 127-128	550.87	0.68	5.66	NA	NA	NA	NA	NA
43R-6, 130-131	552.40	0.70	5.91	NA	NA	NA	NA	NA
44R-3, 118-119	557.08	0.28	2.41	NA	NA	NA	NA	NA
44R-4, 124-125	558.64	0.23	1.96	NA	NA	NA	NA	NA
45R-1, 73-74	563.33	0.12	1.07	NA	NA	NA	NA	NA
45R-3, 108-109	566.68	1.27	10.65	NA	NA	NA	NA	NA
46R-1, 149-150	573.79	1.28	10.72	NA	NA	NA	NA	NA
46R-4, 118-119	577.98	0.27	2.31	NA	NA	NA	NA	NA
46R-7, 42-43	581.72	1.37	11.49	NA	NA	NA	NA	NA
47R-1, 149-150	583.39	0.21	1.78	NA	NA	NA	NA	NA
47R-4, 119-120	587.59	0.24	2.06	NA	NA	NA	NA	NA
48R-2, 134-135	594.44	0.15	1.32	NA	NA	NA	NA	NA
48R-5, 101-102	598.61	0.14	1.22	NA	NA	NA	NA	NA
49R-1, 119-120	602.39	1.69	14.09	NA	NA	NA	NA	NA
49R-3, 99-100	605.19	0.28	2.38	NA	NA	NA	NA	NA
50R-1, 61-62	611.51	0.53	4.42	0.77	0.24	0.09	0.14	0.61
50R-4, 119-120	616.59	0.73	6.11	NA	NA	NA	NA	NA
52R-1, 83-84	630.93	1.16	9.70	NA	NA	NA	NA	NA
52R-6, 116-117	638.76	1.37	11.42	NA	NA	NA	NA	NA
53R-1, 108-109	640.88	0.12	1.07	NA	NA	NA	NA	NA
53R-3, 127-128	644.07	0.13	1.12	NA	NA	NA	NA	NA
53R-4, 15-16	644.45	0.41	3.47	0.60	0.18	0.09	0.11	0.76
54R-3, 126-127	653.66	0.34	2.89	0.72	0.38	0.11	0.33	0.6
54R-5, 97-98	656.37	0.65	5.44	NA	NA	NA	NA	NA
55R-1, 132-133	660.32	0.59	4.97	0.83	0.23	0.10	0	0.63
55R-2, 46-47	660.96	2.00	16.72	NA	NA	NA	NA	NA
55R-5, 91-92	665.91	0.36	3.00	0.64	0.28	0.09	0.04	0.62
56R-1, 115-116	669.85	0.45	3.82	0.77	0.31	0.10	0.10	0.64
56R-2, 134-135	671.54	0.16	1.40	NA	NA	NA	NA	NA
57R-4, 117-118	683.97	0.65	5.43	NA	NA	NA	NA	NA
57R-6, 134-135	687.14	0.69	5.76	NA	NA	NA	NA	NA
58R-2, 75-76	690.25	0.42	3.55	0.64	0.21	0.10	0.15	0.60
58R-4, 80-81	693.30	0.46	3.87	NA	NA	NA	NA	NA
59R-3, 117-118	701.77	0.25	2.12	NA	NA	NA	NA	NA
59R-4, 84-85	702.94	0.07	0.58	NA	NA	NA	NA	NA
59R-5, 128-129	704.88	0.11	0.96	NA	NA	NA	NA	NA
60R-2, 113-114	709.83	0.07	0.65	NA	NA	NA	NA	NA
61R-4, 106-107	722.46	0.63	5.26	NA	NA	NA	NA	NA
61R-5, 119-120	724.09	0.44	3.68	NA	NA	NA	NA	NA
62R-3, 98-99	730.48	0.10	0.87	NA	NA	NA	NA	NA
63R-2, 81-82	738.41	0.06	0.56	NA	NA	NA	NA	NA
63R-5, 137-138	743.47	0.24	2.07	0.66	0.41	0.12	0.17	0.66
64R-1, 106-107	746.76	0.10	0.83	NA	NA	NA	NA	NA
64R-3, 119-120	749.89	0.18	1.51	NA	NA	NA	NA	NA
64R-5, 109-110	752.79	0.06	0.50	0.31	0.25	0.08	0.19	0.64
65R-1, 114-115	756.14	0.18	1.51	NA	NA	NA	NA	NA
65R-4, 84-85	760.34	0.07	0.62	NA	NA	NA	NA	NA
66R-1, 113-114	765.73	0.66	5.55	NA	NA	NA	NA	NA
66R-5, 99-100	771.59	0.16	1.34	NA	NA	NA	NA	NA
67R-2, 99-100	775.43	0.16	1.36	NA	NA	NA	NA	NA
67R-3, 129-130	777.23	0.53	4.42	NA	NA	NA	NA	NA
67R-4, 127-128	778.71	0.35	2.93	0.65	0.29	0.09	0.13	0.66
68R-1, 116-118	785.06	0.25	2.11	NA	NA	NA	NA	NA

Table T16 (continued).

Core, section, interval (cm)	Depth (mbsf)	Inorganic C (wt%)	$CaCO_3$ (wt%)	TOC (wt%)	Organic C (wt%)	N (wt%)	S (wt%)	H (mg HC/g of sediment)
68R-2, 134-136	786.74	0.19	1.60	NA	NA	NA	NA	NA
69R-2, 129-130	795.16	0.21	1.75	NA	NA	NA	NA	NA
69R-3, 96-97	796.33	0.47	3.98	NA	NA	NA	NA	NA
69R-4, 118-119	798.05	1.16	9.71	NA	NA	NA	NA	NA
70R-2, 98-99	805.78	0.96	8.01	NA	NA	NA	NA	NA
70R-4, 148-149	809.28	0.21	1.75	0.43	0.22	0.10	0.79	0.65
70R-5, 148-149	810.78	0.32	2.73	NA	NA	NA	NA	NA
71R-2, 3-4	812.91	0.29	2.49	NA	NA	NA	NA	NA
71R-2, 96-97	813.84	0.49	4.15	NA	NA	NA	NA	NA
71R-3, 79-80	814.95	0.42	3.55	NA	NA	NA	NA	NA
72R-1, 44-45	822.64	1.32	11.04	NA	NA	NA	NA	NA
72R-1, 115-116	823.35	2.34	19.53	NA	NA	NA	NA	NA
72R-3, 104-105	826.24	0.78	6.53	NA	NA	NA	NA	NA
73R-1, 79-80	832.59	0.49	4.16	NA	NA	NA	NA	NA
73R-3, 115-116	835.95	0.21	1.77	0.42	0.21	0.09	0.07	0.68
73R-5, 113-114	838.93	0.72	6.00	NA	NA	NA	NA	NA
73R-7, 50-51	841.30	0.20	1.68	0.45	0.25	0.10	0.22	0.71
74R-1, 128-129	842.68	4.00	33.36	NA	NA	NA	NA	NA
74R-2, 55-56	843.45	0.67	5.64	NA	NA	NA	NA	NA
74R-2, 124-125	844.14	1.06	8.89	NA	NA	NA	NA	NA
74R-CC, 17-18	845.14	0.13	1.16	0.26	0.12	0.10	0.15	0.70
75R-1, 96-97	851.96	0.55	4.64	NA	NA	NA	NA	NA
76R-1, 33-34	861.03	2.83	23.63	NA	NA	NA	NA	NA
76R-1, 68-69	861.38	0.66	5.52	NA	NA	NA	NA	NA
76R-2, 78-79	862.98	0.44	3.68	NA	NA	NA	NA	NA
77R-2, 99-100	872.89	0.19	1.62	0.41	0.22	0.11	0.09	0.63
78R-2, 132-133	882.82	0.04	0.40	NA	NA	NA	NA	NA
78R-3, 99-100	883.99	0.07	0.59	NA	NA	NA	NA	NA
78R-5, 63-64	886.63	7.81	65.08	NA	NA	NA	NA	NA
79R-1, 117-118	890.47	0.08	0.70	0.23	0.15	0.10	0.05	0.65
80R-2, 88-89	901.38	0.06	0.50	NA	NA	NA	NA	NA
80R-3, 116-117	903.16	0.12	1.07	NA	NA	NA	NA	NA
81R-3, 98-100	912.58	0.42	3.53	NA	NA	NA	NA	NA
82R-2, 93-94	920.73	0.11	0.98	NA	NA	NA	NA	NA
83R-2, 147-148	930.87	1.45	12.10	NA	NA	NA	NA	NA
83R-4, 114-115	933.54	0.23	1.95	0.45	0.22	0.10	0	0.64
83R-6, 147-148	936.87	0.06	0.51	NA	NA	NA	NA	NA
84R-2, 115-116	940.15	0.91	7.58	NA	NA	NA	NA	NA
84R-3, 131-132	941.81	1.01	8.43	NA	NA	NA	NA	NA
84R-5, 78-79	944.28	0.06	0.57	0.10	0.03	0	0.04	1.17
85R-1, 121-122	948.31	0.09	0.77	NA	NA	NA	NA	NA
85R-3, 117-118	951.27	1.19	9.96	NA	NA	NA	NA	NA
85R-6, 87-88	955.47	4.77	39.80	NA	NA	NA	NA	NA
86R-2, 116-117	959.46	0.07	0.63	NA	NA	NA	NA	NA
86R-4, 27-28	961.57	6.59	54.89	NA	NA	NA	NA	NA
87R-1, 128-129	967.78	0.06	0.58	0.29	0.22	0.10	0.09	0.68
87R-3, 104-105	970.54	5.88	49.05	NA	NA	NA	NA	NA
87R-5, 8-9	972.58	0.22	1.85	NA	NA	NA	NA	NA
88R-2, 118-119	978.78	0.45	3.78	NA	NA	NA	NA	NA
88R-4, 91-92	981.51	0.33	2.80	NA	NA	NA	NA	NA
89R-2, 144-145	988.24	0.30	2.52	NA	NA	NA	NA	NA
89R-6, 36-37	993.16	0.09	0.77	0.31	0.21	0.11	0.04	0.65
90R-2, 7-8	996.47	0.06	0.57	NA	NA	NA	NA	NA
90R-2, 39-40	996.79	7.94	66.20	NA	NA	NA	NA	NA
91R-1, 86-87	1005.46	0.28	2.40	0.58	0.29	0.10	0	0.69
92R-2, 66-67	1016.36	0.09	0.75	NA	NA	NA	NA	NA
92R-5, 91-92	1021.11	0.23	1.99	NA	NA	NA	NA	NA
93R-3, 73-75	1027.63	6.33	52.79	NA	NA	NA	NA	NA
93R-4, 114-116	1029.54	0.35	2.93	NA	NA	NA	NA	NA
94R-1, 116-118	1034.66	0.49	4.15	NA	NA	NA	NA	NA
94R-3, 130-131	1037.80	1.84	15.38	NA	NA	NA	NA	NA
95R-2, 142-143	1046.02	0.37	3.15	NA	NA	NA	NA	NA
96R-2, 118-119	1055.28	0.73	6.14	NA	NA	NA	NA	NA
96R-3, 16-17	1055.76	0.59	4.99	NA	NA	NA	NA	NA
97R-1, 66-67	1062.96	0.12	1.05	0.35	0.23	0.09	0.19	0.65
98R-1, 25-26	1072.15	1.47	12.27	NA	NA	NA	NA	NA
98R-3, 71-72	1075.61	0.95	7.99	NA	NA	NA	NA	NA
99R-1, 21-22	1081.71	0.09	0.77	0.89	0.80	0.11	0.31	0.66
99R-2, 23-24	1083.23	0.56	4.68	NA	NA	NA	NA	NA

Table T16 (continued).

Core, section, interval (cm)	Depth (mbsf)	Inorganic C (wt%)	$CaCO_3$ (wt%)	TOC (wt%)	Organic C (wt%)	N (wt%)	S (wt%)	H (mg HC/g of sediment)
100R-1, 103-104	1092.23	0.18	1.50	NA	NA	NA	NA	NA
100R-2, 23-24	1092.79	5.41	45.11	NA	NA	NA	NA	NA
101R-1, 50-51	1101.30	1.12	9.36	NA	NA	NA	NA	NA
102R-1, 69-70	1110.89	0.06	0.53	0.19	0.13	0.07	0.05	0.79

Note: TOC = total organic carbon, HC = hydrocarbon.

Table T17. Total bacterial populations in sediments, Site 1174.

Depth (mbsf)	Bacterial cells (cells/cm^3)	
	Hole A	Hole B
2.49	1.47×10^8	
9.98	4.65×10^7	
12.03	2.51×10^7	
16.74	1.15×10^7	
26.24	1.74×10^6	
35.74	1.47×10^7	
54.24	1.93×10^7	
66.47	6.71×10^5	
170.89		2.07×10^6
180.49		1.59×10^6
219.21		1.85×10^6
247.70		2.41×10^6
286.34		2.71×10^6
324.70		6.11×10^6
352.99		1.60×10^6
391.74		2.68×10^5
430.50		1.08×10^5
450.90		2.77×10^5
490.50		2.39×10^5
520.35		5.88×10^4
547.60		1.59×10^4
578.00		BD
598.65		4.76×10^4
623.49		BD
656.49		BD
669.90		BD
709.85		BD
743.60		BD
778.64		7.30×10^5
796.47		7.95×10^5
813.87		BD
826.27		BD
835.99		BD
873.41		BD
901.40		BD
940.19		BD
978.79		BD
1021.10		BD
1055.60		BD
1091.30		BD

Note: BD = below detection (~6×10^4 cells/cm^3).

Table T18. Comparison of near-surface sediment bacterial populations at Site 1174 with data from nine other ODP sites with different overlying-water depths.

Location	ODP leg-site	Depth (mbsf)	Total bacteria (cells/cm^3)
Peru margin	112-681	150	1.05×10^9
Santa Barbara Basin	146-893	577	1.27×10^9
Japan Sea	128-798	900	7.82×10^8
Woodlark Basin	180-1115	1150	2.83×10^8
Cascadia margin	146-890	1326	6.95×10^8
Woodlark Basin	180-1109	2211	3.28×10^8
Juan de Fuca Ridge	139-857	2419	8.28×10^8
Cascadia margin	146-888	2516	5.32×10^8
Lau Basin	135-834	2703	6.12×10^8
Woodlark Basin	180-1108	3188	2.67×10^8
Amazon Fan	155-940	3195	5.62×10^8
Amazon Fan	155-934	3432	6.04×10^8
Eastern Equatorial Pacific	138-851	3760	2.08×10^8
Nankai Trough	190-1173	4791	7.23×10^7
	190-1174	4751	1.47×10^8

Table T19. Drilling fluid intrusion estimated based on PFT tracer experiments, Site 1174.

Core, section	Total sample weight (g)			Bulk density (g/cm³)	PFT peak area			Drilling fluid (µL)/sediment (g)		
	Outside	Quarter	Center		Outside	Quarter	Center	Outside	Quarter	Center
190-1174A-										
4H-2	4.11	3.36	2.45	1.64	1,163	412	296	1.3	0.3	0.2
190-1174B-										
4R-1	2.70	2.13	2.70	1.83	15,022	36,237	26,432	32.7	102.5	57.9
5R-1	3.20	3.79	3.81	1.67	1,060	1,216	9,745	1.5	1.5	14.3
31R-1	2.14	ND	1.17	2.11	3,476	ND	152	9.3	ND	BD
31R-2	ND	1.03	1.66	1.92	ND	4,439	198	ND	25.8	BD
32R-1	1.58	2.28	2.88	1.85	5,675	3,063	4,093	21.3	7.5	8.0
32R-3	2.06	1.13	2.74	2.23	15,896	254	2,377	46.9	0.1	4.8
32R-5	1.39	1.63	1.51	1.86	58,215	1,473	435	259.9	4.7	0.9

Notes: ND = no data. BD = below detection (0.01 µL drilling fluid).

Table T20. Fluorescent microsphere tracer experiments, Site 1174.

Core, section	Total sample weight (g)			Microspheres/sediment (g)		
	Outside	Quarter	Center	Outside	Quarter	Center
190-1174A-						
4H-2	4.11	3.36	2.45	21,381	0	0
190-1174B-						
4R-1	2.70	2.13	2.70	78	106	48
5R-1	3.20	3.79	3.81	13	0	0
31R-1	2.14	ND	1.17	0	ND	0
31R-2	ND	1.03	1.66	ND	0	46
32R-1	1.58	2.28	2.88	0	0	0
32R-3	2.06	1.13	2.74	55	0	23
32R-5	1.39	1.63	1.51	0	0	65

Note: ND = no data.

Table T21. Formation factor data from the needle-probe method, Hole 1174A.

Core, section, interval (cm)	Depth (mbsf)	Lithologic type	Formation factor	
			x	y
190-1174-				
1H-2, 115	2.65	Clayey silt		2.76
1H-2, 140	2.90	Clayey silt	2.67	
2H-2, 7	4.76	Clayey silt	3.10	3.32
2H-2, 82	5.51	Clayey silt	3.47	3.69
2H-3, 64	6.83	Clayey silt	3.21	3.55
2H-3, 133	7.52	Clayey silt	3.26	3.00
2H-5, 122	10.41	Clayey silt	3.48	3.61
2H-6, 69	11.38	Clayey silt	3.91	4.00
3H-1, 70	14.60	Clayey silt	2.92	3.29
3H-1, 142	15.32	Sandy silt	5.21	5.65
3H-2, 15	15.55	Sandy silt	5.65	6.22
3H-2, 91	16.31	Clayey silt	3.11	3.31
3H-3, 87	17.50	Clayey silt	3.16	3.36
3H-4, 60	18.44	Clayey silt	3.59	3.61
3H-5, 85	20.19	Clayey silt	3.56	3.52
4H-2, 4	24.94	Clayey silt	3.75	3.90
4H-3, 33	26.73	Clayey silt	4.25	4.37
4H-3, 36	26.76	Sandy silt		5.71
4H-4, 94	28.84	Sandy silt	4.35	4.56
5H-1, 107	33.97	Clayey silt	3.69	4.25
5H-1, 128	34.18	Sandy silt	4.92	5.31
5H-2, 4	34.44	Clayey silt	3.98	4.66
5H-4, 107	38.47	Clayey silt	4.19	3.94
5H-CC, 30	39.79	Clayey silt	3.62	3.71
7H-1, 76	52.66	Clayey silt	3.70	3.87
7H-4, 1	54.78	Sand	4.21	4.42
8H-2, 46	62.74	Sand	4.65	5.03
8H-3, 25	63.88	Sand	4.99	5.12
8H-4, 110	66.23	Sand	5.69	5.94

Note: x and y = probe axis.

Table T22. Electrical conductivity and formation factor data for cubes, Hole 1174B. (**See table note.** Continued on next two pages.)

Core, section, interval (cm)	Depth (mbsf)	Conductivity (S/m)			Temp (°C)	Formation factor		
		x	y	z		x	y	z
190-1174B-								
7R-1, 84	199.24	1.10	1.16	1.03	25.7	4.89	4.64	5.23
8R-1, 53	208.53	1.03	0.99	0.72	25.7	5.21	5.41	7.44
9R-1, 77	218.47	1.08	1.10	0.92	25.2	4.91	4.83	5.81
9R-2, 35	219.55	1.09	1.12	0.79	25.1	4.88	4.74	6.75
10R-1, 112	228.32	1.03	1.09	0.80	25.3	5.16	4.89	6.63
10R-2, 56	229.26	0.96	0.95	0.75	26.1	5.66	5.71	7.24
11R-1, 57	237.37	1.09	1.03	0.93	25.4	4.89	5.18	5.76
11R-2, 11	238.41	1.19	1.12	0.83	25.5	4.48	4.78	6.42
12R-1, 108	247.58	0.94	0.91	0.76	25.4	5.70	5.84	7.04
12R-1, 69	247.19	1.13	1.10	0.89	25.4	4.71	4.84	6.01
13R-1, 103	257.23	1.10	1.00	0.88	24.8	4.81	5.26	6.02
13R-2, 65	258.35	1.12	1.01	0.85	24.8	4.72	5.23	6.19
13R-3, 3	259.23	0.92	0.90	0.75	24.9	5.75	5.90	7.10
15R-1, 28	275.78	0.66	0.83	0.95	25.0	7.99	6.35	5.59
16R-1, 84	285.94	1.03	1.08	0.91	26.2	5.25	5.03	5.97
17R-1, 114	295.74	1.03	1.00	0.80	26.2	5.26	5.43	6.76
17R-2, 45	296.55	0.89	0.93	0.73	26.2	6.10	5.84	7.46
18R-2, 68	306.48	1.09	1.07	0.80	26.0	4.97	5.06	6.71
18R-4, 77	309.57	1.02	1.03	0.80	25.8	5.28	5.20	6.70
19R-1, 74	314.74	1.05	1.03	0.79	25.8	5.15	5.22	6.80
20R-1, 136	324.86	0.81	0.85	0.66	25.8	6.65	6.31	8.21
20R-2, 106	326.06	0.97	0.88	0.72	26.2	5.60	6.14	7.52
20R-3, 53	327.03	0.92	0.90	0.75	26.2	5.92	6.01	7.20
20R-3, 53	327.03	0.91	0.90	0.75	26.2	5.94	6.05	7.26
21R-1, 117	334.27	0.87	0.87	0.69	25.8	6.19	6.18	7.82
21R-2, 84	335.44	0.93	0.86	0.69	25.8	5.80	6.25	7.83
23R-2, 73	354.23	0.72	0.90	0.69	25.8	7.51	6.01	7.85
24R-1, 83	362.53	0.78	0.93	0.72	25.8	6.92	5.75	7.45
24R-3, 116	365.86	0.95	0.90	0.71	25.8	5.67	5.96	7.60
25R-2, 3	372.83	0.80	0.87	0.61	25.9	6.74	6.23	8.81
27R-1, 121	391.71	0.81	0.85	0.70	26.2	6.69	6.37	7.74
27R-2, 83	392.83	0.92	0.96	0.80	26.2	5.90	5.65	6.78
27R-3, 64	394.14	0.86	0.86	0.68	26.2	6.34	6.34	8.02
28R-1, 82	401.02	0.89	0.94	0.82	26.2	6.12	5.79	6.63
28R-2, 48	402.18	0.86	0.85	0.74	26.2	6.31	6.40	7.33
29R-2, 72	412.02	0.87	0.83	0.67	26.0	6.18	6.51	8.04
29R-3, 129	414.09	0.88	0.86	0.73	26.0	6.10	6.24	7.43
31R-2, 88	431.38	0.80	0.81	0.68	25.5	6.66	6.62	7.92
31R-3, 44	432.44	0.82	0.75	0.54	25.5	6.49	7.12	9.99
32R-6, 58	446.68	0.75	0.77	0.68	25.5	7.16	6.94	7.93
33R-2, 58	450.28	0.79	0.81	0.64	25.5	6.76	6.62	8.42
33R-4, 88	453.58	0.66	0.79	0.65	25.5	8.06	6.75	8.28
34R-2, 79	460.19	0.68	0.78	0.51	25.6	7.86	6.85	10.49
34R-4, 93	463.33	0.77	0.68	0.52	25.6	7.00	7.86	10.28
35R-2, 65	469.25	0.65	0.39	0.56	25.6	8.28	13.60	9.64
36R-2, 54	478.54	0.85	0.69	0.49	25.9	6.36	7.80	11.02
36R-4, 113	482.13	0.65	0.67	0.53	25.9	8.34	8.06	10.10
37R-1, 71	486.41	0.79	0.75	0.59	25.8	6.78	7.19	9.12
37R-3, 128	489.98	0.79	0.81	0.74	26.0	6.81	6.71	7.30
37R-6, 71	493.91	0.68	0.68	0.52	26.4	8.00	8.04	10.43
38R-1, 49	495.79	0.72	0.75	0.57	25.1	7.41	7.12	9.26
38R-2, 62	497.42	0.78	0.74	0.52	25.1	6.85	7.20	10.19
38R-4, 116	500.96	0.72	0.69	0.44	25.3	7.43	7.69	12.08
39R-1, 130	506.20	0.71	0.65	0.46	26.0	7.58	8.29	11.67
39R-4, 116	510.56	0.84	0.80	0.74	26.0	6.46	6.72	7.26
39R-5, 67	511.57	0.79	0.81	0.71	25.9	6.84	6.64	7.60
39R-6, 46	512.86	0.95	0.91	0.85	26.0	5.71	5.91	6.32
40R-2, 86	516.96	0.83	0.92	0.75	25.5	6.41	5.81	7.13
40R-4, 113	520.23	0.74	0.72	0.67	25.5	7.26	7.43	8.02
40R-6, 112	523.22	0.81	0.70	0.70	25.5	6.57	7.63	7.59
41R-2, 69	526.49	0.74	0.66	0.55	27.4	7.52	8.36	10.05
41R-3, 15	527.45	0.74	0.84	0.61	25.4	7.26	6.33	8.69
42R-2, 61	536.01	0.72	0.84	0.64	26.5	7.52	6.52	8.50
42R-4, 49	538.89	0.73	0.84	0.61	26.5	7.42	6.47	8.94
42R-5, 52	540.42	0.76	0.68	0.54	26.2	7.15	7.99	10.06
42R-7, 11	543.01	0.78	0.79	0.60	26.0	6.91	6.87	8.93

Table T22 (continued).

Core, section, interval (cm)	Depth (mbsf)	Conductivity (S/m)			Temp (°C)	Formation factor		
		x	y	z		x	y	z
43R-3, 84	547.44	0.79	0.72	0.58	26.9	6.99	7.57	9.55
43R-5, 125	550.85	0.74	0.76	0.56	26.4	7.40	7.14	9.72
43R-6, 22	551.32	0.74	0.76	0.53	26.4	7.39	7.13	10.35
44R-2, 64	555.04	0.78	0.76	0.58	26.1	6.90	7.13	9.41
44R-4, 115	558.55	0.72	0.80	0.54	26.4	7.57	6.78	9.99
45R-2, 76	564.86	0.76	0.65	0.47	26.1	7.12	8.27	11.58
45R-4, 105	568.15	0.69	0.76	0.52	26.1	7.86	7.14	10.41
46R-2, 81	574.61	0.67	0.67	0.44	26.1	8.05	8.07	12.26
46R-4, 75	577.55	0.70	0.63	0.35	26.1	7.78	8.61	15.40
46R-6, 80	580.60	0.76	0.65	0.49	26.1	7.08	8.29	11.00
47R-2, 96	584.36	0.69	0.75	0.64	26.1	7.81	7.22	8.41
47R-4, 56	586.96	0.73	0.68	0.47	26.1	7.41	7.92	11.49
48R-2, 100	594.10	0.90	0.65	0.48	26.2	6.02	8.31	11.21
48R-4, 82	596.92	0.70	0.64	0.45	26.2	7.79	8.40	12.06
48R-6, 81	599.91	0.64	0.65	0.48	26.0	8.46	8.34	11.14
49R-2, 82	603.52	0.63	0.71	0.44	26.0	8.59	7.60	12.20
49R-3, 96	605.16	0.71	0.72	0.51	26.0	7.60	7.54	10.56
50R-2, 60	613.00	0.85	0.83	0.67	26.0	6.38	6.53	8.10
50R-4, 46	615.86	0.54	0.64	0.50	26.0	9.95	8.38	10.88
52R-1, 84	630.94	0.91	0.83	0.69	26.7	5.98	6.61	7.91
52R-3, 72	633.82	0.87	0.73	0.61	26.7	6.26	7.54	9.02
52R-6, 117	638.77	0.68	0.75	0.51	26.7	8.05	7.30	10.64
53R-1, 105	640.85	0.81	0.82	0.61	26.7	6.75	6.65	8.91
53R-2, 66	641.96	0.75	0.84	0.69	26.7	7.27	6.49	7.88
53R-4, 12	644.42	0.56	0.66	0.59	26.7	9.68	8.23	9.20
54R-2, 40	651.30	0.80	0.71	0.61	26.3	6.80	7.63	8.85
54R-4, 66	654.56	0.62	0.66	0.49	26.3	8.73	8.20	10.98
54R-6, 37	657.27	0.51	0.52	0.41	26.3	10.64	10.47	13.17
55R-2, 98	661.48	0.70	0.67	0.53	26.5	7.76	8.19	10.32
55R-4, 116	664.66	0.68	0.61	0.51	26.5	8.07	8.92	10.60
55R-6, 63	667.13	0.68	0.66	0.49	26.5	8.05	8.29	11.06
56R-2, 81	671.01	0.70	0.68	0.46	26.8	7.78	8.07	11.87
57R-2, 82	680.62	0.65	0.69	0.48	26.8	8.49	7.92	11.46
57R-4, 46	683.26	0.75	0.88	0.57	26.8	7.35	6.24	9.62
57R-6, 55	686.35	0.61	0.56	0.54	26.8	9.02	9.87	10.17
58R-2, 67	690.17	0.67	0.61	0.45	26.8	8.12	8.94	12.10
58R-4, 77	693.27	0.63	0.63	0.47	26.8	8.71	8.75	11.68
59R-2, 32	699.42	0.68	0.59	0.45	26.8	8.12	9.27	12.08
59R-5, 45	704.05	0.58	0.53	0.44	26.8	9.47	10.29	12.47
60R-2, 44	709.14	0.59	0.58	0.41	26.8	9.32	9.40	13.53
60R-6, 34	715.04	0.52	0.62	0.47	26.8	10.57	8.87	11.62
61R-2, 93	719.33	0.65	0.58	0.46	26.6	8.34	9.35	11.91
61R-4, 66	722.06	0.54	0.52	0.38	26.6	10.05	10.54	14.19
61R-6, 56	724.96	0.52	0.58	0.41	26.6	10.55	9.47	13.43
62R-2, 126	729.26	0.61	0.55	0.44	26.7	9.03	10.00	12.40
62R-3, 98	730.48	0.54	0.52	0.38	27.0	10.25	10.63	14.36
62R-4, 126	732.26	0.51	0.53	0.37	28.0	10.98	10.57	15.28
63R-2, 85	738.45	0.56	0.54	0.40	27.5	9.87	10.21	13.71
63R-4, 71	741.31	0.55	0.57	0.39	26.6	9.98	9.65	13.84
63R-6, 11	743.71	0.56	0.59	0.41	26.6	9.75	9.29	13.48
64R-2, 70	747.90	0.58	0.50	0.40	27.1	9.48	11.11	13.79
64R-4, 86	751.06	0.52	0.54	0.40	27.1	10.69	10.29	13.82
64R-5, 108	752.78	0.53	0.56	0.38	27.2	10.43	9.81	14.53
65R-2, 74	757.24	0.58	0.54	0.40	27.0	9.54	10.12	13.71
65R-4, 80	760.30	0.59	0.58	0.42	25.8	9.16	9.31	12.75
65R-6, 40	762.90	0.61	0.54	0.42	25.8	8.88	9.87	12.92
66R-1, 116	765.76	0.53	0.55	0.39	26.0	10.16	9.89	13.76
66R-3, 97	768.57	0.56	0.63	0.44	26.0	9.58	8.64	12.41
66R-5, 102	771.62	0.55	0.57	0.44	26.2	9.89	9.51	12.23
67R-2, 34	774.78	0.58	0.55	0.37	27.4	9.48	10.03	14.83
67R-4, 38	777.82	0.58	0.53	0.38	27.4	9.62	10.45	14.50
67R-6, 56	781.00	0.57	0.52	0.41	27.4	9.68	10.59	13.52
68R-2, 35	785.75	0.58	0.54	0.39	27.4	9.56	10.24	14.37
69R-2, 37	794.24	0.53	0.55	0.39	27.1	10.49	10.08	14.24
69R-4, 34	797.21	0.53	0.50	0.39	27.1	10.42	10.94	14.01
69R-6, 50	800.37	0.52	0.48	0.38	27.1	10.67	11.47	14.54
70R-2, 19	804.99	0.55	0.52	0.37	27.1	10.07	10.62	14.90
70R-5, 50	809.80	0.47	0.46	0.36	27.1	11.78	12.00	15.31
71R-3, 1	814.17	0.53	0.56	0.44	27.1	10.47	9.84	12.44

Table T22 (continued).

Core, section, interval (cm)	Depth (mbsf)	Conductivity (S/m)			Temp (°C)	Formation factor		
		x	y	z		x	y	z
72R-1, 74	822.94	0.34	0.37	0.33	26.7	16.22	14.83	16.34
72R-3, 103	826.23	0.47	0.37	0.42	26.7	11.58	14.77	12.99
73R-5, 118	838.98	0.42	0.39	0.42	26.9	13.11	14.22	13.12
73R-6, 118	840.48	0.45	0.46	0.39	27.2	12.17	12.06	14.03
73R-7, 57	841.37	0.54	0.55	0.44	27.5	10.35	10.11	12.58
74R-1, 40	841.80	0.60	0.54	0.47	27.1	9.18	10.12	11.65
74R-2, 99	843.89	0.60	0.58	0.45	27.1	9.13	9.44	12.30
74R-3, 33	844.73	0.51	0.59	0.41	27.1	10.74	9.34	13.29
75R-1, 93	851.93	0.56	0.56	0.40	27.1	9.89	9.86	13.81
76R-1, 69	861.39	0.63	0.66	0.43	27.1	8.81	8.29	12.95
77R-3, 83	874.23	0.62	0.63	0.36	28.4	9.10	8.97	15.51
77R-5, 67	877.07	0.61	0.60	0.40	28.0	9.14	9.37	14.17
77R-6, 2	877.92	0.66	0.62	0.38	27.9	8.42	9.00	14.82
78R-1, 77	880.77	0.60	0.63	0.40	28.6	9.37	8.93	14.00
78R-2, 130	882.80	0.71	0.79	0.46	28.3	7.93	7.14	12.27
78R-4, 26	884.76	0.61	0.59	0.39	28.3	9.19	9.59	14.61
79R-2, 18	890.98	0.58	0.57	0.37	28.3	9.67	9.85	15.31
80R-2, 24	900.74	0.59	0.56	0.38	28.7	9.60	10.18	14.89
80R-4, 72	904.22	0.60	0.55	0.40	28.7	9.52	10.37	14.29
80R-6, 45	906.95	0.61	0.58	0.37	28.7	9.33	9.75	15.17
81R-2, 68	910.78	0.63	0.61	0.40	28.5	9.04	9.29	14.24
81R-4, 80	913.9	0.63	0.63	0.39	28.5	8.99	8.94	14.49
82R-3, 90	921.95	0.58	0.55	0.37	28.5	9.79	10.33	15.15
83R-2, 25	929.65	0.55	0.54	0.37	27.8	10.08	10.28	15.01
83R-5, 53	934.43	0.70	0.48	0.32	27.8	8.03	11.54	17.41
83R-6, 48	935.88	0.57	0.40	0.37	27.8	9.77	13.83	14.89
84R-2, 48	939.48	0.59	0.56	0.40	27.8	9.48	9.90	14.03
84R-4, 146	945.00	0.55	0.55	0.37	27.8	10.06	10.11	14.88
84R-6, 66	945.66	0.47	0.49	0.34	27.8	11.81	11.45	16.28
85R-2, 70	949.30	0.61	0.59	0.39	28.2	9.26	9.47	14.45
85R-4, 70	952.30	0.58	0.54	0.35	28.5	9.79	10.37	16.01
85R-6, 70	955.30	0.55	0.55	0.34	28.8	10.29	10.41	16.50
86R-2, 110	959.40	0.55	0.55	0.31	27.5	10.01	10.02	17.94
86R-4, 58	961.88	0.50	0.50	0.32	27.4	11.10	11.10	17.14
86R-6, 74	965.04	0.50	0.56	0.36	27.4	11.12	9.89	15.38
87R-1, 24	966.74	0.56	0.51	0.35	27.7	9.90	10.83	15.87
87R-3, 41	969.91	0.53	0.54	0.36	27.8	10.50	10.27	15.50
87R-5, 3	972.53	0.51	0.52	0.32	27.5	10.87	10.58	17.17
88R-2, 116	978.76	0.54	0.53	0.31	26.9	10.09	10.37	17.68
88R-4, 92	981.52	0.55	0.52	0.32	26.9	9.94	10.61	17.29
89R-2, 141	988.21	0.56	0.52	0.31	26.1	9.66	10.47	17.54
89R-4, 74	990.54	0.50	0.53	0.32	26.1	10.74	10.27	16.70
89R-6, 34	993.14	0.54	0.50	0.30	26.1	10.10	10.77	17.77
90R-1, 48	995.38	0.50	0.49	0.30	27.2	11.08	11.21	18.25
90R-2, 4	996.44	0.48	0.49	0.30	27.2	11.40	11.26	18.21
91R-2, 91	1007.01	0.43	0.48	0.30	27.2	12.87	11.43	18.65
92R-2, 66	1016.36	0.56	0.49	0.27	27.2	9.84	11.16	20.14
92R-4, 70	1019.40	0.40	0.47	0.33	27.2	13.71	11.79	16.81
92R-5, 38	1020.58	0.39	0.45	0.29	27.2	14.22	12.31	19.16
93R-2, 20	1025.60	0.46	0.46	0.33	27.2	12.01	12.00	16.92
93R-4, 113	1029.53	0.44	0.49	0.30	27.2	12.41	11.16	18.46
94R-2, 71	1035.71	0.42	0.47	0.30	27.0	12.99	11.68	18.50
94R-4, 85	1038.85	0.49	0.50	0.32	27.0	11.14	11.07	17.21
95R-1, 33	1043.43	0.40	0.42	0.30	26.4	13.61	12.88	18.19
95R-3, 4	1046.14	0.54	0.46	0.27	26.4	10.05	11.89	20.03
96R-2, 35	1054.45	0.45	0.48	0.29	27.1	12.21	11.41	19.19
96R-4, 41	1057.51	0.53	0.47	0.32	27.1	10.35	11.70	17.15
97R-2, 96	1064.76	0.54	0.45	0.27	26.6	10.02	12.06	19.94
97R-4, 110	1067.90	0.46	0.47	0.28	26.6	11.87	11.53	19.65
98R-1, 26	1072.16	0.48	0.44	0.26	27.2	11.50	12.65	21.34
98R-5, 56	1076.98	0.44	0.46	0.25	27.4	12.65	11.95	21.94
99R-1, 19	1081.69	0.47	0.48	0.25	27.3	11.65	11.41	22.01
100R-1, 97	1092.17	0.46	0.46	0.27	27.4	12.05	12.01	20.38
100R-2, 39	1092.95	0.33	0.35	0.22	27.0	16.42	15.57	25.38
101R-1, 51	1101.31	0.43	0.46	0.25	27.0	12.91	11.99	22.43

Note: x, y, z = probe axis. This table is also available in ASCII format.

Table T23. Summary of downhole temperature measurements, Hole 1174A.

Depth (mbsf)	Tool	Measurement location	In situ temperature (°C)
0.0	Adara	Mudline	1.50
32.9	Adara	Bottom of Core 4H	8.74
65.5	DVTP	After Core 8H	12.98
160.8	DVTP	After Core 3R	Bad thermistor
209.1	DVTP	After Core 8R	Unsuccessful

Note: DVTP = Davis-Villinger temperature probe.